IDENTIFICATION AND CHARACTERIZATION OF ISOFORM-SELECTIVE INHIBITORS

FOR PROTEIN ARGININE METHYLTRANSFERASES

by

KUN QIAN

(Under the Direction of Yujun George Zheng)

ABSTRACT

In recent years, the field of epigenetic drug discovery has been rapidly growing and have

resulted in several FDA-approved therapies. Epigenetic mechanisms predominantly consist of

DNA methylation, histone modifications and non-coding RNA regulations. The nine isoforms of

mammalian protein arginine methyltransferases (PRMT1 to PRMT9) are crucial histone

modifying enzymes responsible for arginine methylation, which is an abundant posttranslational

modification in eukaryotic cells. PRMTs are categorized into type I, II and III based on their

catalytic products, which are asymmetric dimethylarginine (ADMA), symmetric

dimethylarginine (SDMA) and monomethylarginine (MMA), respectively. The nine PRMTs

have different roles in cells, many of which are not well understood. Numerous studies have

suggested that PRMTs are promising drug targets for cancers because of their crucial biological

functions. Therefore, PRMT inhibitors are potential therapeutic agents for cancer treatment and

useful chemical tools for cancer research. Despite the steady progress being made in PRMT

inhibitor research, challenges remain in the discovery of potent, isoform-selective, cell-

permeable and *in vivo*-active PRMT inhibitors. This work focuses on the identification and

characterization of small molecule inhibitors for two PRMT isoforms, PRMT1 (type I) and

PRMT5 (type II). Combinatorial inhibitor discovery approaches including virtual screening, target-based high throughput screening, chemical modification applied in this study have resulted in several novel chemical entities for potent and isoform-selective inhibition of PRMT1 or PRMT5 *in vitro* and *in vivo*. These compounds also showed significant anticancer efficacy in PRMT dysregulation-associated cancer models. Furthermore, an innovative stopped flow fluorescence assay was developed to measure PRMT enzymatic activity, representing the first continuous assay for PRMT inhibitor characterization that can determine potency and distinguish the mechanism of inhibition simultaneously.

INDEX WORDS: Epigenetics, Drug Discovery, Protein Arginine Methyltransferases, Small Molecule Inhibitors, Diamidines, Anticancer, Stopped Flow

IDENTIFICATION AND CHARACTERIZATION OF ISOFORM-SELECTIVE INHIBITORS

FOR PROTEIN ARGININE METHYLTRANSFERASES

by

KUN QIAN

B.S. Central China Normal University, China, 2012

A Dissertation Submitted to the Graduate Faculty of The University of Georgia in Partial

Fulfillment of the Requirements for the Degree

DOCTOR OF PHILOSOPHY

ATHENS, GEORGIA

2017

IDENTIFICATION AND CHARACTERIZATION OF ISOFORM-SELECTIVE INHIBITORS

FOR PROTEIN ARGININE METHYLTRANSFERASES

by

KUN QIAN

Major Professor: Yujun George Zheng

Committee: Brian S. Cummings
                     Scott D. Pegan
                     Jeffrey Urbauer
                     Jason Zastre

DEDICATION

I dedicate this dissertation work to my loving family, whose words of encouragement and push have made me who I am today.

This dissertation is also dedicated to the most important person I met in Athens: Ruizhe Lin, I am truly grateful for having you in my life.

I also dedicate this work to Emmiline K. Pritchett, who always has been my best friend for the past five and a half years.

ACKNOWLEDGEMENTS

the diamidine compounds; Sudeepti Kuppa, Lindsay Berman and Dr. Mandy Murph for the examination of K313 activity in melanoma cells.

Lastly, I would like to thank all the other staffs, colleagues and graduate students I have met in the College of Pharmacy at the University of Georgia. I had wonderful experience studying here because of all of you. I would not become who I am today without your positive influence on me.

TABLE OF CONTENTS

LIST OF TABLES

LIST OF FIGURES

LIST OF ABBREVIATIONS

Asymmetrical dimethyl arginine (ADMA)

Arginine methyltransferase inhibitors (AMIs)

Androgen receptor (AR)

Bovine serum albumin (BSA)

Dimethyl sulfoxide (DMSO)

Dimethylformamide (DMF)

1, 4-Dithiothreitol (DTT)

Electrospray ionization (ESI)

Enzyme-linked immunosorbent assay (ELISA)

Ethylenediaminetetraacetic acid (EDTA)

Fluorenylmethyloxycarbonyl (Fmoc)

Fluorescein (FL)

Fast protein liquid chromatography (FPLC)

High-throughput screening (HTS)

2-(6-Chloro-1H-benzotriazole-1-yl)-1,1,3,3-tetramethylaminium hexafluorophosphate (HCTU)

4-(2-hydroxyethyl)-1-piperazineethanesulfonic acid (HEPES)

Histone H4 arginine 3 (H4R3)

Histone methyltransferases (HMTs)

Isopropyl-β-D-thiogalactopyranoside (IPTG)

Matrix assisted laser desorption ionization mass spectrometry (MALDI-MS)

Mixed lineage leukemia (MLL)

Monomethylation of arginine (MMA)

Mode of action (MOA)

Mode of inhibition (MOI)

National Cancer Institute (NCI)

Parallel artificial membrane permeability assay (PAMPA)

Phenylmethanesulphonyl fluoride (PMSF)

Protein arginine methyltransferase (PRMT)

Protein lysine methyltransferase (PKMT)

Protein Database (PDB)

Reverse-phase (RP)

S-Adenosyl-L-methionine (SAM, AdoMet)

S-Adenosyl-L-homocysteine (SAH, AdoHcy)

Symmetrical dimethyl arginine (SDMA)

Sodium dodecyl sulfate polyacrylamide gel electrophoresis (SDS-PAGE)

Solid phase peptide synthesis (SPPS)

Scintillation proximity assay (SPA)

Structure-activity relationship (SAR)

Ultraviolet-visible (UV)

CHAPTER 1

INTRODUCTION

This work is modified from the published book chapter: Qian, K., and Zheng, Y. G. (2016),

Chapter 8 "Current Development of Protein Arginine Methyltransferase Inhibitors", *Epi-*

Informatics: Discovery and Development of Small Molecule Epigenetic Drugs and Probes, 2016,

Medina-Franco, J. L., ed., Academic Press, Waltham. p231-p256

1.1 Targeting Epigenetics in Drug Discovery

Epigenetics is "a bridge connecting phenotype to genotype", which refers to the study of

heritable alterations in gene function other than the changes in DNA sequence [1-2]. It is one of the

most rapidly expanding fields in life sciences. Epigenetics includes several prevailing events in

living cells that record the developmental and environmental cues by modifying genetic material

without altering the nucleotide sequences[3]. The predominant epigenetic mechanisms consist of

DNA methylation, histone modifications and non-coding RNA regulations[4-7]. Typically,

chemical modifications on DNA, histone or other related nuclear proteins control the chromatin

remodeling and switching of the conformational transition of chromatin between

transcriptionally active state and inactive state[8]. Epigenetic regulations can turn-on or turn-off

the expression of certain genes, and determine the normal production of proteins and cellular

differentiation. Therefore, abnormal epigenetic functions are associated with various pathogenic

pathways in human diseases, such as cancers, autoimmune disorders and neurological disorders[9-

10]. Among all, cancer epigenetics have become one of the most studied areas, due to the fact that

the epigenetic events collaborate with genetic alterations in almost all aspects of tumor biology[11-

[12]. Proteins that are directly responsible for the epigenetic changes, including writers that install the chemical marks, erasers that remove the marks and readers that recognize the marks, are widely studied for their potential as anticancer drug targets[13-14]. Until now, seven epigenetic therapies are approved by the FDA to treat hematologic disorders and blood cancers (**Table 1.1**), and many more are in Phase I, Phase II or Phase III clinical trials[14-15]. Mounting evidence in cancer biology studies along with promising clinical and preclinical results have signified that utilization of epigenetic therapies are effective and provide a valuable approach to chemotherapy of cancer[16-18].

Table 1.1 FDA approved epigenetic therapies

Drug	Epigenetic target	Application	Approval year
Azacitidine	DNA methyltransferase 1	Myelodysplastic syndrome	2004
Decitabine	DNA methyltransferase 1	Myelodysplastic syndrome	2006
Vorinostat	Histone deacetylases	Cutaneous T-cell lymphoma	2006
Romidepsin	Class I Histone deacetylases	Cutaneous T-cell lymphoma	2009
Belinostat	Histone deacetylases	Peripheral T-cell lymphoma	2014
Panobinostat	Histone deacetylases	Multiple myeloma	2015

1.2 Protein Arginine Methyltransferases

Among all the epigenetic protein families, enzymes that deposit the marks on the histones are named as histone writers, including protein methyltransferases (PMTs)[19]. PMTs include two families: PKMTs (protein lysine methyltransferases) and PRMTs (protein arginine methyltransferases). The methylation of arginine residues is catalyzed by the PRMTs. To date, eleven PRMT members (PRMT1-PRMT11) have been identified, and nine of them are

mammalian PRMTs (PRMT1-PRMT9)[20-21]. PRMTs are considered as epigenetic regulators

because histone tails are one of their primary targets[22]. Other than functioning on the histones,

PRMTs also methylate other various cellular proteins (**Table 1.2**). In general, most of the

PRMTs prefer to recognize glycine- and arginine-rich (GAR) motifs in their substrates, except

for CARM1 (PRMT4), which instead has an affinity toward proline, glycine, methionine and

arginine-rich (PGM) motifs. PRMT5 also has an affinity for PGM motifs in some cases[23-24]. The

existing crystal structures of PRMTs are shown in **Figure 1.1**.
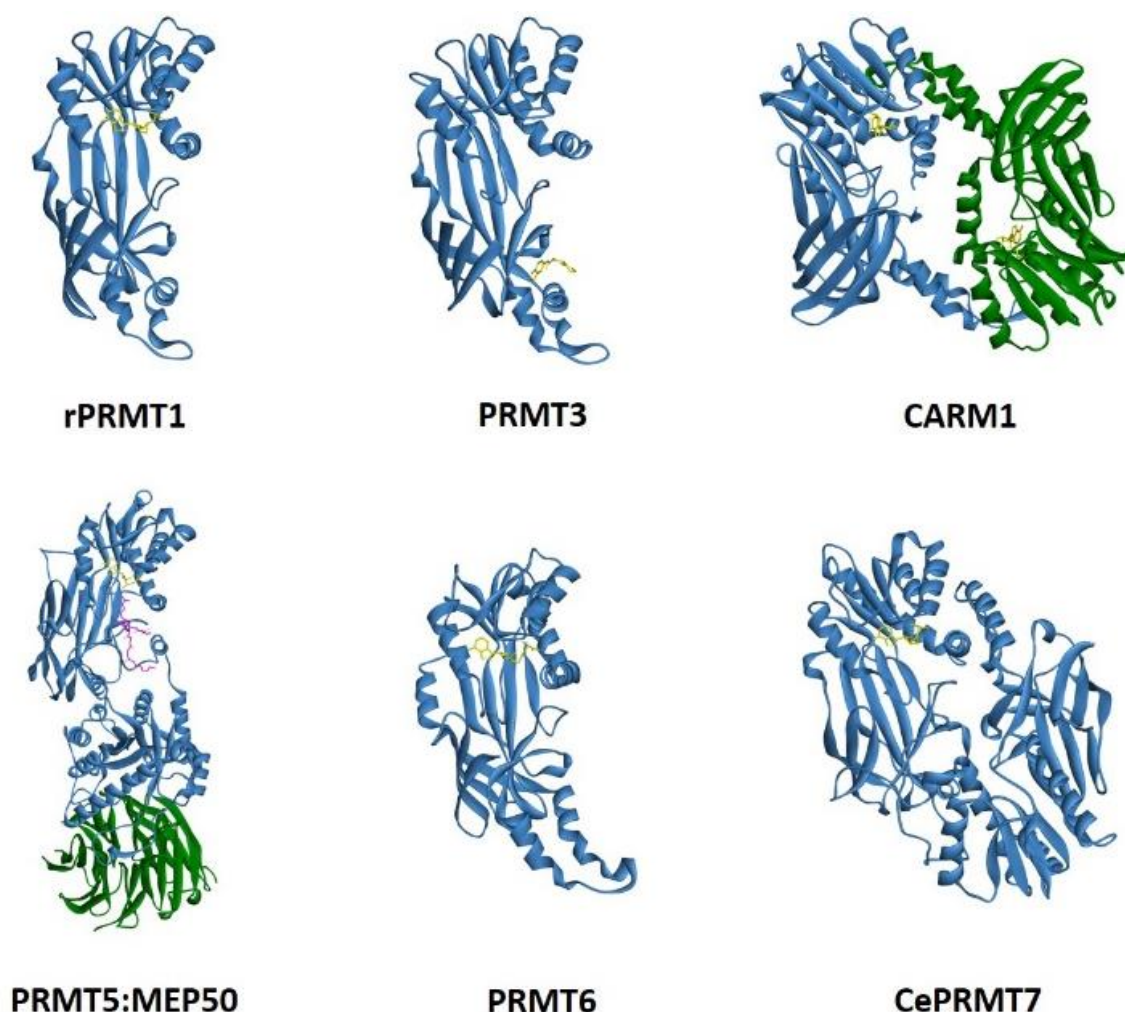
Figure 1.1. Crystal structures of PRMTs. PDB codes: PRMT1:1OR8 (rat, with SAH),
PRMT3: 3SMQ (human, with an allosteric inhibitor), CARM1: 3B3F (rat, dimer, with SAH),
PRMT5-MEP50 complex: 4GQB (human, MEP50 is indicated in green, with a SAM analog),
PRMT6: 4HC4 (human, with SAH), PRMT7: 3WST (C. elegans, with SAH).

The nine human PRMTs share a conserved catalytic site (**Figure 1.2**), which is organized around a Rossman fold for cofactor binding and a β-barrel for substrate binding[25]. Some PRMTs may contain domains for protein-protein interaction at the N-terminus, for example the SH_3 domain in PRMT2, zinc finger of PRMT3, PH domain in CARM1 and a TIM barrel in PRMT5. Current evidences supports that these unique domains are responsible for the recruitment of other proteins, homo-oligomerization and may also take part in substrate binding[26].
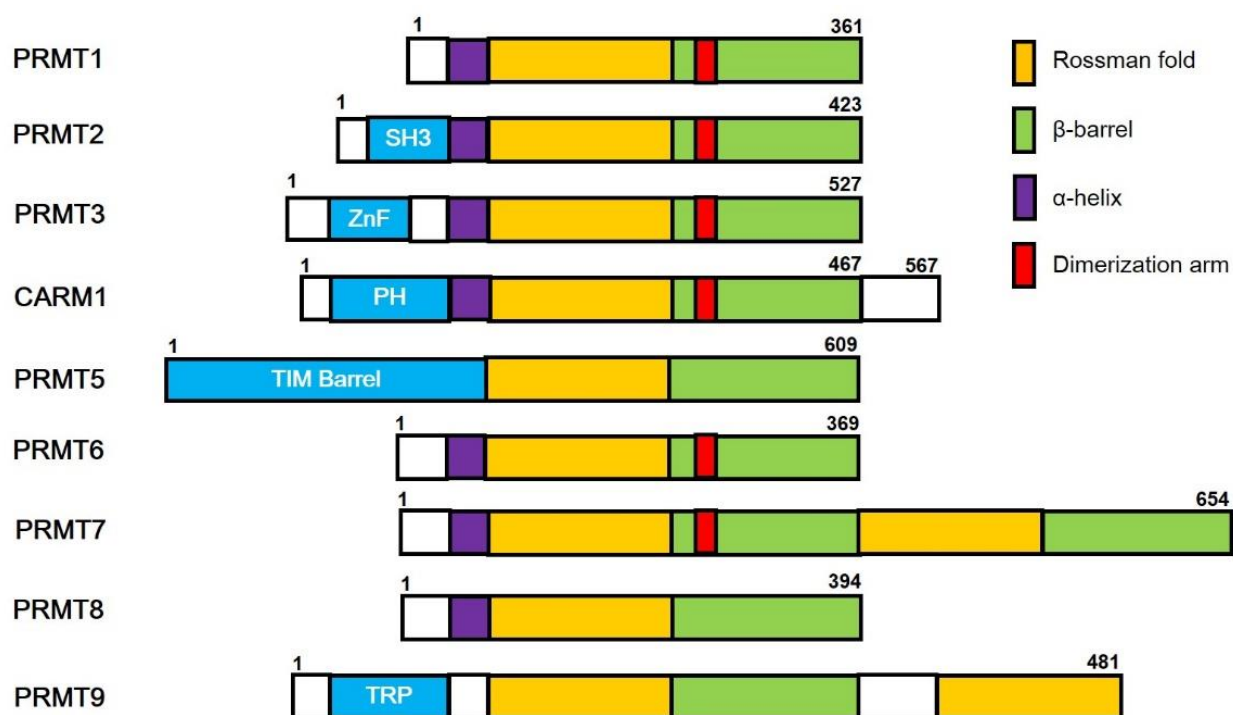
Figure 1.2. Domain architecture of human PRMTs.

1.3 Catalytic Activity of PRMTs

The catalytic reaction mediated by PRMTs are shown in **Figure 1.3**. The terminal guanidino group of an arginine residue on the protein substrates of PRMTs can be methylated in three different ways: monomethylation, asymmetrical dimethylation and symmetrical dimethylation. The methylated arginine products (MMA, ADMA and SDMA) have different functional consequences[27]. The nine mammalian PRMTs are classified into three types: type I

(PRMT1, 2, 3, 4, 6, and 8), type II (PRMT5, PRMT9), and type III (PRMT7)[22, 28-30]. Both type I

and type II PRMTs share MMA (mono-methylated arginine) as intermediate, with difference in

the follow-up step: type I PRMTs further methylate MMA into aDMA while type II PRMTs will

produce sDMA. Type III PRMT can only monomethylate the arginine residue. PRMT7 has been

assigned as type III, but some studies show its ability to catalyze sDMA [29, 31]. PRMT9 is a newly

discovered PRMT, and has been assigned to type II[30, 32]. The global arginine level in cell is

1500:3:2:1 for Arg:ADMA:MMA:SDMA[27]. Among all, PRMT1 is the primary type I enzyme

that is responsible for more than 50% of the total methylation in mouse embryotic fibroblasts

(MEFs); PRMT5 is the primary type II enzyme[33]. Studies have shown that the PRMT1 knockout

or PRMT5 knockdown cells resulted in substrate scavenging by other PRMTs, which supports

the dynamic interplay between different types of PRMTs[34].
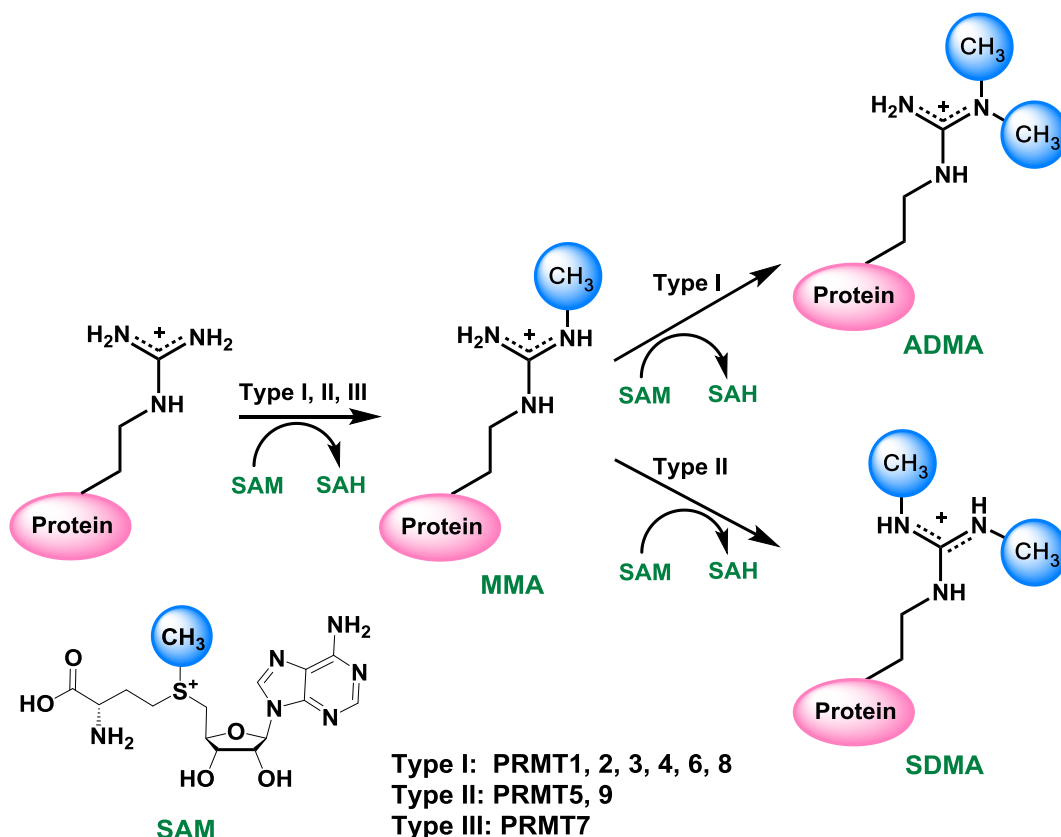
Figure 1.3. Arginine methylation reaction and types of PRMTs. Only theside chain of
arginine is shown. The methyl group transferred from SAM is indicated in blue.

5

An S_N2 like mechanism was proposed for the methylation process. PRMTs transfer a methyl group from S-adenosyl methionine (AdoMet or SAM) to a guanidine nitrogen of arginine, generating methyl arginine with S-adenosyl homocysteine (AdoHcy or SAH) as byproduct[28]. The two conserved glutamate residues (i.e. E144 and E153 of PRMT1) interacting with the substrate arginine were found to be crucial in charge re-distribution during the catalysis[35-37]. Evidence also suggested that a conserved methionine residue was essential for the control SDMA and ADMA formation[38-40]. Each addition of a methyl group to an arginine residue removes a potential hydrogen bond donor and changes its shape[41]. Bulkiness and hydrophobicity are introduced by the additional mono- or dimethyl group(s) on the arginine residue of protein substrates and these properties affects protein–protein interactions. However, methylation does not neutralize the cationic charge of arginine residue[42].

1.4 Pharmacological Significance

Protein arginine methylation is an abundant modification that has been implicated in, but not limited to, signal transduction, gene transcription, DNA repair and mRNA splicing[21]. An increasing amount of evidence shows that abnormity of PRMTs is associated to many diseases, including various cancers[21]. **Table 1.2** shows a brief summarization of the known relevance between PRMTs and cancers. For example, PRMT1 is an essential component of MLL (mixed-lineage leukemia) oncogenic transcriptional complex. One of the major target site, H4R3, is a suggestive marker for the diagnosis of prostate cancer [43]. Aberrant expression of PRMT1 and CARM1 has been observed in breast cancer[44-45]. PRMT5 acts as strong repressor of numerous genes, and the overexpression of PRMT5 has been observed in a variety of lymphoma, leukemia, gastric carcinoma, and immortalized fibro-blast cells[46-48]. PRMT6 is a transcriptional repressor and PRMT7 can down regulate sensitized cancer cells[22]. Overall, dysregulation of PRMTs has

been observed in diverse types of cancers, and the modulation of their levels affects cancer cell growth. This family of enzymes are considered promising therapeutic targets for cancer treatment[20, 49].

Table 1.2. Primary substrates, function and disease relevance of PRMTs. [21, 49-50]

PRMT	Substrate	Function	Disease relevance
PRMT1	H4R3[51] hnRNP A1[52], BTG1[53], TIS2[53], IFNα/β[54], ILF3[55], SPT5[56], SAF-A[57], p53[58], MRE11[59], FMRP[60], Sam68[61], SLM[61], ERα[62], RUNX1[63], TAF15[64], BCR[65], CF Im59 and Im68[66], Ash2L[67], nuclear poly(A)-binding protein (PABP1)[68]	Transcriptional coactivator[69], signal transduction[62, 70], RNA splicing[71] and DNA repair[59]	Overexpressed or aberrant in breast, prostate, lung, colon, bladder cancer and leukemia.[21] Overexpressed or aberrant in pulmonary diseases: pulmonary fibrosis, pulmonary hypertension, chronic obstructive pulmonary disease (COPD) and asthma. [72-74] Play regulatory roles in cardiovascular disease[75-76], diabetes[77-78] and renal disease[79-82].
PRMT2	H3R8[83] ERα[84], Glutathione transferase[85]	Transcriptional coactivator and androgen/estrogen receptor coactivator[86]	Overexpressed or aberrant in breast cancer [87-88]. Overexpressed in pulmonary inflammation [73, 89].
PRMT3	FMRP[60], rpS2[90], PABP1[68]	Ribosomal homeostasis[91]	Enhanced activity in breast tumors [21]. Overexpressed in coronary heart disease [92] and chronic kidney disease [93].
CARM1	H3R2, H3R17, H3R26[94] PABP1[95]; SAP49 (CBP)/p300[96]; FMRP[60]; Sox9[97]; CA150, SmB, U1C and SF3b4[23]	Transcriptional coactivator[69], RNA splicing[23], cell proliferation[98], cell differentiation[99]	Overexpressed in breast, prostate and colorectal cancer [21]. Regulate human t-cell lymphotropic virus type 1 (HTLV1)[100].
PRMT5	H2AR3, H3R8, H4R3[101]; H3R2[102]; MBP (Myelin basic protein) [103]; LSm4, Sm D1 and SmD3[104]; EBNA-2[105]; SPT5[56]; EBNA-1[106]; p53[65]; CBP-	Transcriptional repressor[101], RNA splicing[111], signal transduction[112] and piRNA pathway[113]	Overexpression/increased activity in gastric, colorectal, lung cancer, lymphoma, and leukaemia[21]; mis-localized in prostate cancer cells[114]. Play regulatory roles in renal and cardiovascular disease[115],

	1^{107}; CF Im68[66]; Ash2L[67]; PDCD4[108]; HoxA[109]; NFkB[110]		Huntington's disease[116], Alzheimer's disease[117]
PRMT6	H2AR29[118], H3R2[119] PRMT6[120-121]; HIV Tat[122]; HMGA1a[123], DNA polymerase β[124], PABP1[68]	Transcriptional repressor[125-126] and activator[127]	Overexpressed in bladder and lung cancer [21] Suppress HIV-1 activity[128] Overexpressed or aberrant in pulmonary fibrosis, COPD and asthma[72]
PRMT7	H4R3 and H2AR3[129], H3R2[102], Fibrillarin[29]	DNA damage[129], embryonic stem cell pluripotency[130], male germline gene imprinting[131-132]	Involved in breast cancer metastasis[133]
PRMT8	H2A, H4[134] MBP, PRMT8[134] EWS (Ewing sarcoma)[135]	Brain specific functions[136]	Somatic mutations were found in ovarian, skin and large intestine cancer[21]
PRMT9	SAP145 (SF3B2)[137]	RNA splicing[30]	lymphoma, melanoma, testicular, and pancreatic cancers[138]

1.5 Biochemical Assays in PRMT Inhibitor Study

Discovery of PRMT inhibitors relies on effective assays to detect and quantify the inhibition of PRMT enzymatic activity. Several biochemical assays have been developed for measuring PRMTs activity[139-143], and these assays can be categorized into three types based on the assay method: radiometric assays, antibody-based assays and enzyme-coupled assays for SAH detection. The radiometric methods have been the gold standard for *in vitro* measurements of PRMTs enzymatic activity due to the high sensitivity and reliability of the assay. In a typical radiometric assay, the radioisotope-labeled methyl group from isotope labeled cofactor ([^{3}H]-SAM or [^{14}C]-SAM) is transferred onto a peptide or protein substrate of PRMTs. Then the methylated substrates are separated from unreacted SAM using different approaches, such as gel

electrophoresis[144-148], or filtration through glass fiber or phosphocellulose paper discs[149-160] (**Figure 1.4**). After washing, the signals from the sample are quantitatively detected by a scintillation counter. The scintillation proximity assay (SPA) possesses an advantage of avoiding an additional washing step. In this method, the scintillation signals depend on the micrometer proximity between biotinylated substrates and streptavidin-coated scintillants[152, 161-170], such that SAM molecules present in the bulk solution fall off the SPA distance and do not produce scintillation signals (**Figure 1.4**). Due to its simple mix-and-measure procedure and high sensitivity, the SPA method is applicable in a high throuput format for compound library screening[163, 171-173].

Antibody-based assays represent another type of widely used methods for PRMT activity detection. A typical format is the enzyme-linked immunosorbent assay (ELISA)[174-176], in which methylated substrates are adsorbed onto the microplate, then incubated with primary antibody and further probed with horseradish peroxidase (HRP)-labeled secondary antibody to catalyze the production of chemiluminescence (**Figure 1.4**). The dissociation-enhanced lanthanide fluorescent immunoassay (DELFIA)[140, 145, 177-178] is similar to ELISA, except that the antibody is labeled with a lanthanide probe instead of HRP. Lanthanide is a fluorophore that exhibits large stoke shifts, a long decay time and a narrow emission spectrum, which together minimizes the background interference. By addition of an enhancement cocktail, the lanthanide dissociating from the antibody and results in amplified fluorescence when excited at 340 nm. Other lanthanide-based assays are homogeneous (no-wash) technologies that include time-resolved fluorescence resonance energy transfer (TR-FRET)[179-180] and AlphaLISA[180-182].

The third type of assay utilized a coupled enzymatic reaction for detection of SAH, the side product of the methylation reaction, by converting SAH into derivatives with colorimetric,

fluorescent, or luminescent properties. For example, in the SAHH (SAH hydrolase)-coupled

assay (**Figure 1.4**), SAH is hydrolyzed into adenosine and homocysteine, and homocysteine

subsequently reacts with a thiol-fluorescence reagent ThioGlo or CPM, yielding strong

signals[183-184].
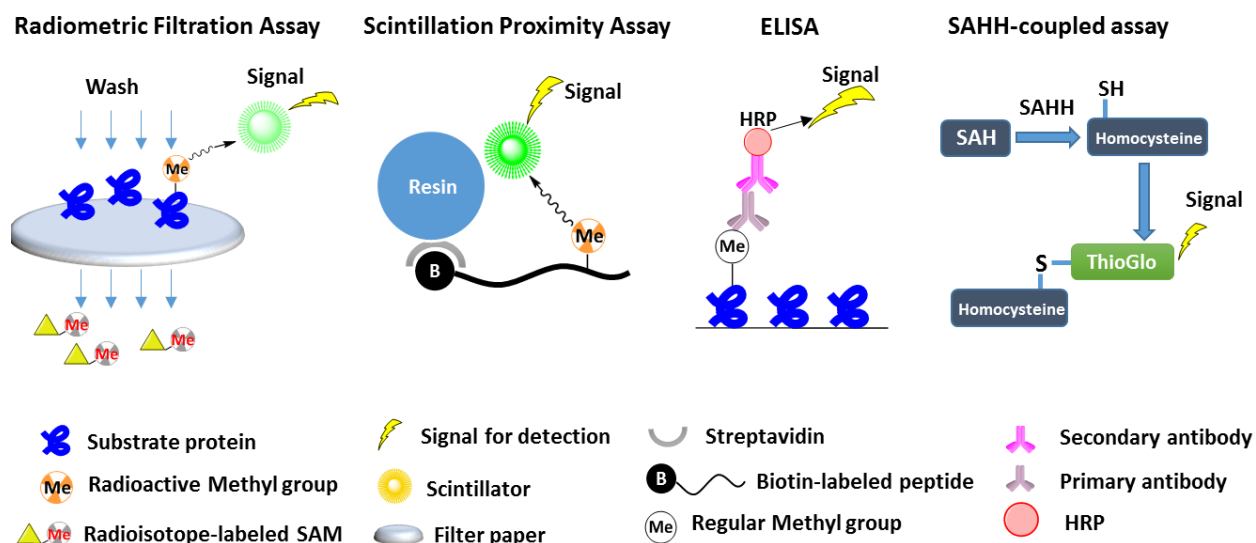
Figure 1.4. Biochemical assays for PRMT inhibitor study.

1.6 PRMT Inhibitors

With mounting evidence suggesting that PRMTs play crucial roles in both physiological

and pathological conditions, understanding their functions in various pathways become

significantly demanded. Since irregular PRMT activities are associated with many human

diseases, they are considered as ideal prognostic biomarkers and therapeutic targets[20, 185].

Therefore, PRMT inhibitors have become important chemical probes to study the various

functions of PRMTs in biological systems, and delivering new therapeutics against diseases and

cancers. Below we categorized the reported PRMT inhibitors by their structural features and

their enzyme targets.

1.6.1 Cofactor mimics

S-Adenosyl methionine (SAM/AdoMet) (**Figure 1.5, 1**) is a small organic cofactor

participating in enzyme catalysis of PRMTs and many other methyltransferases. The structural

analogs of SAM can inhibit the activity of SAM-dependent methyltransferases by competing

with SAM binding. One example is S-adenosyl-homocysteine (SAH, AdoHcy) (**Figure 1.5, 2**),

the reaction product from SAM after the methyl group is removed. However, it is a substrate of

5'-AdoHcy hydrolase, which means that it has a limited availability *in vivo*. Another SAM

analogue is sinefungin (**Figure 1.5**), which is a natural streptomycin antibiotic. SAH and

sinefungin were originally used to inhibit mRNA methyltransferases; later, both were found to

show inhibition for PMTs[186-187]. Many cofactor mimics have been widely used in PRMT protein

crystallization, as indicated in **Figure 1.1**.

Extensive work has been done to develop SAM analogs as PRMT inhibitors. Dowden, et

al. [147] synthesized several SAH derivatives, and found that compound **4** (**Figure 1.5**) inhibited

PRMT1 with an IC_{50} value of 3.9 μM, and was inactive against CARM1 and SETD7. As

described in their studies, the structure activity relationship analysis of the synthesized SAH

derivatives has revealed a way to achieve selective inhibition through various PRMT binding site

sequences. Interestingly, the docking results of compound **4** suggested a bisubstrate binding

mode, although this finding is short of binding and kinetic proofs. The idea of designing a small

molecule bisubstrate inhibitor has been applied by van Haren, et al. [176]. Among the six SAM

analogues that have been synthesized and evaluated, compound **5** (**Figure 1.5**) had an IC_{50} value

of 3.2 μM for PRMT6, and was mostly inactive for PRMT1, CARM1 and G9a. Compound **6**

(**Figure 1.5**) was surprisingly selective for G9a with an IC_{50} value of 3.2 μM. Although the

docking poses suggested that these compounds occupied both the substrate and cofactor binding

site, there is no following study to support this hypothesis. Besides, the activity of the inhibitors mentioned above has not been characterized in cells.
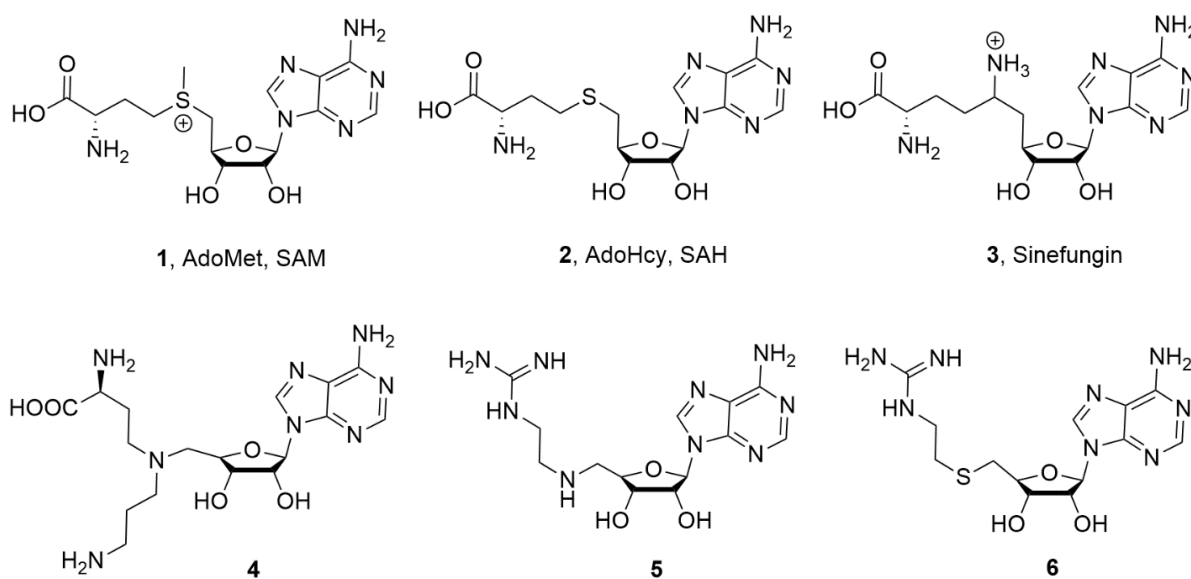
Figure 1.5. Cofactor mimics as PRMT inhibitors.

The idea of designing structural mimics of SAM certainly leads to PRMT inhibitors with promising potency. However, applying this approach is possible to achieve selectivity among PMTs remains a challeng[185]. Recently, a set of SAM analogues were developed as DOT1L-selective inhibitors. The lead inhibitor from this series occupied the SAM binding site of DOT1L with a stronger affinity than SAM, which indicated that the enzyme active site bears a certain degree of flexibility due to the structural nature of the activation loop and substrate binding loop[188-189]. DOT1L is the only PKMT that does not contain a SET domain and is structurally similar to the PRMTs. Since the PRMTs also contain a flexible α-X and α-Y helices in the catalytic pocket, it will be intriguing to see whether this mechanism of inhibition is plausible for PRMTs.

1.6.2 AMI compounds and their analogs

In 2004, the first small molecule inhibitors of PRMTs, named as AMIs (arginine methyltransferase inhibitors) (**Figure 1.6, 7-9**), were identified by Cheng et al. via a high throughput screening of a diverse 9000-compound library[175]. The ELISA-based assay was established to detect methylation of Np13p, an RNA binding protein, by Hmt1p (yeast arginine methyltransferase) or PRMT1. Nine hits were identified to indiscriminately inhibit all tested type I PRMTs (PRMT1, 3, 4, 6), but did not have activity on PKMTs. IC_{50} values of the nine inhibitors ranged from 0.19 µM to 16.3 µM for PRMT1. The leading compound **7** (**Figure 1.6**, AMI-1) inhibited PRMT1 with an IC_{50} value of 8.8 µM and did not compete for SAM binding. It was confirmed to be cell permeable, non-toxic and inhibited *in vitro* methylation of GFP-Npl3 in HeLa cells in a concentration-dependent manner. Subsequent studies showed that **7** was inactive for type II PRMT5[148], and it inhibited sirtuin (a histone deacetylase) with an IC_{50} value of 32 µM[190].

Following the discovery of AMIs, researchers have applied computational approaches to investigate more small molecule inhibitors for PRMTs. Ragno, et al. [191] published the molecular modeling studies based on the dye-like scaffold of compound **8** (AMI-5/eosin), compound **9** (AMI-6) and their analogs. They generated the homology model of PRMT1 from the crystal structure of rat PRMT1 (PDB: 1OR8), yeast homologue RMT1/Hmt1 (PDB: 1G6Q) and rat PRMT3 (PDB: 1F3L). Guided by the docking poses, compound **10** (**Figure 1.6**) was synthesized and identified to have an IC_{50} value of 4.8 µM for PRMT1. The consistency of the modeling studies with the biological results gave confidence that this approach would be further utilized for inhibitor identification.

On the other hand, inhibitor design was pursued through structure modifications. Mai, et al. [192] synthesized simplified analogs based on the pharmacophore of compound **8**, to screen against a panel of PRMTs and PKMTs. Among all, compound **11** (**Figure 1.6**), with an IC_{50} value of 10 μM for RmtA, could inhibit CARM1 but not PRMT1 or SET7/9 at 100 μM. Many of the analogs induced apoptosis of human leukemia cells. Additionally, Bonham, et al. [148] designed compound **13**, which combined the structural features of **7**, **9** and **12** (**Figure 1.6**). It was less polar than **7** and retained its potency (PRMT1 IC_{50} = 4.2 μM; CARM1 IC_{50} = 2.6 μM). Further characterizations on compound **13** (**Figure 1.6**) have shown that it inhibited both type I and type II PRMTs (PRMT5, -6, -8), but was mostly inactive against SET7/9. The cellular activity of compound **13** indicated an enhancement of T helper cell proliferation without affecting viability. In the same year, Castellano, et al. [144] synthesized carboxy analogs of **7**. The PRMT1 IC_{50} values of **7**, **14** and **15** (**Figure 1.6**) are 92.1 μM, 298.0 μM and 111.7 μM, respectively. Compound **7** presented some minor inhibition while both **14** and **15** were inactive against SET7/9. Molecular modeling provided an explanation that **14** and **15** established new interactions with the exposed residues in active site, which positively contributed in the binding process.

AMIs have made a significant impact in advancing the development of PRMT inhibitors. However, there are certain limitations for this type of compounds. First, researchers have not found an inhibitor with potency bellow micromolar value. Second, according to Feng, et al. [160], compound **7** probably interacts with the substrate H4 to achieve inhibition instead of binding to the PRMTs. This proposed mechanism also explains the fact that these compounds were not selective for those enzymes using H4 or H4 peptide as substrates in the assays, and they were mostly inactive to the same enzymes when examined against other substrates such as H3 or H3 peptide. It is also necessary to point out that the potency parameter (IC_{50} or Ki) derived under

different assays or conditions may not be consistent. For example, the potency of **7** was reported to be 8.8 µM on PRMT1 upon discovery; however, later studies showed that the IC_{50} value was 92.1 µM and 76.9 µM[144, 159, 175].
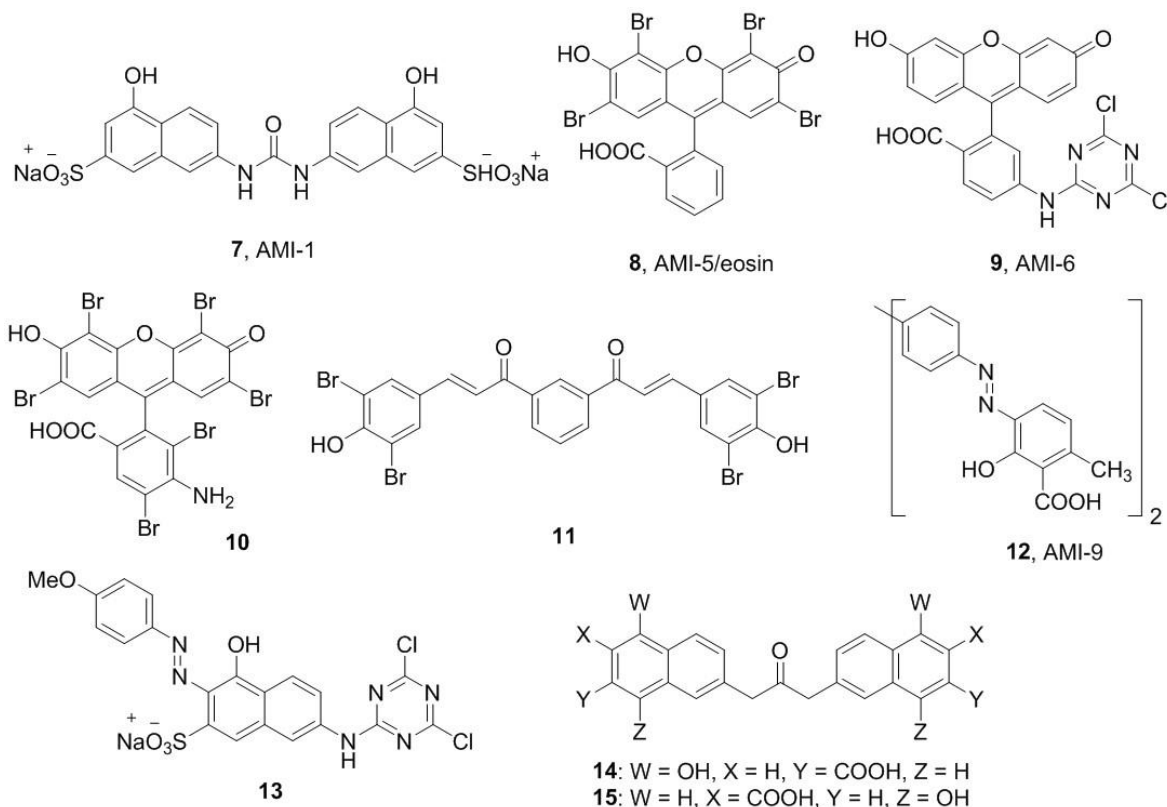
Figure 1.6. Selected structures of AMIs.

1.6.3 Dapsone derivatives, diamidine compounds, and other PRMT1 inhibitors

Dapsone derivatives and diamidine compounds were identified as PRMT inhibitors by Spannhoff, et al. [145] via a target-based screening approach. The authors generated homology models of human PRMT1 and RmtA based on the rat PRMT3 X-ray structure (PDB: 1F3L). The RmtA homology model containing SAH was then used to dock 1630 drug-like compounds derived from the NCI diversity set (140,000 compounds). Compound **17** (**Figure 1.7**, allantodapsone) and compound **19** (**Figure 1.7**, stilbamidine) were one of the best leads that had IC_{50} values of 57 µM and 1.7 µM for PRMT1, respectively. The docking results on human

PRMT1 homology model suggested that these two compounds contain basic or polar group interacting with acidic residue Glu152 in the active site. In cellular assays, these two compounds led to hypomethylation and blocked estrogen receptor activation. Subsequently, Bissinger, et al. [178] reported the structure activity relationship of allantodapsone (**Figure 1.7**, **17**) analogues and identified an improved inhibitor bearing a bis-chloroacetyl amide (**Figure 1.7**, **18**). The IC_{50} value was 1.5 µM for PRMT1 and it was inactive against CARM1 and SET7/9.

The symmetric phenylamidine structure in stilbamidine (**Figure 1.7**, **19**) has been identified as an important pharmacophore. Yan, et al. [150] explored the use of this pharmacophore and identified a series of diamidine compounds as potent and selective PRMT1 inhibitors. Compound **20** (**Figure 1.7**, DB75) inhibited PRMT1 activity with an IC_{50} of 9.4 µM and was selective for PRMT1 over CARM1 (>42-fold), PRMT5 (>18-fold), and PRMT6 (>30-fold). The SAR analysis and molecular modeling results suggested that the interactions between the diamidine functionality and the acidic residues (Glu129, Glu144 and Glu153) in the catalytic site are essential for the overall binding. Compound **20** was primarily competitive with the substrate and noncompetitive with the cofactor. It was also cell permeable and blocked the proliferation of several leukemia cell lines with different lesions.

During the development of PRMT1 inhibitors, researchers have been utilizing and improving various virtual screening methodologies in the drug discovery process. Spannhoff, et al. [140] reported compound **22** (**Figure 1.7**, RM65, IC_{50} = 55 µM), which was identified via the fragment-based virtual screening approach. They started with screening of HKI database (about 9000 compounds) for novel fragment-like leads, and ended up using 900 compounds for RmtA homology model docking followed by primary biological screening. Interestingly, the docking result of **22** on human PRMT1 suggested a bisubstrate inhibition mode in the active site. This

16

compound was further characterized as cell permeable and could cause hypomethylation in cancer cells. Later, Heinke, et al. [177] developed an approach that combined ligand- and target-based virtual screenings. Approximately 328,000 compounds from ChemBridge compound collection were screened by docking into a homology model of human PRMT with SAH. Top ranking compounds were then filtered through a pharmacophore model, which was generated from the known PRMT1 inhibitor structures. Nine compounds were identified to have micromolar potency for human PRMT1, the best among nine was compound **21** (**Figure 1.7**) with an IC_{50} value of 12.75 µM. More recently, Xie, et al. [180] identified compound **26** (**Figure 1.7**, DCLX069) and **27** (**Figure 1.7**, DCX078) through structure-based virtual screening with IC_{50} values of 17.9 µM and 26.2 µM for PRMT1. Both compounds were found to block cell proliferation in breast cancer, liver cancer and acute myeloid leukemia cell lines.

Some of the inhibitors identified by virtual screening strategy have a different mechanism of inhibition. Instead of directly bind to the enzyme, they may target the substrate instead. Feng, et al. [160] reported the identification of compound **23** (**Figure 1.7**, NS-1, naphthalene-sulfo derivative 1) via structure-based virtual screening of the ChemBridge small molecule compound collection (> 400,000 compounds), based on rat PRMT1 structure (PDB: 1OR8). Top 50 hits from the screening were evaluated by a radiometric biochemical assay. Compound **23** (**Figure 1.7**) was then identified with an IC_{50} value of 12.7 µM for PRMT1, while the IC_{50} value of compound **19** was only 105.7 µM in this assay. Kinetic studies suggested a substrate competitive, cofactor non-competitive inhibition mechanism. Interestingly, further studies showed that **23** directly interacted with substrate H4 but not PRMT1. Wang, et al. [159] reported the discovery of PRMT1 inhibitors **24** (**Figure 1.7**, A9) and **25** (**Figure 1.7**, A36) through pharmacophore-based virtual screening. Pharmacophore models were generated from

known PRMT inhibitors and used to filter SPECS database (>300,000 compounds). Top 102 compounds from the screening were evaluated, and compounds **24** and **25** were identified to have PRMT1 IC$_{50}$ values of 41.7 μM and 12.0 μM, respectively. IC$_{50}$ value of compound **7** was tested to be 76.9 µM in this assay. Kinetic data has shown that **24** was a substrate-competitive and cofactor non-competitive inhibitor, while **25** was noncompetitive for both substrate and cofactor. Same as compound **22**, binding studies suggested that they were targeting substrate H4. Compound **24** significantly inhibited the proliferation of castrate-resistant prostate cancer cells.

In addition to virtual screening method, Dillon, et al. [193] developed a high-throughput screening assay based on the fluorescence polarization change of a probe labeled on the SAM-binding cysteine residues of the PRMT1 active site. They successfully identified two mechanism-based inhibitors, compound **28** (**Figure 1.7**, CID5380390) and **29** (**Figure 1.7**, CID2818500), with IC$_{50}$ values of 23 µM and 11 µM, respectively. These compounds also inhibited PRMT8 activity, due to the conserved cysteine residues of PRMT1 and PRMT8, but they were inactive against CARM1 and SETD7/9. Moreover, some PRMT1 inhibitors have strong fluorescence properties that are explored as imaging probes. Sinha, et al. [149] synthesized and evaluated carbocyanine dyes as PRMT1 inhibitors and imaging agents. Compound **30** (**Figure 1.7**) presented low micromolar inhibition on PRMT1 (IC$_{50}$ = 4.1 µM), and was noncompetitive by binding to an allosteric site. This compound was used in optical and fluorescent microscopy to show the chromatin interfering property of cells. However, this compound had very limited selectivity among other PRMTs. Hu, et al. [164] further studied the structure activity relationship of cyanine compounds and was able to identify compound **31** (**Figure 1.7**, E84), with IC$_{50}$ value of 3.38 µM for PRMT1, and have 6- to 25- fold selectivity

over CARM1, PRMT5 and PRMT8. It also inhibited cellular PRMT1 activity and blocked

leukemia cell proliferation.
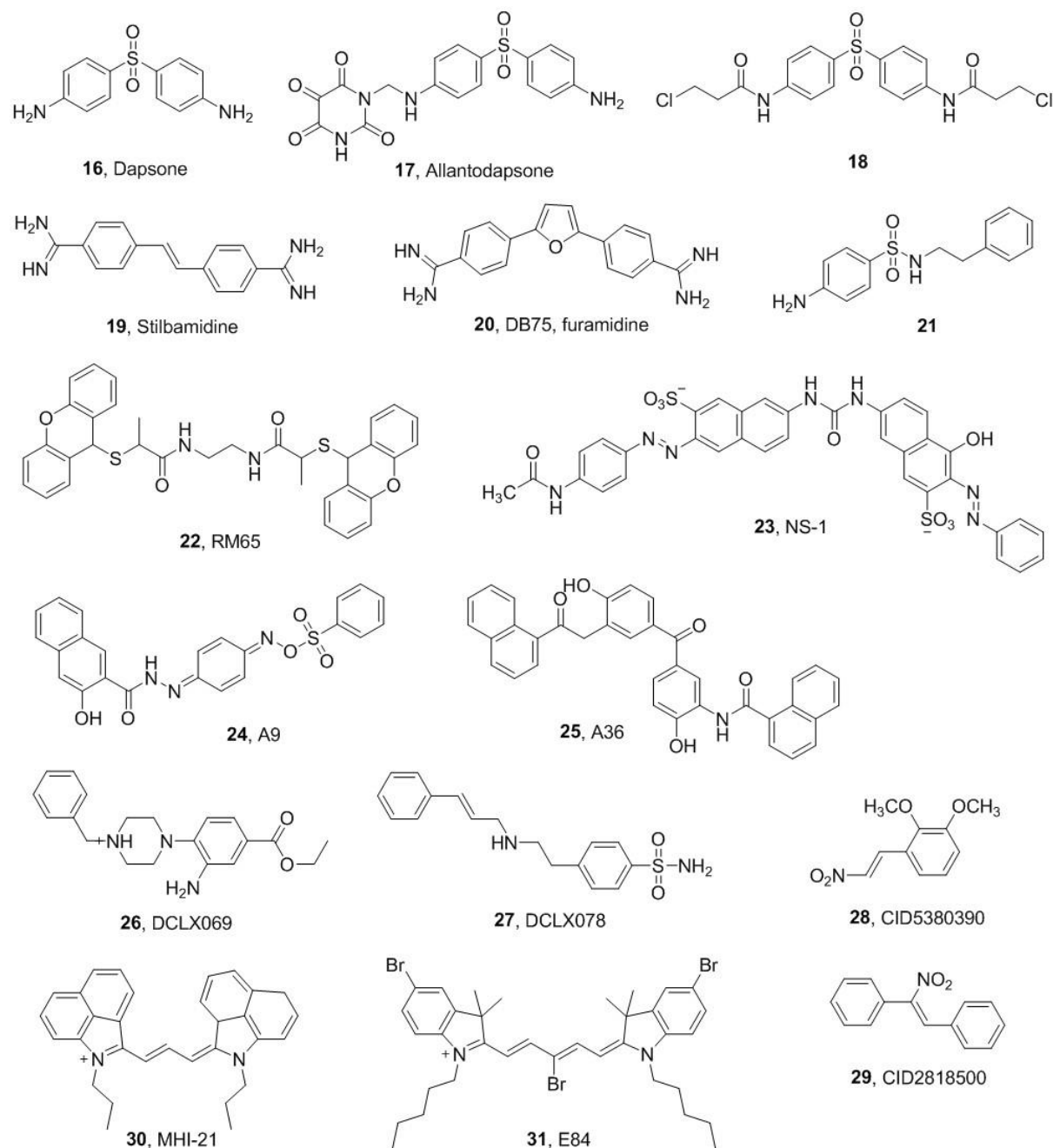
Figure 1.7. Dapsone (compound **16**) **and dapsone derivatives** (compound **17** and **18**), **diamidines** (compound **19** and **20**) **and other PRMT1 inhibitors**.

To conclude, the development of PRMT1 inhibitors has been the most vigorous in the

field, mainly because PRMT1 is the primary type I enzyme of this family[194]. The discovery of

PRMT1 inhibitors has greatly relied on the advancement of computational tools. The above examples included some of the frequently used strategies, which are the structure- or target-based, fragment-based and ligand/pharmacophore-based virtual screening. In many cases, homology model of human PRMT1 was generated instead of using the structure of rat PRMT1 (PDB: 1OR8), because it was crystalized in non-physiological condition (pH = 4.7)[36]. The molecular modeling method was used to help analyze the ligand-protein interactions and guide the chemical modifications. It is also intriguing to see that many inhibitors discovered through this methodology are known drugs that have been applied in other medical practices. For example, compound **19** (**Figure 1.7**, stilbaminine) is a treatment for fungal infections and compound **20** (**Figure 1.7**, furamidine) is for the treatment of parasitic infections such as malaria[195-196]. Besides, the above examples have shown that computational approaches can be extremely helpful in the lead optimization process as well. While computational methods are efficient at identifying drug-like small molecule inhibitors, there are certain limitations. First, theoretical models can often result in artifacts. This may explain why only very few inhibitors from the virtual screening hits were confirmed to have actual activity in the biochemical screening assays. On the other hand, since docking simulation relies on a defined grid or pocket, which is often the enzyme active site, it is extremely challenging to find out whether the inhibitors bind to the other sites on the enzyme. Besides, this class of inhibitors have not been successfully co-crystallized with PRMT1, thus the binding analysis results generated from molecular docking are not conclusive. However, the remaining challenge is to further develop inhibitors with nanomolar potency and isoform selectivity.

1.6.4 Allosteric PRMT3 inhibitors

Siarheyeva, et al. [165] reported the discovery of the first allosteric PRMT3 inhibitor (**Figure 1.8**, compound **32**) proved by the inhibitor-enzyme co-crystal structure. By screening a library containing 16,000 diversity compounds, the authors identified compound **32** to have an IC_{50} value of 1.6 μM for the full length human PRMT3. It was selective over other PKMTs and PRMTs, including G9a, GLP, SUV39H2, SETD7, SETD8, PRMT1, CARM1, PRMT5, and PRMT8. This inhibitor bound to a novel allosteric pocket located at the interface of the PRMT3 dimerization arm, but did not prevent homodimerization of PRMT3. It had a Kd value of 9.5 μM, and was noncompetitive with both SAM and the H4 peptide substrate. Interestingly, the cyclohexenyl moiety of the inhibitor interacted with the α-Y segment, which induced the conformational change that disordered the folding of the α-X helix on the cofactor binding site and resulted in an inactive α-helix structure. This disruption was proposed to have a direct influence on enzymatic activity of PRMT3. Furthermore, Liu, et al. [152] improved the inhibitor potency via SAR studies. Among all the analogs that have been synthesized, compound **34** (**Figure 1.8**) had the best potency (IC_{50} = 230 nM). Resolved crystal structure of PRMT3 with **33** (**Figure 1.8**, IC_{50} = 2.5 μM) showed that it bound to the same site as **32**. Compound **33** showed excellent selectivity for PRMT3 over other protein methyltransferases, including G9a, GLP, SUV39H2, PRMT5, SETD7, PRC2, SETD8, SETDB1, SUV420H1, SUV420H2, MLL1, SMYD3, SMYD2, DOT1L, and DNMT1. However, cellular activities of **33** and **34** remained unknown.

The above results suggest that the allosteric binding site of PRMT3 can be exploited to yield potent and selective inhibitors. According to the multiple sequence alignment of type I PRMTs, there are significant variability by the comparison, however, the structure alignment

showed similarity in the PRMT3 inhibitor binding region[152, 165]. This finding suggested that the

allosteric and selective inhibitors can be exploited by targeting this site in other PRMTs.

Moreover, due to the dynamic nature of α-X and α-Y in PRMTs, it would be exciting to see

whether other PRMT allosteric binding sites can also be explored.
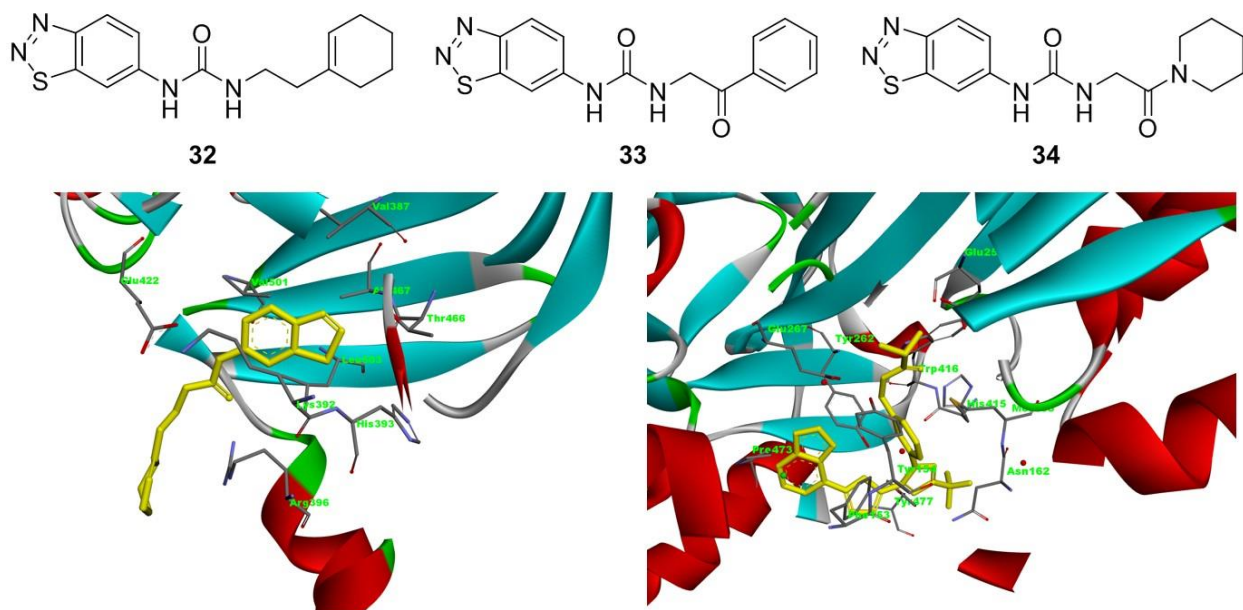
Figure 1.8. **Selected PRMT3 allosteric inhibitors and the co-crystal structure of PRMT3 and CARM1 with their inhibitors.** Inhibitors are indicated in yellow. Interacting amino acid residues are indicated in sticks. Left: PRMT3 (PDB: 3SMQ); right: CARM1 (2Y1W).

1.6.5 Pyrazoles, imidazoles, indoles, and other CARM1 (PRMT4) inhibitors

Purandare, et al. [151] identified pyrazole amide as an initial hit (**Figure 1.9**, **35,** IC$_{50}$ = 1.8

μM) by high throughput screening, and developed the compound **36** as a potent and selective

inhibitor of CARM1 (IC$_{50}$ = 80 nM), albeit poor permeability shown by parallel artificial

membrane permeability assay (PAMPA) and poor PK properties. Further hit-to-lead

optimization of this class of inhibitors led to compound **37** (**Figure 1.9**, IC$_{50}$ = 40 nM)[153].

Compounds **36** and **37** both were found to be significantly less potent against PRMT1 and

PRMT3 (IC$_{50}$ > 25 μM). Through SAR analysis, the replacement of the amide functionality with

the 1,3,4-oxadiazole moiety in **37** improved membrane permeability. Concurrently, Wan, et al.

[156] identified benzo[d]imidazole related analogues as CARM1 inhibitors. Modification made from SAR analysis led to the most potent analog, compound **38** (**Figure 1.9**, IC_{50} = 70 nM). It was significantly less active against PRMT1 and 3 (IC_{50} > 25 μM). Allan, et al. [197] developed compound **39** (**Figure 1.9**) as a CARM1 inhibitor with IC_{50} value of 60 nM, which was also inactive against PRMT1 and SET7/9 (IC_{50} > 100 μM). However, it did not show cellular activity. Therrien, et al. [154] further synthesized 1,2-diamine compounds as CARM1 inhibitors, represented by compound **40** (**Figure 1.9**). Although it only had an IC_{50} value of 0.2 μM and did not show cellular activity, the PK profile was improved. Sack, et al. [155] described the crystal structures of an improved pyrazole/indole-containing inhibitor with CARM1 and SAH/sinefungin. Compound **41** (**Figure 1.9**) is the analogue of **38** that has an IC_{50} value of 30 nM for CARM1, while IC_{50} >10 μM for PRMT1 and PRMT3. The inhibitor was shown to occupy the substrate binding site and the surrounding pocket located in the interface between the N- and C-terminal domains in the presence of SAH (**Figure 1.8,** right). Overall, the pyrazole/imidazole/indole CARM1 inhibitors have nanomolar potency, however there were no further *in vivo* studies reported, possibly due to the low cell permeability or cytoxic side effects. The other limitations include the incomplete selectivity profile and lack of mode of action elucidation.

Other than the pyrazole/imidazole/indole compounds, Selvi, et al. [158] identified compound **42** (**Figure 1.9**, TBBD), which was a natural product from pomegranate extract, as a CARM1 inhibitor. Compound **42** inhibited CARM1 activity in a dose dependent manner, while the IC_{50} value was not determined. It did not inhibit G9a and histone acetyltransferase CBP/p300. This compound was noncompetitive with both H3 and SAM. ITC experiments showed minimal interaction between **42** and CARM1 alone, while the K_d value of CARM1-histone 3 complex was 4 μM. This data suggested a partial inhibition mechanism mediated via

its interaction with the enzyme−substrate complex. Additionally, **42** did not reduce p21

expression in HeLa cells as what was observed in H1299 and HEK293T cells. The other set of

CARM1 inhibitors was reported by Cheng, et al. [198]. Compound **43** had IC$_{50}$ values of 8.6 μM

for CARM1, and had low or no inhibition on a panel of PRMTs (PRMT1, 3, 5 and 6) and

PKMTs (SET7, DOTL1, Suv39H1, and G9a). In human prostate cancer cells, compound **43**

showed a significant dose-dependent reduction of the PSA promoter activity. Although this set of

CARM inhibitors had significantly increased cellular activity and better selectivity profiling, the

potency was not as satisfying as the pyrazoles.
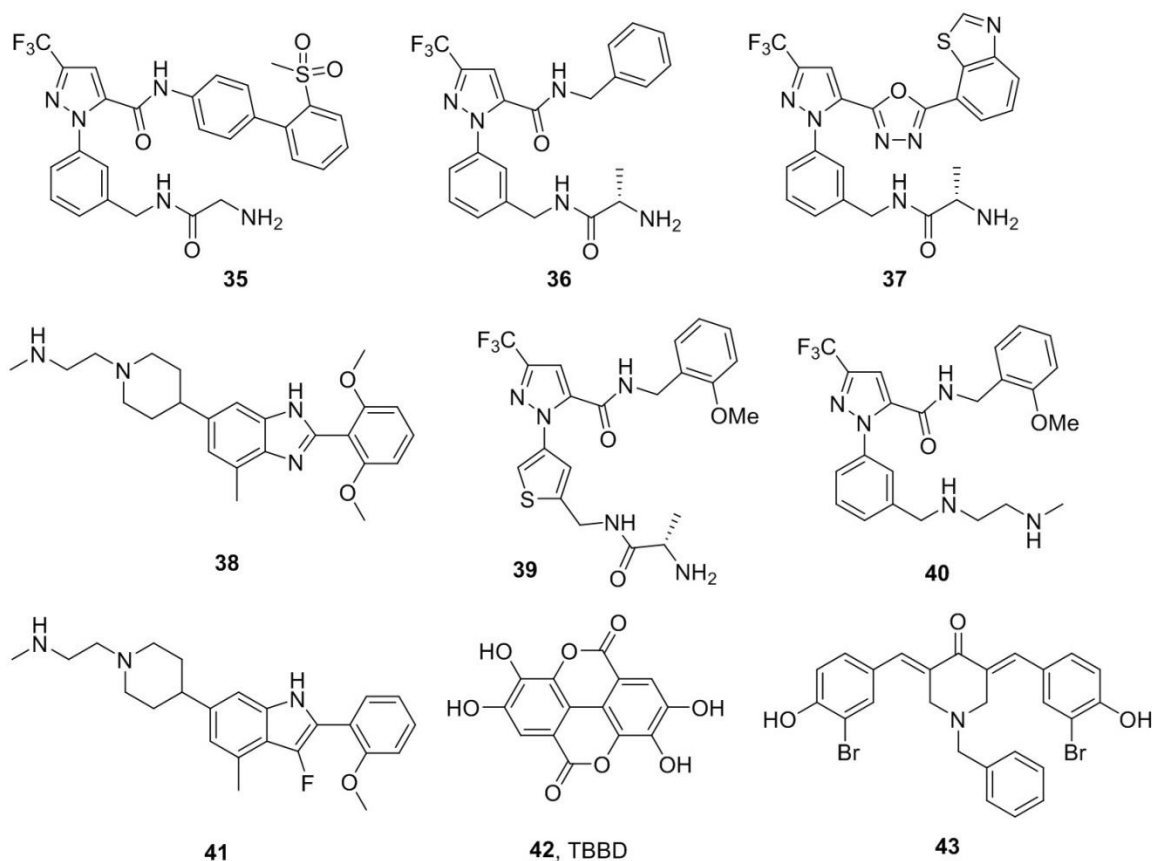
Figure 1.9. Selected CARM1 inhibitors.

1.6.6 PRMT5 inhibitors

Even though PRMT5 is the major type II enzyme and also an important therapeutic target, very few inhibitors are known for PRMT5. Very recently, Alinari, et al. [199] reported compound **44** (**Figure 1.10**, CPD5) as a first-in-class, small molecule PRMT5 inhibitor that blocked initiation and maintenance of B lymphocyte transformation. It was identified via structure-based screening based on a human PRMT5 catalytic site model, which is generated from rat PRMT1 crystal structure (PDB: 1OR8). After screening against the ChemBridge CNS-Set™ library (10,000 small molecule compounds), they further docked the hits and selected the top 8 compounds that had the lowest binding energy for further characterization. A cell-based immunofluorescence assay showed that **44** selectively blocked symmetric dimethylation on H4R3 by inhibiting PRMT5 activity, while others had no effect on H4R3 methylation. Compound **44** did not affect asymmetric methylation of H4R3, and was found to be inactive against PRMT1, CARM1 and PRMT7. Cytotoxicity studies suggested that **44** was selectively toxic to lymphoma cells but not as toxic to normal resting B lymphocytes. The other PRMT5 inhibitor, compound **45** (**Figure 1.10**, EPZ015666), was disclosed by Epizyme, Inc. It was claimed to have a cell biochemical K_i of 8 nM, and > 20, 000-fold K_i of other PMTs. Compound **45** was tested in both *in vitro* and *in vivo* models of mantle cell lymphoma, showing methyl mark inhibition and tumor suppression.
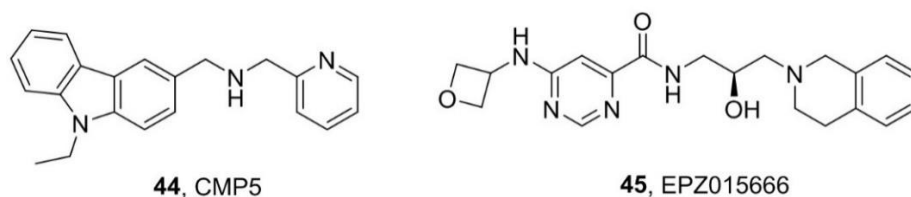
Figure 1.10. Selected PRMT5 inhibitors.

1.6.7 Peptide inhibitors

There are more than fifty peptides or peptide-based therapeutics and diagnostic agents that have been approved by FDA[200]. There has been an increasing amount of studies conducted on peptide inhibitors both for probe design purposes or therapeutic uses. Osborne, et al. [201] reported an *in situ* synthesis strategy of a bisubstrate peptide inhibitor for PRMT1 (**Figure 1.11**). The peptide inhibitor **47** were generated through PRMT1-mediated transfer using a SAM analogue compound **46** (**Figure 1.11**, AAI), which was found to have an IC_{50} value of 18.5 µM. This study indicated that a chemoenzymatic generation of bisubstrate inhibitors was plausible for PRMTs, although the selectivity and cellular activity data was not available. The same group has reported the other PRMT1 peptide inhibitors based on the N terminus of histone H4 incorporating fluoro- and chloroacetamidine warheads (**Figure 1.11**, **48**: C21 and **49**: F21)[202]. Peptide **48** had an IC_{50} value of 1.8 µM for PRMT1, while IC_{50} value of **49** was 94 µM. Peptide **48** was 4.9- fold more selective for PRMT1 compared to PRMT6, and was mostly inactive for PRMT3 and CARM1. These peptides were irreversible inhibitors that could form covalent bond to PRMT1 through a S_N2 attack, and were also proven to selectively inhibit PRMT1 activity in cells.
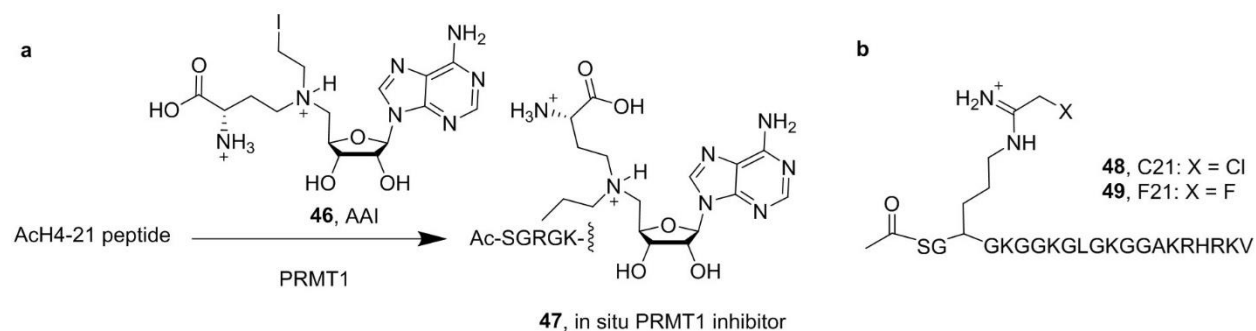
Figure 1.11. Bisubstrate peptide inhibitors. a. In situ generation of a bisubstrate peptide inhibitor. b. Selected bisubstrate peptide inhibitors.

Frankel *et al.* have done a series of studies on the development of peptide inhibitors for PRMTs. The first ones reported were N^η-substituted arginyl peptides **50-53** (**Figure 1.12**, R1-1 to R1-4)[203]. Their IC_{50} values ranged from 4.82 µM to 14.2 µM for PRMT6, and from 27.5 µM to 56.5 µM for PRMT1. The IC_{50} values of these peptide inhibitors were 2.5- to 5- fold lower than the methylation product R1-aDMA. The same group Thomas, et al. [204] synthesized a series of R1 peptides bearing various N^η-substitutions, and described the preferences of PRMTs for those modified peptide substrate-inhibitors. Peptide **54** and **55** (**Figure 1.12**, **54:** R1-can and **55**: R1-NO$_2$) could not be methylated and had micromolar level potency for PRMT1, 4 and 6 (for PRMT1, **54**: $IC_{50} = 30.4$ µM, **55** $IC_{50} = 26.0$ µM). Subsequently, t Hart, et al. [205] reported partial bisubstrate R1 peptide inhibitor **56** (**Figure 1.12**, R1-Orn, PRMT6 $IC_{50} = 36.7$ µM, not active for PRMT1 and 4) and **57** (**Figure 1.12**, R1-Lys, PRMT1 $IC_{50} = 13.9$ µM, PRMT4 $IC_{50} = 35.7$ µM, PRMT6 $IC_{50} = 29.0$ µM), suggesting a six-carbon linker might better mimic the transition state model proposed for PRMT catalytic mechanism. They also pursued a similar approach and synthesized HIV-Tat$_{48-60}$ peptide analogues (**Figure 1.12**, **58**) as potent PRMT substrate-inhibitors, which have 1.31 µM to 11.9 µM K_i values for PRMT1 and 19.9 µM to 77.3 µM K_i values for PRMT6[206].

Therapeutic peptides have great potential as anticancer agents, because they can easily achieve target specificity through rational design. Currently, the modification of PRMT peptide inhibitors are mainly focused on the substrate arginine residues. Since many PRMTs share the same substrates, isoform specific inhibition may rely on the structural differences in PRMT substrate binding sites. One limitation of peptide inhibitors is their low stability *in vivo* and poor membrane penetration.

R1 peptide: NH$_2$-WGGYS-**R**-GGYGGW-OH

50, R1-1   **51**, R1-2   **52**, R1-3   **53**, R1-4   **54**, R1-can: X = O, R = H   **56**, R1-Orn: n = 1
                                                                55, R1-NO$_2$: X = C, R = NO$_2$ **57**, R1-Lys: n = 2
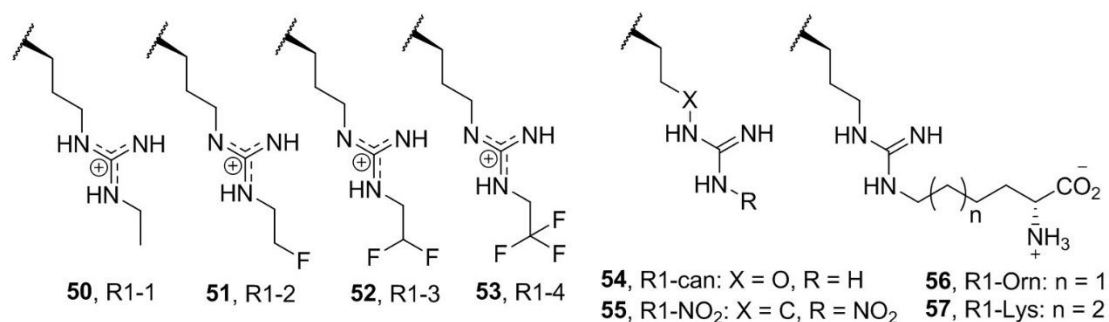
HIV-Tat analogues, **58**:

or R52A mutation
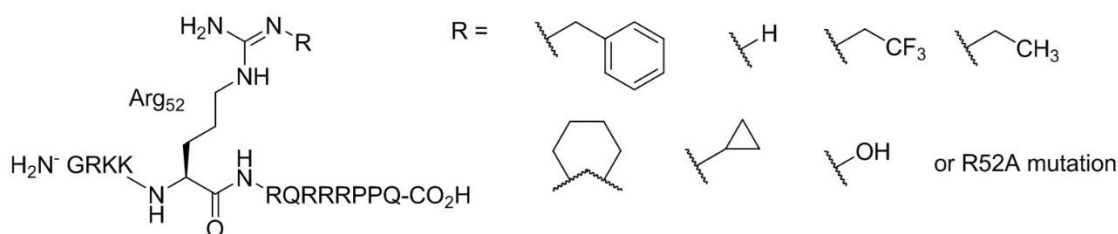
Figure 1.12. Other peptide inhibitors.

1.7 Conclusions

In this chapter, we summarized the current development of PRMT inhibitor discovery to advocate their importance in advancing the field of epigenetic research and clinical application. Inhibitors of PRMTs have drawn plenty of attention by researchers in the field of drug discovery, and so far, marvelous progress has been made. Quite a few potent, isoform-selective, cell permeable small molecule inhibitors were discovered for different PRMTs, such as furamdine for PRMT1 (**Figure 1.7**, **20**), SGC707 for PRMT3 (**Figure 1.8**, **32**), and EPZ015666 for PRMT5 (**Figure 1.10, 45**). Here we conclude some perspectives on the progress and remaining challenges in this field.

First, application of virtual screening approaches has made notable contributions to advance the field of PRMT inhibitor discovery. The combination of virtual screening with target-based biochemical screening has greatly expanded the scale of inhibitor search. For example, the

identification of PRMT1 inhibitors allantodapsone and stilbamidine (**Figure 1.7**) via a target-based virtual screening approach was reported[145]. In another example, a fragment-based method was used to identify RM65 for PRMT1 inhibition[140]. Additionally, based on the known structure of PRMT1 inhibitors, a pharmacophore-based strategy was conducted to identify A9 and A36[160]. Compared to biochemical screening against the large number of compounds in a library, it is more cost-efficient to first use a rational virtual screening to help prioritize the most plausible inhibitor candidates.

Second, structure-guided design is rather beneficial in the lead optimization process. A typical medicinal chemistry strategy is to perform systematic chemical modifications on the lead compound to provide a detailed picture of structure-activity relationship (SAR), based on the hypothesis that subtle changes around the pharmacophore will not change the inhibitor binding site on the target protein. One limitation of this method is that a large amount of organic synthesis is required to gather sufficient information on SAR. When there is a lack of knowledge on binding interactions, the chemical modifications become a "blind" search, which can easily cost a lot of time and effort before valuable conclusions can be made. It can be helpful if co-crystal structures of lead compound with the target protein can be obtained. For example, in the discovery of PRMT5 inhibitor EPZ105666, a structure-directed SAR was conducted to develop compounds with improved ADME profile[181]. In the case when inhibitor-target cocrystal structures are not available, molecular docking was exploited as guidance for chemical modification, such as the discovery of PRMT1 inhibitor **10** by Ragno *et al* [191].

Third, reported results of PRMT inhibitors should be critically interpreted. The frequently used metric for potency is IC_{50}, however, it is possible to have inconsistency in IC_{50} values of the same inhibitor resulted from different assay methods and (or) assay conditions. For example, the

IC_{50} values of AMI1 are reported in a range from 1.2 μM to 376 μM. IC_{50} of an inhibitor can change in different manners as the concentration of substrate increases: it increases for competitive inhibitors, decreases for uncompetitive inhibitor, and remains unaffected for classic noncompetitive inhibitors. The inhibition constant (Ki) or binding affinity constant (Kd) is a more stable metric in potency because it is independent of substrate concentration. However, it is not necessary to measure the intrinsic binding constant for all the initial hits, which is much more laborious to obtain than the IC_{50} values. Practically, it is recommended to include a well-characterized inhibitor control in any assay for new inhibitor identification, to avoid misinterpretation of the results. Additionally, not all the reported inhibitors are sufficiently characterized, some common pitfalls include: incomplete selectivity profile, lack of binding analysis and mode of action, and missing *in cellulo* or *in vivo* studies. Caution should be taken for such missing information before the inhibitors are to be used in further studies.

From the current development of this field, apparently PRMT inhibitors with potencies at nanomolar or lower are still in need. Even though a few patents were newly filed for potent PRMT inhibitors, including PRMT1, CARM1 and PRMT5 inhibitors[207-210], for most of the PRMT inhibitors, gaps exist for the PRMT inhibitors to translate into clinical investigation. The other obstacle is lack of selective inhibitors for all the PRMT members. Great efforts have been devoted to inhibitors for PRMT1, -3, -4 and -5, yet none for PRMT2, -7, -8 and -9. It might partially due to the limited understanding of these enzymes compare to other PRMTs. To conclude, with the rapid development in the field of PRMT inhibitor discovery, we are quite optimistic to expect potent, isoform-selective, *in vivo*-active, pharmacokinetically amenable PRMT inhibitors to be applied in translational and clinical research, and ultimately benefit human well-being in years to come.

1.8 Rationale and Goal of This Work

Growing amount of evidence have suggested that PRMTs are promising protein target in many diseases. These enzymes play essential roles in biology and have intimate association with many pathological conditions, notably cancers. The nine mammalian PRMT isoforms have different roles in various diseases, many of which are not fully understood. Therefore, besides their potential use as therapeutic agents, PRMT inhibitors are ideal chemical tools to dissect the underlying mechanisms of PRMT-dysregulation associated diseases. Tremendous efforts have been invested in the discovery of PRMT inhibitor. However, many of the reported inhibitors have limited application to other researchers because of the incomplete evaluation in isoform-selectivity, mechanism of inhibition or/and cellular activity. Challenges remain in the generation of potent and isoform-selective PRMT inhibitors for translational and clinical research. Moreover, the existing assays for PRMT activity measurement have certain disadvantages, such as cannot achieve continuous measurement, generation of radioactive waste, or complication of the results due to other enzymes and reagents introduced to the assay. Therefore, novel assay methods are needed to further promote PRMT inhibitor discovery.

We set out to test the hypothesis that PRMT inhibitors are potential therapeutic drugs and useful chemical probes for cancers, and to address the remaining challenges in the field of PRMT drug discovery. This work is aimed at discovering novel chemical entities for potent and isoform-selective inhibition of PRMTs in cancers, focusing on the identification and evaluation of small molecule inhibitors for PRMT1 and PRMT5; and also, this work is aimed to develop novel assays for PRMT inhibitor characterization.

CHAPTER 2

DISCOVERY OF DIAMIDINE COMPOUNDS AS ISOFORM-SELECTIVE INHIBITORS

FOR PRMT1

2.1 Introduction

PRMT1 is the predominant mammalian type I enzyme responsible for more than 50% of the asymmetric arginine methylation in mammalian cells[211]. The crystal structures of the PRMTs (PRMT1, PRMT3, CARM1, PRMT5, PRMT6, PRMT7 and PRMT8) revealed a two-domain architecture (**Figure 1.1 and 1.2**): a conserved SAM binding domain and a barrel-like domain, while the active site situated between these two domains[26]. Given that the amino acid sequences of the SAM binding region in PRMTs are mainly identical, substrate protein binding likely plays a key role in the selective methylation. It is not surprising that SAM mimics such as methylthioadenosine and sinefungin are pan inhibitors for all PRMT members. The possibility for PRMT inhibitors to accomplish isoform-selectivity remains in interfering or exploring the interactions of critical amino acid residues within the substrate binding site.

According to our reviews on the reported PRMT1 inhibitors, stilbamidine (**Figure 2.1**) has drawn our attention due to the resemblance of the amidine group to the guanidine group in substrate arginine residue. This compound was reported as a PRMT1 inhibitor with micromolar potency[145], but no follow up studies exploring its structure activity relationship with PRMT inhibition. Stilbamidine represents a group of compounds named diamidines, and their uses as therapeutic agents are previously known. For example, stilbamidine was widely studied as an antifungal agent to treat blastomycosis[212-213] and as an antiparasitic agent to treat Kala-Azar[214].

Furamidine (**Figure 2.1**) is a potent antiparasitic agent shown concentrate in the cell nucleus and delay parasite maturation[215-218]. It is also antimicrobial due to its ability to disrupt mitochondrial membranes[219-220]. Pentamidine (**Figure 2.1**) was reported to be a DNA binder and has been clinically used as an antiparasitic drug in a similar manner to furamidine[217, 221]. Despite such wide applicability, their mode of action as PRMT inhibitors has not been identified.

Based on the inhibitory activity of stilbamidine on PRMT1[145] and the structure similarity of the amidine group to guanidine, we proposed that diamidine structures possess important pharmacophore as PRMT inhibitors. This chapter describes the discovery, development and evaluation of diamidine-type compounds as potent and PRMT1-selective inhibitors, using a combinatorial and comprehensive strategy including biochemical characterization, molecular modeling and cellular activity assessment. The results suggest that diamidines target the catalytic pocket of PRMT1 to inhibit its enzymatic activity. Our cellular studies showed that these compounds were cell permeable and inhibited PRMT1 activity in various cancer cell lines to cause anticancer effects[150].
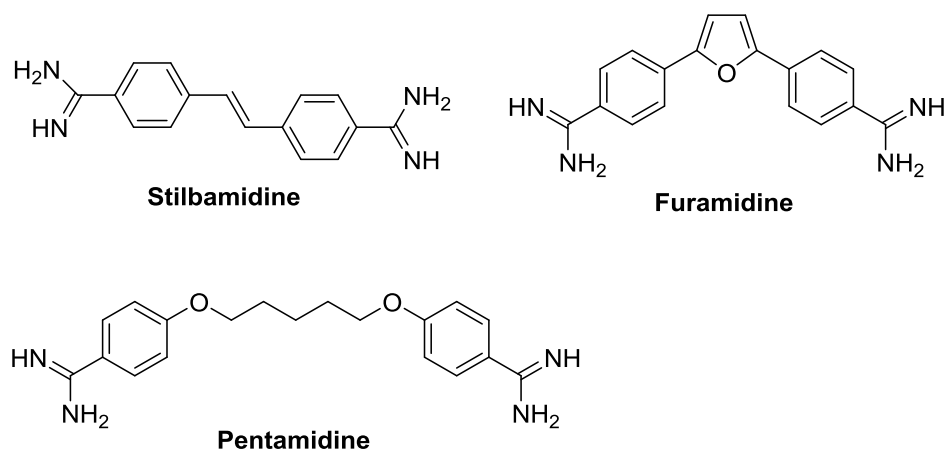
Figure 2.1 Reported diamidine drugs

2.2 Materials and Methods

2.2.1 Protein expression of recombinant methyltransferases.

Recombinant His-tagged rat PRMT1, PRMT3, PRMT8 and G9a were expressed in E. coli. In brief, the corresponding pET28b plasmid was transformed into BL21(DE3) (Stratagene) by heat shock method. Transformed bacteria were incubated in LB media at 37°C for growth and then at 16 °C for protein expression with 0.3 mM IPTG induction. Cells were harvested by centrifuge and lysed by microfluidics cell disrupter. The supernatant containing target protein was loaded onto the Ni-charged His6x-tag binding resin (Novagen) in equilibrium buffer (25 mM Na-HEPES, pH 7.0, 300 mM NaCl, 1 mM PMSF, 10% glycerol (v/v) and 30 mM imidazole). Beads were washed thoroughly by washing buffer (25 mM Na-HEPES, pH 7.0, 300 mM NaCl, 1 mM PMSF, 10% glycerol (v/v) and 70 mM imidazole), and protein was eluted with elution buffer (25 mM Na-HEPES, pH 7.0, 300 mM NaCl, 1 mM PMSF, 100 mM EDTA, 10% glycerol (v/v) and 200 mM imidazole). Recombinant GST tagged CARM1 and PRMT7 on pGEX2T or 4T plasmid were expressed in E. coli. The supernatant containing target protein was loaded onto the Glutathione Sepharose 4B resin (GE Healthcare) in column buffer (25 mM Na-HEPES, pH 7.0, 250 mM NaCl, 1 mm EDTA, 1 mM PMSF, and 0.1% (v/v) Triton x100). Beads were washed thoroughly on a column, and protein was eluted with elution buffer (50 mM Na-HEPES, pH 7.0, 10 mM reduced glutathione and 1 mM PMSF). All the eluted protein solutions were dialyzed into buffer containing 25 mM Na-HEPES, pH 7.0, 300 mM NaCl, 10% glycerol (v/v) and 1 mM DTT. Protein purity were checked by 12% SDS-PAGE, and concentration was determined by Bradford assay[222].

2.2.2 Peptide synthesis

All peptide substrates were synthesized using Fmoc [N-(9- fluorenyl) methoxycarbonyl]-based peptide synthesis protocol on a FOCUS XC peptide synthesizer (aapptec, Louisville, KY). The peptide sequences are as following: H4-20-biotin Ac-SGRGKGGKGLGKGGAKRHRK(biotin), Biotin-H3-20 Biotin-ARTKQTARKSTGGKAPRKQL, SMD1-biotin Ac-AGRGRGRGRGRGRG-biotin. Each amino acid was coupled to the solid phase with 4 equiv of amino acid/HCTU [O-(1H-6-chlorobenzotriazole-1-yl)-1,1,3,3- tetramethyluronium hexafluorophosphate] (Novabiochem or Chempep). The Fmoc group was deprotected with 20% v/v piperidine/DMF, and the N-terminal amino acid was acetylated with acetic anhydride. The peptide was cleaved from the Wang resin by a cleavage solution consisting of 95% trifluoroacetic acid (TFA), 2.5% H_2O, and 2.5% triisopropylsilane. It was then precipitated in cold ether and pelleted by centrifugation. Crude peptides were collected and purified using a Shimadzu liquid chromatography instrument equipped with a C18 reversed-phase high performance liquid chromatography (RP-HPLC) column, where 0.05% TFA containing water and 0.05% TFA-containing acetonitrile were two mobile phases used in gradient purification. The identity of peptides was confirmed with MALDI-MS.

2.2.3 Purchased materials

The PRMT5:MEP50 complex (part number: HMT-22-148) was purchased from Reaction Biology Corp. Cofactor ^{3}H-SAM was purchased from Perkin Elmer (part number: NET155V001MC). DOT1L (part number: HMT-11-101) and nucleosomes (part number: HMT-35-123) were purchased from Reaction Biology Corp. Histone H3.3 was purchased form New England Biolabs (part number: M2507S).

2.2.4 Compound sources

The diamidine compounds were provided by Dr. David Boykin's group at Georgia State University, with >95% purity based on CHN elemental analysis, ^{1}H and ^{13}C NMR, and mass spectrometry. Diamidine analogs with link variations were synthesized by Dr. Jing Zhang, with >95% purity based on ^{1}H NMR, ^{13}C NMR, analytical HPLC and mass spectrometry. The compound library for the high throughput screening were ordered from National Cancer Institute DTP program.

2.2.5 High throughput screening (HTS) of small molecule libraries.

The HTS by scintillation proximity assay (SPA) method was performed on a 96-well plate format as previously described[171]. This assay format has a Z value of 0.65 and a Z′ value of 0.80. Screening compounds were kept at 10 µM and 100 µM in the assay. The DMSO solution of the inhibitors were at 10 or 20 mM, then diluted with ddH$_2$O to 50 or 500 µM. Diluted inhibitor solutions (3 µL) were incubated with 9 µL mixture containing H4-20-Biotin peptide, [^{3}H]-SAM and 2X reaction buffer, then the enzyme (3 µL) was added to initiate the reaction. The reaction buffer contains 50 mM HEPES, 10 mM NaCl, 0.5 mM EDTA, 0.5 mM dithiothreitol (DTT) at pH 8.0. The final concentrations of the enzyme, ^{3}H-SAM, and H4-20-Biotin are 0.02, 0.5, and 1 µM, respectively. The concentrations of [^{3}H]-SAM, and biotinylated H4 peptide in the assay were kept at balanced condition ($\approx$ Km) to indiscriminately identify competitive, uncompetitive and noncompetitive inhibitors. The mixtures were incubated at room temperature for 8 min before it was quenched with 15 µL isopropanol. After mixing with 5 µL of 20 mg/mL streptavidin-coated SPA beads, the plates were incubated in dark for 30 min, and detected by a Microbeta2 scintillation counter (Perkin Elmer). The positive control was carried out with the

corresponding DMSO dilute surrogate, and the background control only contained ^{3}H-SAM, H4-20-biotin peptide and DMSO. The reported data was based on the average of two experiments.

2.2.6 Biochemical selectivity assay

The single point screening and IC$_{50}$ values of inhibitor hits over a panel of methyltransferases were determined. The reaction condition for each enzyme is listed in the following table (**Table 2.1**). The reaction conditions for different enzymes were kept close to the balanced assay condition and the reaction time was controlled under initial rate conditions for reaction yields of less than 10%. The reaction buffer contains 50 mM HEPES pH 8.0, 10 mM NaCl, 0.5 mM EDTA, and 0.5 mM DTT for all the PRMTs. The reaction buffer contains Tris 50 mM pH 9.0, 5 mM MgCl$_2$, 4 mM DTT for all the lysine methyltransferases (G9a and DOT1L). The inhibitor solutions were made at 10 µM for single point screening or as a series of dilution for IC$_{50}$ determination. For the methylation reaction using biotinylated peptides, the procedure was similar to the SPA method described above. The methylation reaction using protein substrates was carried out by radioactive filter plate assay in a 96-well format. Protein substrate and [3H]-SAM were preincubated in the reaction buffer for 2 min prior to initiation of the methyl transfer reaction by adding the enzyme (30 µL total volume). The reaction was quenched by 10 µL of 30% TCA, followed by spotting the reaction mixture on a 96-well 0.2 µm filter plate (Multiscreen filter plates, Millipore cat. Number: MSFBN6B10). Then 40 µL of 10% TCA was added for protein precipitation and the plate was incubated at 4 °C for 20 min. After the plates were washed with 100 µL of 10% TCA for 4 times and 100 µL of 100% ethanol once, they were immersed in 50 µL of liquid scintillation mixture (Microscint PS, PerkinElmer). Scintillation counting was performed by a Microbeta2 to measure the amount of methylated product. The positive control was carried out with the corresponding DMSO dilute surrogate under the same

condition, and the background control only contained [3H]-SAM, protein substrate and DMSO. IC_{50} values were obtained by quantification of formed product at various concentrations of inhibitors, and fit with equation 1. Relative activity of protein in presence of the inhibitor was normalized to the value of product formation without inhibitor present, n is hill coefficient. The reported data was based on the average of two experiments.

$Relative\ Activity =\ 1/(1 + ([Inhibitor]/IC50)^{n})$ (1)

Table 2.1 Conditions for selectivity profiling

Protein	Substrate	Cofactor	Reaction time
PRMT1, 20 nM	H4-20-biotin, 1 uM	SAM, 0.5 uM	8 min, RT
PRMT3, 20 nM	SMD1-biotin, 1 uM	SAM, 0.5 uM	10 min, RT
CARM1, 20 nM	H3.3 protein, 0.4 uM	SAM, 0.5 uM	120 min, RT
PRMT5, 20 nM	H4-20-biotin, 1 uM	SAM, 0.5 uM	8 min, RT
PRMT6, 40 nM	SMD1-biotin, 1 uM	SAM, 0.5 uM	30 min, RT
PRMT7, 40 nM	SMD1-biotin, 1 uM	SAM, 0.5 uM	120 min, RT
PRMT8, 20 nM	H4-20-biotin, 1 uM	SAM, 0.5 uM	8 min, RT
G9a, 20 nM	Biotin-H3-20, 1 uM	SAM, 0.5 uM	30 min, RT
DOT1L, 20 nM	Nucleosomes, 0.3 uM	SAM, 0.5 uM	45 min

2.2.7 Enzyme kinetics assays for mechanism of inhibition determination

Enzyme kinetics measurement by filter binding assay: filter binding assay was carried out in 0.65 mL plastic tubes with a 30 µL reaction volume at 30 °C. The reaction buffer, reagent and enzymes were used as the same as a SPA format described in **2.2.5**. Typically, 6 µL of varied concentrations of each candidate inhibitor was added to the 18 µL of mixture composed of [^{3}H]SAM and one of the PRMTs in reaction buffer. The 24 µL mixture was incubated at room temperature for 5 min before the reaction was initiated by adding 6 µL of H4−20 in distilled water. Reactions without candidate inhibitor were used as positive control. Reactions with neither H4(1−20) nor candidate inhibitor was used as negative control. After incubation, 20 µL of the reaction mixture was aspirated and spread onto anionic P81 filter paper disks (Whatman)

to quench the reaction, and the disks were dried in air for 2 h and washed with 600 mL of 50 mM NaHCO$_3$ (pH 9.0) solution for 15 min three times. Then the disks were dried in air overnight before being transferred into 3.5 mL vials full of scintillation oil, and the amount of the product was quantified by a scintillation counter (Beckman Coulter, Brea, CA) or a MicroBeta2 (PerkinElmer) as CPM. CPM readouts were converted to rate of the reaction based on the readout of total ^{3}HSAM added divided by incubation time. The Kcat and Km of PRMT1 for H4(1−20) was obtained by measuring the initial velocity of reaction at different concentrations of H4(1−20) and fitting the kinetic data with Michaelis−Menten equation.

Enzyme kinetics measurement by SPA: experimental conditions for the SAM or peptide competitions in a 30-μL total volume in 96-well format were similar to those for the IC$_{50}$ experiments. The K280 concentration was a 5,000, 1,250 and 312.5 nM. ^{3}H-SAM was serially diluted two-fold in assay buffer for a seven-point dilution series with a top concentration of 4 μM. Reactions were initiated by the addition of 20 nM enzyme and 1 μM peptide. For the peptide titration assay, H4-20-biotin was serially diluted two-fold in assay buffer for a seven-point dilution series with a top concentration of 4 μM. Reactions were initiated by the addition of 20 nM enzyme and 0.5 μM ^{3}H-SAM. Reactions were incubated at room temperature for 60 min, and then quenched by the addition of 30 μL per well of isopropanol. CPM signals were converted to rate according to a calibration curve.

K$_i$ and αK$_i$ were calculated using the noncompetitive inhibition model by equation 2:

$$\frac{[P]}{t} = \frac{V_{max}[S]}{K_m(1+[I]/Ki)+[S](1+[I]/\alpha K_i)} \tag{2}$$

Where: [P] = product concentration, [S] = substrate concentration, [I] = inhibitor concentration, V$_{max}$ = maximum velocity, K$_m$ = Michaelis constant, K$_i$ = inhibitor constant for binding to enzyme, and αK$_i$ = inhibitor constant for binding to enzyme-substrate complex.

Stopped flow assay: experimental detailed are described in **Chapter 3.2**.

2.2.8 Molecular docking

Docking was carried out with Discovery Studio 4.0. A previously described PRMT1 homology model[150] was used as the receptor model for docking of furamidine and decamidine. The docking boxes were identified through the cavities of the protein structure in Discovery Studio 4.0. CDOCKER docking module was applied for molecular dynamic enforced optimization. Docking poses were ranked based on CDOCKER energy from the lowest to highest, and the lowest energy confirmation was chosen for binding interaction analysis.

2.3 Furamidine is a Lead PRMT1-Selective Inhibitor

2.3.1 Identification of furamidine as a PRMT-1 selective inhibitor

A single concentration (10 µM) screening assay was performed in Scintillation Proximity Assay (SPA) format to examine the inhibition of a diamidine series (DB compounds from Dr. David Boykin, Georgia State University) on PRMT1 and PRMT5, with PRMT1 representing type I enzyme while PRMT5 representing type II[150]. Among all the compounds tested in the assay, DB75 (also known as furamidine, **Figure 2.1**) stood out due to the selective inhibition toward PRMT1, although it was not the most potent inhibitor for PRMT1 or PRMT5. Dose-dependent assay revealed that the IC_{50} of furamidine was 9.4 ± 1.1 µM for PRMT1, while the IC_{50} values for PRMT5, PRMT6 and CARM1 were 166 ± 2 µM, 283 ± 37 µM and >400 µM, respectively[150].

2.3.2 Mechanism of action studies of furamidine

Steady state kinetic characterization was conducted to elucidate the inhibition mode of furamidine against PRMT1, as described in **2.2.7**. The initial velocities of PRMT1 were

measured at varying concentrations of the inhibitor over a range of substrate H4-20 peptide

concentrations with fixed concentration of the cofactor SAM. Similarly, when the concentration

of H4-20 was fixed, the initial velocities of PRMT1 were measured at varying concentrations of

SAM and inhibitor. The data were plotted in double reciprocal format as shown in **Figure 2.2**. In

H4-20 peptide titration assay, the linear curves were intersected closely in the second quadrant,

indicating that furamidine is primarily competitive to the substrate peptide. In the SAM titration

assay, the intersection is close to the X-axis, supporting a noncompetitive pattern to SAM. These

inhibition patterns suggest that the inhibition of PRMT1 is likely achieved through the

interference of substrate arginine binding in the catalytic pocket of the enzyme.
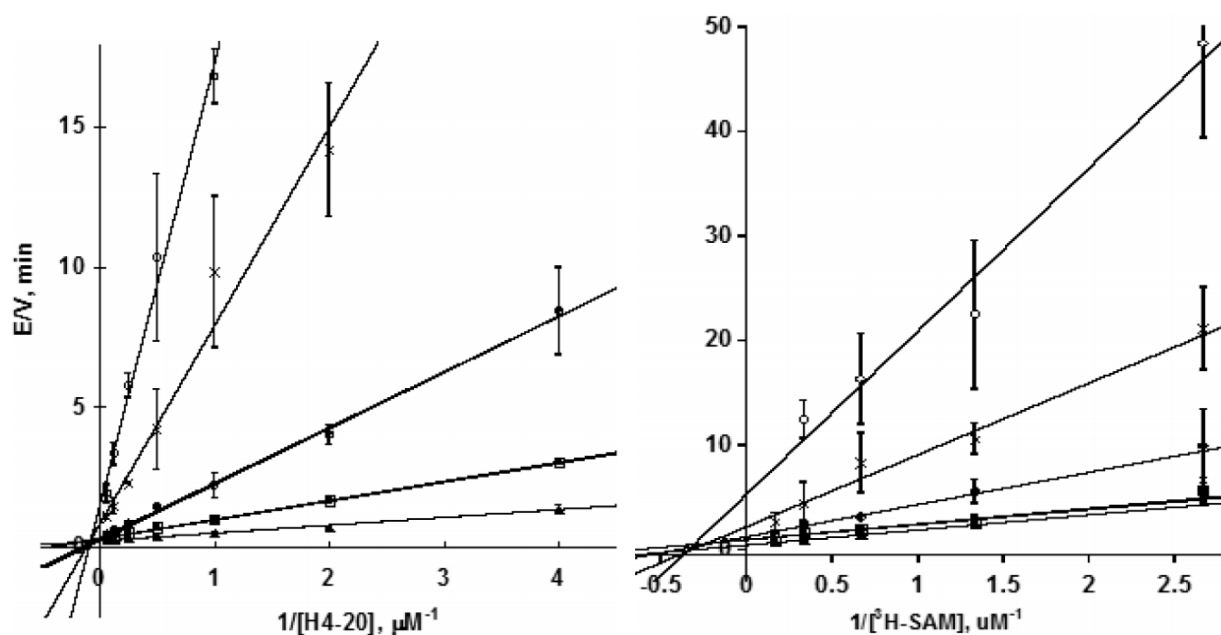
Figure 2.2 Kinetic analysis of PRMT1 inhibition by furamidine. The concentration of
inhibitor was selected at 0 μM (▲), 10 μM (■), 20 μM (●), 30 μM (×), and 40 μM (○). In H4-20
titration assay (left), the concentration of SAM was fixed at 3 μM, and in SAM titration assay
(right), the concentration of H4-20 was fixed at 15 μM.

Molecular docking analysis was performed to better understand the mode of action of furamidine,, in which the SAM-binding site and substrate arginine site was included in the binding cavity (**Figure 2.3**). The amidine groups of furamidine is interacting (via salt bridge) with the acidic residues Glu129, Glu144, and Glu153 of hPRMT1 (**Figure 2.3A** and **B**). One amidine group is binding with Glu144 and Glu153, which are reported to be essential for substrate binding and catalysis. The second amidine group is binding with residue Glu129, which is slightly overlapping the SAM adenine binding. This binding mode can explain why furamidine showed mixed-type inhibition with a substrate-competitive feature. Additionally, extensive molecular dynamics (MD) simulations and molecular mechanics/Poisson−Boltzmann solvent-accessible surface area (MM-PBSA) calculations have shown that the amidine interactions with Glu129 and Glu144 has the most contribution to ligand binding[150] (**Appendix A Figure S2.1**).
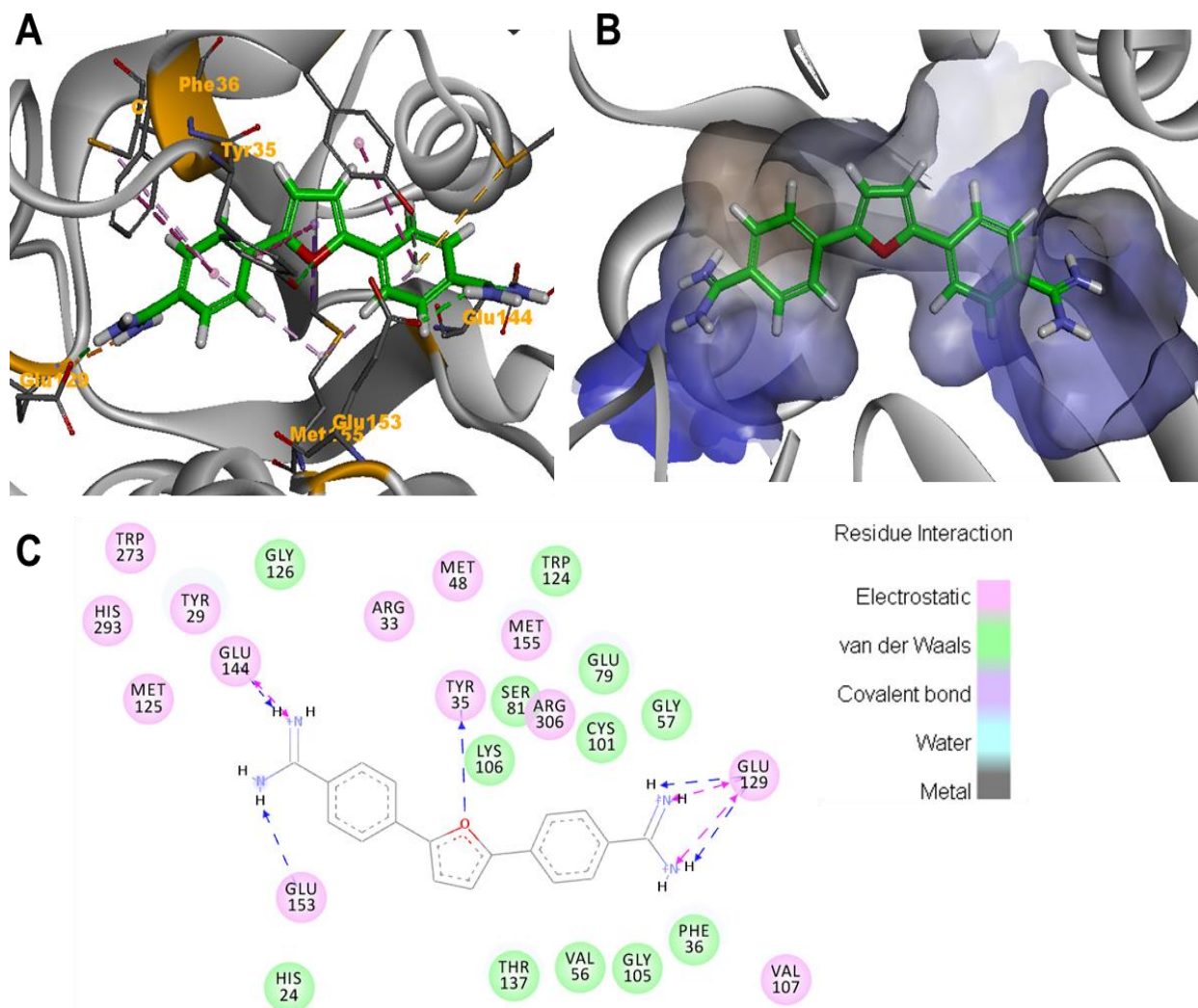
Figure 2.3 Proposed binding pose of furamidine in PRMT1 catalytic cavity. A. Furamidine (green) binding interactions in the catalytic cavity of PRMT1 (grey). Interacting residues of PRMT1 are in orange. **B**. Hydrophobic surface of PRMT1 in furamidine binding site (darker blue is less hydrophobic). **C**. 2D diagram of **A**. The above figures were generated using Discovery Studio 4.0.

2.3.3 Structure activity relationship of diamidines in PRMT inhibition

The original series of diamidines contains 40 compounds (DB compounds from Dr. David Boykin, Georgia State University) with multiple structural variations. Here we summarize the structure activity relationship of the 15 compounds bearing furan and amidine functional groups modifications (**Table 2.3**) in PRMT1 and PRMT5 inhibition. The PRMT1 inhibition of the diamidine compounds is sensitive to alkylation of the terminal amidine moiety. DB242, DB244, and DB249 have alkyl substituents, while DB256 and DB569 have phenyl substituents on the amidine all showed reduced activity. In accordance to the docking analysis, the salt bridges between the two amidines and the two glutamate residues, which contribute most in furamidine binding, is likely disturbed by the hydrophobic substituents (**Figure 2.3A** and **C**). Replacing the oxygen in the furan ring of furamidine with S or Se (DB351 and DB1213A) had minimal effect on PRMT1 inhibition, probably because their similar stereoelectronic properties. However, replacement with alkylated N in DB320A, DB1304, DB2235 and DB2236 caused bigger loss in activity with increasing bulkiness; possibly due to the steric hindrance with the small cavity surrounding that area (**Figure 2.3B**). The SAR of the diamidines for PRMT5 inhibition is quite different from that of PRMT1. The most striking feature is that bulky substitution in the amidine group seems to be preferred, based on the increased inhibitory activity of DB256, DB244 and DB249. This phenomenon may indicate that hydrophobicity is favored in PRMT5 bonding, and possibly a larger size of the molecule can better fit the cavity. Overall, our biochemical data suggest that PRMT5 prefers to bind molecules with higher hydrophobicity and more bulkiness. This difference could explain the selective inhibition of PRMT1 by a smaller and more polar compound like furamidine.

Table 2.2 SAR summary table of furan and amidine derivatives. Compounds were screened at 10 µM concentration. Remaining activity of PRMT1 and PRMT5 (R.A. P1 and R.A. P5) were presented relative to control without inhibitor presence. Results are the average of two experiments.
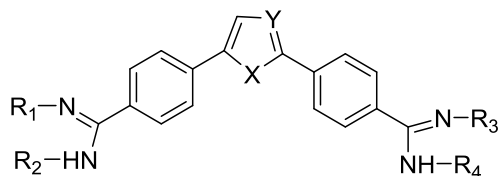
Compound	X	Y	R_1	R_2	R_3	R_4	R.A P1	R.A P5
DB1213A	Se	C	H	H	H	H	0.17	0.38
DB75	O	C	H	H	H	H	0.19	0.66
DB351	S	C	H	H	H	H	0.21	0.61
DB256	O	C	H	(4-methoxyphenyl ethyl)	H	(4-methoxyphenyl ethyl)	0.31	-0.058
DB244	O	C	H	(cyclopentyl)	H	(cyclopentyl)	0.43	0.39
DB1052	N	S	H	H	H	H	0.48	0.78
DB320A	N—	C	H	H	H	H	0.49	0.44
DB690	C	O	H	H	H	H	0.51	0.55
DB417	O	C	H	CH3	H	CH3	0.58	0.51
DB249	O	C	H	(cyclohexyl)	H	(cyclohexyl)	0.59	0.32
DB1304	N—(ethyl)	C	H	H	H	H	0.62	0.72
DB2236	N—(cyclopropyl)	C	H	H	H	H	0.65	0.77
DB2235	N—(phenyl)	C	H	H	H	H	0.70	0.48
DB242	O	C	H	(cyclopropylmethyl)	H	(cyclopropylmethyl)	0.76	0.59
DB569	O	C	H	(phenyl)	H	(phenyl)	0.79	0.75

2.3.4 Inhibitory activity of furamidine in leukemia cells (this work was conducted through collaboration with Hairui Su and Dr. Xinyang Zhao)

PRMT1 is overexpressed in many kinds of tumors, including leukaemia. To verify whether furamidine can inhibit the PRMT1 enzymatic activity in cells, studies were conducted in leukemia cell lines as reported previously[150]. Asymmetric methylated arginine (ASYM24) antibody was used to detect the protein methylation status of GFP-ALY fusion protein in 293T cells. GFP-ALY was immunoprecipitated with GFP antibody, which showed that the level of the methylation was significantly reduced in presence of the 20 μM furamidine (**Appendix A Figure 2.2A**). This result confirmed that the drug is permeable to cell membrane and inhibits cellular PRMT1 activity. The cell viability of leukemia cell lines treated with 20 μM furamidine was examined. The result showed inhibited cell growth for the two leukemia cell lines CHRF and MOLM13 (**Appendix A Figure 2.2B**). These results agree with the expected role of PRMT1 in cell proliferation, and indicated that treatment of furamidine is inhibitory to the leukemia cells. Furamidine was further used as a chemical probe to elucidate the regulatory function of PRMT1 in RNA splicing through methylation of RBM15[223].
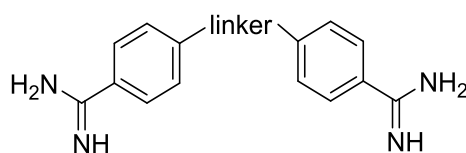
2.4 Discovery of Decamidine as an Improved PRMT1 Inhibitor

2.4.1 Diamidines varying the linker length

The diamidine series (DB compounds from Dr. David Boykin, Georgia State University) of compounds had very limited variation in the linker modifications connecting the two phenylamidine functional groups. In the preliminary structural modification efforts, we found that linker variation in stilbamidine (**Figure 2.1**) was well tolerated, which inspired us to further explore the effect of middle linker lengths on these diamidine compounds. We synthesized amidine analogs with different hydrocarbon linkers between the two benzamidine functional

groups, and purchased pentamidine (Sigma) for this study[224] (**Table 2.4**). The inhibitory activity

of these compounds on PRMT1 and PRMT5 was measured with the scintillation proximity

assay (SPA), using furamidine as a positive control. The IC_{50} values were listed in **Table 2.4**, in

which the most active compound being the 10-carbon linker molecule, decamidine. The

improved potency of decamidine in PRMT1 inhibition was further validated by mass

spectrometric analysis and radiometric gel assay (**Appendix A Figure S2.3**)[224].

Table 2.3 IC_{50} values of diamidines for PRMT1 and PRMT5.

Pentamidine, linker = $-O(CH_2)_5O-$
Hexamidine, linker = $-O(CH_2)_6O-$
Decamidine, linker = $-O(CH_2)_{10}O-$

Compounds	IC_{50}, μM	
	PRMT1	PRMT5
Stilbamidine	52.3 ± 2.3	712.7 ± 161.1
Furamidine	21.6 ± 2.1	256.8 ± 0.8
Pentamidine	81.0 ± 2.7	582.6 ± 100.4
Hexamidine	52.2 ± 3.4	357.3 ± 155.0
Decamidine	12.7 ± 1.0	42.6 ± 0.8

2.4.2 Binding pose analysis of decamidine in PRMT1

To decipher the structural basis for the linker length influence on the enhanced potency of

decamidine, docking analysis was performed (**Figure 2.4**). The results show that the first

amidine group occupies the SAM adenosine site via two hydrogen bonds to the backbone

carbonyl group of Pro24 and Ala26, and a hydrogen bond with the side chain of Glu129. For the

second amidine group, the flexible 10-carbon linker allowed stretching of the amidine into the

SAM methionine binding site. In this orientation, the amidine forms hydrogen bonds with

ASP76 side chain and the backbone carbonyl group of Ser79. The deep placement of the amidine

in the cofactor pocket with multiple interactions accounts for the stronger binding with PRMT1.
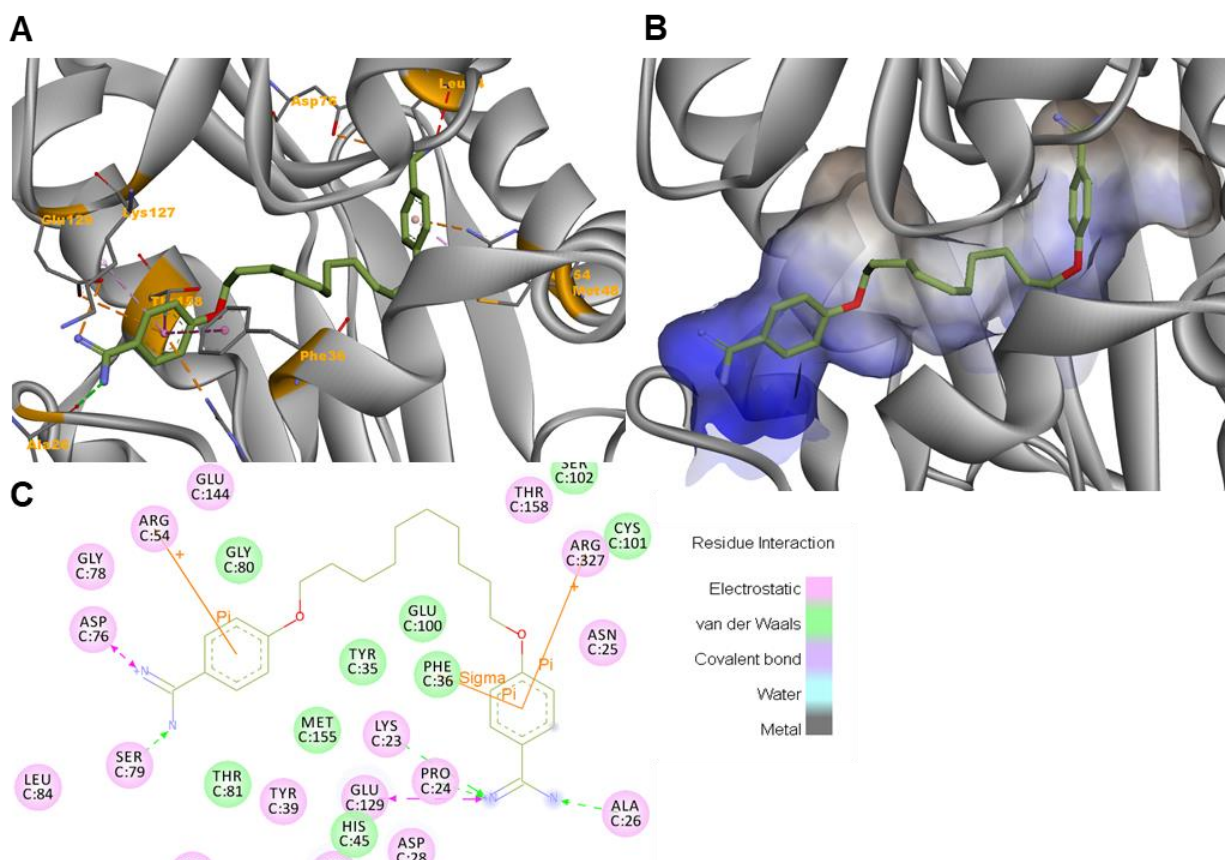
Figure 2.4 Proposed binding pose of decamidine in PRMT1 catalytic cavity. A. Detailed view of decamidine displaying the key PRMT1 residues. Decamidine is shown in green sticks, PRMT1 residues involved in binding are labeled in orange. B. Shape of the binding cavity of PRMT1 (grey) with decamidine (green stick) shown as hydrophobic surface (darker blue is less hydrophobic). C. 2D diagram of A. All figures are generated with Discovery Studio 4.0.

2.5 Discovery of K313 as a Potent PRMT1 Inhibitor

 2.5.1 Identification of K313 through combinatorial high throughput screening

In addition to the chemical modification-based lead optimization approach based on the furamidine structure, a ligand-based virtual screening was applied to gain better diversity of the diamidine moiety from the existing commercial compound libraries. The rigid, crescent and planar structure of the lead PRMT1 inhibitor furamidine was used as a structural template for both charge and shape similarity filtration in the virtual screening (**Appendix A Figure S2.4**). A furamidine structure-derived compound library containing the top 406 hits was generated, sourced from the NCI Diversity Set (total of 260071 compounds). 406 compounds (namely K1 to K406) from this smaller library were subject to a biochemical high throughput screening (HTS) against PRMT1 and PRMT5, using scintillation proximity assay (SPA). Since the IC50 of furamidine is 9.4 µM under the assay condition, a single concentration screening was performed at 10 µM concentration of the compounds. The top 33 compounds inhibited PRMT1 activity to less than 50% at 10 µM were identified as the biochemical screening hits (**Figure 2.5A**), which have better inhibition than furamidine. A parallel screening against PRMT5 (type II PRMT enzyme) was also conducted for preliminary selectivity assessment. Further characterization of these hits led to the lead inhibitor, K313 (**Figure 2.6**). Compound K313 possesses an IC_{50} value of 0.84 ± 0.14 µM, which is >10-fold more potent than furamidine (**Figure 2.6B**). To obtain more structure analogs of K313, we conducted a second-round search on the NCI Diversity Set using the established virtual screening method, based on the structure template of K313. The K313-derived library containing 89 compounds (K415 to K503) were screened at 10 µM and 100 µM, and 14 compounds inhibited PRMT1 activity to less than 50% at 10 µM (**Figure 2.5B**). Selected compounds from the K313-derived library were used for SAR analysis in **2.5.2**.
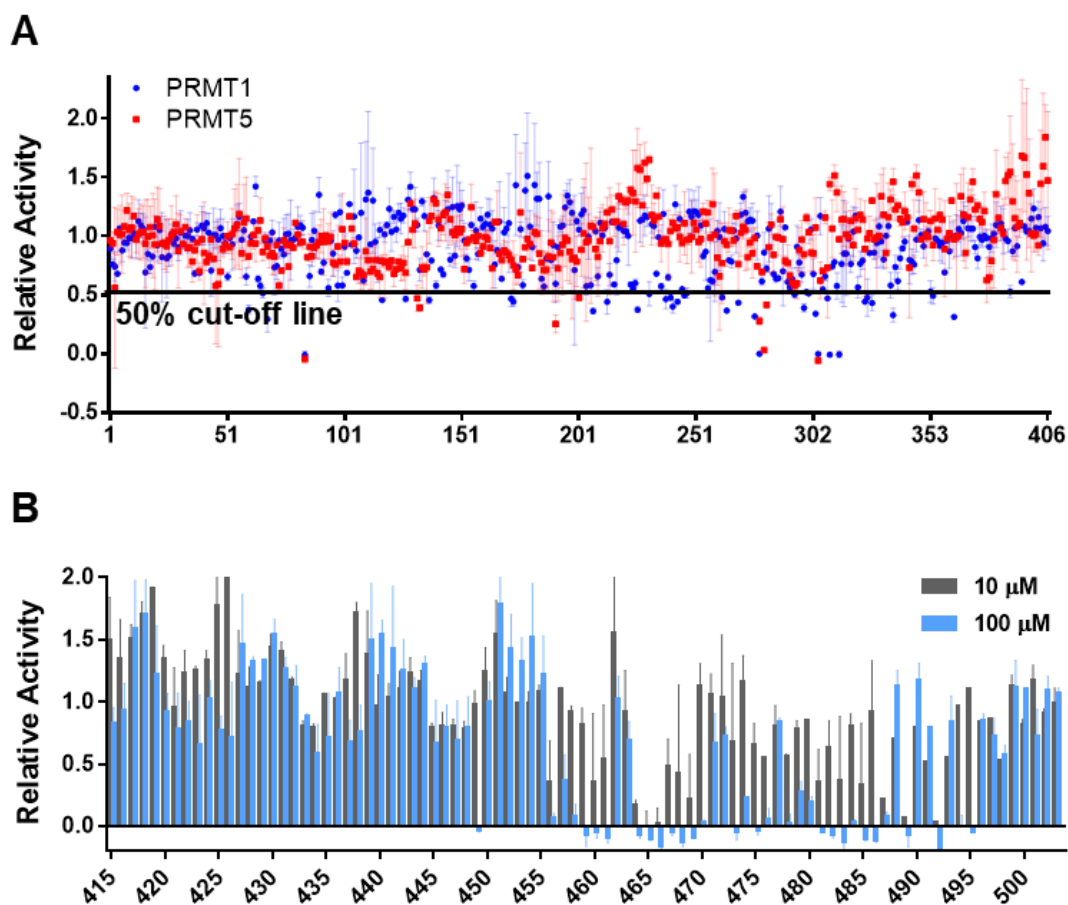
Figure 2.5 Results of high throughput screening on compound libraries. **A**. Single concentration screening result of the furamidine-derived library against PRMT1 (blue) and PRMT5 (red). **B**. Two-concentration (10 μM, grey and 100 μM, blue) screening result of the K313-derived library.
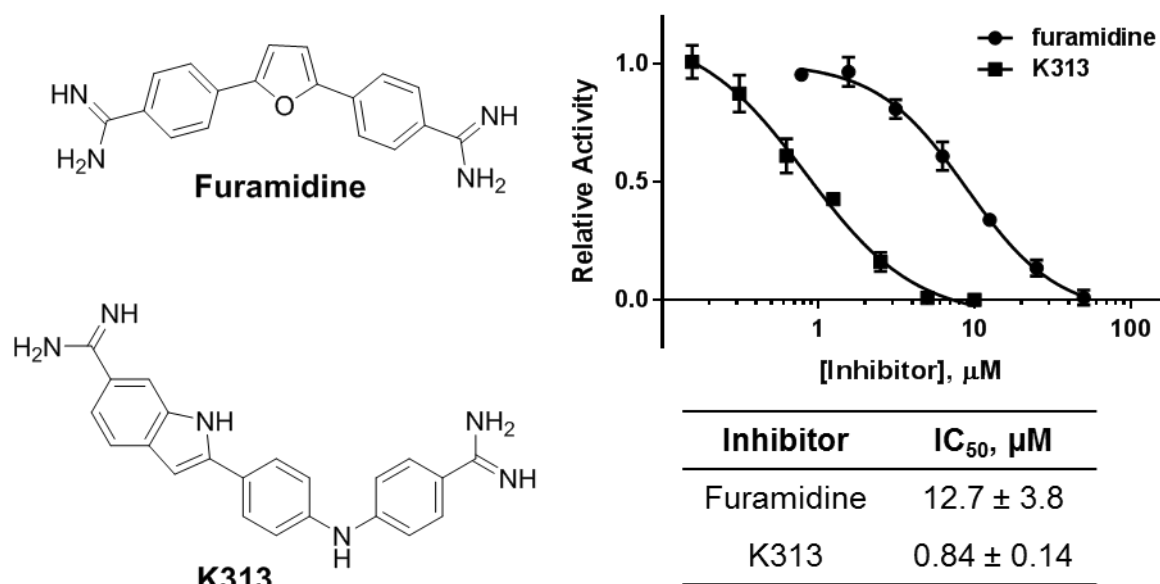
Figure 2.6 Structures, IC$_{50}$ curves and potency comparison of K313 and furamidine.

Furthermore, to obtain the selectivity profile of K313, the inhibition potencies were

determined by SPA using a protein methyltransferase panel containing seven PRMT isoforms

(PRMT1, PRMT3, CARM1, PRMT5:MEP50, PRMT6, PRMT7 and PRMT8) and a lysine

methyltransferase (G9a) (**Figure 2.7**). Single concentration screening at 10 µM of K313 showed

that this compound significantly inhibited the activity of PRMT1, PRMT3 and PRMT8, which

are type I PRMTs (**Figure 2.7A**). The dose-dependent selectivity profile indicates that K313 is a

strong PRMT1 inhibitor with an IC$_{50}$ of 0.84 ± 0.14 µM, which is more potent than it is for the

other methyltransferases in the panel (**Figure 2.7B**). Due to the poor fitting of a three-parameter

logistic equation (Relative Activity= $1/(1+([\text{Inhibitor}]/\text{IC}_{50}))$) to some target enzymes, the four-

parameter logistic equation (Relative Activity= $1/(1+([\text{Inhibitor}]/\text{IC}_{50})^{n})$) was used to derive the

Hill coefficient (n). Hill coefficients may give information on the number of interacting sites, and

the Hill coefficients different from one are proof for multiple ligand binding, possibly inducing

allosteric changes to the target protein. The Hill coefficient of K313 is close to 1 for PRMT1 and

PRMT5, while the values had a large variation among other proteins. This phenomenon

suggested different binding modes of K313 on these protein targets.

A	Relative activity		B		
			Enzyme	IC$_{50}$, μM	Hill
PRMT1			PRMT1	0.84 ± 0.14	1.25 ± 0.14
PRMT3			PRMT3	3.4 ± 0.30	3.9 ± 0.95
CARM1	50.7%		CARM1	27.6 ± 3.5	0.88 ± 0.10
PRMT5	35.1%		PRMT5	6.8 ± 0.77	1.1 ± 0.12
PRMT6	22.9%		PRMT6	2.8 ± 0.06	4.4 ± 0.43
PRMT7	32.1%		PRMT7	23.6 ± 7.2	3.1 ± 0.14
PRMT8			PRMT8	8.2 ± 0.76	1.8 ± 0.29
G9A	10.5%		G9a	3.7 ± 0.16	4.7 ± 0.80
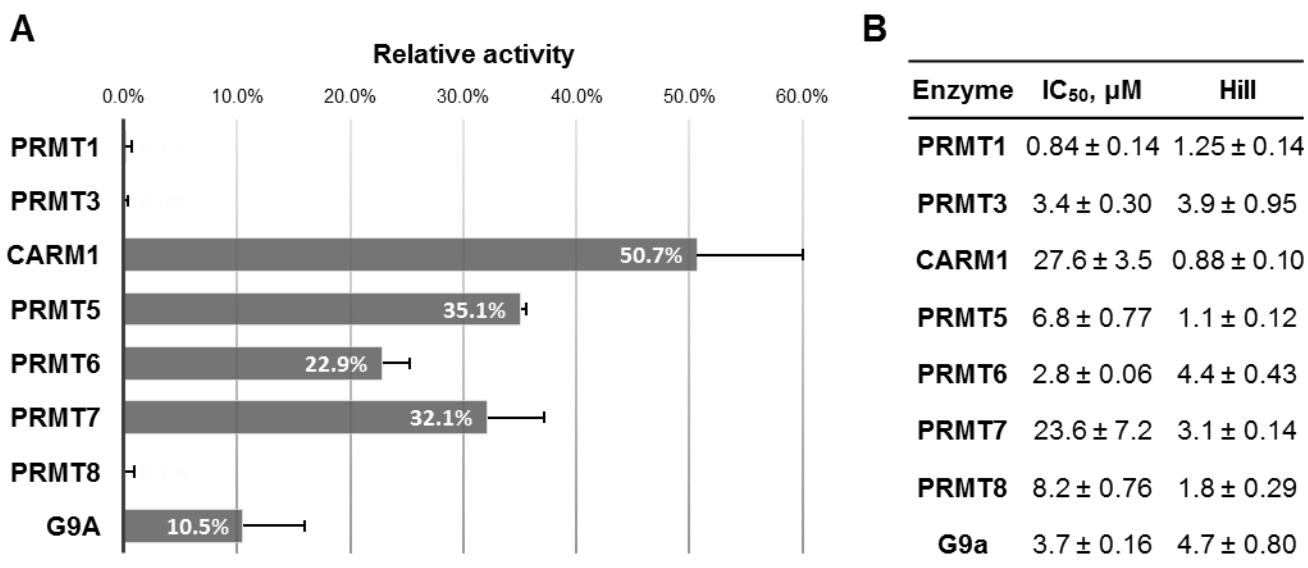
Figure 2.7 Selectivity of K313. A. Single concentration screening at 10 μM of K313. **B.** IC$_{50}$ of K313 against a panel of protein methyltransferases.

The selectivity of less potent PRMT1 hits (K278, K309, K336 and K413) from the

screening was also evaluated (**Figure 2.8**). K413 is selective against CARM1 with an IC$_{50}$ of 9.1

± 0.9 μM, while is 4-fold less potent over PRMT5, 6-fold over PRMT3, 7-fold over PRMT1 and

-6, 9-fold over G9a and more than 13-fold over PRMT1 and PRMT8. K336 showed selectivity

against PRMT3 and CARM1, which is 2-fold less potent for PRMT1, 4-fold for PRMT8, 7-fold

for PRMT6, more than 20-fold for PRMT7 and almost inactive against PRMT5. The IC$_{50}$ values

of K309 for PRMT1, -3 and 6 are very close, while it is about 3-fold less potent for G9a, 5-fold

for PRMT8, 10-fold for CARM1, 15-fold for PRMT7 and almost inactive for PRMT5. K278 is

less selective for all the enzymes in the panel with IC$_{50}$ values range from 4.7 to 23.3 μM, in

which the most potent for G9a. A large variation in the values of the Hill coefficient was

observed, which suggested different binding modes exists for these small molecules inhibiting

the protein targets.
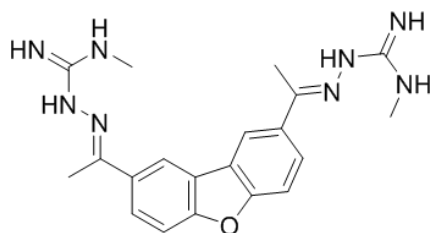
K278	IC$_{50}$, µM	hill
PRMT1	6.9 ± 0.12	2.5 ± 0.10
PRMT3	8.2 ± 0.31	4.4 ± 0.49
CARM1	15.5 ± 1.35	0.67 ± 0.05
PRMT5:MEP50	18.9 ± 2.50	1.1 ± 0.16
PRMT6	6.01 ± 0.19	6.9 ± 4.2
PRMT7	23.3 ± 9.52	1.7 ± 1.1
PRMT8	17.6 ± 3.03	2.1 ± 0.65
G9a	4.7 ± 0.52	1.2 ± 0.16

K278
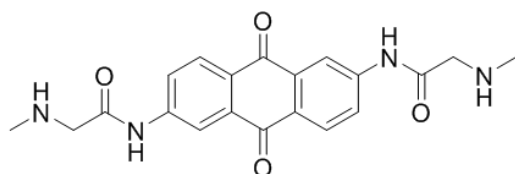
K336	IC$_{50}$, µM	hill
PRMT1	34.7 ± 1.7	0.98 ± 0.55
PRMT3	11.6 ± 0.46	1.6 ± 0.09
CARM1	12.4 ± 2.1	0.68 ± 0.09
PRMT5:MEP50	>500	
PRMT6	84.5 ± 14.4	1.9 ± 0.57
PRMT7	287.8 ± 92.3	3.0 ± 2.5
PRMT8	43.7 ± 9.6	0.97 ± 0.21
G9a	>1000	

K336
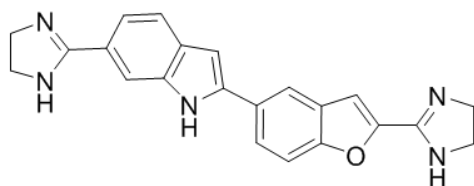
K309	IC$_{50}$, µM	hill
PRMT1	18.7 ± 0.99	2.3 ± 0.25
PRMT3	19.0 ± 1.1	3.6 ± 0.56
CARM1	154.6 ± 14.5	0.96 ± 0.14
PRMT5:MEP50	>500	
PRMT6	12.9 ± 0.78	5.4 ± 3.3
PRMT7	247.7 ± 48.9	1.0 ± 0.20
PRMT8	60.1 ± 12.3	1.5 ± 0.49
G9a	39.7 ± 4.2	2.8 ± 0.68

K309
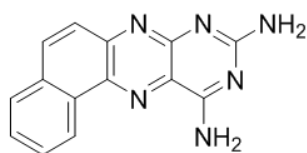
K413	IC$_{50}$, µM	hill
PRMT1	65.4 ± 5.7	1.3 ± 0.14
PRMT3	55.7 ± 4.4	1.6 ± 0.19
CARM1	9.1 ± 0.90	0.77 ± 0.07
PRMT5:MEP50	62.1 ± 3.1	0.62 ± 0.11
PRMT6	62.9 ± 5.8	2.3 ± 0.43
PRMT7	125.5 ± 34.9	1.2 ± 0.37
PRMT8	166.5 ± 33.5	1.4 ± 0.40
G9a	81.5 ± 5.1	1.5 ± 0.13

K413

Figure 2.8 Selectivity of other hits against the protein methyltransferase panel.

53

2.5.2 Structure activity relationship (SAR) of K313 analogues in PRMT1 inhibition

The 30 most structurally-related compounds from the furamidine-derived library and K313-derived library were chosen for SAR analysis, which were further categorized into three series according to their central frame structures (**Figure 2.9**, **2.10** and **2.11**). In series 1, compounds share two indene-like cores connected by butene or butyl linkers. The substitution of the 5-membered ring affects the activity of the compounds, and K465 showed lowest IC_{50} at 2.4 ± 1.0 µM among all (**Figure 2.9A**). The additional methyl group on the double-bond linker of K457 did not bring significant change on the potency, comparing to K467 (**Figure 2.9A**). The replacement of diamidine group with imidazole in K473 decreased its inhibition compare to K464 (**Figure 2.9B**), which is supportive to our previous SAR analysis in **2.3.3** that the amidine group is essential for ligand-protein binding by contributing hydrogen bonds. The *cis* conformation in K466 slightly reduced the potency than the *trans* compound K465 (**Figure 2.9C**). Flexible linker was generally not favored, comparing K461 to K465 or K466, and K458 to K469 (**Figure 2.9D**).

A

Inhibitor	X_1	X_2	X_3	X_4	R	IC$_{50}$, µM
K465	NH	O	C	C	H	2.4 ± 1.0
K468	C	O	NH	C	H	7.5 ± 1.6
K460	C	C	NH	O	H	7.7 ± 1.3
K464	O	O	C	C	H	14.1 ± 5.0
K456	C	O	S	C	H	16.5
K467	C	O	O	C	H	34.7 ± 21.5
K457	C	O	O	C	CH$_3$	~ 40

B

Inhibitor	X_1	X_2	X_3	X_4	IC$_{50}$, µM
K483	NH	NH	C	C	6.2 ± 1.4
K473	O	O	C	C	~ 35

K492 IC$_{50}$ = 5.0 ± 1.2 µM

C

Inhibitor	X_1	X_2	X_3	X_4	IC$_{50}$, µM
466	NH	O	C	C	7.6 ± 2.0
469	O	C	C	NH	7.9 ± 0.97

D

Inhibitor	X_1	X_2	X_3	X_4	IC$_{50}$, µM
461	NH	O	C	C	> 10
458	O	C	C	NH	~ 50
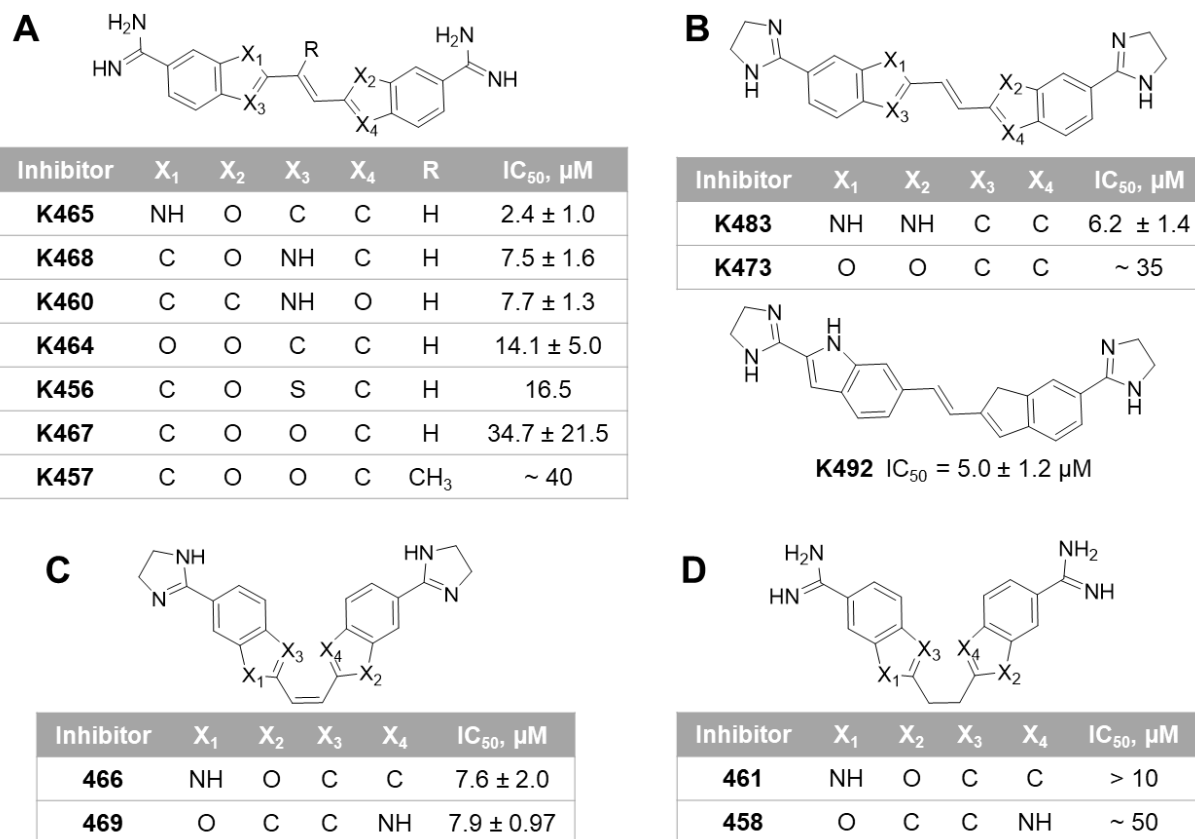
Figure 2.9 Structure activity relationship of the K313 analogs, series 1.

A

Inhibitor	X_1	X_2	IC$_{50}$, µM
K476	C	O	~ 10

Inhibitor	X_1	X_2	IC$_{50}$, µM
K487	C	O	~ 15
K486	NH	C	~ 50
K484	C	S	~ 70
K480	C	O	~ 80

B

Inhibitor	X_1	X_2	IC$_{50}$, µM
K471	O	C	> 100
K462	C	O	> 100

Inhibitor	X_1	X_2	IC$_{50}$, µM
K470	NH	C	~ 50
K472	O	C	> 100
K463	C	O	> 100
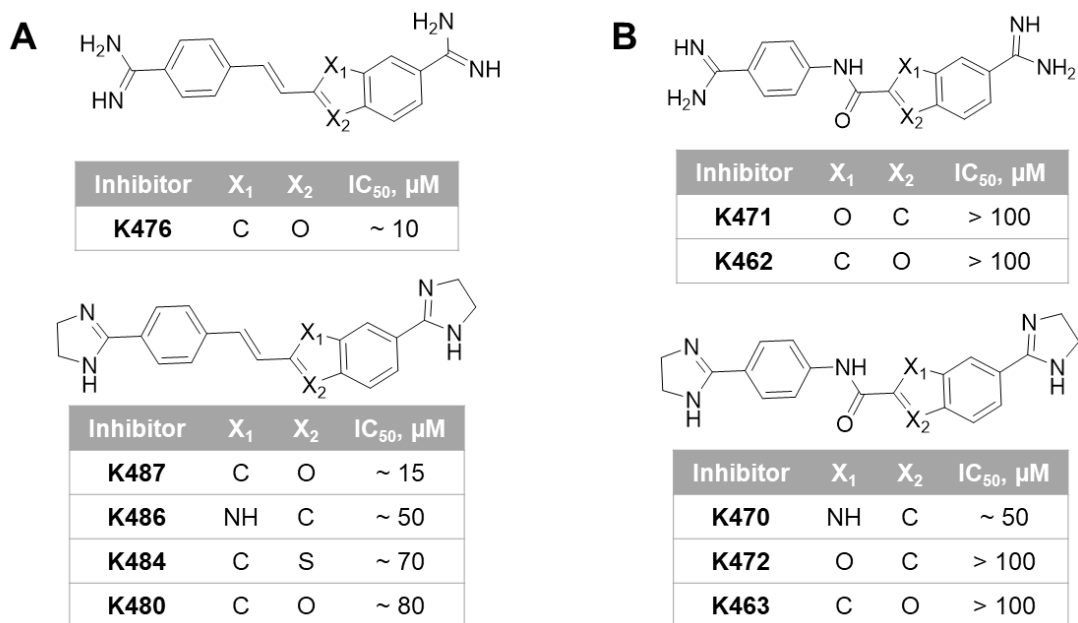
Figure 2.10. Structure-activity relationship of the K313 analogs, series 2.

The compounds in series 2 are featured with a benzene ring connected to an indene-like core (**Figure 2.10**). Similar to series 1, substitution of the 5-membered ring altered the potency of the inhibitors (**Figure 2.10A**), and the imidazole side group was not as favored as the amidine group (**Figure 2.10B**). It is likely that either the steric hindrance or hydrophobicity of the additional alkyl carbons can interrupt the hydrogen bonding from the amidine groups.

In series 3, the potencies of compounds bearing different lengths of the linkers are listed and compared (**Figure 2.11**). The shorter linker (K309 and K489) is preferred than the four-carbon diene linker (K475 and K481), which is again consistent with the linker variation studies in **2.4.1**. The lengths of the linker mainly contribute to the overall ligand binding through positioning the amidine groups into the appropriate pocket where strong hydrogen bonds or salt bridges can form between the terminal amidines and amino acid residues.
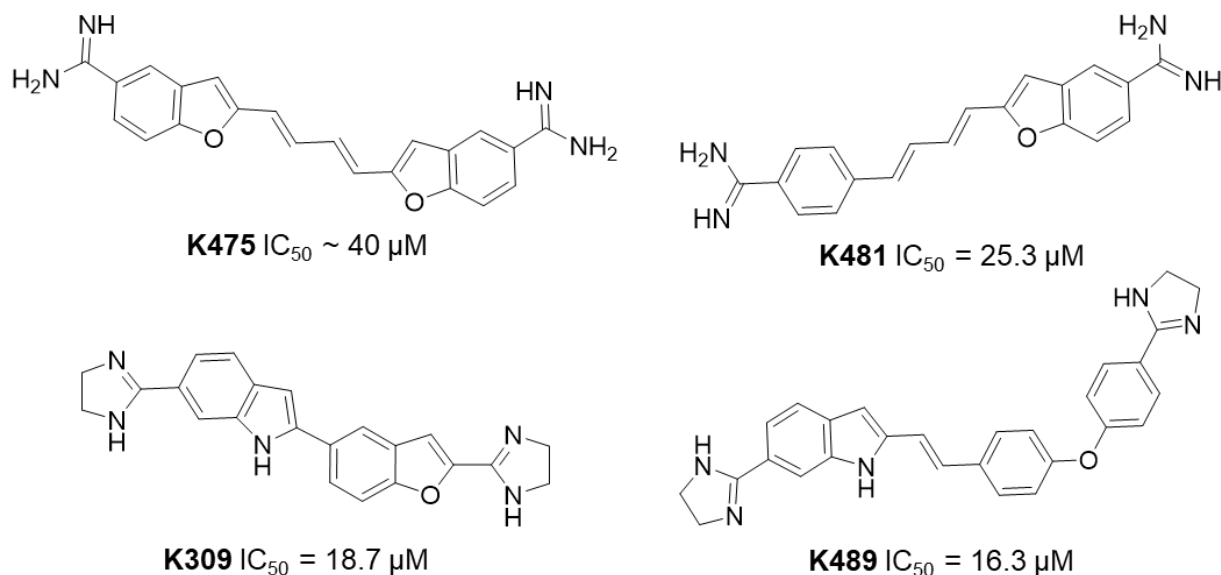
Figure 2.11 Structure-activity relationship of the K313 analogs, series 3.

2.5.3 Mechanism of action studies of K313

As soon as K313 was identified, the compound was sent to a collaborator expertized in protein crystallography (Dr. Joseph Ho, Academia Sinica, Taiwan) for co-crystallization

screening on PRMT1, PRMT3 and PRMT8. After condition optimization, yellow crystals were formed for PRMT3 with K313, which was likely from this yellow-colored ligand. The yellow color remained after back wash (soaked the crystal in the solution without K313), which suggested that K313 was bound to the protein. However, the density of the K313 was not observed in PRMT3. Docking of K313 in the PRMT1 pocket was performed, and this proposed binding model was overlapped with a rat PRMT3 structure in presence of SAH (SAM analogue) (PDB code 1F3L, **Figure 2.12A**). The two protein structures overlapped very well, and K313 (blue) clearly appeared in the SAM binding site overlapping with SAH (magenta), which suggested that K313 is probably competitive to SAM, but it could not exclude the possibility of being the mixed-type of inhibition. In order to obtain a docking structure of K313 in PRMT1, the previously described PRMT1 homology model was overlapped with the K313-PRMT3 cocrystal structure, and the docking site was defined by the position of K313 in PRMT3. The *in situ* ligand minimization protocol in Discovery Studio 4.0 was used to further dock K313 in PRMT1. The obtained results show that K313 was sitting in an overall hydrophobic environment, except the slightly hydrophilic residues surrounding the two terminal amidine groups (**Figure 2.12B**). From a more detailed view in **Figure 2.12C** and **D**, a hydrogen bond formed between the Glu129 and one amidine group of K313, which was also found in the case of furamidine. However, the other amidine group of K313 did not interact with Glu144 but rather extended to the SAM carbonyl binding site and formed hydrogen bond with Thr81. The middle aromatic rings in K313 formed several interactions with hydrophobic side chain residue, which helped positioning the ligand and tightened binding.
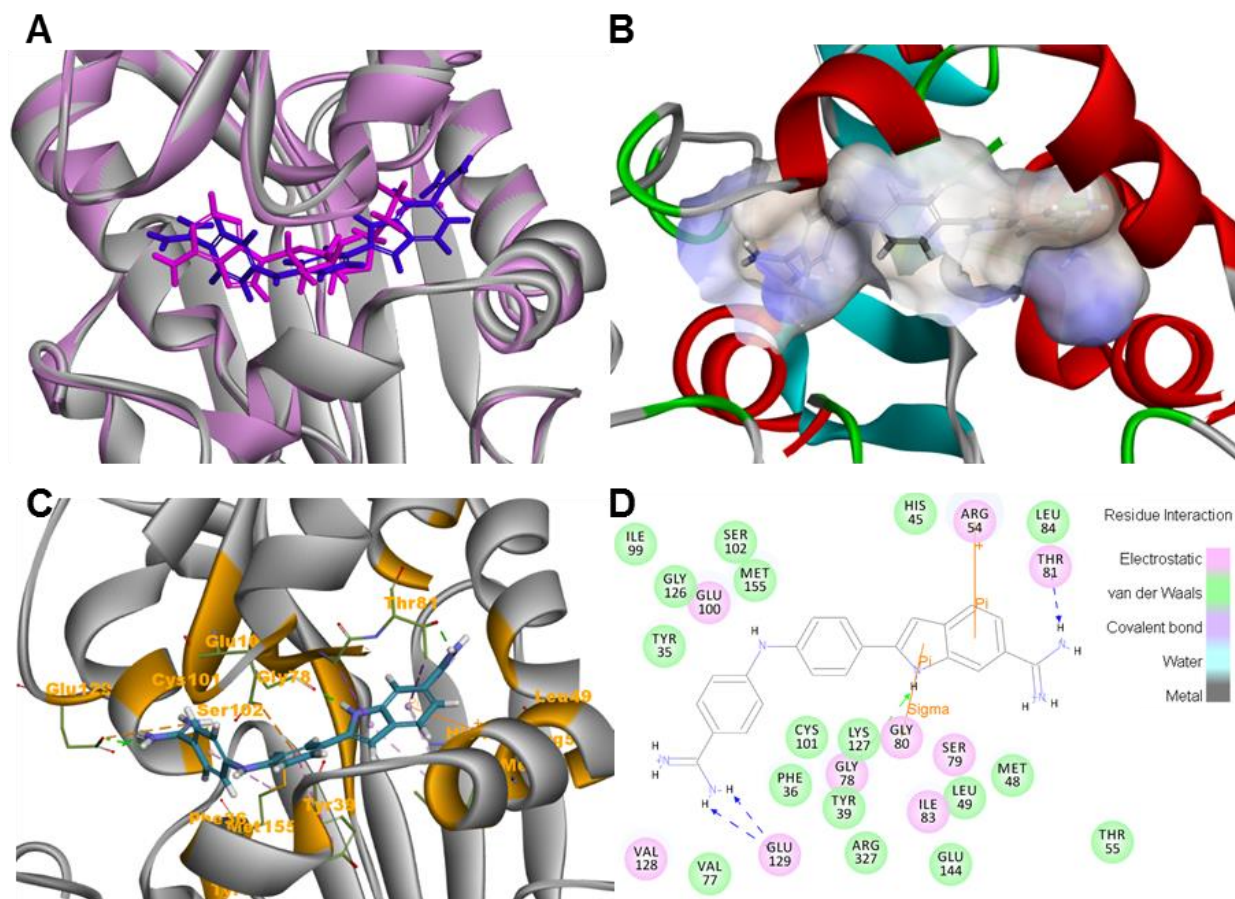
Figure 2.12 Proposed binding pose of K313 in PRMT1 catalytic cavity. A. Overlapped structures of K313 (blue) in PRMT1 (grey), with SAH (magenta) in PRMT3 (pink) (PDB: 1F3L). **B**. Hydrophobic surface of PRMT1 at K313 binding site (darker blue is less hydrophobic). **C**. Detailed interactions of K313 with PRMT1 catalytic pocket residues. K313 is shown in blue sticks, PRMT1 residues involved in binding are labeled in orange. **D**. 2D diagram of **C**. All figures are generated with Discovery Studio 4.0.

The mechanism of inhibition was carried out using stopped flow spectrometer (details about this assay is described in Chapter 4). The curve of Phase I rate with concentration of K313 showed an ascending trend rather than descending trend (**Figure 2.13**), which is similar the SAH titration result (**Figure 4.5**). However, the decreasing trend of the Phase I rate curve is steeper than SAH, which indicated it could also affect substrate binding. These results suggested a mix-type inhibition with primarily SAM competitive pattern, which agreed with the proposed docking model where K313 is interrupting the binding of the cofactor SAM.
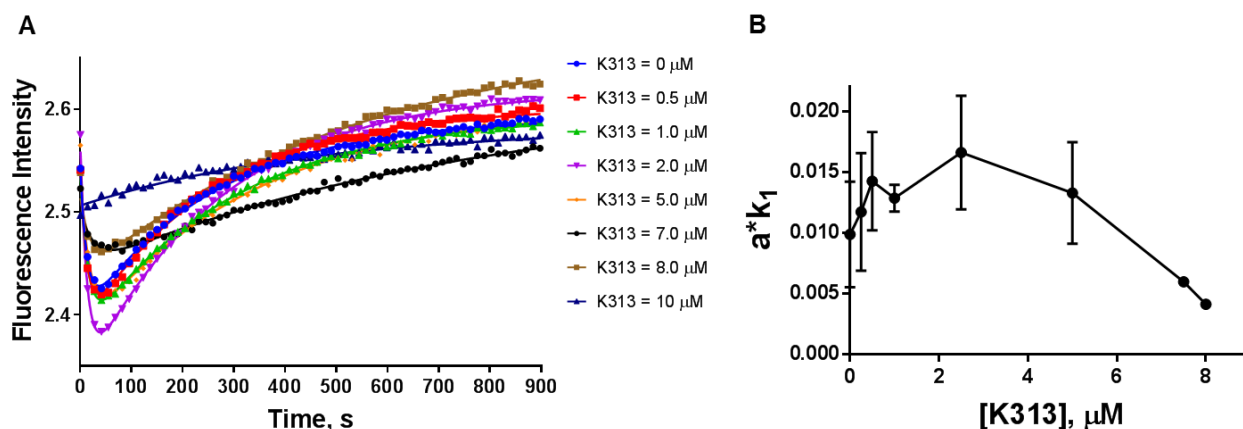
Figure 2.13 Stopped flow fluorescence assay of K313. A. PRMT1 methylation time curves in presence of different concentrations of K313**. B.** The relationship of Phase I slope values with varying concentrations of K313. The condition of the assay is as the following: [PRMT1] = 0.2 µM, [SAM] = 3.5 µM and [H4FL] = 0.4 µM.

2.5.4 Cellular efficacy of K313

(This work was conducted through collaboration with Hairui Su, Dr. Xinyang Zhao on Leukemia cells; Sudeepti Kuppa, Lindsay Berman and Dr. Mandy Murph on Melanoma cells.)

The cellular efficacy of K313 in leukemia cells was tested through collaboration. Dose-dependent cell viability assay was performed on MEG01, CMK, K562, and HEL cells by K313 treatment, with DMSO as control (**Appendix B Figure S2.5 A-B**). Cell viability inhibition IC_{50} was calculated after 3 days and 4 days of treatment (**Appendix B Figure S2.5C**). Immunoblots of asymmetric arginine methylation level of with or without K313 treatment in MEG01 cells was shown in **Appendix B Figure S2.5D**. The results validated the inhibition of PRMT1 by K313 in cells, according to the decreased methylation level of the PRMT1 substrates, including RBM15. K313 was potent enough to significantly inhibit ADMA levels at 100 nM and 200 nM after 24-hour treatment. K313 was also tested in melanoma MeWo cells. In a parallel growth inhibition assay, the IC_{50} of K313 is 1.1 µM while the IC_{50} of furamidine (DB75) is 13.5 µM (**Appendix B Figure S2.6**). The IC_{50} result on MeWo cells is consistent with that of the leukemia cells, which also reflected the 10-fold lower potency of K313 than furamidine in biochemical assays.

2.6 Conclusions

The results of this chapter have demonstrated that diamidine compounds are capable of selectively inhibiting the methyl transfer activity of PRMT1 with varied potencies, evidenced by the identification and characterization of furamidine, decamidine and K313 (**Table 2.5** and **Figure 2.14**).

Furamidine was identified as a potent and selective inhibitor for PRMT1 compared with the other PRMTs such as CARM1, PRMT5, and PRMT6. It effectively inhibited PRMT1 activity intracellularly, which also inhibited leukemia cell proliferation. The computational

studies of ligand-protein interactions suggested that the rigid crescent-shaped compound spans the adjacent substrate and cofactor binding sites, through strong salt bridges formed between the positively charged amidine functional group and glutamate side chains in the substrate site and cofactor site. This mode of inhibition was confirmed by enzyme kinetic results, wherein furamidine showed a primarily substrate competitive mode of inhibition and a noncompetitive inhibition toward the cofactor. The SAR analysis also supported that amidine residues are essential for the inhibitory activity of the compounds, in which any modification resulted the deprotonation or bulkiness on the amidine groups caused a decrease in inhibitory activity.

Following this work[150], a series of phenyl diamidines bearing different middle linker length were synthesized for a complimentary SAR study to the original set of compounds. Among the newly obtained analogs[224], the inhibition potencies increased as the linker length elongated, and the most potent inhibitor in this series was decamidine with a C10 linker. Compared to stilbamidine and furamidine, this compound showed moderately increased PRMT1 inhibition but slightly decreased selectivity against PRMT5. Molecular docking studies suggested that the increase inhibitory activity for PRMT1 could be attributed to the extension of the linker that positioned the amidine group to the far end of the SAM binding site. It appears that only a linker length over five methylene groups is long enough for transitioning from one binding mode (like furamidine) to the other (like decamidine).

K313 was identified using a combinatorial approach - furamidine was the template for ligand-based virtual screening to search for compounds with similar shape and charge in a diverse compound library, and ranked by similarity scores. A furamidine-derived library containing top hits from virtual screening was subjected to biochemical high throughput screening. A total of 30 compounds were found more potent than furamidine for PRMT1

inhibition, among which K313 was identified as the most potent inhibitor with 10-fold improved

IC_{50} for PRMT1 compare to that of furamidine. Stopped flow fluorescence assay and

computational studies together indicated that K313 directly interfere with cofactor binding. K313

significantly decreased ADMA level in leukemia cells at concentration as low as 100 nM. The

IC_{50} value of K313 for growth inhibition is 1 μM in leukemia cell and melanoma cell studies,

and for melanoma cells, K313 is at least 10-fold more potent than furamidine.

The SAR studies of the diamidines together demonstrated the importance of amidine

moiety in the inhibitory activity of compounds: the substitution on the amidines resulted in

decreased inhibition for PRMT1, while the linker lengths and structures could also affect the

PRMT1 inhibition. This conclusion is also supported by the computational studies of the three

inhibitors. The proposed binding mode of the three inhibitors in PRMT1 is shown in **Figure

2.14**. From the overlapped structure, the three compounds have a common binding region in the

SAM adenosine site (left side amidine of **Figure 2.14**), whereas furamidine and K313 interacted

with Glu129 while decamidine stretched a little further. On the other side, the amidine group of

furamidine pointed downward to interact with the arginine binding site residues Glu144 and

Glu153, while both decamidine and K313 extended in the SAM binding site. It is likely that the

larger molecule size and more hydrophobic middle linker of K313 and decamidine are more

suitable for the environment of the SAM binding site (**Figure 2.4 B**, **Figure 2.12B**). As for

furamidine, the relatively short distance between the two amidine groups allowed the

complimentary shape and space to interact with the three glutamate residues from SAM site

(Glu129) and substrate arginine site (Glu144 and Glu153) (**Figure 2.3B**). Interestingly,

furamidine has the best selectivity for PRMT1 inhibition (**Table 2.5**) among the three

compounds, which also had the most interactions to the arginine binding site residues. It is

possible that decamidine and K313 bind to the conserved SAM binding site of the PRMT isoforms and their selectivity was compromised, but the increased hydrophobic interactions enhanced the binding of the molecules.

In all, this work has provided several potent, selective and cell-active PRMT1 inhibitors for further structure optimization. These potent and selective inhibitors can be used as chemical probes to study the biological functions of PRMT1, and they are potential therapeutic agents for PRMT1 dysregulation-associated cancers.
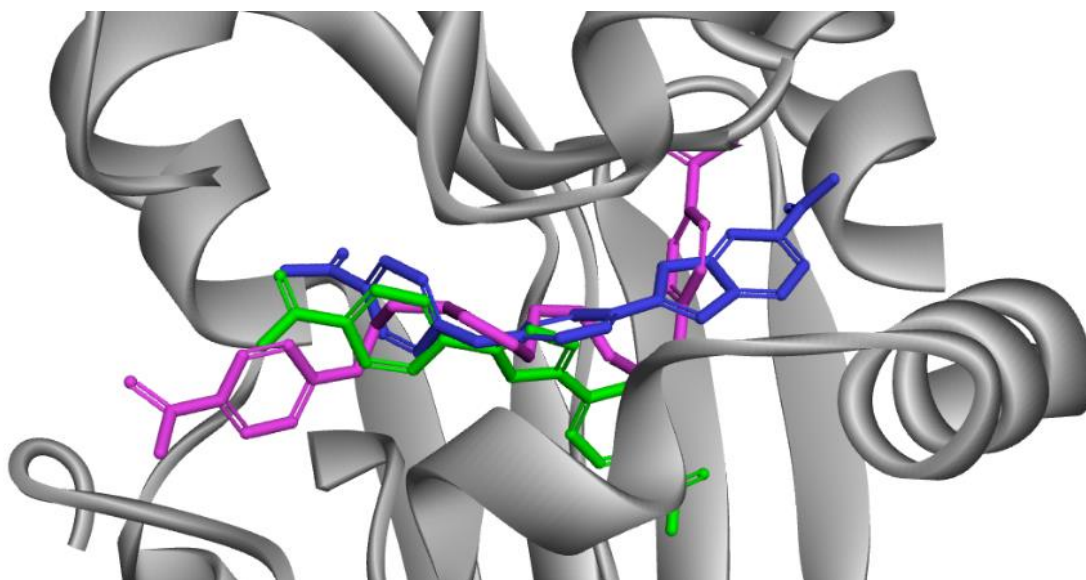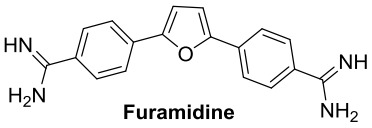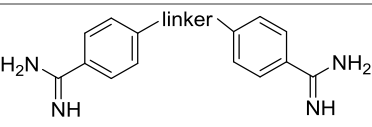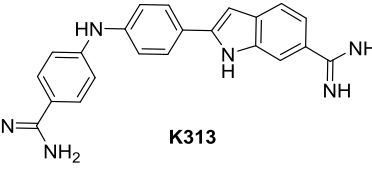
Figure 2.14. Overlapped structure of furamidine, decamidine and K313 in PRMT1 catalytic pocket. PRMT1 is shown in grey, furamidine is in green, decamidine is in magenta and K313 is in blue.

Table 2.4. Comparison of PRMT1 inhibitors in Chapter 2.

Structure	MW, g/mol	LogP	IC$_{50}$ for PRMT1, µM	IC$_{50}$ increase for PRMT5	Cellular activity
Furamidine	304.35	2.34	9.4 ± 1.1	17.6-fold	Reduced ADMA level in 293T; inhibited growth of leukemia cells; cell viability IC$_{50}$ is 13.5 µM in MeWo (melanoma)
Decamidine, linker = -O(CH$_2$)$_{10}$O-	410.56	4.92	12.7 ± 1.0 (furamidine: 21.6 ± 2.1)	3.4-fold	Not determined
K313	368.44	3.06	0.84 ± 0.14 (furamidine: 12.7 ± 3.8)	8.1-fold	Reduced ADMA level in MEG01 cell (leukemia); cell viability IC$_{50}$ 1.03 µM in MEG01 and 1.08 µM in MeWo (melanoma)

64

CHAPTER 3

K280S IS A DUAL-TARGET INHIBITOR FOR PRMT5 AND MICROTUBULIN IN

PROSTATE CANCER

Part of this work is submitted to *Proc. Natl. Acad. Sci.* as: Zhang, J.*, **Qian, K.**, Quach, N.*

Yan, C., Missori, W., Ghoshe, D., Dawsone, M., Guo, T., Ivanov, I., Cummings, B., Zheng, Y.G.

(*equal contribution) (2017) Anticancer Candidate CI-980 Is a Dual Inhibitor of PRMT5 and

Microtubule.

3.1 Introduction

PRMT5 is the predominant type II enzyme that symmetrically dimethylates arginine

residues of histones and non-histone protein substrates (**Table 1.2**)[225]. One of the major role of

PRMT5 in epigenetics is to repress gene expression[101, 226]. PRMT5 also participates in various

cellular processes by the symmetrically demethylation of critical signaling proteins involved in

cell cycle progression, apoptosis and DNA repair [28, 225]. Recently, PRMT5 has garnered attention

as a new molecular target in various diseases: PRMT5 is overexpressed in gastric, colorectal,

lung cancer, lymphoma, leukaemia[21] and prostate cancer[114]; it also plays regulatory roles in renal

and cardiovascular disease[115], Huntington's disease[116] and Alzheimer's disease[117] (**Table 1.2**).

The elevated activity of PRMT5 was found to correlate with progression and poor prognosis in

many cancers, and evidence suggests that PRMT5 functions as an oncogene to promote cancer

development[46, 108, 225, 227-231]. The therapeutic potential of PRMT5 inhibition is supported by

numerous studies. For example, silencing PRMT5 expression in lung cancer A549 cells reduced

cell proliferation[228]. In neuroblastoma, PRMT5 overexpression is intensely associated with

oncogene MYCN amplification[232]. The growth inhibition of ER-negative breast cancer cell with 17-β-estradiol treatment is accompanied by decreased PRMT5 expression[233]. PRMT5 relates to adaptive changes in several signaling pathways typical of prostate cancer type[20, 234], and studies show that silencing PRMT5 in prostate cancer cells causes slow cell growth.[114] These studies suggest that PRMT5 overexpression plays important roles in prompting cancer cell growth, and silencing or reduce expression of PRMT5 is a plausible way to prevent or slow down the development of cancer. Therefore, PRMT5 inhibitors are potential therapeutic agents to treat cancers that associated with elevated PRMT5 activity.

Despite the emerging need, to date, a very limited number of PRMT5 inhibitors were reported (refer to **Chapter 1.6.6**). Compound CMP5 (**Figure 1.9**, **44**) was used in cells but not much information about its selectivity profile and mode of action was reported[199]. EPZ015666[235] is a potent, selective and orally bioavailable PRMT5 Inhibitor with a biochemical K_i of 5 nM. It has >20,000-fold selectivity over a panel of protein methyltransferases. Enzyme kinetics studies showed competitive inhibition to the peptide substrate, and uncompetitive to SAM. The crystal structure of EPZ015666 with SAM in PRMT5:MEP50 (PDB: 46X1) explained this mechanism of inhibition. The compound was found to bind in the peptide-binding site, interacting directly with many of the residues for peptide binding and catalytic reaction. Interestingly, it forms a π-π stacking interaction with Phe327, which is postulated to be a crucial residue that differentiates type I and type II activity[40, 236]. This unique interaction can also explain why this compound is extremely selective for PRMT5 – based on the known crystal structures of PRMTs, PRMT5 is the only enzyme that has this residue in arginine binding site[26]. Treatment of MCL cell lines with EPZ015666 resulted in inhibition of SmD3 methylation and decreased cell proliferation. However, the treatment time lasted for 12 days for the nanomolar potency in proliferation

inhibition, which suggested that the treatment onset of EPZ015666 was slow in MCL cells. Oral dosing with EPZ015666 demonstrated dose-dependent antitumor activity in multiple MCL xenograft models. In all, EPZ015666 is a validated chemical probe to study PRMT5 biological function in cancer and other diseases.

In this chapter, the inhibitory activity of 1,2-dihydropyrido[3,4-b]pyrazine compounds on PRMT5 was identified and characterized. This group of compounds were previously reported as tubulin binders. This inhibitor is more potent than EPZ015666 in inhibiting prostate cancer cell growth. Our studies suggested that the synergetic effect of K280 inhibiting PRMT5 activity and microtubule formation is beneficial to cancer treatment.

3.2 Materials and Methods

3.2.1 Materials

Experimental or purchasing details are described in Chapter 2: protein expression of Recombinant methyltransferases refer to 2.2.1; peptide synthesis refer to 2.2.2; purchased materials refer to 2.23.

3.2.2 Compound sources

Compound library for high throughput screening were ordered from National Cancer Institute DTP program. K280 and K280 derivatives were synthesized and purified by Dr. Jing Zhang, with >95% purity based on ^{1}H and ^{13}C NMR, analytical HPCL and mass spectrometry, with an exception of hydrogenated K280 (K280+2H) with 90% purity due to the instability nature of this compound.

3.2.3 Biochemical assays

Experimental details are described in Chapter 2: high throughput screening (HTS) of small molecule libraries refer to 2.2.5; biochemical selectivity assay refer to 2.2.6; mechanism-of-inhibition studies refer to 2.2.7.

3.2.4 Molecular docking

Docking was carried out with Discovery Studio 4.0. The reported PRMT5:MEP50 crystal structure (PDB: 4GQB) was used as the receptor model for docking of K280. The docking boxes were identified through PDB recorded catalytic pocket of the protein structure in Discovery Studio 4.0. CDOCKER docking module was applied for molecular dynamic enforced optimization. Docking poses were ranked based on CDOCKER energy from the lowest to highest, and the lowest energy confirmation was chosen for binding interaction analysis.

3.2.5 PRMT5:MEP50 protein complex expression using Bac-to-bac baculovirus expression system

Recombinant human PRMT5:MEP50 complex was expressed in baculovirus-infected SF9 cells. Full-length protein arginine methyltransferase 5 (PRMT5) including residues 1–637 with an amino terminal his-TEV tag (MGHHHHHHSSGVDLGTENLYFQ*SM, *is TEV cleavage site) was cloned into pFastBac vector between Lic205 and Bse221. Full-length MEP50 including residues 1–342 was cloned into the same vector. The two bacmids were extracted and purified using form the two pFastBac plasmids inoculated culture of DH10Bac *E coli*, using PureLink HiPure DNA midiprep Kit (life technologies). Insertion of the target genes in the two bacmids was verified by PCR using pUC/M13 primers. The two bacmids were then transfected separately in SF9 adherent culture on a 6-well plate, cultured in SF900II serum free medium. PRMT5 and MEP50 were harvested 10 days after transfection, when > 80% cell death was

observed. The two viruses were used to infect more SF9 cells in adherent culture or suspension culture to generate P2, and the titer of P2 viruses was determined by a modified baculovirus rapid titer protocol (Clontech). The infection condition was optimized in a 12-well or 24-well assay varying MOI from 1 to 10 and infection time from 24 hr to 72 hr. An optimal condition was determined to be MOI = 1 for both viruses with 72 hr infection. The 250 mL suspension cultures of SF9 cells were then infected at MOI=1 for 72 hr before the cell pellets were harvested. Purification of the PRMT5:MEP50 complex was carried out at 4 °C. Cell pellets were lysed by resuspension in buffer containing 50 mM Tris pH 8, 300 mM NaCl, 20 mM imidazole pH 8, 1 mM TCEP, 10% (vol/vol) glycerol, 0.1% (vol/vol) Triton X-100, and freshly added 1 mM PMSF followed by centrifugation for 30 min at 39,191 g. The clarified lysate was mixed with Ni-NTA resin (Qiagen) pre-equilibrated in the equilibrium buffer containing 50 mM Tris pH 8.0, 250 mM NaCl, 10% (vol/vol) glycerol, 1 mM TCEP, 30 mM imidazole and freshly added 1 mM PMSF. Resin was sedimented and washed with the washing buffer (50 mM Tris pH 8.0, 250 mM NaCl, 10% (vol/vol) glycerol, 1 mM TCEP, 80 mM imidazole and freshly added 1 mM PMSF), and eluted in buffer supplemented with 300 mM imidazole pH 8.0. Concentrated protein was dialyzed and then loaded onto a Superdex 200 size-exclusion column (GE Healthcare LifeSciences) in a buffer containing 50 mM Tris pH 8.0, 250 mM NaCl, 10% (vol/vol) glycerol, and 1 mM TCEP. FPLC fraction of the complex was collected, and the purity of the protein complex was checked by SDS-PAGE and western blot. The enzyme activity was confirmed by methylation time courses measured by SPA, in comparison to the purchased PRMT5:MEP50 complex from Reaction Biology Inc. (part number: HMT-22-148).

3.2.6 Crystallization of PRMT5:MEP50 protein with MTA and histone H4-20 peptide, or K280S

MTA (5'-Methylthioadenosine) or K280S was solubilized at 100 mM in DMSO, H4-20 peptide was dissolved in sterilized distilled water at 20 mM. MTA and H4-20 or K280S at a final concentration of 1 mM were mixed with PRMT5:MEP50 complex at 10.5 mg/mL, and the samples were incubated on ice for 1 hour. Hanging drop vapor-diffusion methods was used in a 0.5-mL reservoir 24-well tray for protein crystallization. Typically, 2 μL protein was added to 2 μL reservoir solution containing 20% - 30% PEG3350 and 200 mM ammonium sulfate. Trays were incubated at 8 °C for two weeks before the pictures of the needle-shaped crystal were taken using a camera attached to the microscope.

3.3 Identification of K280 as a Potent and Selective PRMT5 Inhibitor

To identify novel PRMT5 inhibitors, a ligand-based virtual screening (**Appendix A Figure S1**) was performed based on the reported PRMT1 inhibitor furamidine (**Figure 1.7**, **20**). The NCI Diversity Set was used as the library compound source, which contains 260,071 compounds. Biochemical screening of the top 406 hits was conducted using the previously described scintillation proximity assay. The screening yielded 8 compounds based on a cut-off of 50% inhibition at 10 μM (**Figure 2.5A**), and one dihydropyrazine compound K280 (**Figure 3.1A**) was identified with potent PRMT5 inhibition (IC$_{50}$ = 371 nM, **Figure 3.1B**).
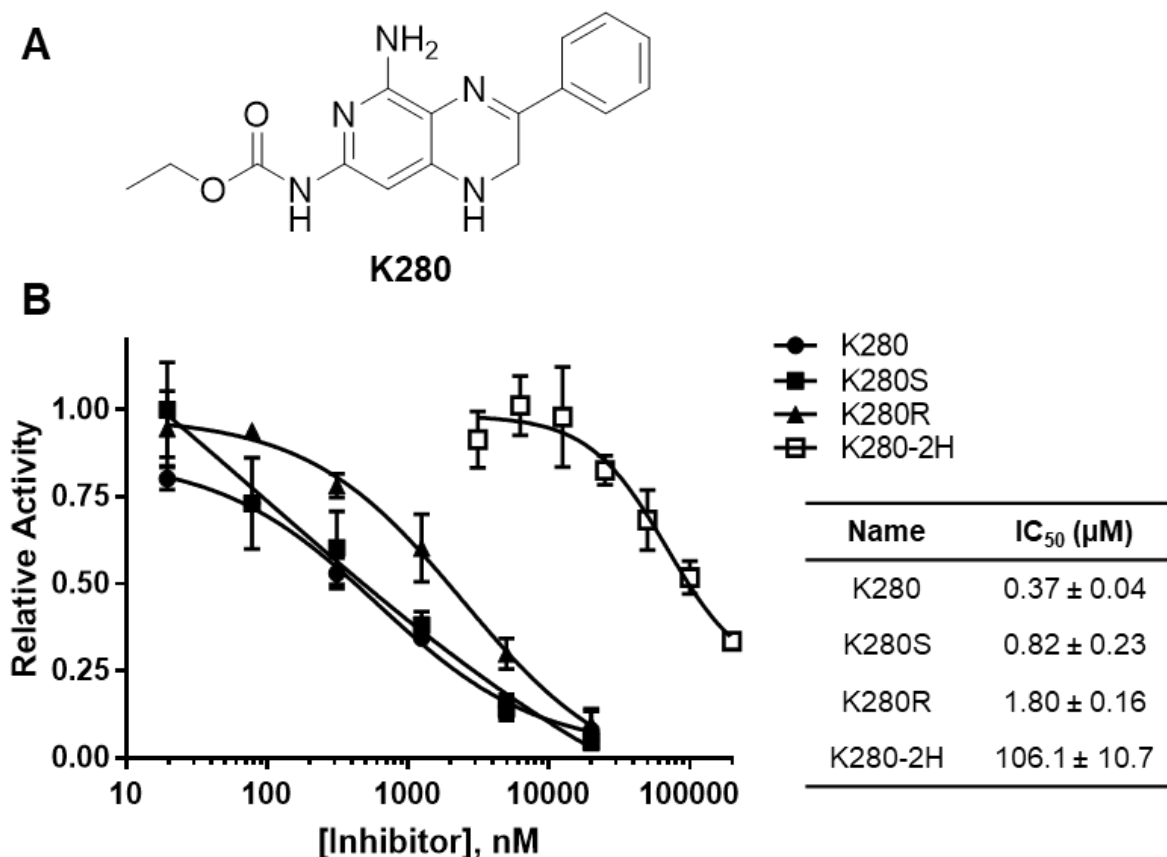
Figure 3.1 K280 is a potent PRMT5 inhibitor. A. Chemical structures of K280. **B**. Representative IC_{50} plots of K280, K280-2H, K280S and K280R in semi-log format measured by SPA.

Inhibitory activity of K280 was measured using a panel of PRMTs and lysine methyltransferases (**Figure 3.2**). At 10 µM concentration of K280, PRMT5 is inhibited to 10% remaining activity, while other enzymes are almost not inhibited; At 100 µM concentration of K280, PRMT5 is fully inhibited and G9a has 2% remaining activity, while inhibition of other enzymes is minimal (**Figure 3.2A**). The IC_{50} values of K280 for each tested protein methyltransferases are shown in **Figure 3.2B.** The IC_{50} value of K280 (0.37 µM) is 150-fold lower than G9a ($IC_{50} = 55.8$ µM) and more than 300-fold lower than the other enzymes. These results together suggested that K280 was highly selective for PRMT5.

A.

B.

Enzyme	Substrate	Remaining activity at 10 µM	Remaining activity at 100 µM	IC$_{50}$, µM
PRMT1	H4-20-biotin	98%	93%	>200
PRMT3	SmD1-biotin	No inhibition	97%	>200
CARM1	H3.3 protein	No inhibition	No inhibition	>200
PRMT5	H4-20-biotin	10%	0%	0.37 ± 0.04
PRMT6	SmD1-BTN	92%	70%	>200
PRMT7	SmD1-BTN	98%	72%	>200
PRMT8	H4-20-biotin	No inhibition	99%	>200
G9a	Biotin-H3-20	96%	2%	55.8 ± 4.4
DOT1L	Nucleosomes	No inhibition	No inhibition	>100

Figure 3.2 K280 selectively inhibits PRMT5 but not other PRMTs and PKMTs. A. Single concentration (10 µM) selectivity screening of K280 against protein methyltransferases. **B.** Summary table of K280 inhibition on protein methyltransferases. The corresponding substrates used in the assays, remaining activity of the enzymes in presence of 10 µM or 100 µM of the inhibitor and the IC$_{50}$ values are listed.

Since K280 is known to bind to the colchicine binding site of tubulin[237-239], we also tested the activity of colchicine, which has a completely different chemical scaffold (**Figure 3.3B**), on the PRMT5:MEP50 enzyme complex. As shown in **Figure 3.3A,** colchicine showed very weak inhibition against PRMT5 (IC$_{50}$ of ~1 mM), indicating that PRMT5 inhibition specificity is unique for the dihydropyrazine scaffold.
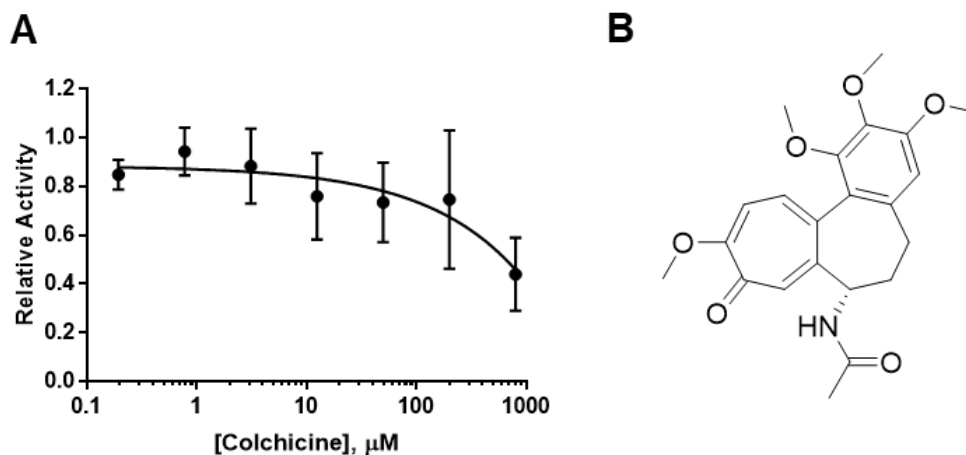
Figure 3.3 Colchicine is not a PRMT5 inhibitor. A. IC_{50} plot of colchicine in semi-log format measured by SPA. **B.** Chemical structure of colchicine.
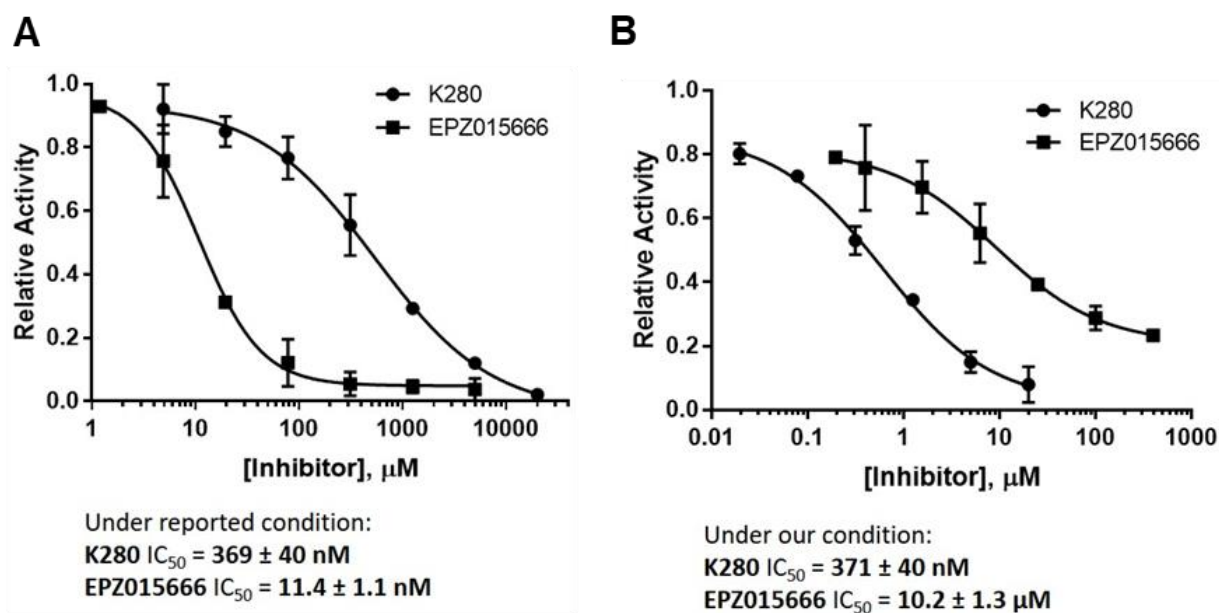
Figure 3.4 IC_{50} values of EPZ015666 and K280 against PRMT5:MEP50. A. Under the reported assay condition: [PRMT5:MEP50] = 4 nM, [^{3}H-SAM] = 75 nM, [H4-20-BTN] = 40 nM, room temperature, 2 hr, n = 2; **B.** under our assay condition: [PRMT5:MEP50] = 20 nM, [^{3}H-SAM] = 0.5 µM, [H4-20-BTN] = 1 µM, room temperature, 30 min, n = 2.

The PRMT5 inhibitory activity of K280 was compared with that of PRMT5-specific

probe EPZ015666 under the reported assay[235] and current assay conditions (**Figure 3.4**). Under

the reported assay condition, the IC_{50} value of K280 was measured as 369 nM, which is very

close to the value of 371 nM measured under our assay condition. Interestingly, compound

EPZ015666 showed two distinctive inhibition profiles. Under the reported condition, the IC_{50} of EPZ015666 was measured as 11.4 nM, close to the reported IC_{50} value of 22 nM. However, under our assay condition, its IC_{50} increased to 10.2 µM. The weakened PRMT5 inhibitory potency of EPZ015666 in response to increased substrate concentration may be explained by its inhibitory mechanism as peptide competitive and cofactor dependent[235]. In other words, the higher concentration of H4-20 in our assay (1 µM) and a relatively lower SAM concentration (0.5 µM) may increase the IC_{50} of EPZ015666, because more peptide is competing with the compound and less cofactor is available for the inhibitor binding under this condition.

3.4 K280S Showed Improved Stability Compared to K280

In the follow-up biochemical tests and chemical characterization, we found that K280 was easy to degrade over time (**Figure 3.5A** and **Appendix B Figure S3.1**), and this degradation dramatically reduced its ability to inhibit PRMT5 (**Figure 3.5B**). The degradant was confirmed to be aromatized K280 (hereafter referred to as K280-2H) by NMR (**Appendix B Figure S3.2**) as a result of oxidative aromatization of dihydropyrazine ring. Since K280-2H was a very weak PRMT5 inhibitor (IC_{50} = 106 µM, **Figure 3.1B**), we further performed structural modifications of K280 to improve its chemical stability (**Table 3.1**). This led to the identification of (*S*)-2-methyl-K280 (referred to as K280S) as a chemically stable PRMT5 inhibitor. K280S displayed improved stability with no sign of degradation over 1 month (**Figure 3.5**). This enhanced stability likely results from the steric shielding of the added methyl group. It should also be noted that K280S had been previously studied as a Phase II clinical candidate, named as CI-980[240-241].

74
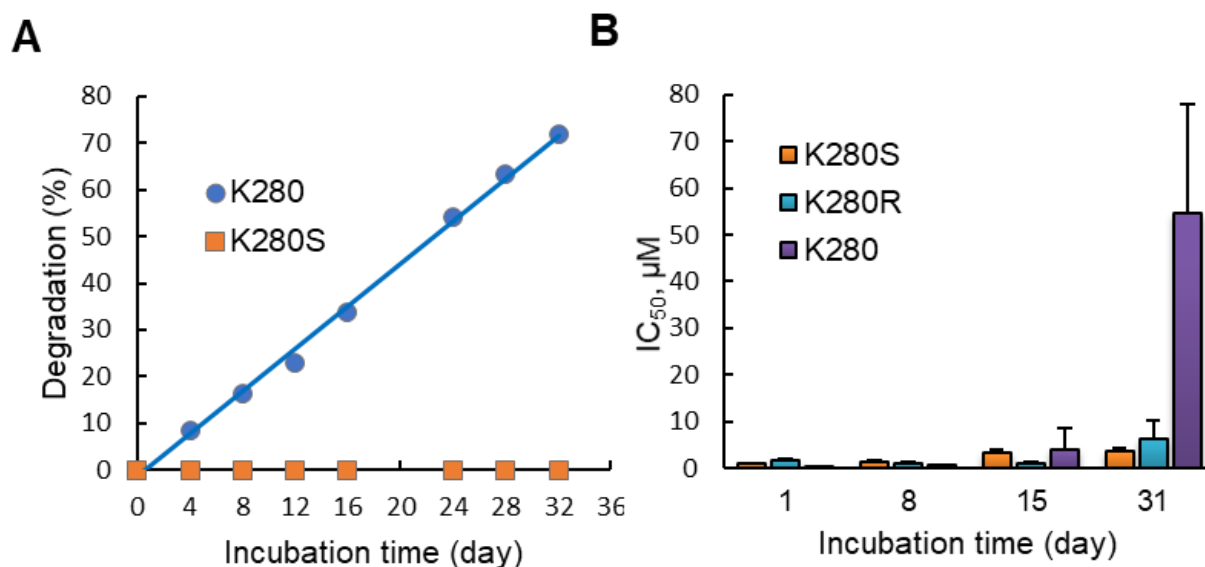
Figure 3.5 Improved stability of compound K280S as compared to K280. A. Degradation rate of K280 and K280S quantified from NMR spectra. **B**. IC_{50} values of K280, K280R and K280S over time.

3.5 Structure Activity Relationship of K280 Derivatives in PRMT Inhibition

Table 3.1 summarizes the SAR of the synthesized K280 derivatives in PRMT5 inhibition. The IC_{50} plots of the representative dihydropyrazine compounds are also shown in **Figure 3.1B**. Compound K280 displayed the most potent PRMT5 inhibition with IC_{50} of 371 nM, followed by K280S (IC_{50} = 818 nM) and K280R (IC_{50} = 1.8 μM). The R_1 hydrogen is essential for the activity: the two derivatives replacing the hydrogen with methyl or Boc significantly decreases the inhibitory activity; and the aromatized form (K280-2H) without this hydrogen also loses activity. The R_2 position can tolerate a single methyl substitution but not double methylations, probably due to the steric hindrance from the two methyl groups. Interestingly, the inhibitory activity of S form is better than the R form, which suggested the microenvironment in this region favors the S conformation over R. Bulkier R3 groups such as 4'-Cl-phenyl and 4'-biphenyl resulted in decreased inhibition, which may also due to the steric hindrance. Similar to R_1, the R_4 hydrogen is also very important, wherein replacing with acetyl

or Boc led to a significant decrease in inhibition. This position may form another hydrogen bond crucial for the inhibitor binding to the protein. The variance in R_5 resulted in several potent derivatives with submicromolar potencies, all bearing subtle extended alkyl groups connecting to the amide bond, which suggested that there is extra space in that area for further exploration. However, the hydrogen on the amide nitrogen is not replaceable (both $N(Me)CO_2Et$ and $N(Ac)$ CO_2Et lost activity). The carbonyl group is also essential, for which replacing with NH_2 decreases activity. In all, the above SAR suggested the importance of several positions that may potentially contribute to hydrogen bonds: the R_1 and R_4 hydrogens, R_5 amide hydrogen and the carbonyl group oxygens.

Table 3.1 SAR of K280 derivatives in PRMT5 inhibition
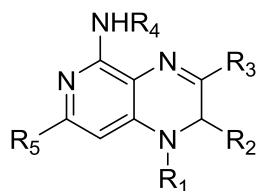
R_1	R_2	R_3	R_4	R_5	IC_{50} (μM, PRMT5)	Relative activity at 10 μM		Relative activity at 100 μM	
						PRMT5	PRMT1	PRMT5	PRMT1
Me	H	Ph	H	$NHCO_2Et$	-	74%	130%	3%	102%
Boc	H	Ph	H	$NHCO_2Et$	-	97%	103%	77%	90%
H	(S)-Me	Ph	H	$NHCO_2Et$	0.82	10%	-	0%	-
H	(R)-Me	Ph	H	$NHCO_2Et$	1.80	21%	-	2%	-
H	di-Me	Ph	H	$NHCO_2Et$	138	-	-	-	-
H	H	4'-Cl-phenyl	H	$NHCO_2Et$	-	49%	-	22%	0.49%
H	H	4'-biphenyl	H	$NHCO_2Et$	121	-	-	-	-
H	H	Ph	Ac	$NHCO_2Et$	-	123%	119%	-	-
H	H	Ph	Boc	$NHCO_2Et$	-	91%	87%	32%	34%
H	H	Ph	H	NH_2	23	67%	105%	21%	31%
H	H	Ph	H	$NHCONHCH_2Ph$	1.35	11%	95%	0%	58%
H	H	Ph	H	$NHCONHC_6H_{13}$	4.2	54%	93%	4%	47%
H	H	Ph	H	$NHCONHCH_2CH_2OH$	1.16	18%	93%	5%	77%
Aromatized K280 (K280 – 2H)			H	$NHCO_2Et$	200	79%	87%	81%	100%
Hydrogenated K280 (K280 + 2H)[1]			H	$NHCO_2Et$	0.47	-	-	-	-

[1]The purity of this compounds is 90%.

3.6 Mechanism of Action studies of K280

A molecular docking model was conducted to predict the binding mode of K280 to PRMT5 catalytic pocket and to explore mechanism underlying selective binding of K280 to PRMT5 (**Figure 3.6**). The protein sequence and crystal strucutre of PRMT5:MEP50 with a cofactor analog and the peptide substrate revealed that PRMT5 had a two-domain structure (**Figure 1.1** and **1.2**). The catalytic domain adopts the canonical arginine methyltransferase tertiary structure similar to type I PRMTs, with an AdoMet binding domain containing the nucleotide binding Rossmann fold, followed by a barrel-like domain involved in substrate binding (**Figure 1.1**, PRMT5 in blue, cofactor in yellow and peptide in magenta). However, the N-terminal domain (residues 13–292) of PRMT5 is a TIM barrel, which directely interacts with the MEP50 protein (**Figure 1.1**, MEP50 in green). The SAM-binding site and substrate arginine site were included for docking. **Figure 3.6B** showed the interaction mode of K280 with PRMT5. In this model, the amino groups of the the dihydropyrazine ring (R_1 and R_4) are stabilized by hydrogen bonds to the side-chains of Glu392 and Glu435 (**Figure 3.6D**). The residue Ala366 stabilizes K280 by accepting a proton from the amino group of $NHCO_2Et$ (R_5), while the residue Arg368 donates a proton to the carbonyl group of $NHCO_2Et$ (R_5) to form another hydrogen bond. The far end phenyl ring is in a hydrophobic environment surounding by Pro314, Leu315 and Cys449 (**Figure 3.6C**), further enhanced the binding of K280. This docking model suggested the importance of the hydrogen bonding between R_1, R_4 and R_5 to the receptor protein, which is conssistent with the SAR studies.
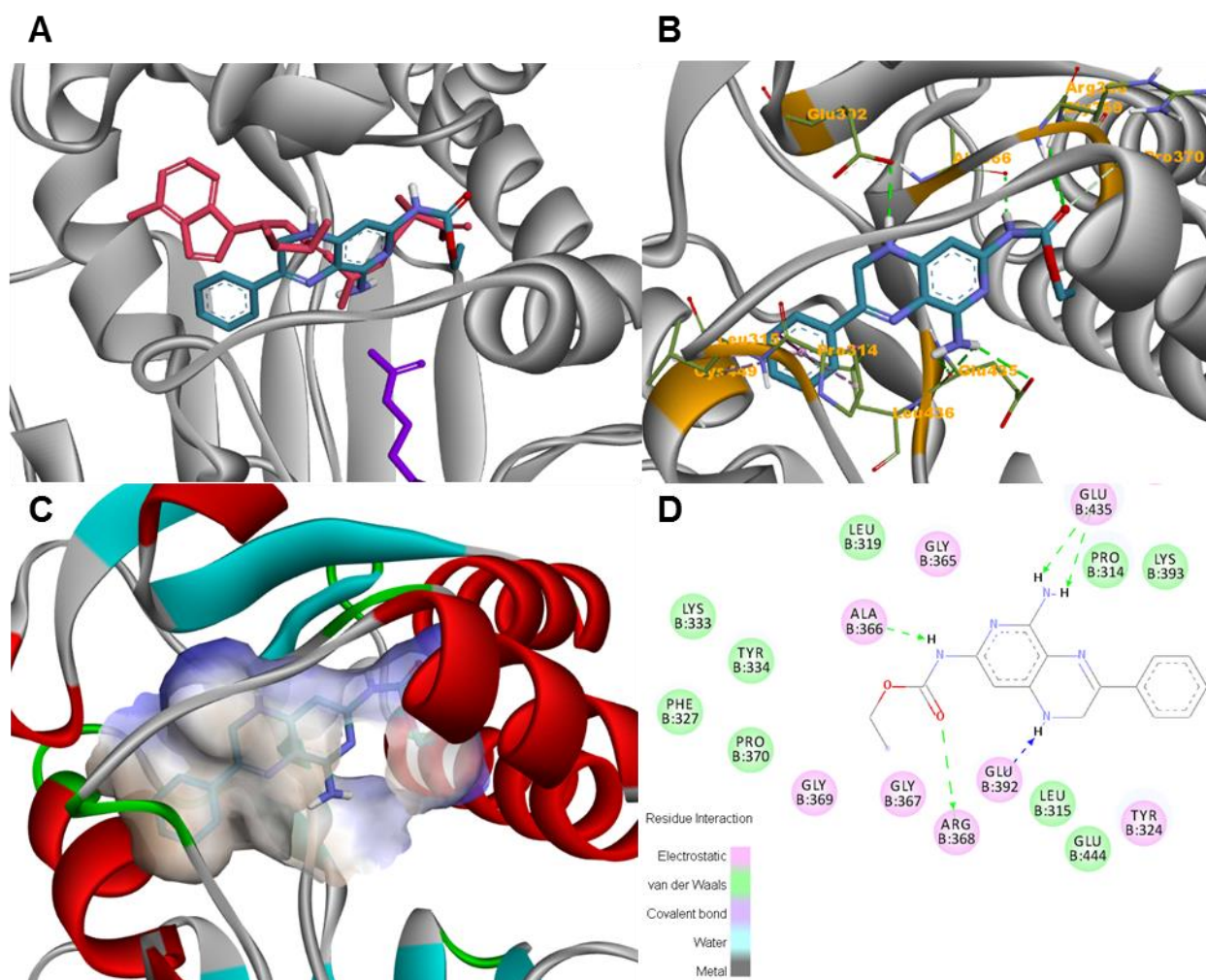
Figure 3.6 Proposed binding pose of K280 in PRMT5 catalytic cavity. A. Overlapped structures of K280 (orange) with cofactor analog (green) and substrate arginine (purple) in PRMT5 (grey, PDB: 4GQB) catalytic pocket. **B**. Detailed interactions of K280 with PRMT5 catalytic pocket residues. K280 is shown in blue sticks, PRMT5 residues involved in binding are labeled in orange. **C**. Hydrophobic surface of PRMT5 at K280 binding site (darker blue means less hydrophobic). **D**. 2D diagram of B. All figures are generated with Discovery Studio 4.0.

Further mechanistic study using enzyme kinetics indicated that compound K280 displayed a mixed type inhibition (**Figure 3.7**). The values of the K_{ii}/K_{is} parameter α (**Figure 3.7, A**. α = 0.19 for peptide and **B**. α = 0.34 for cofactor) were less than 1, which suggested that K280 uncompetitive feature of inhibition with respect to peptide and cofactor. This finding is consistent with the docking model, which shows that K280 partially overlaps with the SAM pocket and further extends toward the substrate arginine binding site (**Figure 3.6A**).
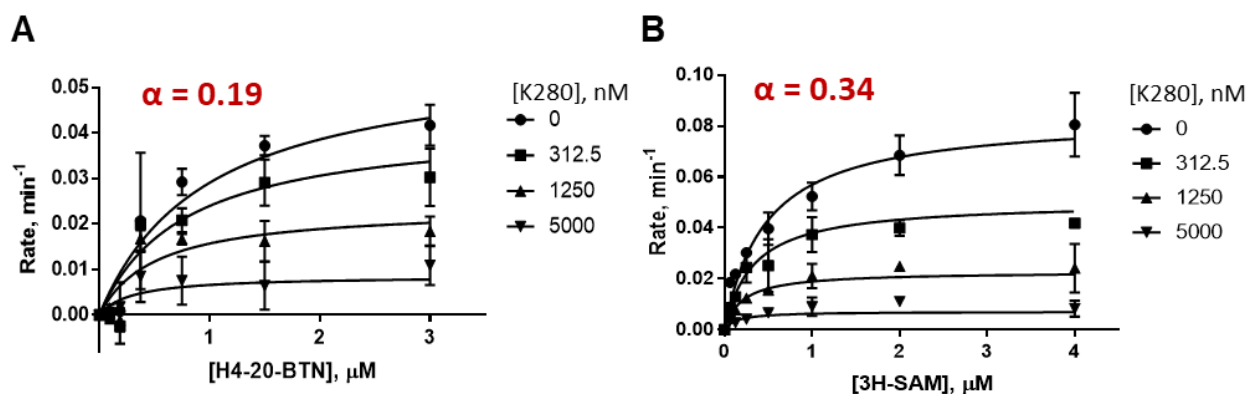
Figure 3.7 Mechanism of inhibition studies of K280. K280 displayed a mixed type inhibition, which is predominantly uncompetitive to the peptide (α = 0.19, **A**) and also predominantly uncompetitive to the cofactor (α = 0.34, **B**).

To obtain the structural information of this group of inhibitors binding to PRMT5 and to further validate the mode of action, attempts have been made to generate the co-crystal structure of K280S with PRMT5:MEP50 complex. Baculovirus protein expression system was adapted to allow large-scale production of PRMT5:MEP50 complex. Recombinant human PRMT5 [His-PRMT5 (1-637)] and MEP50 [His-MEP50(2-342)] baculoviruses were generated according to the Bac-to-bac protocol (Invitrogen) to co-infect SF9 cells. The harvested protein complex was purified on Ni-column and then size exclusion FPLC (Fast protein liquid chromatography), before it was concentrated to 10.5 mg/mL. The purity of the obtained complex is shown in **Figure S3.3A.** The enzymatic activity of the obtained protein complex is the same as the commercially available product from Reaction Biology Corp. (**Figure S3.3B**). In our preliminary

hanging-drop vapor diffusion experiment of the purified PRM5:MEP50 complex with 1 mM

MTA and 1 mM H4-20 peptide using 20% PEG3350 w/vol in the presence of 200 mM

ammonium sulfate as reservoir solution, needle-shaped crystals were observed (**Figure S3.3C**).

Unfortunately, this crystal would not render ideal X-ray diffraction. Further experiments are

needed to optimize the condition of the K280S co-crystallization with the protein complex.

**3.7 Target Validation and Anticancer Efficacy Assessment of K280S in Prostate Cancer
Cells and TRAMP-C2 Induced Prostate Cancer Mice Model**

(This work was conducted through collaboration with Nhat Quach, Wided Missaoui, Dr. Brian

Cummings and Dr. Tai Guo.)

PRMT5 expression was increased in prostate cancer LNCap and PC-3 cells, as compared

to non-cancerous prostate RWPE-1 cells (**Appendix B Figure S3.3a**). In order to validate that

K280 and K280S can inhibit PRMT5 activity *in vitro* and *in vivo*, and to assess their anti-cancer

efficacy, a series of experiments were conducted in prostate cancer cell lines and prostate cancer

mice.

First, the anti-proliferative effects of the inhibitors were examined in prostate cancer

cells. The growth inhibition potencies of K280 and K280S on RWPE-1 and PC-3 cells were

compared, along with colchicine (**Appendix B Figure S3.5a**). Colchicine showed a strong

toxicity to both non-cancer and cancer cells after 72-hr treatment, while K280S and K280

demonstrated a selectivity for PC-3 cells (**Appendix B Figure S3.5a)**. The PRMT5 inactive

analog, K280-2H, did not induce cytotoxicity in any cell line (**Appendix B Figure S3.5a)**, which

suggested minimal side effects were caused by this type of structures. The PRMT5-specific

inhibitor EPZ015666 only exhibited cytotoxicity after a longer exposure time up to 14 days with

a GI_{50} of ~500 nM (**Appendix B Figure S3.5b**). Further comparison of GI_{50} values from 24 to

72 hr showed that the effect of K280 derivatives on PC-3 cell growth was escalated in the later time points (**Appendix B Table S3.1**). To further profile the PRMT5 inhibitory activity of K280 and K280S, PRMT5 knockdown PC-3 cells (PRMT5 KD cells) was generated using PRMT5-targeting shRNA (**Appendix B Figure S3.3c**). With PRMT5 KD cells as a positive control, a reverse correlation of K280S concentration and global SDMA level was observed, while the ADMA level was not affected (**Appendix B Figure S3.4b**). Additionally, inhibition of PRMT5 resulted in a decrease in SDMA formation for histone H4R3, which is one of the major PRMT5 target sites in histones (**Appendix B Figure S3.4b**). Similar results were obtained for compound K280 (**Appendix B Figure S3.3d**). The above results indicated that K280 and its derivatives could target both PRMT5 enzymatic activity in prostate cancer cells, and the anti-proliferative selectivity of K280 and K280S for prostate cancer cells with PRMT5 overexpression suggested that PRMT5 might contribute to prostate cancer cell growth.

Second, because K280 and K280S were reported as tubulin binder that can inhibit microtybule formation, their inhibitory activity on tubulin polymerization was assessed by observing the changes of tubulin structure in cells treated with K280 or K280S (**Appendix B Figure S3.3d and Figure S3.4c**). Exposure of cells to 25 nM of K280S resulted in microtubule fibers degradation. In contrast, microtubule fibers remained relatively intact in PRMT5 KD cells. The above results indicated that K280 and K280S could inhibit tubulin polymerization in prostate cancer cells, however, PRMT5 enzymatic activity might not directly associate to the microtubule structure change.

Third, the therapeutic potential of K280S was assessed by its ability to inhibit cancer cell migration, cell adhesion and spheroid formation. Decreased migration was observed in the trans-well assay of both K280S treated PC-3 cells and shRNA-mediated PRMT5 KD cells (**Appendix**

B Figure S3.6a). Similar results were observed in cell adhesion assay (**Appendix B Figure S3.6b**). Further, we assessed spheroid formation of both 10 nM K280S-treated cells and shRNA-mediated PRMT5 KD cells, and showed that they reduced spheroids growth as compared with control cells (**Appendix B Figure S3.6c**). We correlated this to cell cycle using flow cytometry, and demonstrated that both K280S and PRMT5 KD induced a G2-M cell cycle arrest (**Appendix B Figure S3.6d**). Assessment of apoptotic markers (Bcl2 and Bax) showed that K280S did not alter their expression at a concentration of 25 nM, although changes were noticed at higher concentration (125 nM) (**Appendix B Figure S3.6e**).

To further verify the therapeutic potential of K280S *in vivo*, the ability of K280S to inhibit PRMT5 and tumor growth was examined using the xenograft C57BL/6 mice model induced with TRAMP-C2 cells[242]. Prior to conducting the animal study, we confirmed that PRMT5 expression was increased in TRAMP-C2 cells, as compared with host mouse tissues (**Appendix B Figure S3.8a**). We also confirmed the *in vitro* efficacy of K280S against TRAMP-C2 cells with GI_{50} of 35 nM, while no reduction in cell growth was detected with K280-2H with a concentration up to 1 μM (**Appendix B Figure S3.8b**). Initial K280S dosing studies resulted in the identification of doses ranging from 0.25 to 0.5 mg/kg. Doses higher than these tended to induce toxicity as indicated by reduced weight gain and morbidity when delivered via i.p. injection every 4 days. Increased tolerance was observed when a variable dose regimen was used, especially at the higher dose of 0.5 mg/kg. This resulted in the use of 3 dose regimens (0.25 mg/kg, 0.35 mg/kg and 0.5-0.25 mg/kg) (**Appendix B Figure S3.7a and Figure S3.8c**). Compared with the vehicle group, the dosing of 0.35 mg/kg and 0.5-0.25 mg/kg K280S markedly lowered tumor volume (**Appendix B Figure S3.7c**) and tumor weight (**Appendix B Figure S3.7d**) with no significant effect on body weight (**Appendix B Figure S3.7b**). Further,

western blot analysis of tumor samples showed dramatic reductions in total SDMA and H4R3 SDMA levels, as compared with vehicle control (**Appendix B Figure S3.7e**), which demonstrated that K280S had similar effect on PRMT5 inhibition and anti-cancer efficacy *in vivo* and *in vitro*.

3.8 Conclusions

Together, the work in this chapter demonstrated that compound K280 and K280S featuring the 1,2-dihydropyrido[3,4-b]pyrazine scaffold are potent PRMT5 inhibitors *in vitro* and *in vivo*. The biochemical potency of K280 is 371 nM for PRMT5:MEP50, while a more stable compound K280S is 818 nM. Enzyme kinetics analysis of K280 showed a mixed-type inhibition pattern, which uncompetitive feature to both substrate and cofactor. The proposed binding pose of K280 also supported this mode of inhibition. The SAR and docking analysis results suggested a few important interactions formed by the amine hydrogens and carbonyl group of K280 to the receptor catalytic pocket residues. K280 and K280S showed strong anticancer efficacy selective to the prostate cancer cells, and K280S reduced tumor growth in prostate cancer mice.

These compounds possess interesting profile targeting both PRMT5 and tubulin in cancer treatment. The previous pre-clinical studies of its representative compound K280S (CI-980) had showed significant activity against a broad spectrum of tumors including multidrug resistance tumors, and favored a prolonged treatment[243]. Interestingly, cellular studies of K280S showed a discrepancy with its ability to inhibit microtubule formation, which led to the suspicion that K280S had "multiple and independent mechanisms of action"[237]. Our data demonstrated that one of these mechanisms might be PRMT5 inhibition. In previous clinical studies, K280S was generally well tolerated. The main obstacle for its advance was the limited efficacy[244], and the reason is not clear yet. Based on our data and the prior study that PRMT5 inhibition may favor a

long-term treatment[235], we think drug schedule could be one possible reason. In Phase II clinical trials, CI-980 was delivered as a 72- hour continuous intravenous infusion every three weeks. Under this circumstance, it is likely that the PRMT5 inhibitory activity was not fully executed due to the rapid clearance of this compound. Therefore, alternate schedule or formulation favoring sustained long-term delivery would be more beneficial for tumors with PRMT5 overexpression. Another reason could be the misregulation of PRMT5 is not the same in different cancers, meaning some cancer types may not be sensitive to PRMT5 inhibition. Regardless, this combinatory inhibition of PRMT5 and tubulin is unique and warrants further study. Although the interaction and coordination of these two targets are not clear at this moment, both targets are intensively involved in carcinogenesis in their own respective. Further tailoring the potency of K280S for these two targets may enhance optimal synergistic benefits while minimizing the side effects of drug.

CHAPTER 4

DETECTION OF PRMT INHIBITORS WITH STOPPED FLOW FLUORESCENCE

This work was submitted to *Signal Transduct. Target Ther.* as: Qian, K., Hu, H., Xu, H., Zheng, Y.G. (2017) Detection of PRMT1 Inhibitors with Stopped Flow Fluorescence.

4.1 Introduction

Protein arginine methylation as one of the universal posttranslational modifications (PTMs) plays substantial biological roles in eukaryotic organisms, which is mediated by the family of protein N-arginine methyltransferases (PRMTs)[14]. Thus far, nine PRMT members are found in mammalian cells[29], which are classified into three major types: type I, type II and type III PRMTs. Type I enzymes (PRMT1, -2, -3, -4, -6, and -8) convert arginine residue to monomethyl arginine (MMA) and further to asymmetric dimethyl arginine (ADMA); type II enzymes (PRMT5 and PRMT9) produce MMA and symmetric dimethyl arginine (SDMA); PRMT7 is the only type III enzyme that generates MMA. The global arginine levels in the mouse embryo fibroblast (MEF) cells are found to be 1500:3:2:1 for Arg:ADMA:MMA:SDMA, while PRMT1 is the major type I enzyme that accounts for 50% of ADMA formation[2, 13]. During PRMT catalysis, one or two hydrogen atom(s) on the ω-N^G of arginine substrate is (are) replaced by the methyl group from S-adenosylmethionine (SAM or AdoMet), generating methylated arginine and leaving S-adenosyl homocysteine (SAH or AdoHcy) as the side product[29]. PRMTs methylate numerous protein substrates in nucleus, cytoplasm, and membranes[14]. Studies reveal the diverse function of PRMTs in signal transduction, transcriptional coactivation, RNA splicing and DNA repair, while its many other roles remain unclear[36]. Moreover, misregulation or aberrant expression of PRMTs are

associated with various pathological conditions. For example, PRMT1 was found overexpressed or aberrant in breast, prostate, lung, colon, and bladder cancers, and leukemia[10, 36]. It is also upregulated in pulmonary diseases such as pulmonary fibrosis, pulmonary hypertension, chronic obstructive pulmonary disease (COPD), and asthma[22]. Further, PRMT1 plays regulatory roles in cardiovascular disease, diabetes, and renal diseases[4]. Therefore, development of PRMT inhibitors has become an emerging and imperative task for their potential use as novel therapeutic agents to treat diseases and as tools to investigate biological functions of PRMTs[9, 22, 31].

In the past decade, both academic and industrial laboratories have invested numerous efforts to discover and develop PRMT inhibitors possessing adequate potency and isoform selectivity[12, 18, 22, 25, 31]. Discovery of PRMT inhibitors relies on efficient and effective biochemical assays for PRMT activity measurement and inhibitor characterization[3, 7, 20, 22, 27, 28, 32]. Radiometric assays are the gold standards for biochemical methyltransferase activity measurement of PRMTs due to their high sensitivity and reliability[22]. In this type of assay, the radioisotope-labeled methyl group from cofactor ($[^3H]$-SAM or $[^{14}C]$-SAM) is transferred to a peptide or protein substrate during the enzymatic reaction[22]. Then the products are separated from unreacted SAM and quantified by autoradiography or liquid scintillation counting. The scintillation proximity assay (SPA) is able to achieve mix-and-measure procedure without product separation, in which the signal is induced through micrometer proximity of the biotinylated substrates with ^3H labeled methyl group to the streptavidin-coated scintillants, while the excessive SAM molecules in solution are too far away to produce signals[34]. This format can be applied to high-throughput library compound screening[34]. However, one obvious drawback of this type of assays is the involvement of radioactive reagents, which requires strict environmental safety regulation. Another type of assays is antibody-based, represented by enzyme-linked immunosorbent assay

(ELISA), in which a methylarginine-specific antibody is used to recognize products of the reaction and a secondary antibody is used as probe for signal detection[22]. A few enzymatically-coupled assays have also been developed to detect generation of the side product SAH for PRMT activity measurement, which often convert SAH into derivatives bearing colorimetric, fluorescent, or luminescent properties for the measurement[1, 8, 15, 19, 23, 33]. These assays are nonradioactive and sensitive, however, introducing additional components in the assay potentially complicate the results. Especially for inhibitor screening, the coupling components could possibly interact with the inhibitors and lead to false positives. Furthermore, due to the limitation of detection methods, all of the above assays require quenching the reaction at certain time points and convert products into other chemical species for signal generation, therefore difficult to monitor the reaction progression *in situ*. In this article, we have developed a stopped flow fluorometric platform to detect and characterize PRMT1 inhibitors, which possesses advantages of being homogeneous and nonradioactive, and can be implemented through simply mix-and-measure procedure. To our knowledge, this is the first continuous assay for PRMT reaction detection and inhibitor characterization.

4.2 Materials and Methods

4.2.1 Protein expression

Recombinant His-tagged rat PRMT1 was expressed in *E. coli* and purified with Ni-charged His6x-tag binding resin as reported previously[17, 21]. In brief, the mouse PRMT1-pET28b plasmid was transformed into BL21(DE3) (Stratagene) by heat shock method. Transformed bacteria were incubated in LB media at 37°C for growth and then at 16°C for protein expression with 0.3 mM IPTG induction. Cells were harvested by centrifuge and lysed using a microfluidics cell disrupter. The supernatant containing PRMT1 protein was loaded onto the Ni-charged His6x-tag binding

resin (Novagen) in equilibrium buffer (25 mM Na-HEPES, pH 7.0, 300 mM NaCl, 1 mM PMSF, and 30 mM imidazole). Beads were washed thoroughly by washing buffer (25 mM Na-HEPES, pH 7.0, 300 mM NaCl, 1 mM PMSF, and 70 mM imidazole), and protein was eluted with elution buffer (25 mM Na-HEPES, pH 7.0, 300 mM NaCl, 1 mM PMSF, 100 mM EDTA, and 200 mM imidazole). Protein purity was checked using a 12% SDS-PAGE, and concentrations were determined by the Bradford assay[5].

4.2.2 Peptide synthesis

In all the stopped flow fluorescence assays, H4FL peptides (N-terminal 20 amino acids of histone H4, fluorescein labeled on Lys-10 substituting for Leu-10) were used as probes[16]. H4FL was synthesized using Fmoc-based solid phase peptide synthesis (SPPS) protocol on a PS3 peptide synthesizer (Protein Technology, Tucson, AZ) as described previously. Each amino acid was coupled to the solid phase with 4 equiv of amino acid with HCTU [O-(1H-6-chlorobenzotriazole-1-yl)-1,1,3,3- tetramethyluronium hexafluorophosphate] (Novabiochem, Darmstadt, Germany). The Fmoc group was deprotected with 20% v/v piperidine/DMF, and the N-terminal amino acid was acetylated with acetic anhydride. The peptide was cleaved from the Wang resin by a cleavage solution consisting of 95% trifluoroacetic acid (TFA), 2.5% H_2O, and 2.5% triisopropylsilane. It was then precipitated in cold ether and pelleted by centrifugation. Crude peptides were collected and purified using a Varian Prostar instrument equipped with a C18 reversed-phase high performance liquid chromatography (RP-HPLC) column, where 0.05% TFA containing water and 0.05% TFA-containing acetonitrile were two mobile phases used in gradient purification. The identity of peptides were confirmed by MALDI-MS. Concentrations of the peptides were calibrated according to the absorption of fluorescein at 492 nm.

4.2.3 Stopped-flow fluorescence assay

In a stopped flow fluorescence assay, binding of H4FL to PRMT1 (or PRMT1−cofactor complex) quenches the peptide fluorescence, while release of the peptide restores the fluorescence. The fluorescence signal change was detected at room temperature on an Applied Photophysics Ltd (UK) stopped flow equipment using an excitation wavelength of 495 nm and a long pass emission filter centered at 510 nm. The widths of the entrance and exit slits of the monochromator were set to 0.5 mm. An equal volume of samples from two syringes was driven into the observation cell for mixing measurement. The H4FL concentration of all experiments were 0.4 μM. Typically, the enzyme PRMT1 was pre-mixed with H4FL and loaded into one syringe, while the mixture of SAM and H4FL with or without the inhibitor was loaded into the other syringe. For inhibition assay measurements, the enzyme and H4FL solution were mixed with the SAM, H4FL and inhibitor solution at the following final concentrations: 0.2 μM PRMT1, 0.4 μM of H4FL, 3.5 μM of SAM, with increasing concentration of different inhibitors. The fluorescent signal was recorded up to 900 seconds, with a total data points of 10000. Data of four to six drives were collected and averaged for each curve.

After averaging the shot data, the association time courses were fitted to a double-exponential function (equation 2) using GraphPad Prism. The methylation time course exhibited two distinct kinetic phases. F is the fluorescence intensity at time t, k_1 and k_2 are the rate constants for Phase I and Phase II, a is the amplitude of the fluorescence change for k_1, and b is the amplitude of the fluorescence change for k_2. Simulation curves based on the values of a, b, k_1 and k_2 at fixed $c = 1$ were produced by Matlab. The IC$_{50}$ value of inhibitors is determined by equation 1 using GraphPad Prism. The equation 1 and 2 are shown below:

Relative Activity= $1/(1+([\text{Inhibitor}]/\text{IC}_{50}))$ (1)

$$F = a \cdot exp(-k_1 \cdot t) + b \cdot \exp(-k_2 \cdot t) + c \qquad (2)$$

4.2.4 Radiometric filter-binding assay

Peptide substrate, inhibitor and [^{3}H]-SAM were preincubated in the reaction buffer for 2 min prior to initiation of the methyl transfer reaction by adding the enzyme (30 µL total volume) at room temperature. The final concentrations of PRMT1, ^{3}H-SAM, and H4 peptide are 0.02, 0.5, and 1 µM, respectively. The reaction buffer contains 50 mM HEPES (pH 8.0), 50 mM NaCl, 1 mM EDTA, and 0.5 mM DTT. The reaction was quenched by 30 µL of isopropanol, followed by spotting the reaction mixture on separate squares of P81 Ion Exchange Cellulose Chromatography Paper (Reaction Biology Corp, item number: IEP-01). Then the paper was air dried for 30 min before washed with 50 mM NaHCO$_3$, pH 9 for 3 times. Then the paper squares were dried in air overnight before transferred into 3.5 mL vials full of scintillation oil, and the amount of methylation was quantified by scanning the vials on a scintillation counter (Beckman Coulter, Brea, CA). The background control only contained [^{3}H]-SAM and the substrate. Reaction sample readouts subtracted by the background were normalized with the reaction without inhibitor and fitted by **equation 1** to obtain IC$_{50}$ values. The reported value was calculated based on the average of two experiments and shown with standard deviations.

4.3 Fluorescent Changes of Fluorescein-Labeled Histone H4 Peptide during PRMT1 Catalysis

PRMT1 is the major type I enzyme responsible for asymmetric arginine dimethylation[2]. PRMT1 transfers the methyl group from SAM to a guanidine nitrogen of arginine to form MMA, which can be further methylated into ADMA (**Figure 4.1A**) [2]. Stopped-flow is a powerful technique to study transient kinetics of enzymes[6]. Recently, by detecting intrinsic tryptophan fluorescence changes of PRMT1 together with global fitting analysis, we elucidated the major

kinetic steps of PRMT1 catalysis with resolved rate constants (k_{on} and k_{off}) for individual steps, which provided important mechanistic insights of how PRMTs interact with their substrates and catalyze the methyl transfer reaction[21]. In addition, we designed and synthesized fluorescein-labeled substrate peptides as fluorescent reporters to probe arginine methylation reaction[16]. One such probe is a fluorescein-labeled 20-residue histone H4 N-terminus tail peptide: acetyl-SG**R**GKGGKGK(FL)GKGGAKRHRK (abbreviated as H4FL), which the methylation site resides on arginine-3 and fluorescein group is attached to the side chain of residue lysine-10 (**Figure 4.1B**). The kinetic parameters[17] of the fluorescent peptide are comparable to the natural substrate, the 20 residue H4 N-terminus tail peptide (H4-20: SGRGKGGKGKGKGGAKRHRK). The apparent K_m and k_{cat} values for H4-20 are 0.64 ± 0.04 μM and 0.81 ± 0.01 min^{-1}, while the K_m and k_{cat} values for H4FL are 0.50 ± 0.05 μM and 0.43 ± 0.01 min^{-1}. In the previous study[17], we observed a biphasic progression curve of PRMT1-catalyzed methylation of H4FL under the condition that the cofactor SAM is saturating the enzyme ([PRMT1] = 2 μM, [SAM] = 100 μM, [H4FL] = 0.4 μM). In this study, we measured the stopped flow fluorescence curve of PRMT1 catalysis under a different condition ([PRMT1] = 0.2 μM, [SAM] = 3.5 μM, [H4FL] = 0.4 μM) and the same pattern of progression curves was observed, in which there was a decay phase (Phase I) until a minimum (the lowest point) was reached, followed by an increasing phase (Phase II) until it approached to a plateau, as illustrated in **Figure 4.2**.
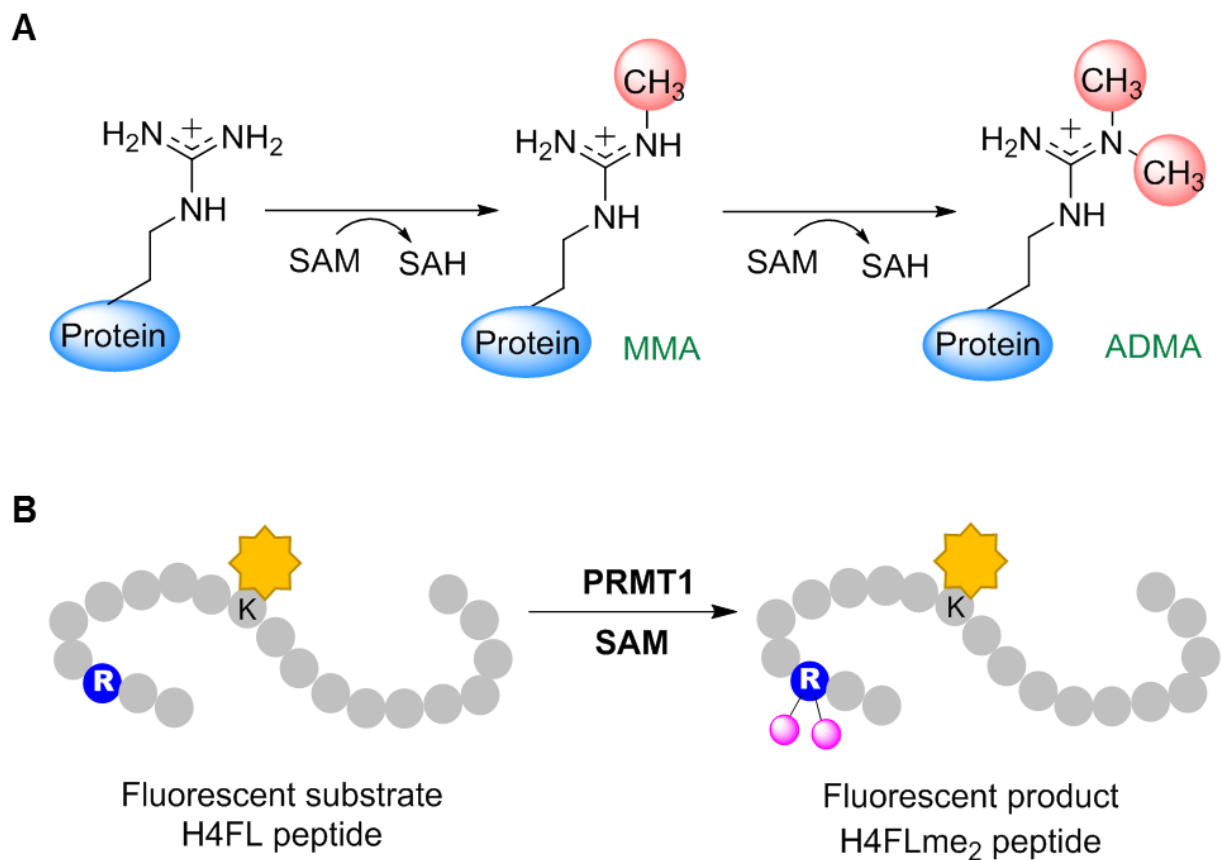
Figure 4.1 Arginine methylation by PRMT1. A. PRMT1-mediated methylation reaction. **B.** Symmetric dimethylation of the fluorescent peptide H4FL.
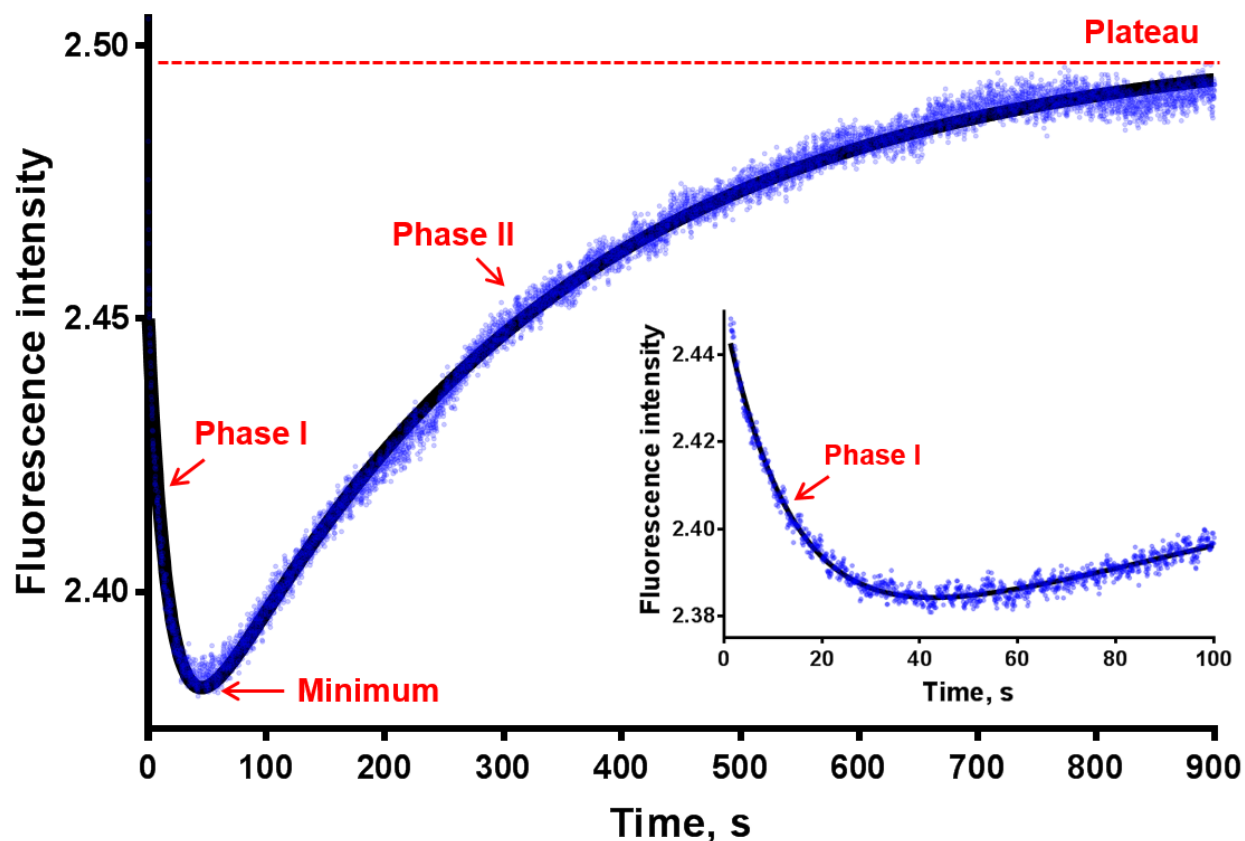
Figure 4.2 Time course of PRMT1 methylation (1 s to 900 s). The raw data (total of 10,000 points) are shown in blue dots. The curve fitted by **equation 2** is shown in solid black line, which is an average of 4 or 5 replicates. An amplified view of 1 s - 100 s is shown on the side. The concentrations of the enzyme, cofactor and substrate are as following: [PRMT1] = 0.2 μM, [SAM] = 3.5 μM, [H4FL] = 0.4 μM.

A critical question is regarding the mechanism underneath the biphasic phenomenon of the progression curve of H4FL methylation (i.e. the fluorescence first decreased and then went up). During the progression of methylation reaction, the substrate peptide H4FL, monomethylated peptide H4FLme$_1$ (acetyl-SG**Rme**GKGGKGK(FL)GKGGAKRHRK), asymmetric dimethylated peptide H4FLme$_2$ (acetyl -SG**Rme$_{2a}$**GKGGKGK(FL)GKGGAKRHRK) and many intermediate species of binary or ternary complexes were involved. Based on our established PRMT1 kinetic model[21], we used KinTek Explorer 5.2 to simulate the concentration changes of the relevant species during the methylation time course under the condition of [PRMT1] = 0.2 μM, [SAM] = 3.5 μM and [H4FL] = 0.4 μM (**Figure S4.1A**). In the very beginning of the reaction, substrate H4FL quickly forms enzyme-H4FL complex (E•H4) and enzyme-cofactor-H4FL complex (E•SAM•H4), and undergoes a conformational change (F•SAM•H4), which overall reflected as a sharp decrease in total free H4FL concentration. Later, the F•SAM•H4 ternary complex turns into mono-methylated product (H4FLme$_1$), and the concentration of free H4FLme$_1$ increases while the concentration of free H4FL decreases. H4FLme$_1$ can form binary or ternary complexes with the enzyme and the cofactor during the process. The mono-methylated peptide is further converted into the dimethylated product, H4FLme$_2$. As the reaction moves forward, substrate H4FL and H4FLme$_1$ concentrations continues to decrease while the H4FLme$_2$ concentration increases. The concentrations of all the other binary or ternary intermediates also decreases, except for E•H4me$_2$, E•SAM•H4me$_2$ and F•SAM•H4me$_2$. Overall, the expected conversion of the substrate H4FL to the intermediate H4FLme1 and to the product H4FLme2 is observed.

The key to deconvolve such biphasic fluorescent signal changes is the relative fluorescence intensity values of the free peptides and the related complexes. In the binary binding assay of the fluorescein-labeled peptides (H4FL, H4FLme$_1$ and H4FLme$_2$) and PRMT1, we noticed that the

fluorescent signal decreased over time[17]. The observed overall fluorescence intensity can be defined as $f_p \cdot [\text{H4FL}] + f_c \cdot [\text{E} \bullet \text{H4FL}]$, in which the fluorescence factor is f_p, μM^{-1} for the free peptide and f_c, μM^{-1} for the complex. In the stopped flow assays, we mixed excess amounts of PRMT1 in three concentrations (2, 4 or 6 μM) with H4FL, H4FLme$_1$ and H4FLme$_2$ peptides at 0.4 μM. The raw data in **Figure S4.2**, **Figure S4.3** and **Figure S4.4** were analyzed by global fitting function of KinTek explorer 5.2 software based on the reported k_{on} and k_{off} values[17] of each fluorescent peptide. For H4FL, the values of f_p and f_c are 6.4 μM^{-1} and 5.6 μM^{-1}; for H4FLme$_1$, the values of f_p and f_c are 5.4 μM^{-1} and 3.8 μM^{-1}; for H4FLme$_2$, the values of f_p and f_c are 5.9 μM^{-1} and 3.9 μM^{-1}. Not surprisingly, f_p is always larger than f_c. The f_p values of the three fluorescent peptides are similar, possibly because the small size of the methyl group and the long distance between the methylation site arginine-3 and the fluorescein on lysine-10 have minimized the effect of methylation on the fluorescence. Upon binding with PRMT1, the fluorescein group on the peptide substrate is likely exposed to a different physicochemical environment, which results in reduced fluorescence from the complexes.

Based on the above observations and analysis, we propose that the two phases of the H4FL methylation time course is an overall result of the concentration changes of the species involved in the methylation process and their differences in fluorescence intensity. The fluorescence intensity of the free peptides are relatively higher than their corresponding complexes; consequently, when there are more free peptides in the mixture, the overall florescence intensity is higher. Similarly, if there are less free peptides, the overall florescence intensity will be lower. Therefore, upon mixing the reaction components, H4FL first forms binary or ternary complexes with E and SAM while the amount of the free H4FLme$_1$ or H4FLme$_2$ is very small, which leads to a decreased total concentration of free peptides reflected as overall decreasing curve in Phase I.

In the later stage, as more substrates have been reacted, the methylated products are formed and released from the enzyme due to its intrinsic low affinity[21], and the total concentration of the free peptides increases, which is reflected as the increasing curve of Phase II. As a result, the methylation process of the fluorescein-labeled substrate is represented by the overall fluorescence intensity change, and Phase I is likely related to peptide substrate binding while Phase II is likely related to peptide product formation.

4.4 Use of the Stopped Flow Fluorescence Assay for PRMT1 Inhibition Measurement

Compared to non-continuous methods, stopped flow spectroscopic measurement can rapidly mix two components within a few milliseconds. This technology allows to measure the fluorescent signals at any stage of the reaction and to continuously monitor the entire process. The total progression time curve can provide mechanistic and quantitative information of how an enzyme regulator, such as a small molecule inhibitor, affects the enzymatic reaction. In the stopped flow fluorescence assay, we chose the balanced condition ([PRMT1] = 0.2 µM, [H4FL] = 0.4 µM and [SAM] = 3.5 µM), which the concentration of substrate H4FL and cofactor SAM is close to their Km values (Km of H4FL is 0.50 ± 0.05 µM, Km of SAM on H4FL is 3.1 ± 0.46 µM)[17, 24], in order to indiscriminately characterize competitive, uncompetitive and noncompetitive PRMT1 inhibitors. Again, the methylation time course of H4FL peptide showed a biphasic pattern: the fluorescence first decreased until the minimum (at 40 seconds), then raised up to a plateau (**Figure 4.2**). This biphasic time course was analyzed using a double exponential equation (**equation 2**), which resulted in five parameters: $a = 0.06974 \pm 1.90\text{E-04}$, $k_1 = 0.06161 \pm 3.34\text{E-04}$ s^{-1}, $b = -0.1115 \pm 9.25\text{E-05}$, $k_2 = 0.004804 \pm 1.15\text{E-05}$ s^{-1} and $c = 2.501 \pm 1.03\text{E-04}$ (**Table S4.1A**). The first part of the equation $F1 = a \cdot exp(-k_1 \cdot t)$ is dominant in Phase I (the decay phase), the amplitude parameter a and the rate constant k_1 (s^{-1}) together describe the decreasing trend of the

curve. The second part of the equation $F2 = b \cdot \exp(-k_2 \cdot t)$ is dominant in Phase II (the increasing phase), while the amplitude parameter b and rate constant k_2 (s^{-1}) together describe the increasing trend of the curve. The plateau of the curve represents the endpoint when no more methylated product is generated. The parameter c is the fluorescence intensity of the endpoint. The value of c can be normalized to any number without affecting the fluorescence amplitude values (a and b) and the rate constant values (k_1, k_2).

To obtain the IC$_{50}$ of a specific inhibitor, the relative activities of the enzyme in presence of different concentrations of the inhibitor are required (**equation 1**)[11]. In a typical non-continuous assay (e.g. radiometric filter binding assay), we need to determine a time course under the desired experimental condition for optimal reaction time. The chosen reaction time should stay within the initial condition to ensure the relationship between the readouts, i.e., counts per minute (CPM), and the time (t) is linear. Within this period, the concentration of the product has minimal influence on the rate of the reaction, and the reaction time course can be described as $y = K \cdot t$, where K is the rate of the reaction (e.g. μM·s^{-1}) as well as the slope value of the linear curve. By adding different concentrations of the inhibitor to the reaction mixture, the relative activity of the enzyme can be obtained by normalizing K with the reaction rate without the inhibitor, and calculate the IC$_{50}$ value using **equation 1**. In our stopped flow fluorescence assay, the reaction rate of Phase I and Phase II can be obtained from approximation and derivation of the double exponential equation (**equation 2**). In Phase I, during a very short period of time (t is small), the curve is nearly linear and the exponential equation can be approximately described as $F1 = a \cdot (-k_1) \cdot t$. Therefore, the derivation of the function F1 equals to $-k_1 \cdot a$, which is the slope value of Phase I. Similarly, the curve of Phase II at early stage can be approximately described as $F2 = b \cdot (-k_2) \cdot t$. The derivation of this function F2 equals to $-k_2 \cdot b$, which is the slope value of Phase II. The slope

values at various inhibitor concentrations are normalized to the slope value without the inhibitor present to obtain the corresponding relative enzyme activity, which can be used to calculate the potency value (IC_{50}) of the inhibitor using **equation 1**.

4.5 Effect of Enzyme Concentrations on the Stopped Flow Time Courses

Firstly, to observe the effects of enzyme on the stopped flow fluorescence response, we measured the time courses at different concentrations of PRMT1 from 0.05 μM to 0.4 μM. The obtained progression curves are shown in **Figure 4.3A** and **Figure 4.3B**, which were fitted by **equation 2**. The calculated *a*, *b*, k_1, k_2 values are summarized in **Table S4.1A**. Since the concentration of the substrate H4FL was fixed for all the reactions, we can arbitrarily normalize the plateau fluorescence intensity value *c* to 1 (**Figure 4.3B**). When the enzyme concentration increased, the minima shifted from 65 s to 24 s and the shape of the curve near the minimum became sharper (**Figure 4.3B**), which indicated that the rates of both Phase I and Phase II increased when more PRMT1 was present in the reaction mixture. Indeed, the values of *a*, k_1, |*b*| and k_2 increased with increasing concentration of PRMT1: *a* increased from 0.01079 to 0.09437, k_1 increased from 0.04187 to 0.09452 s^{-1}, |*b*| increased from 0.01117 to 0.156 and k_2 increased from 0.00287 to 0.006924 (**Table S4.1A**). The calculated slope values of Phase I increased from 4.52E-04 to 8.92E-03 s^{-1}, and the slope values of Phase II increased from 4.52E-04 to 8.92E-03 s^{-1} (**Table S4.1B**). When we plotted the *a*·k_1 or -*b*·k_2 values with respect to the PRMT1 concentrations, a linear relationship was observed (**Figure 4.3C** and **4.3D**). This result indicated that the initial rates, reflected by the slope values, of Phase I and Phase II was linearly proportional to the concentration of PRMT1 under the assay condition.

Figure 4.3. **Time course of PRMT1 methylation by varying the enzyme concentrations. A**. The curves are fit with **equation 2** to generate values in **Table S4.1A**. Each fitting curve used 10,000 data points, but only 50 data points are shown. Each curve is an average of 4 to 6 replicates. **B** is the simulation results from values in **Table S4.1A** at fixed c = 1. **C** and **D** represent the relationship of slope values (a·k_1 and b·k_2) with varying concentrations of PRMT1 (values listed in **Table S4.1B**). The linear fitting curves are shown in solid black line. The concentrations of the cofactor and the substrate are fixed at [SAM] = 3.5 µM, [H4FL] = 0.4 µM in these experiments.

4.6 Effect of Cofactor SAM Concentrations on the Stopped Flow Time Courses

After we measured the effects of enzyme on the reaction, we measured the stopped flow fluorescence responses at varied SAM concentrations (1.5 µM, 3.5 µM, 7.5 µM and 15 µM). The obtained progression curves were shown in **Figure 4.4A** and **Figure 4.4B**, and the calculated a, b, k_1, k_2 values were summarized in **Table S4.2A**. For clarity, again we normalized the plateau fluorescence intensity value c to 1 (**Figure 4.4B**). The time reaching the minimum was shortened as the SAM concentration increased (the minima were shifting to the left). It was also clear that when the concentration of SAM went higher, the slopes of the curve near the minimum became sharper. The values of all the parameters, a, k_1, $|b|$ and k_2, increased with increasing concentration of SAM: a increased from 0.0482 to 0.1992, k_1 increased from 0.04402 to 0.2476 s^{-1}, $|b|$ increased from 0.07363 to 0.2664 and k_2 increased from 0.002713 to 0.01175 (**Table S4.2A**). We plotted the values of $a \cdot k_1$ or $-b \cdot k_2$ against the SAM concentrations (**Figure 4.4C** and **Figure 4.4D**). The slope values of Phase I increased from 2.12E-03 to 4.93E-02 s^{-1} and the slope values of Phase II increased from 2.00E-04 to 3.13E-03 s^{-1} (**Table S4.2B**). The above results indicated that the slope values of Phase I or Phase II and the concentrations of SAM are in a linear relationship.
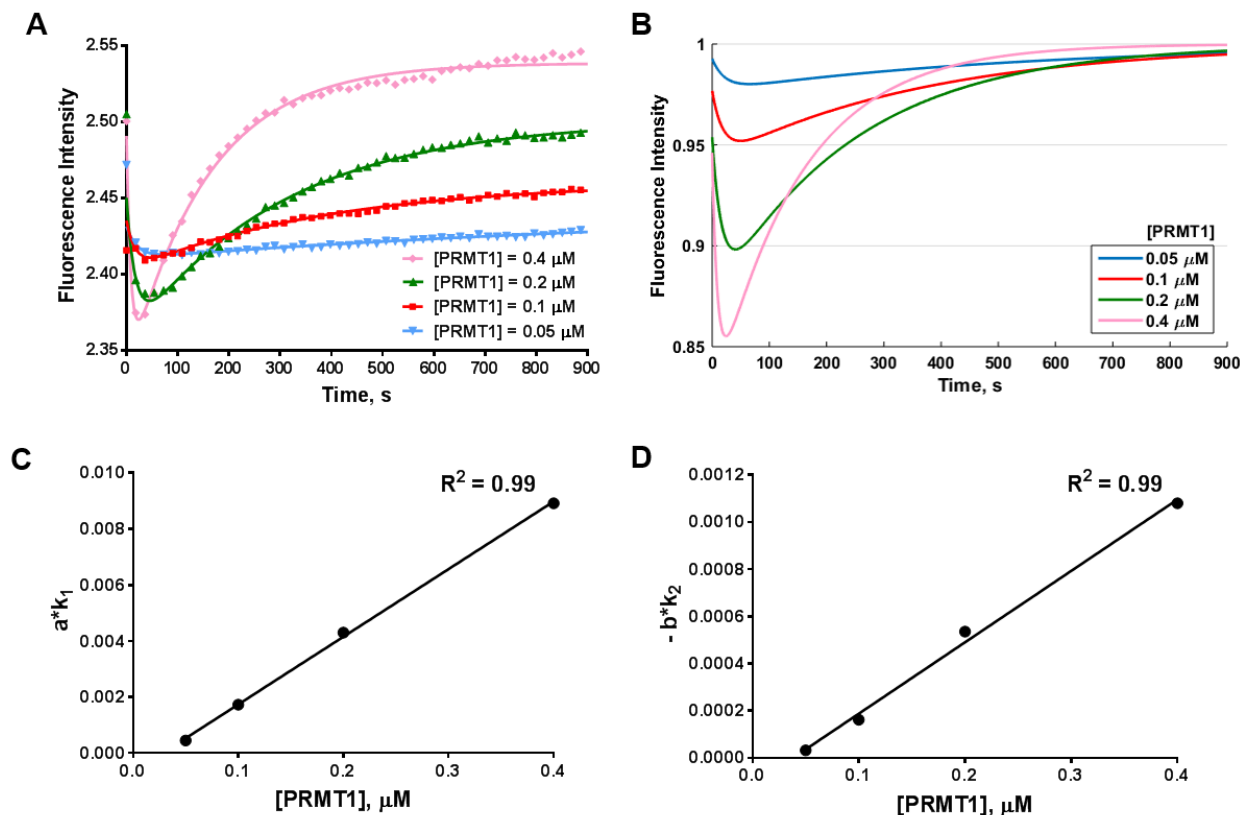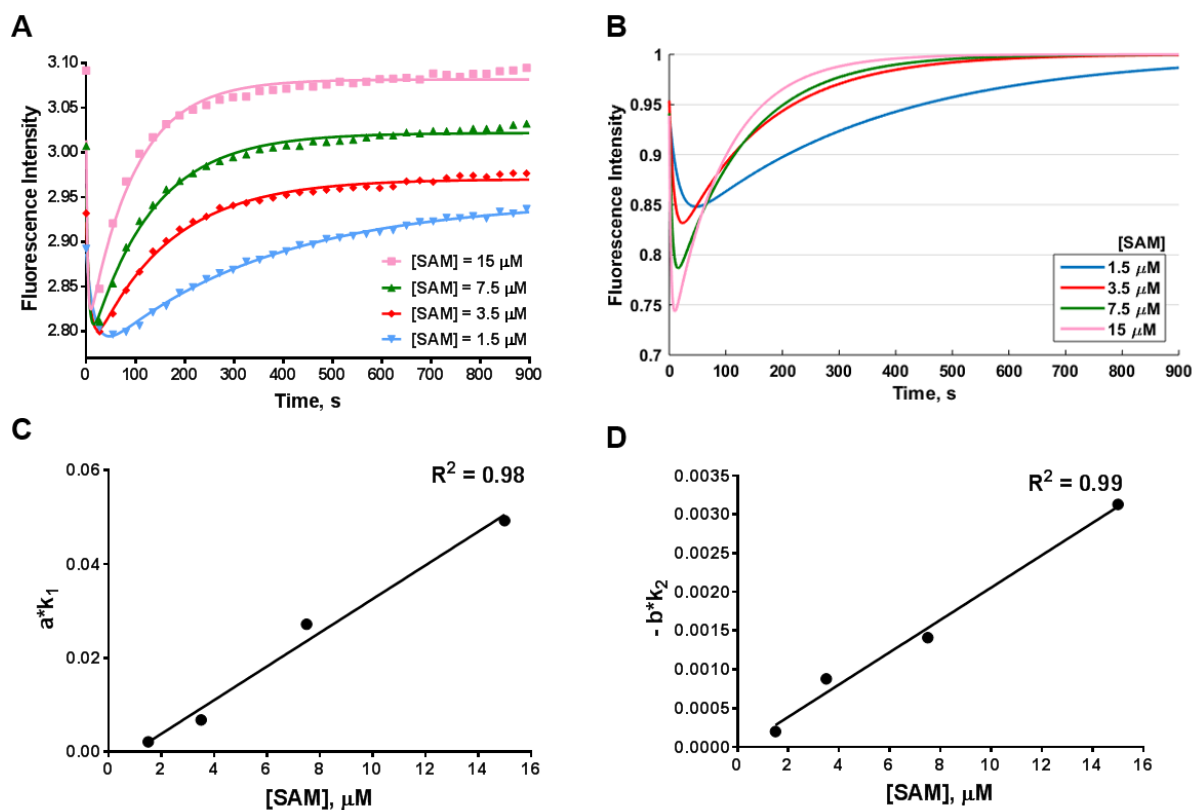
Figure 4.4. **Time course of PRMT1 methylation by varying the cofactor concentrations. A**. The curves are fit with **equation 2** to generate values in **Table S4.2A**. Each fitting curve used 10,000 data points, but only 50 data points are shown. Each curve is an average of 4 to 6 replicates. **B** is the simulation results from values in **Table S4.2A** at fixed c = 1. **C** and **D** represent the relationship of slope values (a·k_1 and b·k_2) with varying concentrations of SAM (values listed in **Table S4.2B**). The linear fitting curves are shown in solid black line. The concentrations of the enzyme and the substrate are fixed at [PRMT1] = 0.4 µM, [H4FL] = 0.4 µM in these experiments.

4.7 Detection of PRMT1 Inhibition by cofactor-Competitive Inhibitors SAH and

Sinefungin

With the assay condition defined ([PRMT1] = 0.2 μM, [H4FL] = 0.4 μM and [SAM] = 3.5 μM), we examined changes of the stopped flow fluorescence time course in response to different PRMT1 inhibitors. First we tested the inhibition of the SAM analog, SAH (**Figure 4.5A**), on the methylation time course. With a series of concentrations of SAH added to the mixture, the obtained progression curves showed the reaction was inhibited by SAH in a dose-dependent manner (**Figure 4.5B**). When the concentration of SAH was at 0.1 μM, there was very little difference compared to the control group without SAH presence. When the concentration of SAH was up to 10 μM, the increasing trend of Phase II was almost abolished. Higher concentrations of SAH resulted in steeper decreasing curves in Phase I and milder increasing curves in Phase II (**Figure 4.5B**). The changes of the parameters, a, k_1, $|b|$, and k_2 did not follow a simple rule with SAH concentrations (**Table S4.3A**). The relationship between the slope values $a \cdot k_1$ and $-b \cdot k_2$ with respect to the SAH concentrations is shown in **Figure 4.5C** and **Figure 4.5D**, and the corresponding values are listed in **Table S4.3B**. Interestingly, the $a \cdot k_1$ values of Phase I were boosted when the inhibitor concentrations were lower than SAM (from 0.1 μM to 2.5 μM); and when the inhibitor concentrations were higher than SAM, the $a \cdot k_1$ values started to decrease (**Figure 4.5C** and **Table S4.3B**). The initial slope values of Phase II, $-b \cdot k_2$, decreased with more SAH in the reaction mixture (**Figure 4.5D**), which indicated a dose-dependent inhibition manner. We used the dose response of $-b \cdot k_2$ to determine the IC_{50} of SAH to be 0.66 ± 0.07 μM, which falls into the range of the IC_{50} values reported in the literature[9].

We performed similar stopped flow study of PRMT1 inhibition by sinefungin (**Figure S4.5**), another SAM analog and a universal methyltransferase inhibitor[30, 37]. The obtained reaction

curves showed that sinefungin inhibited PRMT1 activity in a dose-dependent manner (**Figure S4.5**) very similar to the SAH inhibition (**Figure 4.5**). The relationship between $a{\cdot}k_1$ or $-b{\cdot}k_2$ and the sinefungin concentration is shown in **Figure S4.5C** and **S4.5D**. The values of all parameters are listed in **Table S4.4**. Similar to SAH inhibition, the $a{\cdot}k_1$ values of Phase I increased with higher concentration of sinefungin up to 3 μM, followed by a slight decrease (**Figure S4.5C**). The value $-b{\cdot}k_2$ decreased with more inhibitor present, and the IC$_{50}$ of sinefungin was calculated to be 0.12 ± 0.08 μM, close to previously reported data[9, 22, 31].
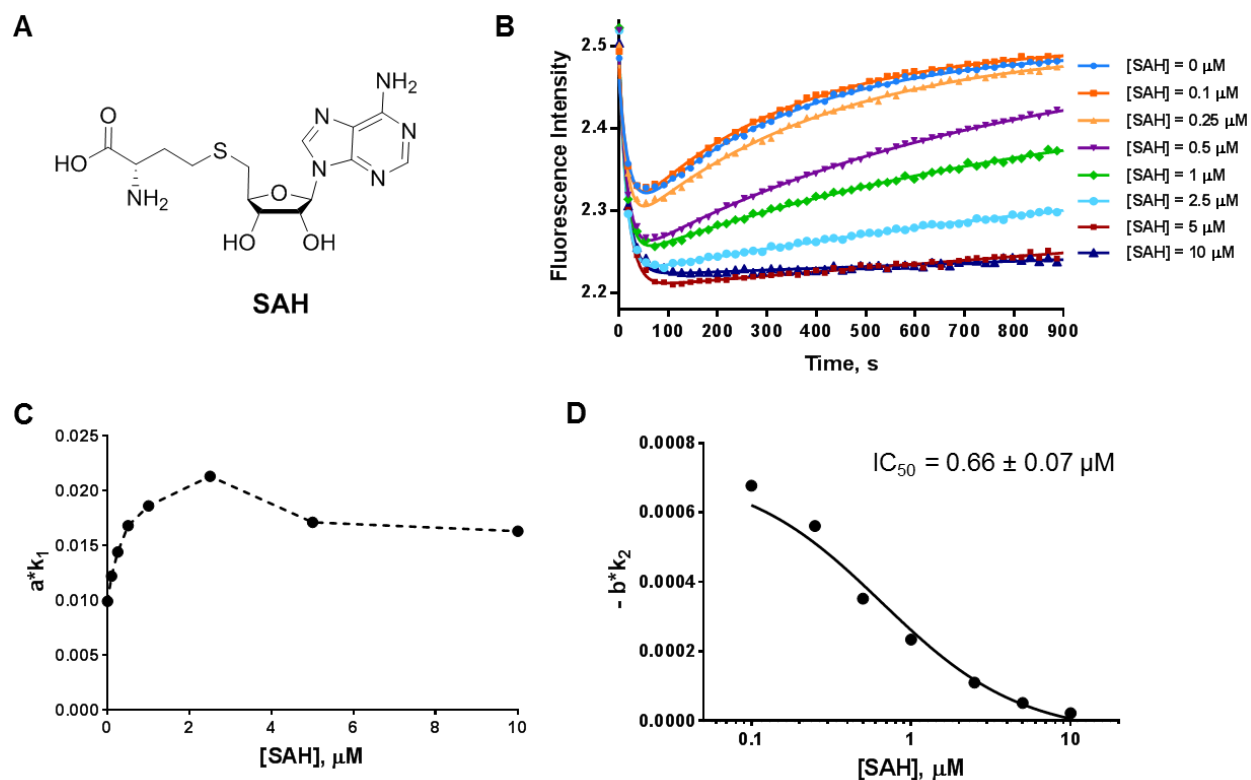
Figure 4.5. **Stopped flow fluorescence assay of the cofactor-competitive inhibitor, SAH. A**.
Structure of SAH. In **B**, the curves are fit with **equation 2** to generate values in **Table S4.3A**.
Each curve used 10,000 data points, but only 50 data points are shown. Each curve is an average
of 4 to 6 replicates. **C** and **D** represent the relationship of $a \cdot k_1$ or $b \cdot k_2$ with inhibitor
concentrations (values listed in **Table S4.3B**). In **D**, the IC_{50} is calculated using **equation 1**. The
reaction condition used for all the experiments is [PRMT1] = 0.2 µM, [SAM] = 3.5 µM, [H4FL]
= 0.4 µM, with varying concentrations of SAH.

4.8 Detection of PRMT1 Inhibition by Substrate-Competitive Inhibitor, H4R3me2a

Next, we investigated the peptide-based product inhibitor, the asymmetrically dimethylated peptide, H4R3me2a (acetyl-SGRme$_{2a}$GKGGKGLGKGGAKRHRKVL, **Figure 4.6A**). The obtained stopped flow fluorescence curves of the H4R3me2a inhibition assay are shown in **Figure 4.6B**. When the concentration of H4R3me2a was as low as 0.25 μM, no obvious difference was observed (**Figure 4.6B**). When the H4R3me2a concentration was above 0.5 μM, the shape of the curves changed significantly with increased minima and milder slopes in Phase II. Again, the changes of a, k_1, $|b|$ and k_2 did not follow a simple rule with respect to the inhibitor concentration (**Table S4.5A**). However, the slope values $a \cdot k_1$ and $-b \cdot k_2$ clearly showed a dose-dependent inhibition pattern. Different from the SAH or sinefungin assay, the Phase I was strongly inhibited by increasing concentrations of H4R3me2a (**Figure 4.6C**), and the $a \cdot k_1$ values were lessened from $1.10E\text{-}02 \pm 5.14E\text{-}05$ s^{-1} to $1.79E\text{-}03 \pm 1.72E\text{-}05$ s^{-1} (**Table S4.5B**). Phase II showed similar pattern to that of the SAM-competitive inhibition: $-b \cdot k_2$ values were reduced with more inhibitor present (**Figure 4.6D** and **Table S4.5B**). The IC$_{50}$ of H4R3me2a calculated from the $a \cdot k_1$ curve (**Figure 4.6C**) was 0.99 ± 0.12 μM, and 1.18 ± 0.17 μM from the $-b \cdot k_2$ curve (**Figure 4.6D**). The two IC$_{50}$ values are very comparable, and both are close to the IC$_{50}$ determined by a radiometric filter binding biochemical assay, which was 1.32 ± 0.20 μM (**Figure S4.6**).
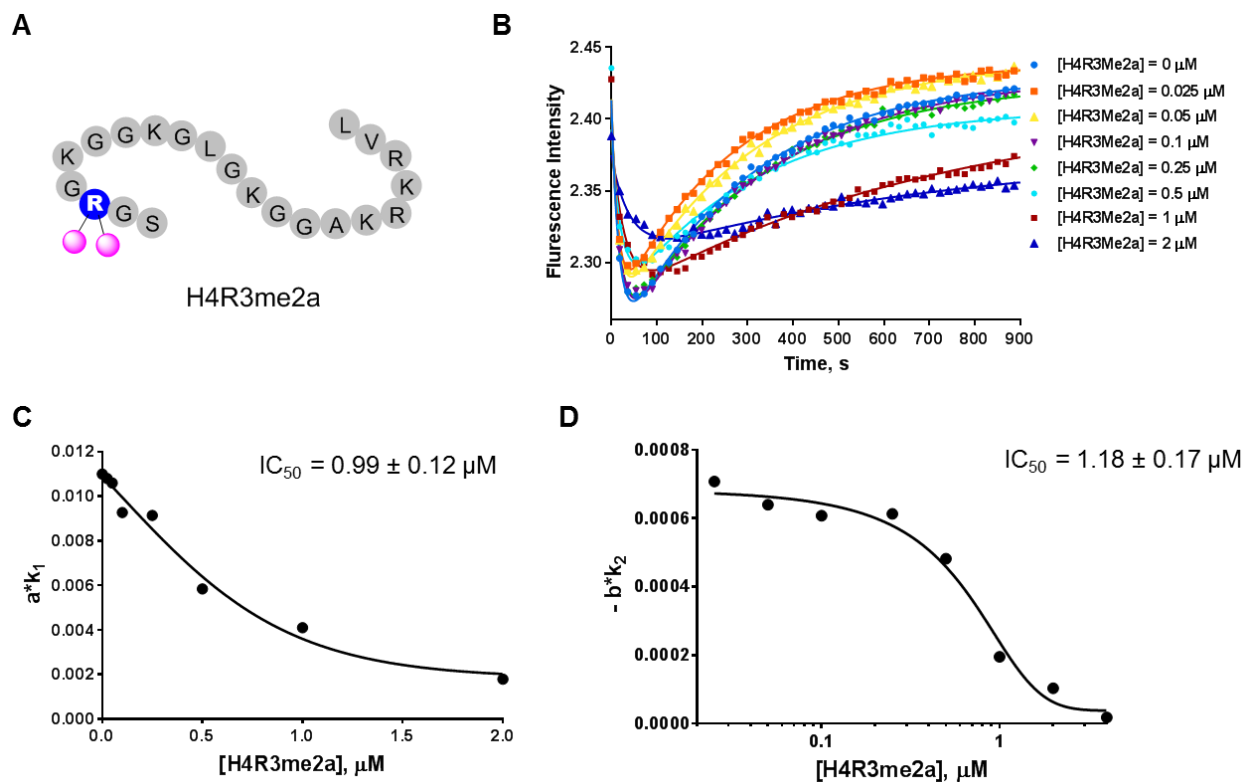
Figure 4.6. **Stopped flow fluorescence assay of the substrate-competitive inhibitor, H4R3Me2a.** A. Illustration of H4R3Me2a. In **B**, the curves are fit with **equation 2** to generate values in **Table S4.5A**. Each curve used 10,000 data points, but only 50 data points are shown. Each curve is an average of 4 to 6 replicates. **C** and **D** represent the relationship of $a \cdot k_1$ or $b \cdot k_2$ with inhibitor concentrations (values listed in **Table S4.5B**). In **C** and **D**, the IC$_{50}$ is calculated using **equation 1**. The reaction condition used for all experiments are [PRMT1] = 0.2 µM, [SAM] = 3.5 µM, [H4FL] = 0.4 µM, with varying concentrations of H4R3Me2a.

4.9 Detection of PRMT1 Inhibition by DB75

Next, we performed stopped flow characterization on two recently reported small molecule inhibitors of PRMT1. DB75 (furamidine) is a diamidine molecule with a rigid, crescent and planar scaffold (**Figure 4.7A**). According to our previous study[35], its IC_{50} for PRMT1 was 9.4 ± 1.1 µM and it showed a favorable inhibition selectivity against PRMT1 over the other PRMT members: 42-fold over CARM1, 30-fold over PRMT6 and more than 15-fold over PRMT5. We tested DB75 using the stopped-flow fluorescence assay, and obtained methylation curves at a series concentrations of DB75 (**Figure 4.7B**). In general, as the inhibitor concentration went up, the minima of the curves leveled and the Phase I and Phase II slopes became less steep. When the concentrations of DB75 were higher than 10 µM, Phase II was almost fully inhibited. The relationship of $a \cdot k_1$ or $-b \cdot k_2$ with the inhibitor concentration is plotted in **Figure 4.7C** or **Figure 4.7D** with corresponding values listed in **Table S4.6B**. In this measurement, we observed that both the $a \cdot k_1$ of the first phase and $-b \cdot k_2$ of the second phase were strongly inhibited, in a pattern that was similar to the H4R3me2a inhibition, suggesting that DB75 was substrate-competitive. This conclusion is in good agreement with our previous steady-state kinetic analysis that DB75 is primarily substrate competitive[35]. From the $a \cdot k_1$ curve, the IC_{50} of DB75 was calculated to be 7.9 ± 0.2 µM; from the $-b \cdot k_2$ curve, the IC_{50} was 9.1 ± 0.6 µM, consistent with the result from the radiometric filter binding assay, which was 9.4 ± 1.1 µM[35].

Figure 7. **Stopped flow fluorescence assay of DB75. A.** Structure of DB75. In **B**, the curves are fit with **equation 2** to generate values in **Table S4.6A**. Each curve used 10,000 data points, but only 50 data points are shown. Each curve is an average of 4 to 6 replicates. In **C** and **D**, the IC_{50} is calculated using **equation 1**. The reaction condition used for all experiments are [PRMT1] = 0.2 µM, [SAM] = 3.5 µM, [H4FL] = 0.4 µM, with varying concentrations of DB75.

4.10 Detection of PRMT1 Inhibition by MS023

Lastly, we performed stopped flow florescence assay on another compound, MS023 (**Figure 4.8A**), a type I PRMT inhibitor recently discovered by Kaniskan *et al*, which showed an IC_{50} of 30 nM against PRMT1[26]. In this measurement, MS023 was titrated from 10 nM to 200 nM in the reaction mixture. From **Figure 4.8B**, we observed that the higher the concentration of MS023, the milder the slope of Phase II became. At 200 nM, Phase II was almost fully inhibited. The relationship of $a \cdot k_1$ or $-b \cdot k_2$ with the inhibitor concentration is shown in **Figure 4.8C** and **Figure 4.8D**, and values listed in **Table S4.7B**. For Phase II, the $-b \cdot k_2$ values decreased with more inhibitor present, and the calculated IC_{50} of MS023 was 43 ± 8.9 nM (**Figure 4.8D**), close to what was reported ($IC_{50} = 30$ nM)[26]. Interestingly, for Phase I, the $a \cdot k_1$ values modestly decreased with the increasing MS023 concentration, and the calculated IC_{50} from this curve was more than 200 nM (**Figure 4.8C** and **Table S4.7B**). This result is different from those of the substrate-competitive inhibitors (e.g. DB75, H4R3me2a) nor the cofactor-competitive inhibitors (e.g. SAH and sinefungin). The partial inhibition of MS023 on Phase I (**Figure 4.8C**) suggests that MS023 is possibly a mixed-type noncompetitive inhibitor, which is partially substrate-competitive. Indeed, the mechanism of action of MS023 was reported as noncompetitive with both the cofactor SAM and the substrate peptide[26]; and according to the X-ray co-crystal structure of PRMT6 in complex with MS023, the inhibitor occupied the substrate arginine-binding site[26].

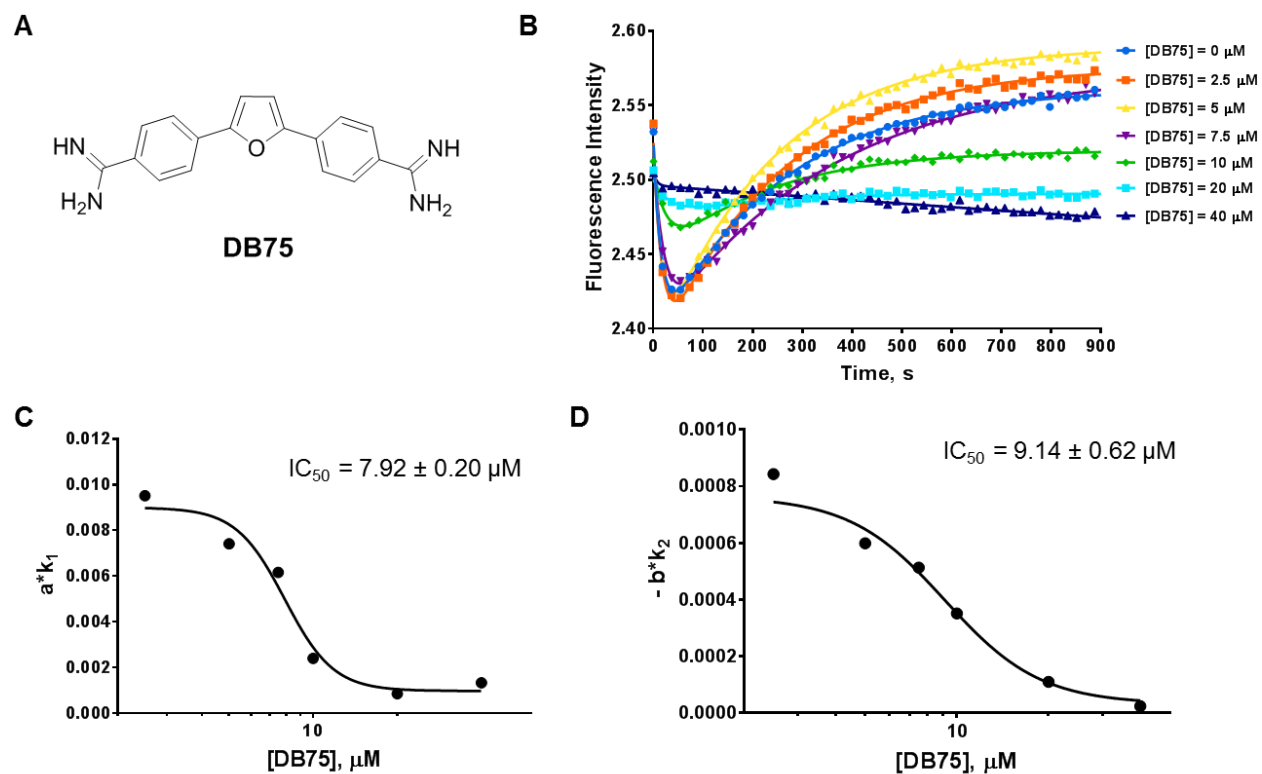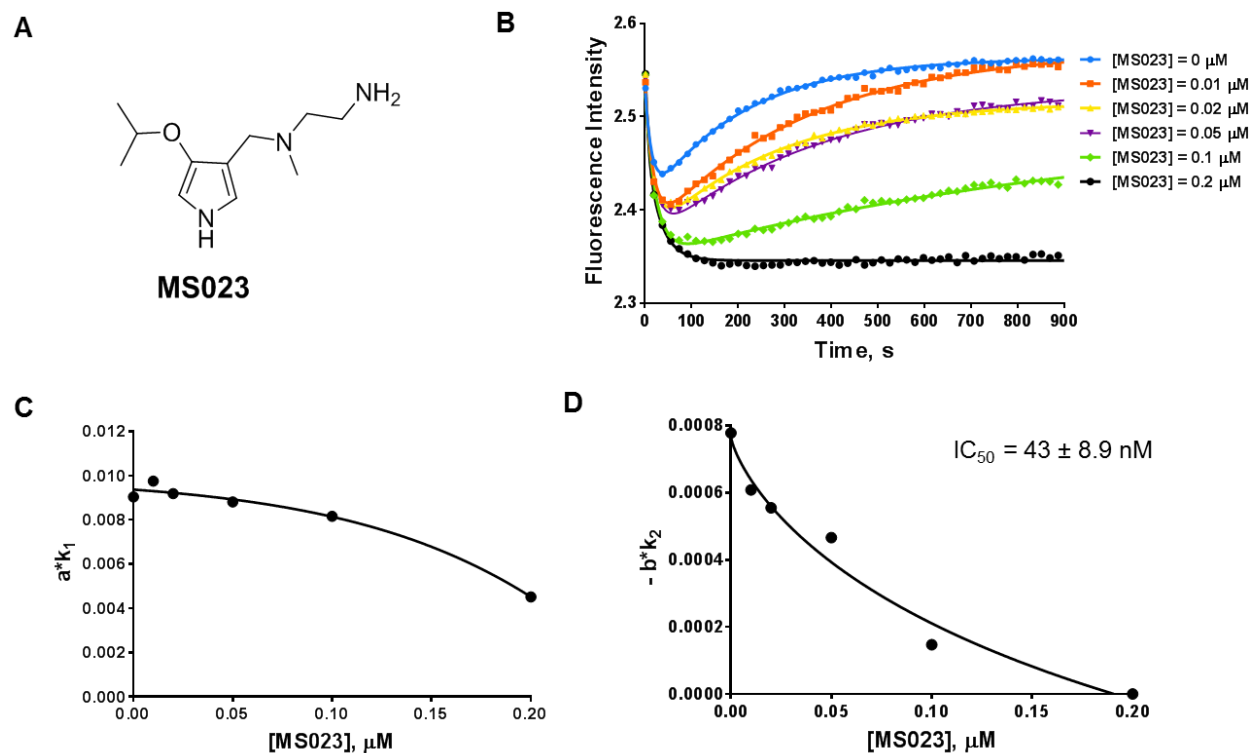**Figure 4.8**. **Stopped flow fluorescence assay of MS023. A.** Structure of MS023. In **B**, the curves are fit with **equation 2** to generate values in **Table S4.7A**. Each curve used 10,000 data points, but only 50 data points are shown. Each curve is an average of 4 to 6 replicates. In **C** and **D**, the IC_{50} is calculated using **equation 1**. The reaction condition used for all experiments are [PRMT1] = 0.2 μM, [SAM] = 3.5 μM, [H4FL] = 0.4 μM, with varying concentrations of MS023.

4.11 Conclusions

There is an emerging need of PRMT inhibitors for use as novel therapeutic agents to treat diseases and as tools to investigate biological functions of PRMTs. Development of PRMT inhibitors relies on robust biochemical assay to evaluate candidate inhibitors. We have designed and applied a stopped flow fluorescence platform for PRMT inhibitor characterization utilizing a fluorescein-labeled peptide as the substrate. According to our study on PRMT1 inhibitors, this assay can provide more information of an inhibitor than just potency: the relationship of the Phase I initial rates ($a \cdot k_1$) with respect to inhibitor concentrations can cast light on the mode of action. A decrease in $a \cdot k_1$ with increasing inhibitor concentration in a dose-dependent manner similar to the Phase II inhibition, such as the H4R3me2a and DB75 curves (**Figure 4.6C** and **Figure 4.7C**), and a consistent IC$_{50}$ values calculated from Phase I and Phase II rate inhibition curves, suggests that the inhibitor is substrate-competitive. However, a pattern similar to SAH or sinefungin, which a moderate inhibition in Phase I (**Figure 4.5C** and **Figure S4.5C**) was observed, suggests that the inhibitor is cofactor-competitive. The noncompetitive inhibitor MS023 slightly decreases the Phase I initial rates, not as evident as the substrate-competitive inhibitors, and the resulted IC$_{50}$ from Phase I rate inhibition curve is much higher than that of the Phase II, suggests that it is a mixed-type inhibitor that partially substrate-competitive. In conclusion, the stopped flow fluorescence assay is effective to characterize the potency (IC$_{50}$) of the PRMT1 inhibitors and provide mechanistic insights for the mode of action. This assay bears the advantages of being homogeneous, nonradioactive, mix-and-measure featured, and allowing for continuous measurement of methylation inhibition. This assay format can be potentially adapted to detect and characterize inhibitors for other PRMTs and histone modifying enzymes using a fluorescent peptide substrate.

CHAPTER 5

SUMMARY AND FUTURE DIRECTIONS

Identification and characterization of potent and isoform-selective PRMT inhibitors have become a timely demand for their applications in clinical research as drug candidates and also for their potential use as chemical tools to dissect the underlying mechanisms of PRMT-dysregulation in diseases. Both academic laboratories and pharmaceutical companies have great interest in the field of PRMT inhibitor discovery, evidenced by the numerous high-quality articles published in prestigious journals and the various reports of small molecule or peptide inhibitors for PRMTs. Despite the emerging need, many of the reported compounds have limited application due to incomplete characterization in isoform-selectivity, mechanism of action and cellular efficacy. Challenges remain in the identification of inhibitors with nanomolar or lower potencies that achieve selective inhibition of the structurally conserved PRMT members for translating to clinical research. Furthermore, the existing assays for PRMT activity measurement have certain disadvantages, such as non-continuous measurement, generation of radioactive waste, or complication of the results due to introduction of other enzymes and reagents for assay detection. Therefore, novel assay methods are needed to further promote the field of PRMT inhibitor discovery.

To address the remaining challenges, this work aimed at discovering novel chemical entities for potent and isoform-selective inhibition of PRMTs in cancers, with a focus on the identification and characterization of small molecule inhibitors for PRMT1 and PRMT5; and also to develop novel biochemical assays for PRMT inhibitor evaluation. We focused on a

compounds that have two amidine functional groups named diamidines. Because of the similarity between amidine and guanidine in arginine residue, we proposed that diamidine compounds could be potential PRMT inhibitors with a similar binding manner to that of the substrate arginine in PRMT catalytic site. We discovered furamidine as a PRMT1-selective inhibito[150] from a diamidine compound library obtained from Dr. David Boykin. Because the existing diamidine compounds lack structure variation of the linker region, we designed and synthesized a series of diamaidine analogs with various linker lengths, and discovered decamidine as an improved PRMT1 inhibitor[224]. On the other hand, using the lead compound furamidine as a structure template, a combined approach including virtual screening, biochemical high throughput screening and various chemical modifications were applied to build PRMT-targeting small molecules with improved inhibition characteristics. The hits from the inhibitor screening were subjected to detailed biochemical characterization, in order to profile their selectivity over a panel of protein methyltransferases and investigate their mechanism of action in isoform-selective inhibition. With proper controls in each study, their ability to inhibit PRMT enzymatic activity as well as anti-proliferative activity were validated in PRMT dysregulation-associated cancer models. As a result, compound K313 was discovered as a PRMT1-selective inhibitor, which is 10-fold more potent than the initial lead compound furamidine in enzymatic activity inhibition of PRMT1 and in growth inhibition of leukemia and melanoma cells. Compound K280S was discovered as a dual-target inhibitor for PRMT5 and microtubule, which exhibits strong synergetic anticancer efficacy in prostate cancer cells and prostate cancer mice. Additionally, we designed a novel stopped flow assay platform that can determine the inhibition potency of PRMT inhibitor and distinguish their mechanism of inhibition simultaneously. To our knowledge, this is the first continuous assay for PRMT

114

inhibition measurement, which also possesses advantages of being homogeneous, nonradioactive, mix-and-measure featured. This assay can serve as a counter screening and validation method for PRMT inhibitor characterization in addition to the existing detection methods.

To conclude, this work presented several small molecule inhibitors for selective inhibition of PRMT1 and PRMT5, which can be used for structure modification to achieve further improvements. These compounds have significant anti-cancer efficacy in various PRMT-dysregulation associated cancer cell lines, and studies are required to further elucidate their mode of action. Moreover, this work provides an innovative assay based on the stopped flow method to promote the field of PRMT inhibitor discovery. The results and future directions of this work are further discussed in the following aspects:

(1) The structure features of the identified small molecules provide rich information for PRMT inhibitor design.

Initially, the investigation on the diamidine compounds was started due to the reasoning that the amidine group can mimic the substrate arginine to bind to the PRMTs. The SAR analysis and docking models demonstrated that the diamidine moiety is crucial for the ligand binding, but the binding interactions are not solely dependent on mimicking the substrate arginine. For furamidine, indeed one of the amidine groups interacted with two glutamate side chains (Glu144 and Glu153, **Figure 2.3**), which are conserved on the "double-E-loop" among PRMTs proposed to participate in positioning the guanidine group of arginine for methyl transfer[26]. However, decamidine and K313 did not interact with the two glutamate side chains in the arginine binding site, instead, these two inhibitors stretched into the cofactor site. The three compounds had common interactions formed between one of the amidine groups and the Glu129 side chain of

115

PRMT1. Glu129 in PRMT1 is also conserved in other PRMTs, which is known to form hydrogen bonds with the adenine hydroxyl groups of the cofactor[36]. PRMT5 also has the three conserved glutamate residues in its catalytic pocket: Glu392 in the cofactor site as well as Glu435 and Glu444 in the substrate arginine site[38]. In the proposed binding model of K280, the two glutamate residues in the catalytic pocket of PRMT5 (Glu392 and Glu435) directly participated in hydrogen bonding with the amine groups of the inhibitor (**Figure 3.6**); and SAR analysis on K280 derivatives also supported that these interactions are essential for their inhibitory activity on PRMT5. The above results suggested that the conserved glutamate side-chain residues in the catalytic pocket of PRMTs can be utilized for specific binding of small molecule inhibitors, and the amidine groups represent an important pharmacophore interacting with the glutamate side-chain interactions.

Another interesting finding is that furamidine and K280 had better isoform selectivity than decamidine and K313. A common feature of furamidine and K280 was that they interact closely with the residues in the substrate arginine site, whereas the interactions of decamidine and K313 were relatively closer to the cofactor site. Given that PRMTs share a structurally preserved Rossman fold for cofactor-binding but the substrate binding pocket is significantly more diverse[26], it is possible that inhibitors interacting with residues in the substrate site have a higher probability to be a selective inhibitor. While several reported potent and isoform-selective inhibitors were substrate competitive[155, 235], our results indicated that selective inhibitors do not necessarily follow this inhibition pattern. According to the enzyme kinetics studies, furamidine and K280 both showed mixed-type inhibition, while furamidine was primarily substrate competitive and K280 was uncompetitive to either substrate or cofactor. Their mechanisms of action are closely related to the binding poses in the enzymes: docking analysis showed that

116

furamidine and K280 interacted with residues from both cofactor and substrate site. Our observations in this study can help the rational design and structure modification of the PRMT inhibitors.

In all, this work provided important chemical entities for further optimization to achieve potent and selective inhibition of PRMTs: diamidine compounds for PRMT1 selective inhibition and 1,2-dihydropyrido[3,4-b]pyrazine compounds for PRMT5 selective inhibition. These lead inhibitors possess important structural features for specific binding to the PRMTs. The SAR and mechanism of action studies of these inhibitors provided critical information for further structure modifications and rational drug design. One limitation of the proposed binding models is that the molecular docking was performed based on an assumption that the inhibitors bind to the PRMT catalytic cavity. However, the inhibitors may potentially bind to an unexplored region of the protein to cause an allosteric effect to reduce enzymatic activity. Besides, cofactor, substrate and water molecules are not included in docking, but they might be potentially important for inhibitor binding. Therefore, the proposed binding models will be further verified using inhibitor co-crystallization with the target protein, and/or the site mutagenesis of the interacting residues in the enzyme catalytic site.

(2) Novel pharmacological mechanisms of the identified PRMT inhibitors are important for translating the compounds to clinical research.

Diamidine compounds are well-studied drugs for antifungal, antimicrobial and antiparasitic purposes[217, 245-246]. Their potential antitumor activity have also been reported[219]; however, their inhibitory activity for PRMTs was never shown before this work. In our cellular studies, the two diamidine compounds, furamidine and K313 presented strong inhibition on PRMT1 enzymatic activity in cells. Their anti-proliferative activity was also validated in

117

leukemia or/and melanoma cell lines. These results suggested that the two diamidine compounds are cell membrane permeable with anticancer activities. Previous studies showed that these compounds can be transported into the mammalian cells[247] and accumulate in the cancer cell nuclei[248-249]. Given that PRMT1 distributes in both cytoplasm and nuclues[33], and it is overexpressed in various cancers (**Table 1.2**), one mechanism for the diamidine compounds to inhibit cancer cell growth might be through reducing the abnormally elevated enzymatic activity of PRMT1. Additional studies are necessary to further elucidate this mechanism.

In another case, compound K280S was reported as a tubulin binder named as CI-980. This compound was a candidate chemotherapy agent used to treat a broad spectrum of cancers[243]. Previous cellular studies of K280S showed a discrepancy in results[237], which led to suspicion that microtubule inhibition was not the only mechanism for the compound's anticancer efficacy. Our studies demonstrated that one of these mechanisms might be PRMT5 inhibition. This new finding may help justify the limited efficacy showed in the previous clinical studies on K280S[244]. Results in phase I clinical trials indicated that K280S had high systemic clearance and a well-tolerated toxicity[250-251]. In phase II clinical trials, K280S was delivered as a 72- hour or 24-hour continuous intravenous infusion every three weeks at a dosage of 4.5 mg/m^2/day [252-256]. The previous dosing regimen was likely scheduled based on the phase I results and previous experience with mitotic inhibitors, but might not be appropriate for PRMT5 inhibition. Recent pre-clinical studies together with our data suggested that PRMT5 inhibitors may favor a long-term treatment to fully exhibit their anticancer efficacy[235]. Another reason for the limited efficacy seen in the K280S trials could be that some cancers are not dependent on PRMT5 regulation and thus may not be sensitive to PRMT5 inhibition. Therefore, we propose that the treatment schedule could be altered, or the formulation of drug could be adjusted to a sustained

long-term delivery for tumors with elevated PRMT5 activity. Although it is not yet clear whether there is an interplay between PRMT5 and tubulin in cancer cells, these two targets individually are intimately involved in carcinogenesis. Our data suggested that the synergistic anticancer effect resulted from the combinatory inhibition of PRMT5 and tubulin is unique and warrants further investigation.

Overall, this work presented novel pharmacological mechanisms for previously studied drugs and drug candidates, which can help in repurposing the use of these previously known compounds to treat cancers. A significant advantage is that since these compounds have already passed a number of toxicity and PK/PD tests, their safety profiles are well-established, and hence the risk of adverse events are reduced. Our observations in the mode of action studies for these drugs and drug candidates can provide guidance for future preclinical and clinical research.

(3) Innovative and powerful assay methods are crucial for promoting the field of PRMT inhibitor discovery.

To identify PRMT inhibitors from the NCI Diversity Set library containing 260,071 compounds, we first conducted ligand-based virtual screening using furamidine as a template to prioritize the most likely hits from the lengthy list. The benefits of virtual screening include reduced time and cost for hit identification as well as increasing the hit identification rates[257-259]. The top 406 compounds with high similarity scores to furamidine were selected for single concentration biochemical screening at 10 µM, which resulted in 33 PRMT1 inhibitor hits and 8 PRMT5 inhibitor hits with less than the 50% remaining enzyme activity. This combinatorial approach led to a hit identification rate of 8.1% for PRMT1 inhibitors and a rate of 2.0% for PRMT5 inhibitors, which are significantly higher than typical experimental high throughput screening methods (hit identification rates between 0.01% and 0.14%)[257]. Since furamidine is a

PRMT1 inhibitor, it is reasonable that the rate of PRMT1 inhibitor identification is higher than that of PRMT5. The strategy of combining virtual screening and biochemical high throughput screening was proven to be efficient in this work, which have resulted in several potent and selective PRMT inhibitors. In the future, since we have obtained significant amount of SAR data of these inhibitors, it is worthwhile to generate a more defined pharmacophore model to help improve the hit identification rate for further virtual screening against other existing compound libraries.

Additionally, the scintillation proximity assay platform for PRMT activity measurement[171] played a crucial role in the inhibitor discovery process. This 96-well assay format was adapted for target-based biochemical high throughput screening, dose-dependent enzyme activity measurement, inhibitor selectivity profiling, as well as the mechanism of inhibition determination by enzyme kinetics. Despite its robustness, a reliable secondary assay is necessary for counter screening and validation purposes. In this work, we developed a novel stopped flow assay platform for PRMT inhibitor characterization. In this assay, a fluorescein-labeled substrate peptide was applied to continuously probe the methylation process of PRMT1 over time, using the fluorescence changes of the substrate converting to the product. The obtained curves were analyzed based on a complete kinetic model of PRMT1 methylation[260] to quantify the dose-dependent methylation inhibition caused by the PRMT inhibitors. Currently, this assay used PRMT1 as an example for inhibitor characterization. Given that the enzyme kinetics of the other PRMTs are similar[83, 236, 261-263], further studies are desired to adapt this assay for mechanistic and selectivity studies using other PRMTs. This format can also be potentially adapted to other histone writers or erasers using the fluorescein-labeled peptide substrates.

A   Supporting information for Chapter 2
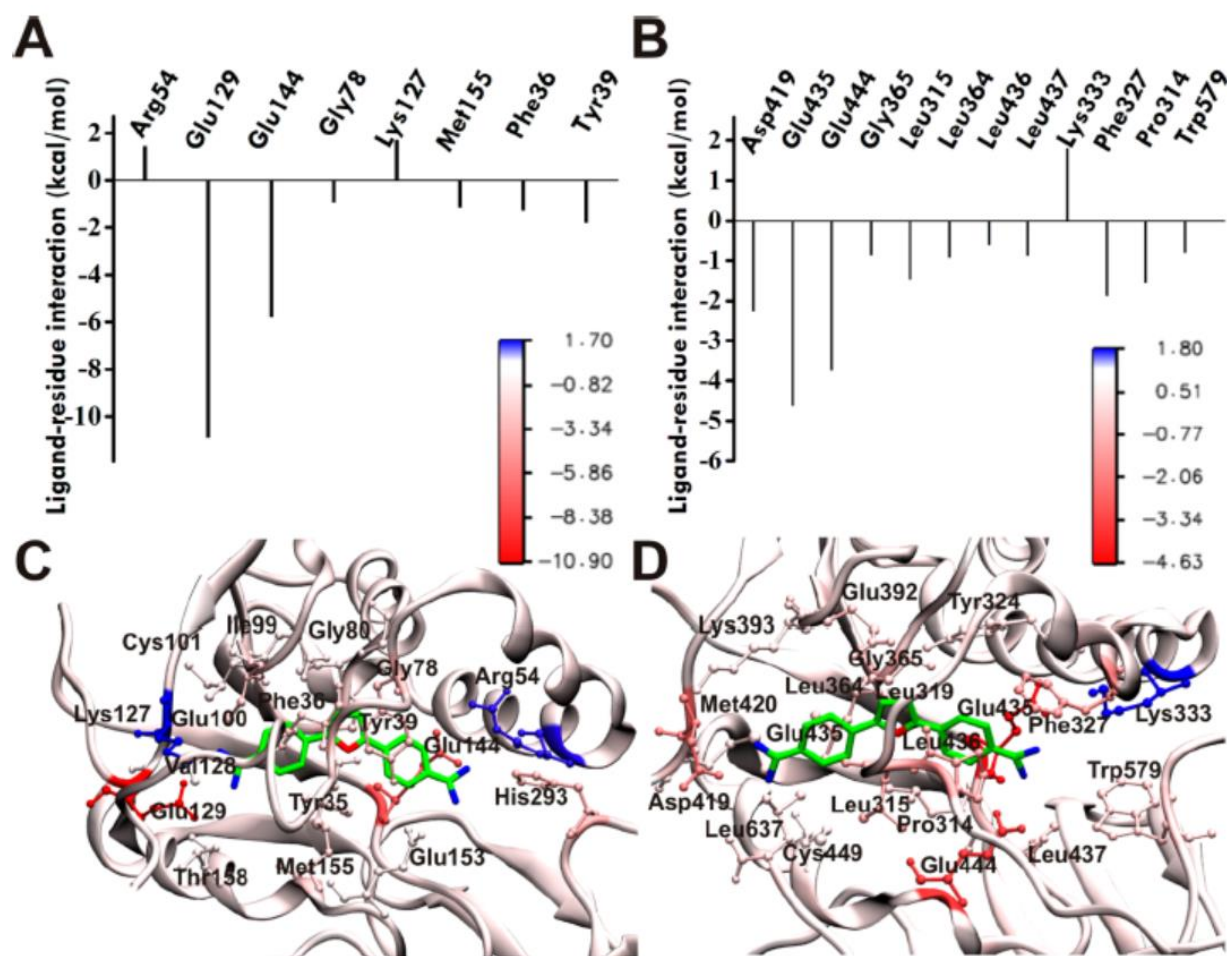
Figure S2.1. **Predicted binding modes of furamidine in PRMT1 and PRMT5 from docking (AutoDock 4.2) and molecular dynamics simulation (NAMD 2.8).**[150] Ligand−residue interaction energies from MM/PBSA energy decomposition for (A) PRMT1 and (B) PRMT5. (C, D) Binding modes of furamidine with (C) PRMT1 and (D) PRMT5. The best docking pose obtained from AutoDock in complex with the hPRMT1 homology model (based on 1F3L and 3SMQ) and X-ray hPRMT5 (4GQB) was selected for MD simulation. Dominant structures for the hPRMT1·furamidine and hPRMT5·furamidine complexes from the last 20 ns of MD trajectory clustering analysis were used for visualization. PRMT residues engaging the ligand are explicitly shown in ball and stick representation. The protein (in cartoon representation) is colored according to the residue contribution values in the free energy decomposition from red (negative) to blue (positive).
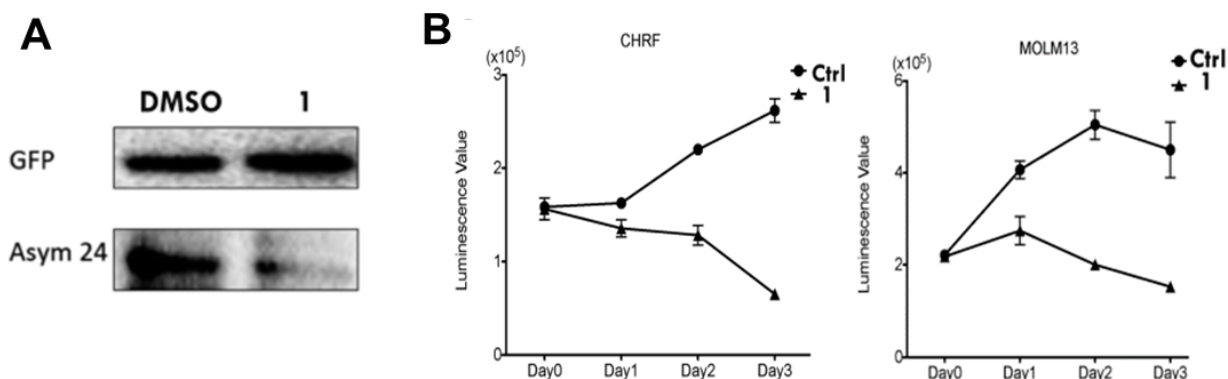
Figure S2.2 Furamidine was cell permeable and inhibited leukemia cell growth. A. Furamidine inhibited methylation of GFP-ALY in 293T cells. **B**. Furamidine inhibited the growth of CHRF and MOLM13 cells.
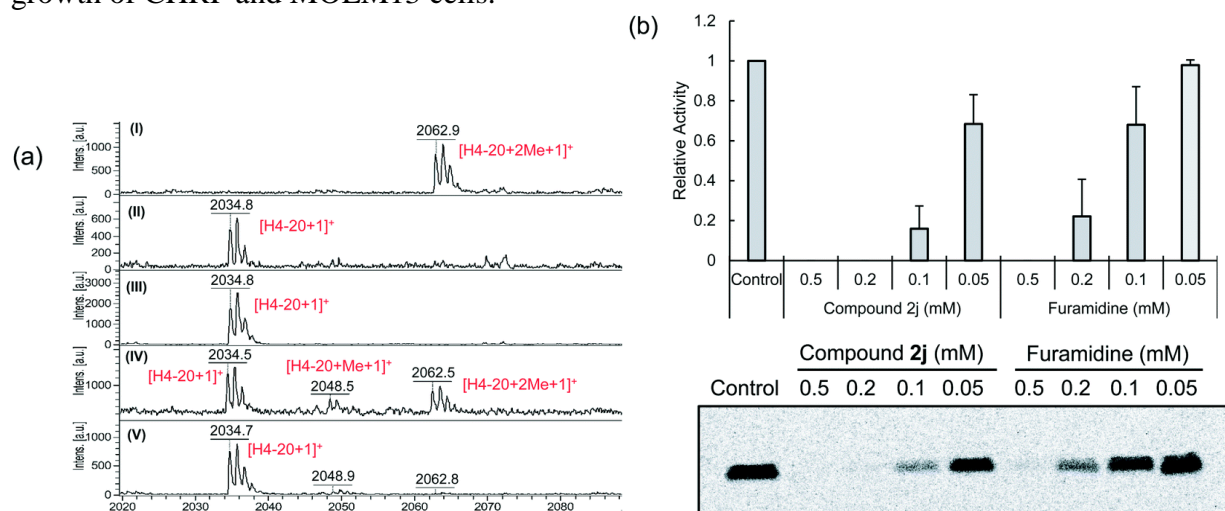
Figure S2.3 The comparison of PRMT1 inhibition by decamidine (2j) and furamidine.[224] (a) Mass spectra of the reaction mixture with different concentrations of compounds 2j and furamidine. From spectra I to V: DMSO control, compound 2j (0.2 mM), compound 2j (0.5 mM), furamidine (0.2 mM), furamidine (0.5 mM). The concentrations of PRMT1, SAM, and H4-20 were 1, 200, and 50 µM, respectively. The mixtures were incubated at 30°C for 3.5 h. (b) Radiometric gel assay and its quantification. The concentrations of PRMT1, [14C]SAM, and H4-20 are 0.1, 20, and 100 µM, respectively. The reaction time was 30 min at 30°C before it was quenched with $5 \times$ SDS-loading buffer, separated by 15% SDS-PAGE, dried under vacuum and visualized by storage phosphorimaging. The quantification was based on two experiments.
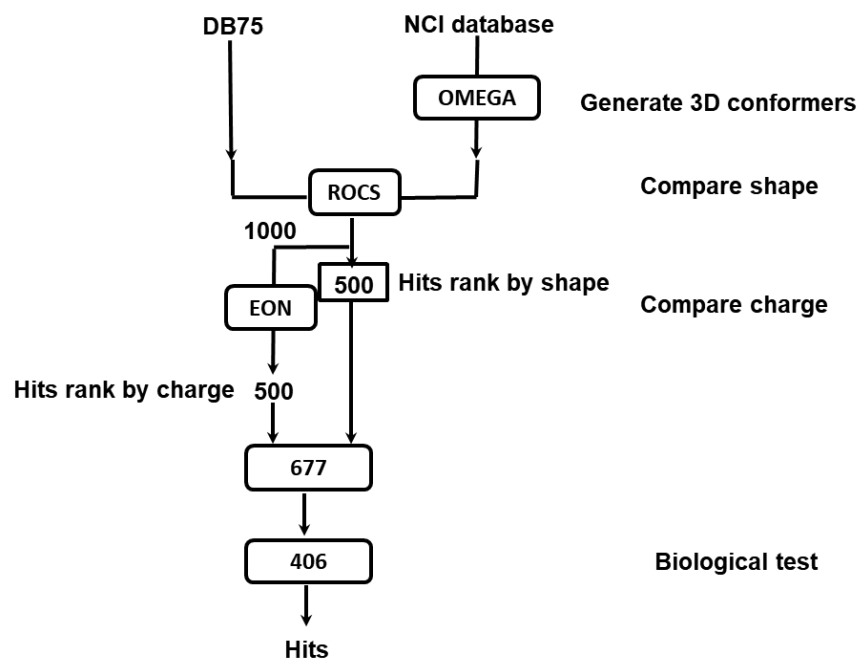
Figure S2.4. Flow chart overview of ligand-based virtual screening.
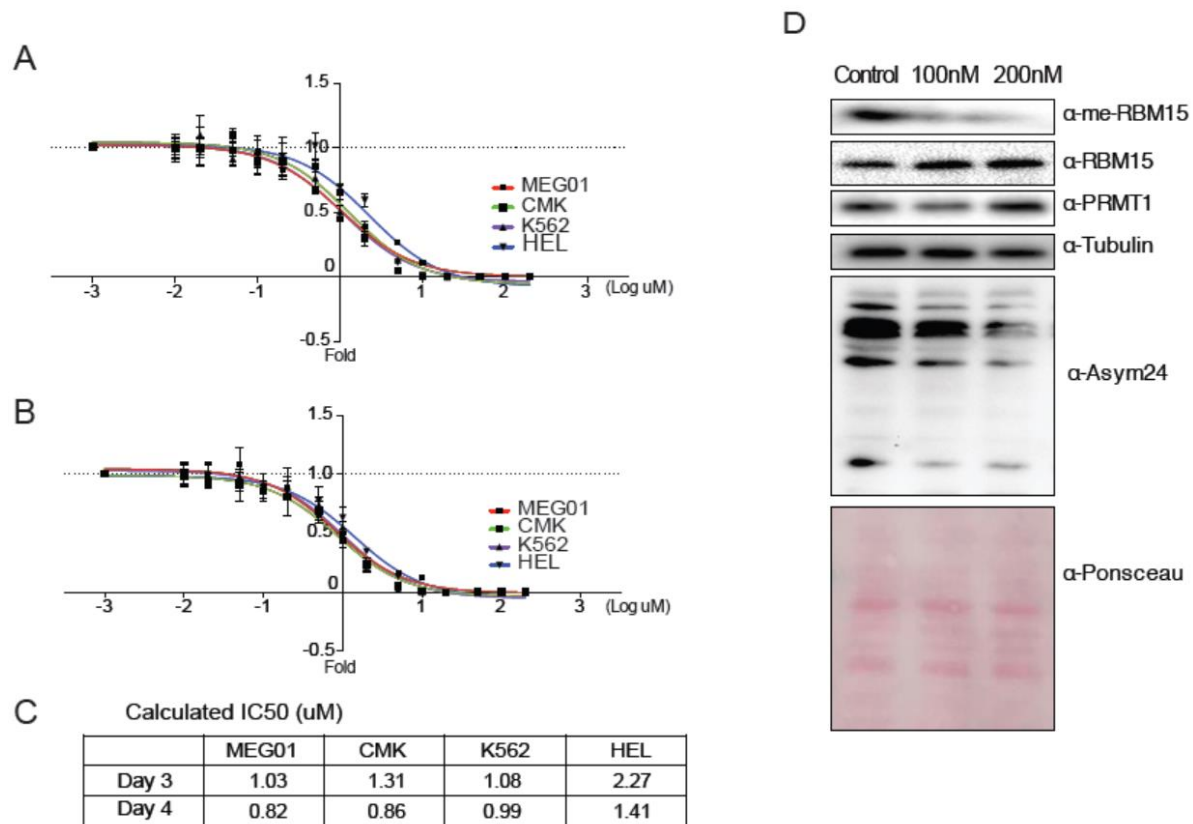
Figure S2.6 K313 inhibits proliferation of leukemia cell lines via blocking of PRMT1 activity. (**A−C**) K313 inhibited leukemic cell growth. Serial diluted K313 was added to the MEG01, CMK, K562, and HEL cell cultures and cell growth was measured by viability assay. As a control, the cells were treated with the same volume of DMSO. Sensitivity curves of day 3 (**A**) and day 4 (**B**) are plotted based on viability assay results and IC_{50} was calculated (**C**). (**D**) Arginine methylation level of K313-treated MEG01cells. MEG01 cells were cultured with the presence of DMSO or K313. Cell extract was harvested after 24 h of treatment, and samples were resolved by SDS−PAGE. Arginine methylation status was detected using anti-methyl-R antibody Asym24. PRMT1 activity was measured by the methylation status of substrate protein RBM15. Equal loading was confirmed by Ponceau S staining.
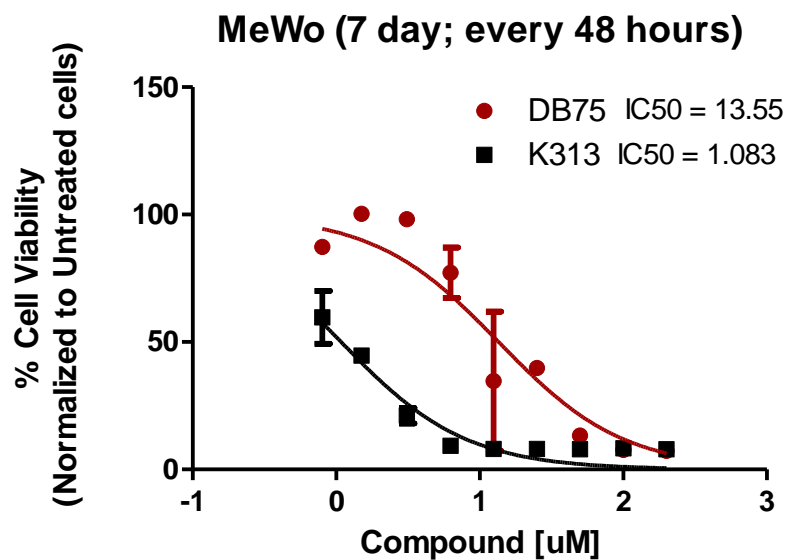
Figure S2.7 K313 inhibits proliferation of melanoma cell line MeWo. Serial diluted K313 was added to the MeWo cell cultures and cell growth was measured by viability assay. Treatment lasted for 7 days with media change every 48 hours.
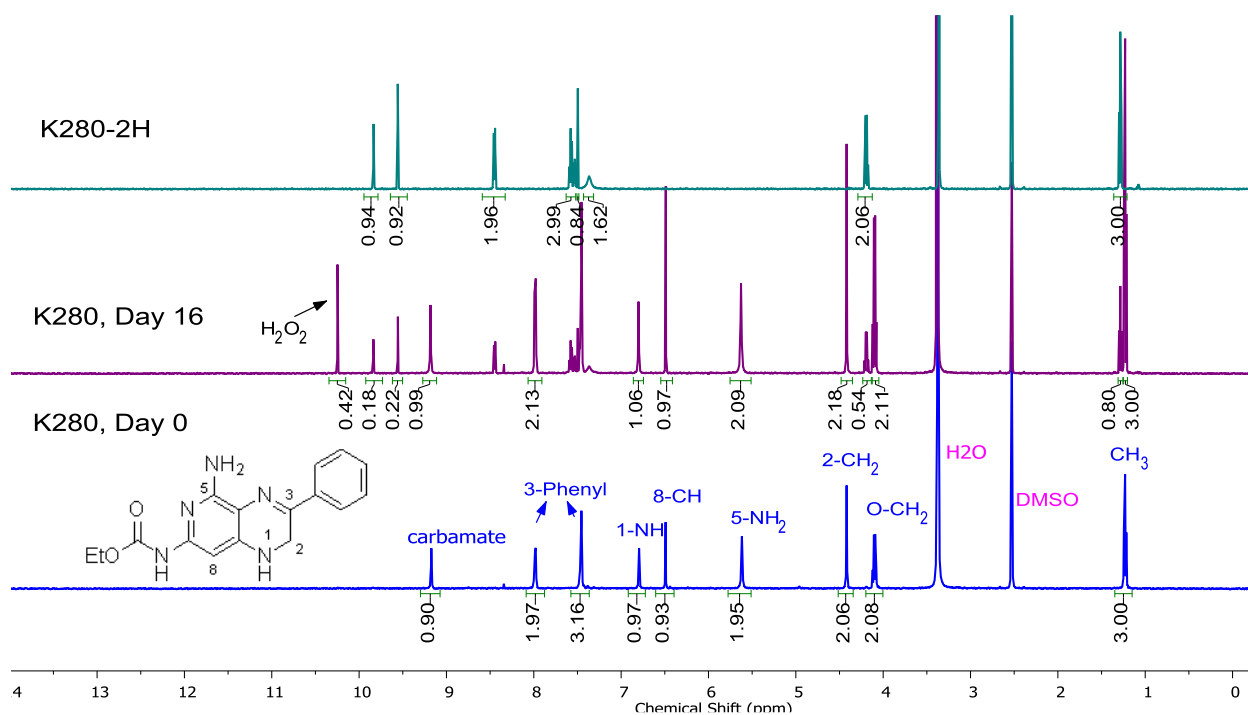
Figure S3.1 Compound K280 is unstable as revealed by ^{1}H NMR spectrum. Top: K280-2H standard in d6-DMSO; Middle: 16 mM K280 in d6-DMSO after 16 day incubation at room temperature; Bottom: 16 mM K280 in d6-DMSO, day 0. The middle spectrum demonstrated a combinatory profile of top and bottom spectra, suggesting that the degradant is K280-2H. H_2O_2 was observed in the degradation progress probably as a byproduct of O_2-mediated oxidation.
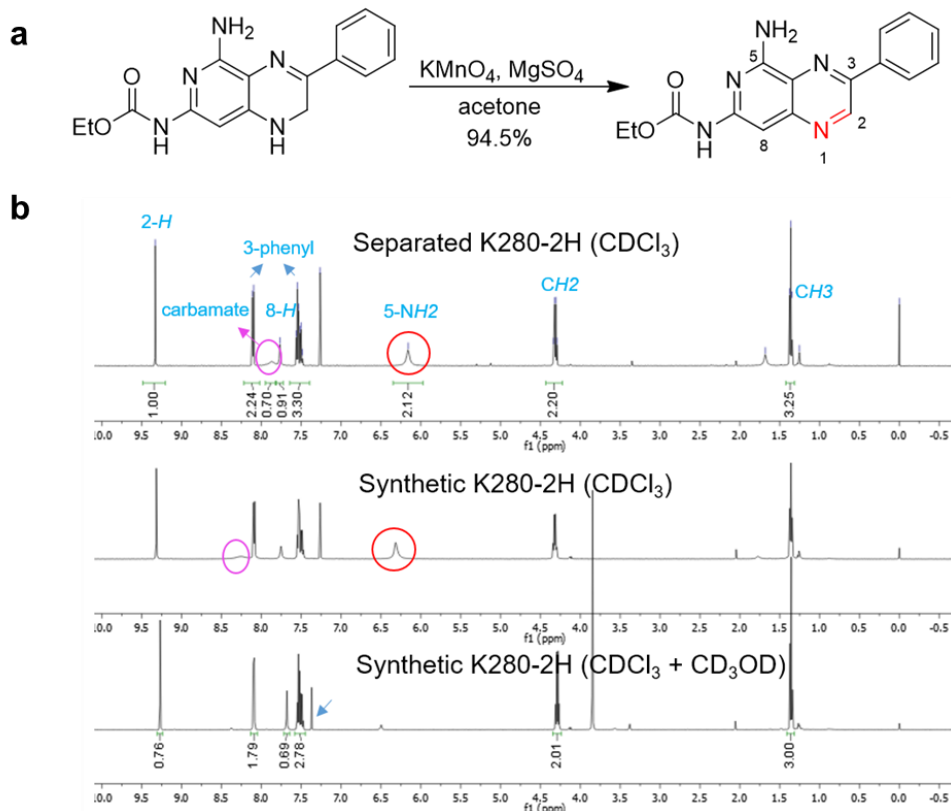
Figure S3.2 (a) Synthetic routine for compound K280-2H. (b) ^{1}H NMR comparison of separated K280 degradant (top, CDCl$_3$), synthetic K280-2H (middle, CDCl$_3$), and synthetic K280-2H (bottom, CDCl$_3$/CD$_3$OD). Note that the active hydrogens (carbamate and 5-NH$_2$) in the three spectra are circled in purple and red, respectively. And both disappeared due to hydrogen/deuterium exchange when CD$_3$OD was added (bottom panel of ^{1}H NMR spectrum). The alignment of top and middle spectra indicated that the K280 degradant is K280-2H.

127
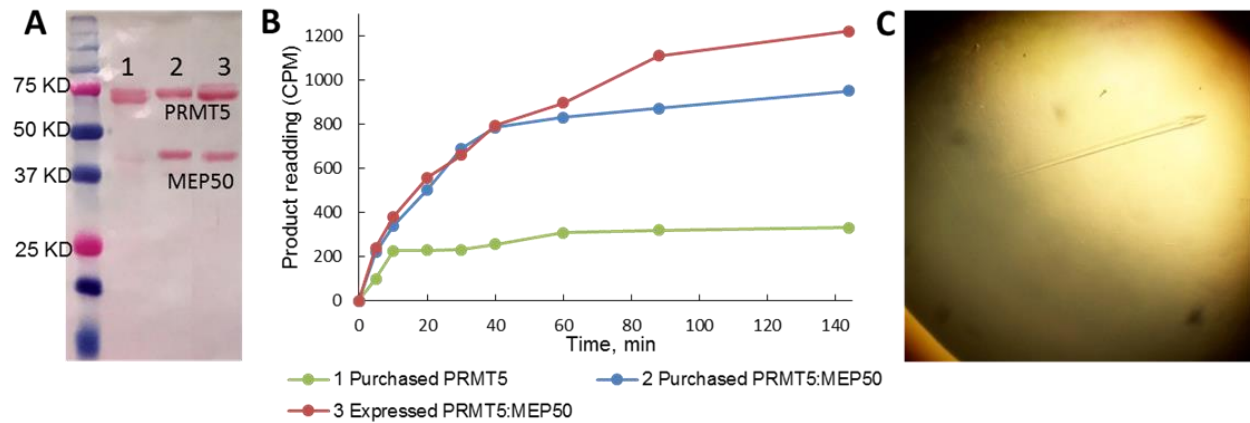
Figure S3.3 Crystallization of PRM5:MEP50. A. purity of expressed PRMT5:MEP50 complex shown in a Ponceau stained nitrocellulose membrane; **B**. time course of the purchased and expressed enzymes; **C**. the needle-shaped crystal from PRMT5:MEP50 with MTA and H4-20 peptide in a 24-well tray for hanging-drop vapor diffusion experiment.
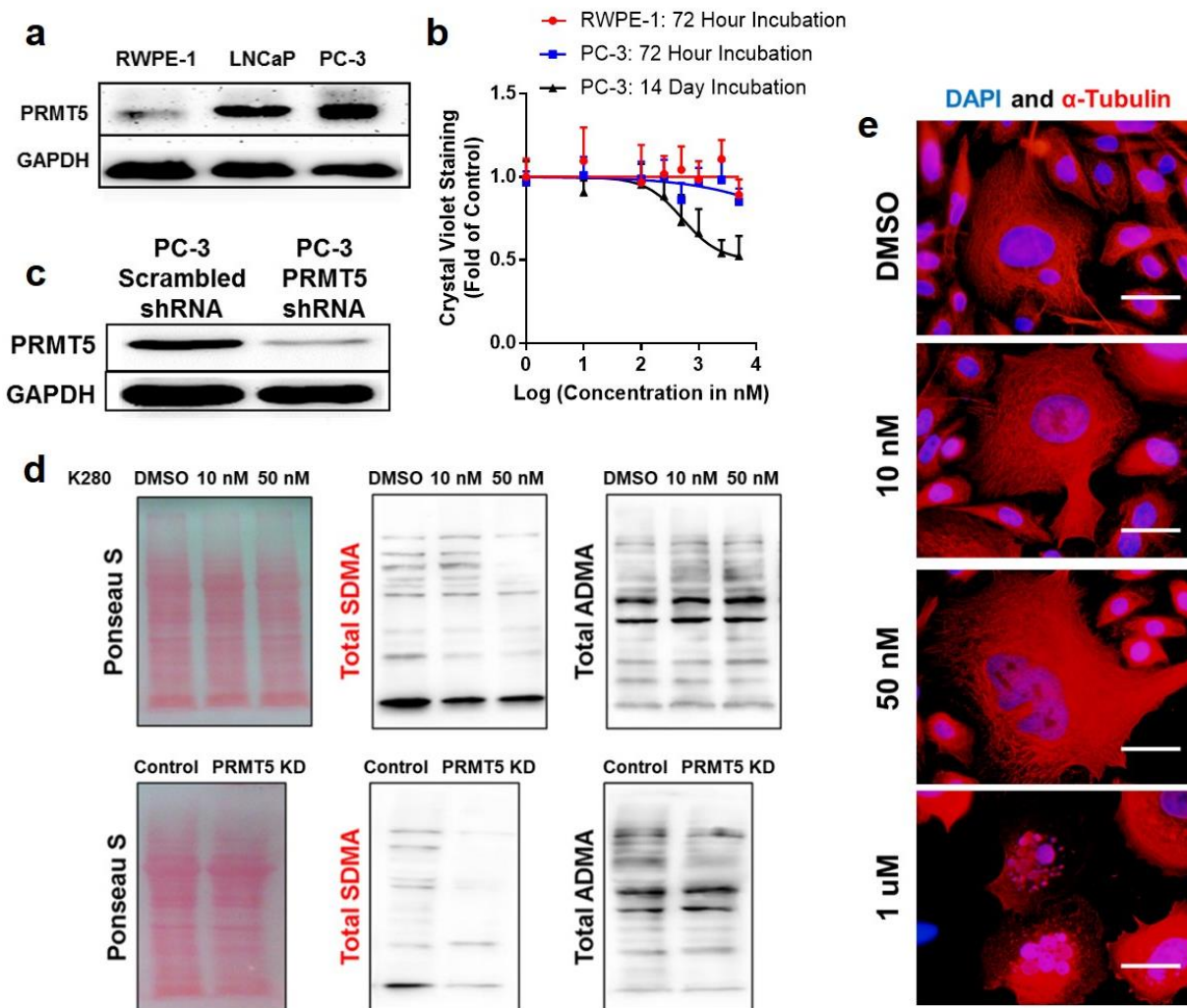
Figure S3.4 (**a**) PRMT5 expression in non-cancer (RWPE-1) and cancer (LNCaP and PC-3) cells were determined by immunoblot analysis. (**b**) Effect of EPZ015666 on RWPE-1 and PC-3 cell growth. RWPE-1 and PC-3 cells were treated with EPZ015666 at various concentrations for 72 hours or 14 days. Crystal violet staining assays were used to determine cell density. (**c**) PRMT5 knockdown (PRMT5 KD) of PC-3 cells were established using PRMT5-targeting shRNA while scrambled shRNA was used as a control. (**d**) Effect of K280 on SDMA and ADMA formation. (**e**) Effect of K280 on tubulin polymerization was examined using fluorescent microscopy. Scale bar, 10 µm. Data were replicative of three independent experiments. Data is presented as mean ± SD.
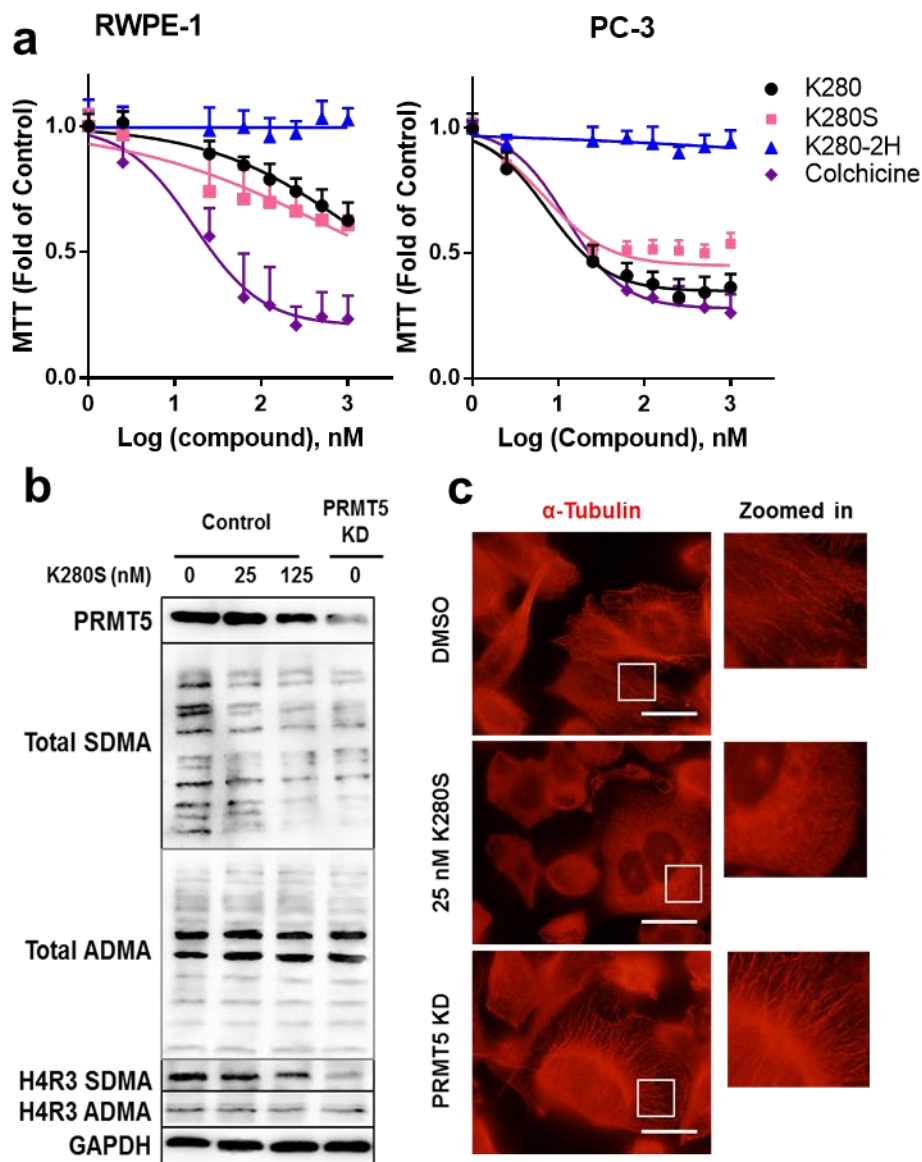
Figure S3.5 K280S induces PRMT5 inhibition and tubulin disruption on prostate cancer cells. (**a**) Cytotoxic effects of K280, K280S, K280-2H and colchicine on non-cancer (RWPE-1) and bone-derived metastatic prostate cancer (PC-3) cells after 72 hours as measured by MTT assay. (**b**) Western blot analysis of total and specific SDMA and ADMA formation of PC-3 cells after 24-hour treatment of K280S and shRNA-mediated PRMT5 KD cells. (**c**) Representative fluorescence micrographs of microtubule depolymerization on PC-3 cells after 24- hour of K280S treatment and shRNA-mediated PRMT5 KD cells. Scale bar, 10 µm.
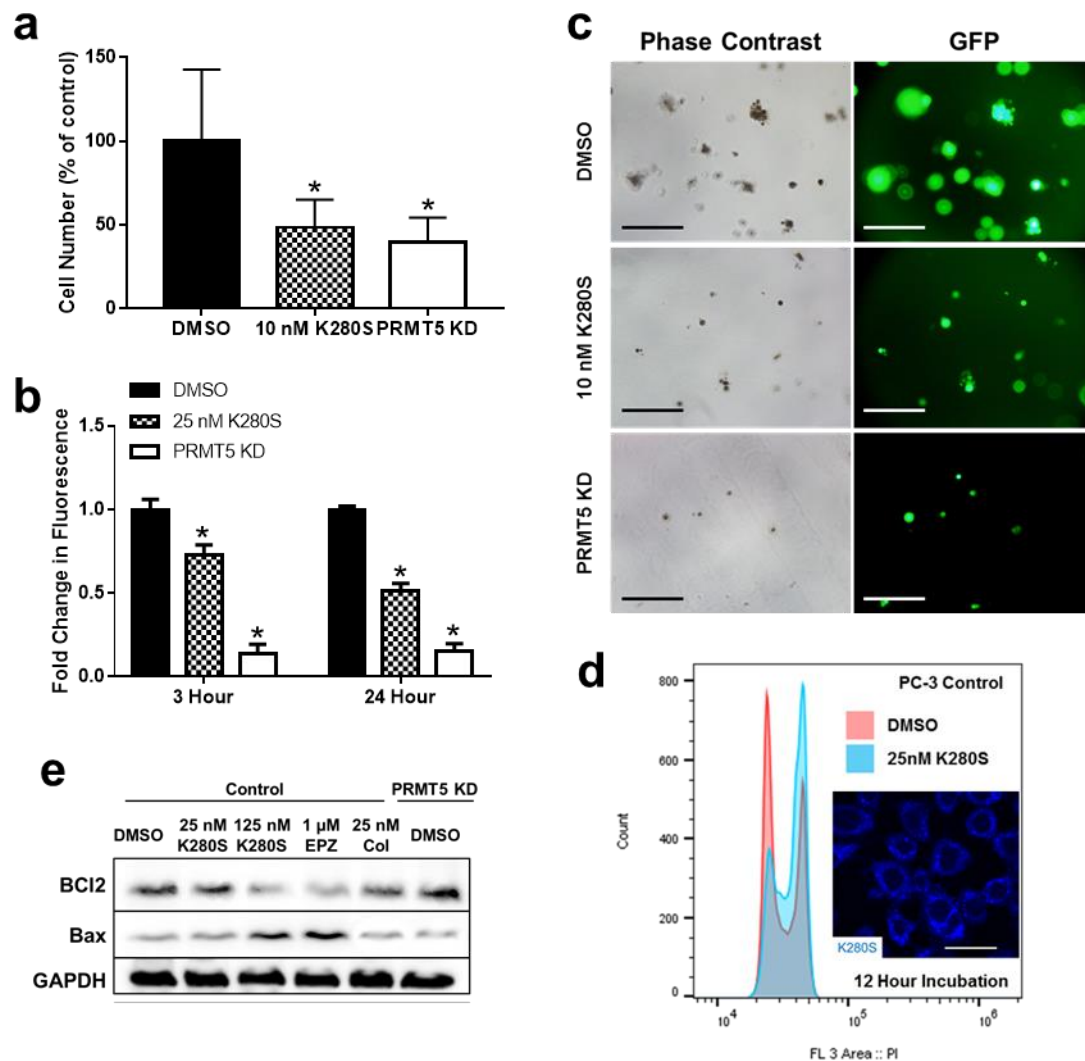
Figure S3.6 K280S inhibits migration, adhesion, cause cell cycle arrest and induce apoptosis in prostate cancer cells. (**a, b**) Cell migration quantification of K280S-treated group and shRNA-mediated PRMT5 KD group as determined by trans-well assays (**a**) and adhesion assays (**b**). (**c**) Representative 10-day spheroid formation with K280S treatment and shRNA-mediated PRMT5 KD. Left: phase contrast. Right, GFP. Scale bar, 200 µm. (**d**) K280S induced G2-M cell cycle arrest in PC-3 cells after 12-hour treatment. (**i**) Western blot analysis of apoptotic markers (BCl2 and Bax) in PC-3 cells of 24-hour drug treatment and shRNA-mediated PRMT5 KD cells.
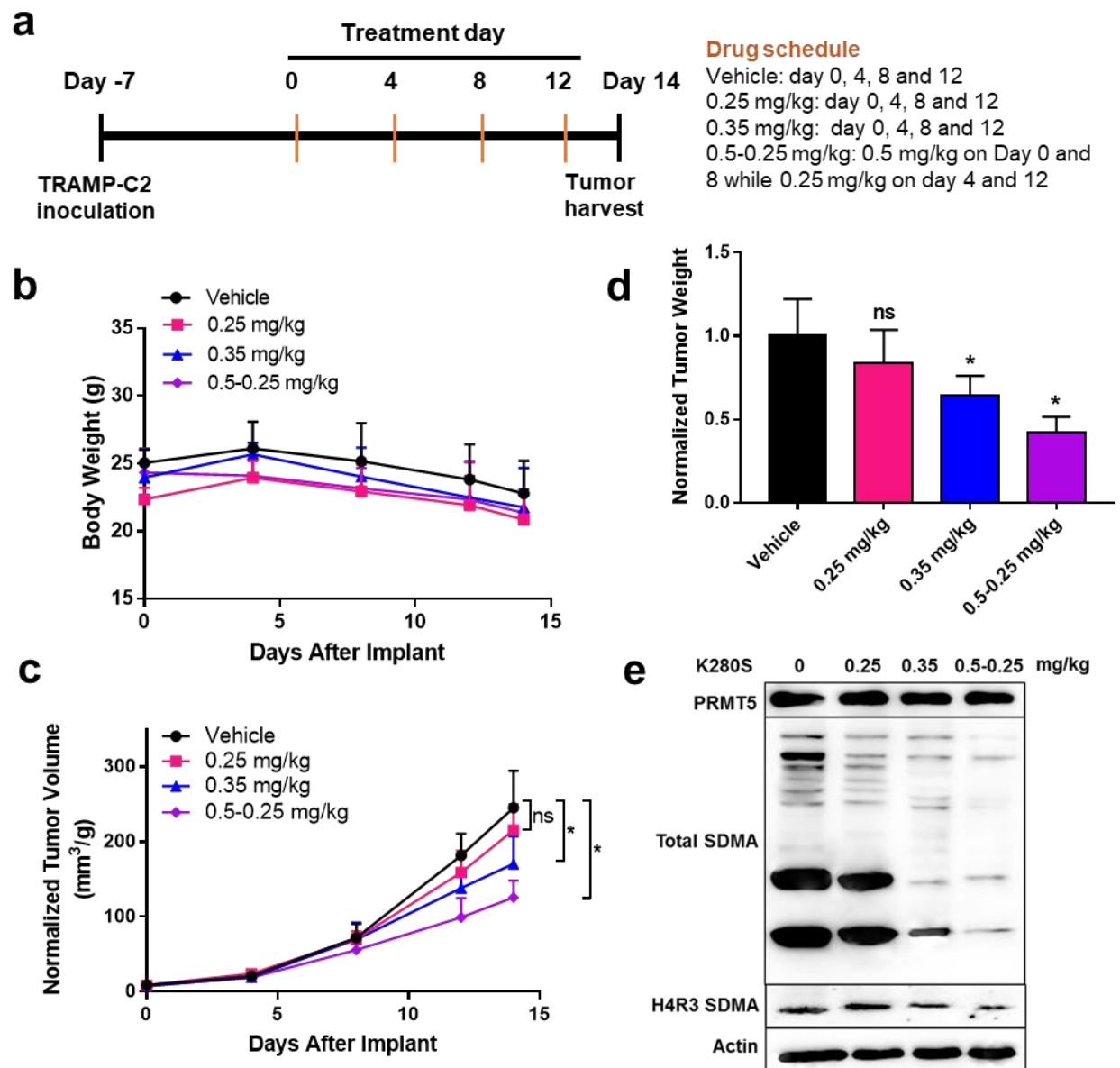
Figure S3.7 Effect of K280S in TRAMP-C2 xenograft model. (**a**) Schematic illustration of *in vivo* treatment of TRAMP C-2 prostate xenograft models. Tumor cells were seeded 7 days prior to the experiment. The tumor-bearing mice were treated with vehicle, 0.25 mg/kg, 0.35 mg/kg and 0.5-0.25 mg/kg K280S via intraperitoneal injection every 4 days for four courses. (**b-d**) Changes in body weight (**b**), tumor volume (**c**) and tumor weight (**d**) with and without K280S treatment. (**e**) Immunoblot analysis of PRMT5, SDMA, ADMA from tumor samples of untreated and treated mice. Data is presented as mean $\pm$ SD, n = 6. * $p < 0.05$.
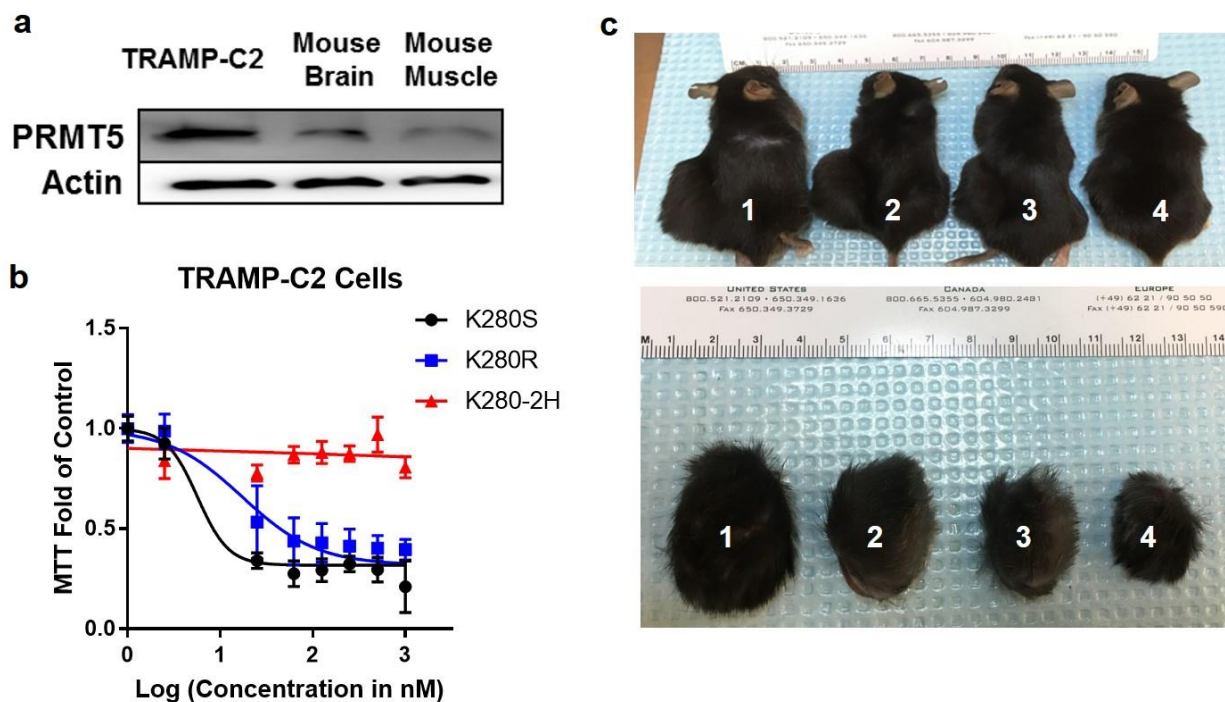
Figure S3.8 (**a**) PRMT5 expression in TRAMP-C2 cells, host mouse brain and muscle tissue. (**b**) Effect of K280 analogues on TRAMP-C2 cells. TRAMP-C2 cells were treated with various concentration of the indicated compounds and incubated for 72 hours. MTT assays were used to measure cell density. Data is presented as mean ± SD with n = 3. (**c**) Top: representative photograph of mice bearing tumor; Bottom: representative photograph of dissected tumors. Groups 1-4 represent different treatments. **1**: Control Vehicle; **2**: 0.25 mg/kg; **3**: 0.35 mg/kg; **4**: 0.5 – 0.25 mg/kg.

Table S3.1 GI$_{50}$ (nM) of compounds on PC-3 cells at specific time points.

Compounds	24 Hour	48 Hour	72 Hour
K280	475.4 ± 1.221	23.58 ± 1.183	5.867 ± 1.205
K280S	1036 ±1.598	35.49 ± 1.286	6.938 ± 1.136
K280R	1195 ± 1.651	34.92 ± 1.302	13.29 ± 1.362
Colchicine	138 ± 1.221	18.79 ± 1.159	11.21 ± 1.171

C   Supporting information for Chapter 4

Table S4.1A. Parameter values[a] of the enzyme-dependent time courses[a].

[PRMT1], µM	a	k_1, (s^{-1})	b	k_2, (s^{-1})	R^2
0.05	0.01079 ± 1.32E-04	0.04187 ± 1.05E-03	-0.01117 ± 8.97E-05	0.00287 ± 1.03E-04	0.9972
0.1	0.03605 ± 1.42E-04	0.04810 ± 3.86E-04	-0.05688 ± 9.80E-05	0.002841 ± 1.99E-05	0.9898
0.2	0.06974 ± 1.90E-04	0.06161 ± 3.34E-04	-0.1115 ± 9.25E-05	0.004804 ± 1.15E-05	0.7915
0.4	0.09437 ± 2.85E-04	0.09452 ± 5.45E-04	-0.156 ± 1.35E-04	0.006924 ± 1.12E-05	0.9977

[a]The standard deviation values of fitting with equation 2 are shown.

Table S4.1B. Slope values[a] of the enzyme-dependent time courses[a].

[PRMT1], µM	$a·k_1$, (s^{-1})	$-b·k_2$, (s^{-1})
0.05	4.52E-04 ± 1.26E-05	3.21E-05 ± 1.17E-06
0.1	1.73E-03 ± 1.55E-05	1.62E-04 ± 1.16E-06
0.2	4.30E-03 ± 2.61E-05	5.36E-04 ± 1.35E-06
0.4	8.92E-03 ± 5.81E-05	1.08E-03 ± 1.99E-05

[a]The standard deviation of the slope values are calculated from the fitting standard deviation values of a, b, k_1 and k_2.

Table S4.2A. Parameter values[a] of the cofactor SAM-dependent time courses.

[SAM], μM	a	k_1, (s⁻¹)	b	k_2, (s⁻¹)	R^2
1.5	0.0482 ± 2.31E-04	0.04402 ± 4.06E-04	-0.07363 ± 8.97E-05	0.002713 ± 1.28E-05	0.9905
3.5	0.0846 ± 3.83E-04	0.08016 ± 6.88E-04	-0.1161 ± 2.14E-04	0.007565 ± 1.73E-05	0.9937
7.5	0.1529 ± 1.79E-03	0.1778 ± 2.91E-03	-0.2054 ± 3.40E-04	0.006848 ± 1.85E-05	0.9883
15	0.1992 ± 2.65E-03	0.2476 ± 4.40E-03	-0.2664 ± 5.21E-04	0.01175 ± 3.03E-05	0.9886

[a]The standard deviation values of fitting with equation 2 are shown.

Table S4.2B. Slope values[a] of the cofactor SAM-dependent time courses.

[SAM], μM	$a \cdot k_1$, (s⁻¹)	$-b \cdot k_2$, (s⁻¹)
1.5	2.12E-03 ± 2.20E-05	2.00E-04 ± 9.72E-07
3.5	6.78E-03 ± 6.58E-05	8.78E-04 ± 2.58E-06
7.5	2.72E-02 ± 5.47E-04	1.41E-03 ± 4.46E-06
15	4.93E-02 ± 1.09E-03	3.13E-03 ± 1.01E-05

[a]The standard deviation of the slope values are calculated from the fitting standard deviation values of a, b, k_1 and k_2.

Table S4.3A. Parameter values[a] of the SAH inhibition curves.

[SAH], μM	a	k_1, (s^{-1})	b	k_2, (s^{-1})	R^2
0	0.1944 ± 4.03E-04	0.05093 ± 1.97E-04	-0.2213 ± 1.47E-04	0.003031 ± 6.73E-06	0.9972
0.1	0.2027 ± 4.00E-04	0.05995 ± 2.11E-04	-0.2201 ± 1.26E-04	0.003078 ± 5.86E-06	0.9978
0.25	0.2214 ± 4.39E-04	0.06487 ± 2.18E-04	-0.2306 ± 1.33E-04	0.002434 ± 5.47E-06	0.9977
0.5	0.2658 ± 3.49E-04	0.06324 ± 1.36E-04	-0.2629 ± 3.89E-04	0.00134 ± 4.32E-06	0.9983
1	0.2726 ± 3.65E-04	0.06815 ± 1.45E-04	-0.2134 ± 6.03E-04	0.001095 ± 5.70E-06	0.997
2.5	0.2961 ± 3.73E-04	0.07177 ± 1.40E-04	-0.1862 ± 2.16E-03	0.0005933 ± 9.36E-06	0.9944
5	0.2962 ± 3.74E-04	0.05757 ± 1.17E-04	-0.3000 ± 3.18E-02	0.0001714 ± 1.98E-05	0.9919
10	0.2774 ± 5.02E-04	0.05889 ± 1.70E-04	-0.2999 ± 2.24E-01	7.42E-05 ± 5.74E-05	0.9836

[a]The standard deviation values of fitting with equation 2 are shown.

Table S4.3B. Slope values[a] of the SAH inhibition curves.

[SAH], μM	$a \cdot k_1$, (s^{-1})	$-b \cdot k_2$, (s^{-1})
0	9.90E-03 ± 4.35E-05	6.71E-04 ± 1.55E-06
0.1	1.22E-02 ± 4.90E-05	6.77E-04 ± 1.35E-06
0.25	1.44E-02 ± 5.59E-05	5.61E-04 ± 1.30E-06
0.5	1.68E-02 ± 4.24E-05	3.52E-04 ± 1.25E-06
1	1.86E-02 ± 4.67E-05	2.34E-04 ± 1.38E-06
2.5	2.13E-02 ± 4.93E-05	1.10E-04 ± 2.16E-06
5	1.71E-02 ± 4.08E-05	5.14E-05 ± 8.08E-06
10	1.63E-02 ± 5.57E-05	2.22E-05 ± 2.71E-05

[a]The standard deviation of the slope values are calculated from the fitting standard deviation values of a, b, k_1 and k_2.

Table S4.4A. Parameter values[a] of the sinefungin inhibition curves.

[sinefungin], μM	a	k_1, (s⁻¹)	b	k_2, (s⁻¹)	R^2
0	0.1624 ± 4.09E-04	0.06256 ± 2.85E-04	-0.1869 ± 1.53E-04	3.88E-03 ± 7.52E-06	0.9970
0.0375	0.1645 ± 3.77E-04	0.0653 ± 2.62E-04	-0.1699 ± 1.17E-04	3.38E-03 ± 6.86E-06	0.9975
0.075	0.2064 ± 3.83E-04	0.05564 ± 1.79E-04	-0.2170 ± 1.94E-04	1.94E-03 ± 5.83E-06	0.9972
0.15	0.2215 ± 4.17E-04	0.05703 ± 1.83E-04	-0.2165 ± 3.17E-04	1.62E-03 ± 6.43E-06	0.9964
0.3	0.2200 ± 4.51E-04	0.05374 ± 1.88E-04	-0.1711 ± 6.89E-04	1.23E-03 ± 1.02E-05	0.9913
0.75	0.2668 ± 5.02E-04	0.05576 ± 1.77E-04	-0.1045 ± 8.19E-04	1.18E-03 ± 1.83E-05	0.984
1.5	0.287 ± 5.51E-04	0.05722 ± 1.79E-04	-0.1776 ± 8.27E-03	4.06E-04 ± 2.33E-05	0.9822
3	0.2925 ± 5.44E-04	0.05659 ± 1.69E-04	-4.517	9.13E-06 ± 3.36E-05	0.9824
7.5	0.2481 ± 5.15E-04	0.05968 ± 1.97E-04	-4.223	3.37E-06 ± 8.82E-05	0.979
15	0.2592 ± 5.43E-04	0.05599 ± 1.89E-04	-0.5239	5.08E-06 ± 5.23E-04	0.9798

[a]The standard deviation values of fitting with equation 2 are shown.

Table S4.4B. Slope values[a] of the sinefungin inhibition curves.

[sinefungin], μM	$a \cdot k_1$, (s^{-1})	$-b \cdot k_2$, (s^{-1})
0	1.02E-02 ± 5.29E-05	7.24E-04 ± 1.53E-06
0.0375	1.07E-02 ± 4.96E-05	5.74E-04 ± 1.23E-06
0.075	1.15E-02 ± 4.27E-05	4.20E-04 ± 1.32E-06
0.15	1.26E-02 ± 4.69E-05	3.51E-04 ± 1.48E-06
0.3	1.18E-02 ± 4.79E-05	2.10E-04 ± 1.94E-06
0.75	1.49E-02 ± 5.48E-05	1.23E-04 ± 2.15E-06
1.5	1.64E-02 ± 6.01E-05	7.22E-05 ± 5.34E-06
3	1.66E-02 ± 5.83E-05	4.12E-05 ± 1.52E-04
7.5	1.48E-02 ± 5.77E-05	1.42E-05 ± 3.72E-04
15	1.45E-02 ± 5.77E-05	2.66E-06 ± 2.74E-04

[a]The standard deviation of the slope values are calculated from the fitting standard deviation values of a, b, k_1 and k_2.

Table S4.5A. Parameter values[a] of the H4R3me2a inhibition curves.

[H4R3Me2a], μM	a	k_1, (s^{-1})	b	k_2, (s^{-1})	R^2
0	0.1800 ± 3.96E-04	0.06112 ± 2.52E-04	-0.1961 ± 1.47E-04	0.003422 ± 7.36E-06	0.9967
0.025	0.1544 ± 3.91E-04	0.06982 ± 3.27E-04	-0.1795 ± 1.47E-04	0.003946 ± 7.72E-06	0.9967
0.05	0.1589 ± 4.16E-04	0.06665 ± 3.21E-04	-0.1863 ± 1.43E-04	0.003437 ± 7.65E-06	0.9963
0.1	0.1731 ± 3.91E-04	0.05356 ± 2.31E-04	-0.1960 ± 1.50E-04	0.003104 ± 7.73E-06	0.9963
0.25	0.1692 ± 4.25E-04	0.05400 ± 2.60E-04	-0.1883 ± 1.69E-04	0.003253 ± 8.83E-06	0.9953
0.5	0.1282 ± 4.32E-04	0.04557 ± 3.06E-04	-0.1431 ± 2.10E-04	0.003370 ± 1.35E-05	0.9903
1	0.1156 ± 3.30E-04	0.0355 ± 2.01E-04	-0.1396 ± 5.20E-04	0.001394 ± 1.31E-05	0.9878
2	0.0723 ± 3.03E-04	0.02475 ± 2.15E-04	-0.07524 ± 5.65E-04	0.001365 ± 2.82E-05	0.9577

[a]The standard deviation values of fitting with equation 2 are shown.

Table S4.5B. Slope values*ᵃ* of the H4R3me2a inhibition curves.

[H4R3Me2a], μM	$a \cdot k_1$, (s^{-1})	$-b \cdot k_2$, (s^{-1})
0	1.10E-02 ± 5.14E-05	6.71E-04 ± 1.53E-06
0.025	1.08E-02 ± 5.74E-05	7.08E-04 ± 1.50E-06
0.05	1.06E-02 ± 5.80E-05	6.40E-04 ± 1.51E-06
0.1	9.27E-03 ± 4.52E-05	6.08E-04 ± 1.59E-06
0.25	9.14E-03 ± 4.96E-05	6.13E-04 ± 1.75E-06
0.5	5.84E-03 ± 4.38E-05	4.82E-04 ± 2.06E-06
1	4.10E-03 ± 2.60E-05	1.95E-04 ± 1.96E-06
2	1.79E-03 ± 1.72E-05	1.03E-04 ± 2.25E-06

*ᵃ*The standard deviation of the slope values are calculated from the fitting standard deviation values of a, b, k_1 and k_2.

Table S4.6A. Parameter values[a] of the DB75 inhibition curves.

[DB75], µM	a	k_1, (s^{-1})	b	k_2, (s^{-1})	R^2
0	0.1445 ± 3.59E-04	0.06205 ± 2.82E-04	-0.1741 ± 1.41E-04	0.004015 ± 7.30E-06	0.9973
2.5	0.1608 ± 3.86E-04	0.05913 ± 2.65E-04	-0.203 ± 1.66E-04	0.004151 ± 7.18E-06	0.9975
5	0.1114 ± 3.10E-04	0.06653 ± 3.34E-04	-0.14 ± 1.20E-04	0.004282 ± 7.68E-06	0.9971
7.5	0.1285 ± 3.57E-04	0.04791 ± 2.52E-04	-0.1789 ± 1.33E-04	0.002865 ± 7.66E-06	0.9965
10	0.06466 ± 3.90E-04	0.03706 ± 4.47E-04	-0.07628 ± 3.14E-04	0.004596 ± 2.82E-05	0.9754
20	0.02855 ± 5.16E-04	0.02992 ± 8.36E-04	-0.01837 ± 5.38E-04	0.005985 ± 1.62E-04	0.6643
40	0.009937 ± 5.73E-04	0.1335 ± 1.03E-02	-	-	0.9104

[a]The standard deviation values of fitting with equation 2 are shown.

Table S4.6B. Slope values[a] of the DB75 inhibition curves.

[DB75], µM	$a \cdot k_1$, (s^{-1})	$-b \cdot k_2$, (s^{-1})
0	8.97E-03 ± 4.64E-05	6.990E-04 ± 1.39E-06
2.5	9.51E-03 ± 4.83E-05	8.427E-04 ± 1.61E-06
5	7.41E-03 ± 4.25E-05	5.995E-04 ± 1.19E-06
7.5	6.16E-03 ± 3.66E-05	5.125E-04 ± 1.42E-06
10	2.40E-03 ± 3.23E-05	3.506E-04 ± 2.59E-06
20	8.54E-04 ± 2.84E-05	1.10E-04 ± 4.39E-06
40	1.33E-03 ± 1.28E-04	0

[a]The standard deviation of the slope values are calculated from the fitting standard deviation values of a, b, k_1 and k_2.

Table S4.7A. Parameter values[a] of the MS023 inhibition curves.

[MS023], µM	a	k_1, (s^{-1})	b	k_2, (s^{-1})	R^2
0	0.1306 ± 3.23E-04	0.06923 ± 3.11E-04	-0.1598 ± 1.36E-04	0.004868 ± 7.47E-06	0.9976
0.01	0.1705 ± 4.53E-04	0.05716 ± 2.73E-04	-0.2028 ± 1.46E-04	0.002997 ± 7.44E-06	0.9964
0.02	0.1706 ± 3.73E-04	0.05384 ± 2.22E-04	-0.1507 ± 1.57E-04	0.003684 ± 9.45E-06	0.9951
0.05	0.1741 ± 5.03E-04	0.05062 ± 2.70E-04	-0.1701 ± 1.74E-04	0.002741 ± 1.07E-05	0.9924
0.1	0.1833 ± 4.85E-04	0.04454 ± 2.11E-04	-0.1468 ± 1.36E-03	0.0010 ± 1.66E-05	0.9797
0.2	0.1330 ± 2.05E-03	0.03397 ± 3.62E-04	-	-	0.9648

[a]The standard deviation values of fitting with equation 2 are shown.

Table S4.7B. Slope values[a] of the MS023 inhibition curves.

[MS023], µM	$a \cdot k_1$, (s^{-1})	$-b \cdot k_2$, (s^{-1})
0	9.04E-03 ± 4.64E-05	7.78E-04 ± 1.36E-06
0.01	9.75E-03 ± 5.33E-05	6.08E-04 ± 1.57E-06
0.02	9.19E-03 ± 4.29E-05	5.55E-04 ± 1.54E-06
0.05	8.81E-03 ± 5.35E-05	4.66E-04 ± 1.88E-06
0.1	8.16E-03 ± 4.42E-05	1.47E-04 ± 2.79E-06
0.2	4.52E-03 ± 8.45E-05	-

[a]The standard deviation of the slope values are calculated from the fitting standard deviation values of a, b, k_1 and k_2.
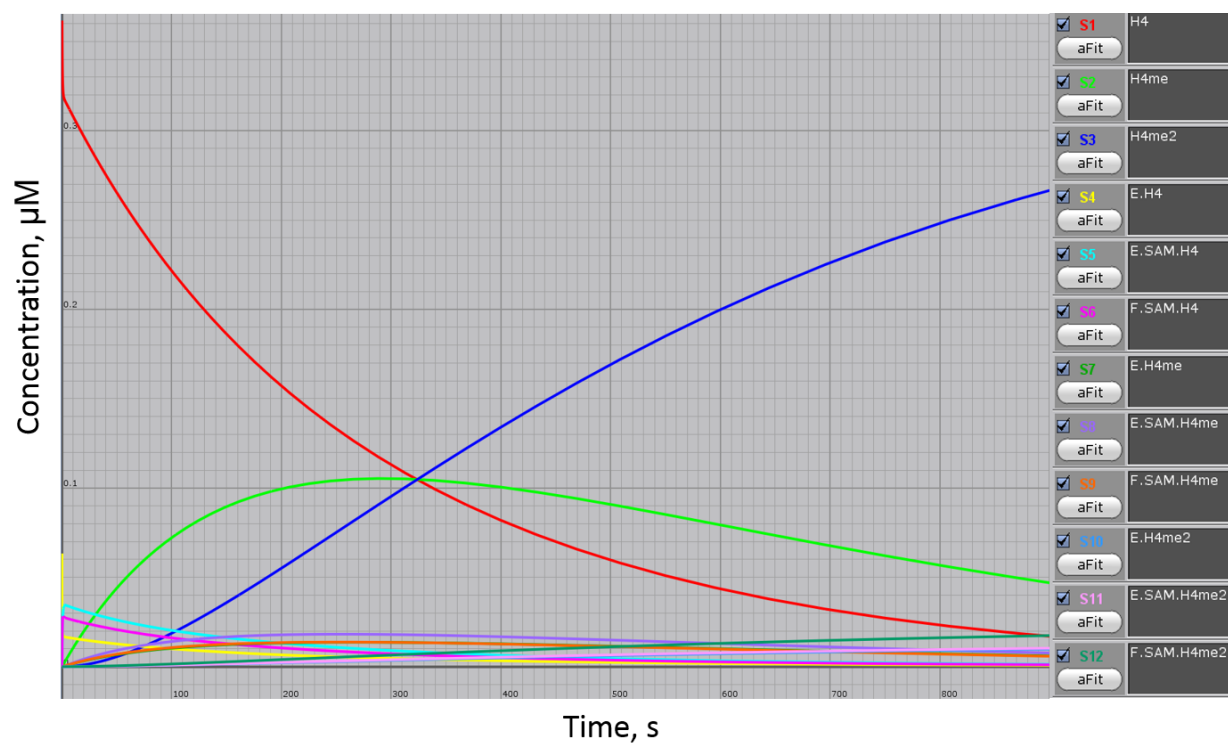
Figure S4.1A. Concentration changes of peptide-related species during the reaction ([PRMT1] = 0.2 µM, [SAM] = 3.5 µM, [H4] = 0.4 µM), simulated based on the complete kinetics model of PRMT1[1] using KinTek Explorer 5.2.

Reactions

```
E + SAM = E.SAM = F.SAM
E + H4 = E.H4
E.H4 + SAM = E.SAM.H4
E.SAM + H4 = E.SAM.H4
E.SAM.H4 = F.SAM.H4
F.SAM + H4 = F.SAM.H4
F.SAM.H4 = F.SAH.H4me
F.SAH = E.SAH = SAH + E
F.SAH + H4me = F.SAH.H4me = E.SAH.H4me
E.SAH + H4me = E.SAH.H4me
E.SAH.H4me = SAH + E.H4me
E + H4me = E.H4me
E.H4me + SAM = E.SAM.H4me
E.SAM + H4me = E.SAM.H4me
E.SAM.H4me = F.SAM.H4me
F.SAM + H4me = F.SAM.H4me
F.SAM.H4me = F.SAH.H4me2
F.SAH + H4me2 = F.SAH.H4me2 =
E.SAH.H4me2
E.SAH + H4me2 = E.SAH.H4me2
E + H4me2 = E.H4me2
E.SAH.H4me2 = SAH + E.H4me2
E.H4me2 + SAM = E.SAM.H4me2
E.SAM + H4me2 = E.SAM.H4me2
E.SAM.H4me2 = F.SAM.H4me2
F.SAM + H4me2 = F.SAM.H4me2
E.H4 + SAH = E.SAH.H4
E.SAH + H4 = E.SAH.H4
E.SAH.H4 = F.SAH.H4
F.SAH + H4 = F.SAH.H4
```

Thermodynamic Cycles:

E.H4me2=E=E.SAM=E.SAM.H4me2=E.H4me2   1.183

E.SAM.H4me=E.SAM=F.SAM=F.SAM.H4me=E.SAM.H4me   1.005

E.SAM=E.SAM.H4me2=F.SAM.H4me2=F.SAM=E.SAM   1.089

E.SAM=E=E.H4=E.SAM.H4=E.SAM   1.698

E.SAH.H4=F.SAH.H4=F.SAH=E.SAH=E.SAH.H4   1.000

E.SAH.H4me2=E.SAH=F.SAH=F.SAH.H4me2=E.SAH.H4me2   0.958

E.SAM.H4me=E.H4me=E=E.SAM=E.SAM.H4me   1.514

E.SAH.H4me=E.SAH=F.SAH=F.SAH.H4me=E.SAH.H4me   1.070

F.SAM.H4=F.SAM=E.SAM=E.SAM.H4=F.SAM.H4   0.928

Reactions	k+	k-
E + SAM = E.SAM	1.14	41
E.SAM = F.SAM	13	7
E + H4 = E.H4	79	115
E.H4 + SAM = E.SAM.H4	0.0025	0.014
E.SAM + H4 = E.SAM.H4	12	1.6
E.SAM.H4 = F.SAM.H4	0.0019	0.0022
F.SAM + H4 = F.SAM.H4	55	17
F.SAM.H4 = F.SAH.H4me	0.062	0
F.SAH = E.SAH	4	27.5
E.SAH = SAH + E	5.43	0.78
F.SAH + H4me = F.SAH.H4me	23	15
F.SAH.H4me = E.SAH.H4me	0.04	1.01
E.SAH + H4me = E.SAH.H4me	0.0067	0.015
E.SAH.H4me = SAH + E.H4me	0.03	0.001
E + H4me = E.H4me	74	34
E.H4me + SAM = E.SAM.H4me	0.12	0.67
E.SAM + H4me = E.SAM.H4me	5.1	0.24
E.SAM.H4me = F.SAM.H4me	0.00047	0.00082
F.SAM + H4me = F.SAM.H4me	60	9.1
F.SAM.H4me = F.SAH.H4me2	0.034	0
F.SAH + H4me2 = F.SAH.H4me2	38	62
F.SAH.H4me2 = E.SAH.H4me2	0.013	0.35
E.SAH + H4me2 = E.SAH.H4me2	0.003	0.02
E + H4me2 = E.H4me2	90	144
E.SAH.H4me2 = SAH + E.H4me2	0.048	0.0017
E.H4me2 + SAM = E.SAM.H4me2	0.1	0.61
E.SAM + H4me2 = E.SAM.H4me2	0.48	0.11
E.SAM.H4me2 = F.SAM.H4me2	0.0023	0.0017
F.SAM + H4me2 = F.SAM.H4me2	45	13
E.H4 + SAH = E.SAH.H4	0.04	0.16
E.SAH + H4 = E.SAH.H4	0.0092	0.0076
E.SAH.H4 = F.SAH.H4	0.67	0.2
F.SAH + H4 = F.SAH.H4	46	78

Figure S4.1B. The parameter values used for the simulation.
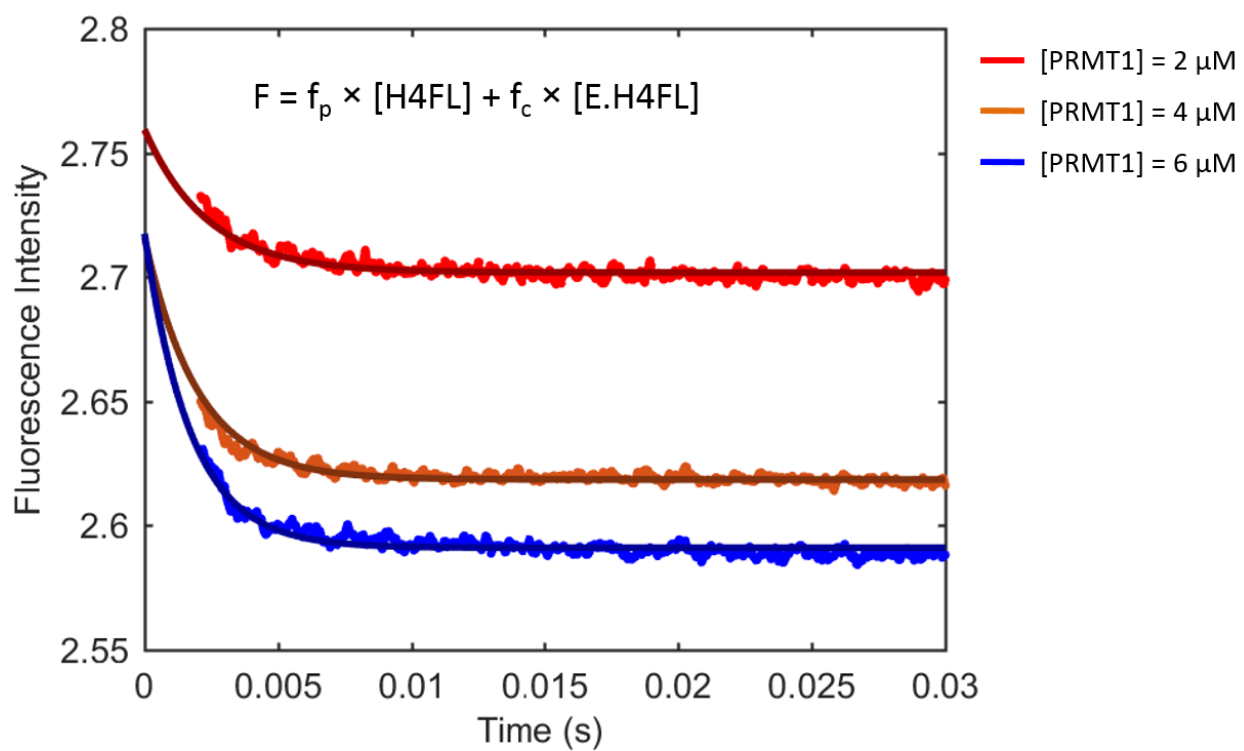
Figure S4.2. Global fitting result based on the binary binding model of PRMT1 and H4FL. The values of k_{on} and k_{off} 40 $\mu M^{-1}s^{-1}$ and 333 s^{-1} were used[2], respectively. The values of fp and fc are 6.4 μM^{-1} and 5.6 μM^{-1}, respectively. The raw data are shown in colored points and the smooth lines are the simulation results. H4FL concentration is fixed at 0.4 μM.
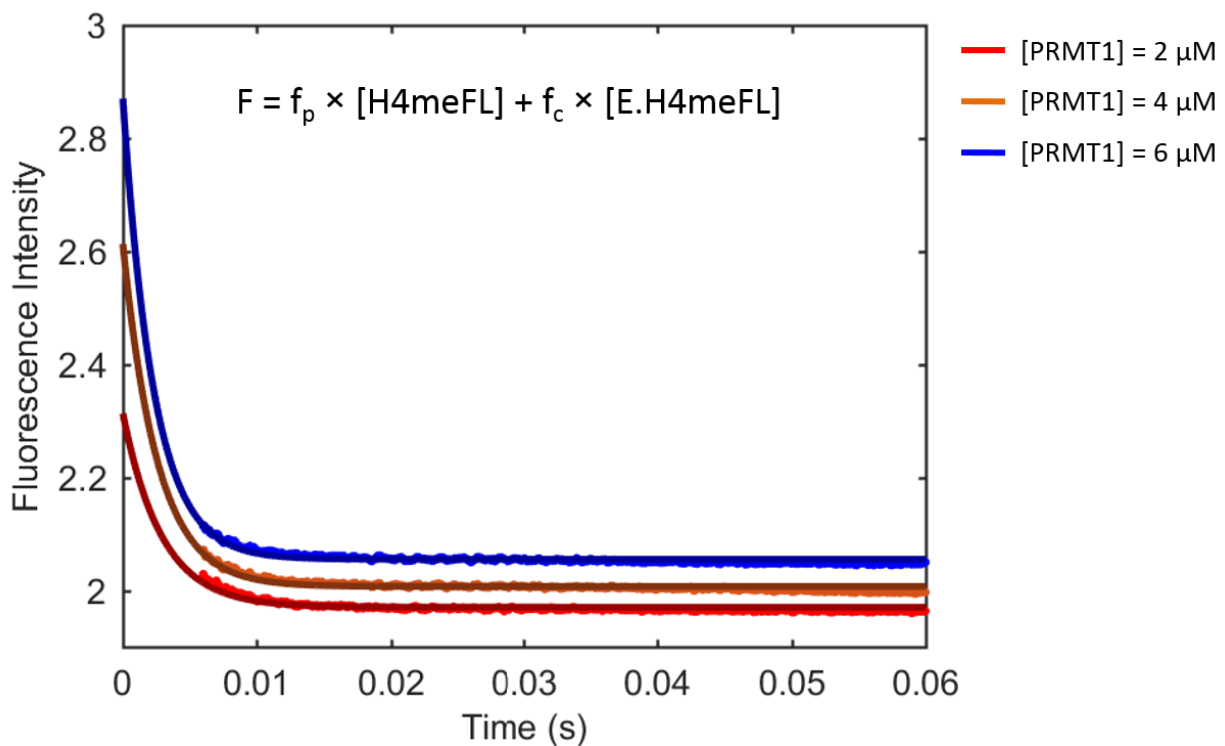
Figure S4.3. Global fitting results based on the binary binding model of PRMT1 and H4meFL. The values of k_{on} and k_{off} of 23 $\mu M^{-1} s^{-1}$ and 292 s^{-1} were used[2], respectively. The values of f_p and f_c are 5.4 μM^{-1} and 3.8 μM^{-1}, respectively. The raw data are shown in colored points and the smooth lines are the simulation results. H4meFL concentration is fixed at 0.4 μM.
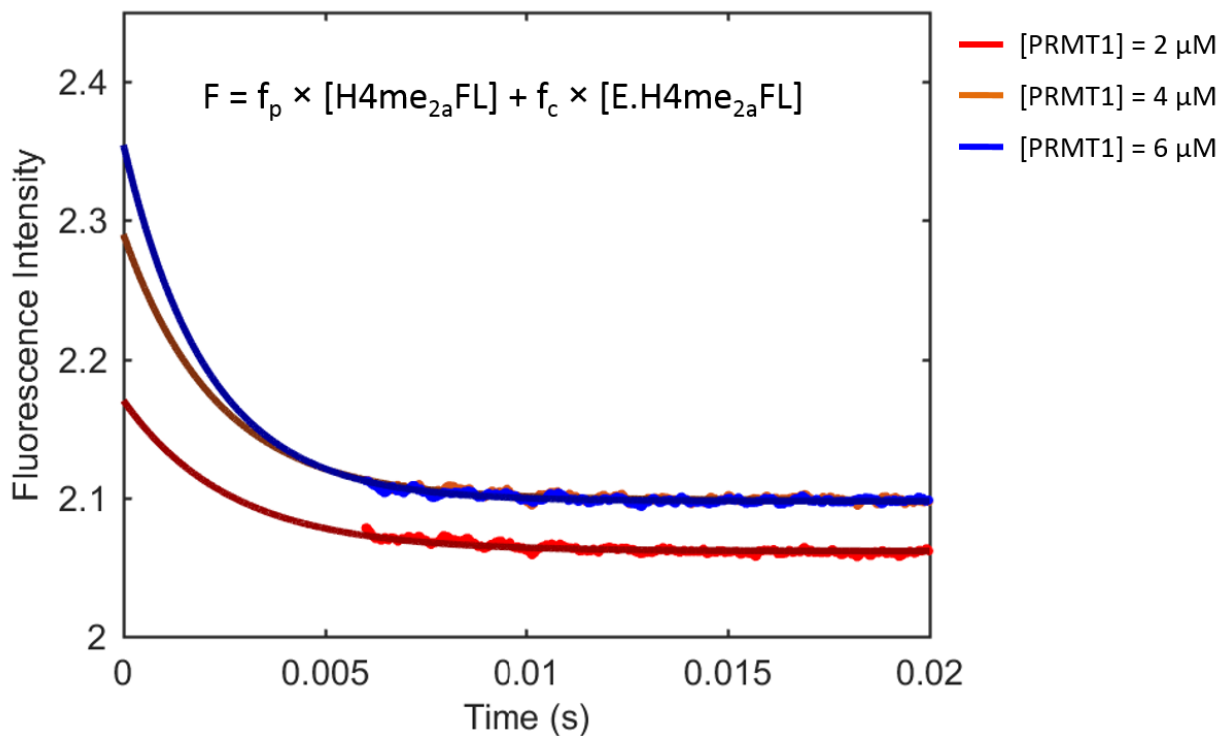
Figure S4.4. Global fitting results based on the binary binding model of PRMT1 and H4me$_{2a}$FL. The values of k_{on} and k_{off} of 26 μM^{-1}s^{-1} and 319 s^{-1} were used[2], respectively. The resulted value of f_p and f_c are 5.9 μM^{-1} and 3.9 μM^{-1}, respectively. The raw data are shown in colored points and the smooth lines are the simulation results. H4me$_2$FL concentration is fixed at 0.4 μM.
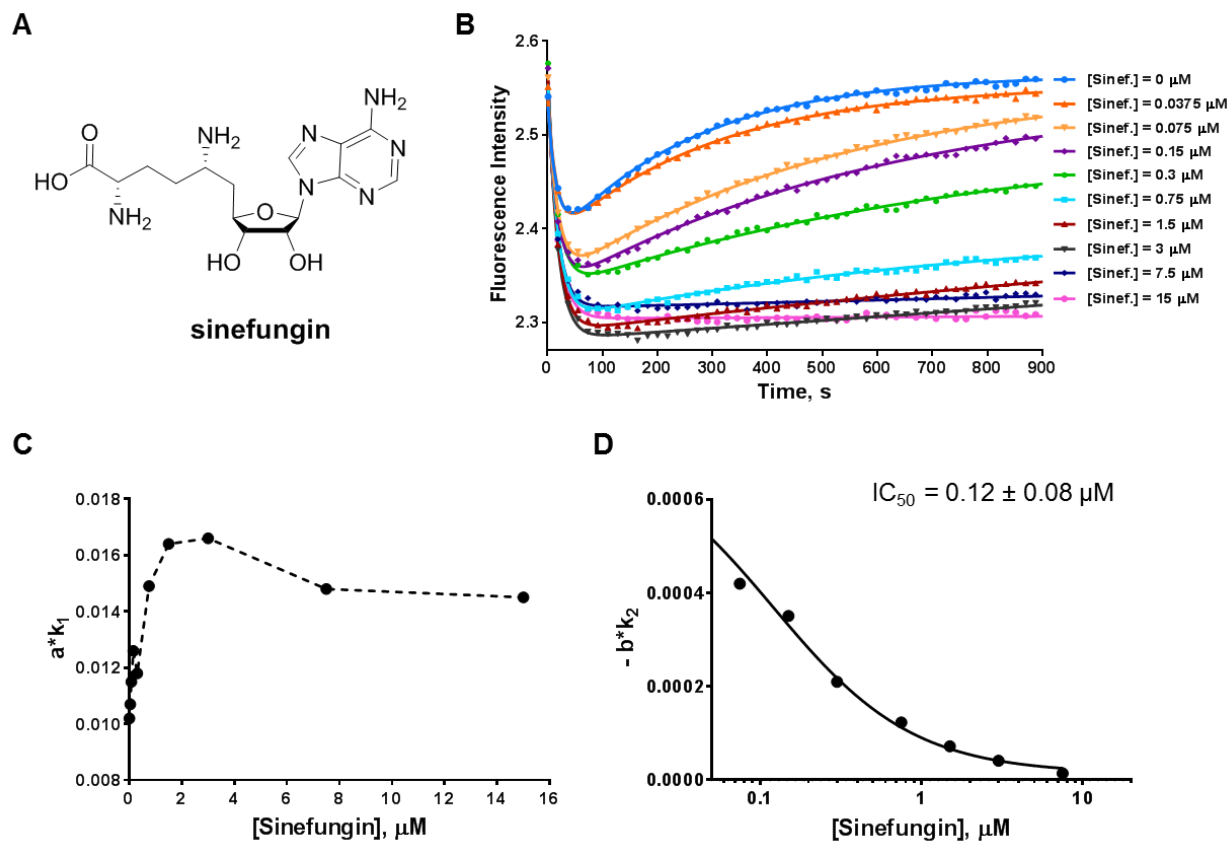
Figure S4.5. **Stopped-flow fluorescence assay of the cofactor competitive inhibitor, sinefungin**. **A.** Structure of sinefungin. In **B**, the curves are fit with equation 2 by Prism to generate values in **Table S4.4A**. Each curve used 10,000 data points, but only 50 data points are shown. Each curve is an average of 4 or 5 replicates. **C** and **D** represent the relationship of $a \cdot k_1$ or $b \cdot k_2$ with inhibitor concentrations, values listed in **Table 4B**. In **D**, the IC_{50} is calculated using **equation 1**. The reaction condition used for all experiments are [PRMT1] = 0.2 µM, [SAM] = 3.5 µM, [H4FL] = 0.4 µM, with varying concentrations of sinefungin.
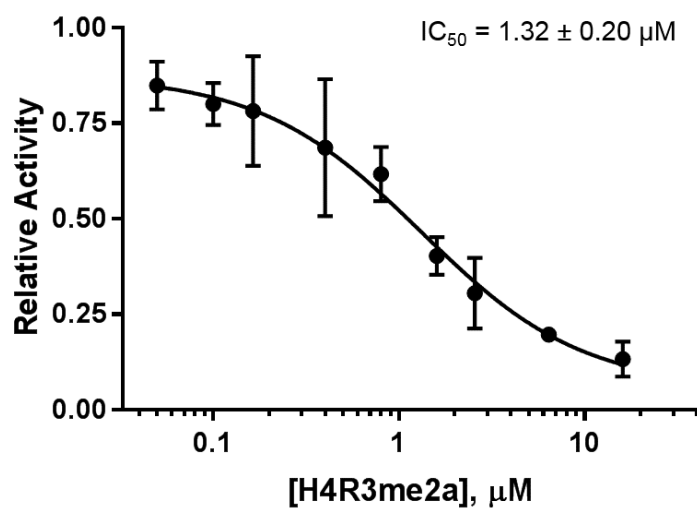
Figure S4.6. IC$_{50}$ of H4R3Me2a by filter binding assay, at the following condition: [PRMT1] = 0.2 μM, [SAM] = 3.5 μM, [H4FL] = 0.4 μM, with varying concentration of H4R3Me2a.

REFERENCES

1.   Bird, A., Perceptions of epigenetics. *Nature* **2007,** *447* (7143), 396.

2.   Berger, S. L.; Kouzarides, T.; Shiekhattar, R.; Shilatifard, A., An operational definition of epigenetics. *Genes Dev.* **2009,** *23* (7), 781-3.

3.   Riddihough, G.; Zahn, L. M., What is epigenetics? *Science* **2010,** *330* (6004), 611-611.

4.   Mohammad, F.; Mondal, T.; Kanduri, C., Epigenetics of imprinted long non-coding RNAs. *Epigenetics* **2009,** *4* (5), 277-286.

5.   Jones, P. A.; Takai, D., The Role of DNA Methylation in Mammalian Epigenetics. *Science* **2001,** *293* (5532), 1068-1070.

6.   Cedar, H.; Bergman, Y., Linking DNA methylation and histone modification: patterns and paradigms. *Nature reviews. Genetics* **2009,** *10* (5), 295.

7.   Lee, J. T., Epigenetic Regulation by Long Noncoding RNAs. *Science* **2012,** *338* (6113), 1435-1439.

8.   Finley, A.; Copeland, R. A., Small molecule control of chromatin remodeling. *Chem. Biol.* **2014,** *21* (9), 1196-210.

9.   Egger, G.; Liang, G.; Aparicio, A.; Jones, P. A., Epigenetics in human disease and prospects for epigenetic therapy. *Nature* **2004,** *429* (6990), 457.

10.   Feinberg, A. P., Phenotypic plasticity and the epigenetics of human disease. *Nature* **2007,** *447* (7143), 433.

11.   Esteller, M., Epigenetics in cancer. *N. Engl. J. Med.* **2008,** *2008* (358), 1148-1159.

12.   Jones, P. A.; Laird, P. W., Cancer-epigenetics comes of age. *Nat. Genet.* **1999,** *21* (2).

13.   Arrowsmith, C. H.; Bountra, C.; Fish, P. V.; Lee, K.; Schapira, M., Epigenetic protein families: a new frontier for drug discovery. *Nat. Rev. Drug Discov.* **2012,** *11* (5), 384-400.

14.   Pfister, S. X.; Ashworth, A., Marked for death: targeting epigenetic changes in cancer. *Nat. Rev. Drug Discov.* **2017,** *16* (4), 241-263.

15.   Kelly, A. D.; Issa, J.-P. J., The promise of epigenetic therapy: reprogramming the cancer epigenome. *Curr. Opin. Genet. Dev.* **2017,** *42*, 68-77.

16.   Dawson, Mark A.; Kouzarides, T., Cancer Epigenetics: From Mechanism to Therapy. *Cell* **2012,** *150* (1), 12-27.

17.   Campbell, R. M.; Tummino, P. J., Cancer epigenetics drug discovery and development: the challenge of hitting the mark. *The Journal of Clinical Investigation* **2014,** *124* (1), 64-69.

18.   Chadwick, R.; O'connor, A., Epigenetics and personalized medicine: prospects and ethical issues. *Per. Med.* **2013,** *10* (5), 463-471.

19.   Wang, G. G.; Allis, C. D.; Chi, P., Chromatin remodeling and cancer, Part I: Covalent histone modifications. *Trends Mol. Med.* **2007,** *13* (9), 363-72.

20.   Boksik Cha, E.-H. J., Protein arginine methyltransferases (PRMTs) as therapeutic targets. *Expert Opin. Ther. Targets* **2012,** *16* (7), 651-664.

21.   Yang, Y.; Bedford, M. T., Protein arginine methyltransferases and cancer. *Nat. Rev. Cancer* **2013,** *13* (1), 37-50.

22.   Di Lorenzo, A.; Bedford, M. T., Histone arginine methylation. *FEBS Lett.* **2011,** *585* (13), 2024-31.

23.   Cheng, D.; Cote, J.; Shaaban, S.; Bedford, M. T., The arginine methyltransferase CARM1 regulates the coupling of transcription and mRNA processing. *Mol. Cell* **2007,** *25* (1), 71-83.

24.   Bedford, M. T.; Reed, R.; Leder, P., WW domain-mediated interactions reveal a spliceosome-associated protein that binds a third class of proline-rich motif: the proline glycine and methionine-rich motif. *Proceedings of the National Academy of Sciences* **1998,** *95* (18), 10602-10607.

25.   Cheng, X.; Collins, R. E.; Zhang, X., Structural and sequence motifs of protein (histone) methylation enzymes. *Annu. Rev. Biophys. Biomol. Struct.* **2005,** *34*, 267-94.

26.   Schapira, M.; Ferreira de Freitas, R., Structural biology and chemistry of protein arginine methyltransferases. *Med. Chem. Commun.* **2014,** *5* (12), 1779-1788.

27.   Bedford, M. T., Arginine methylation at a glance. *J. Cell Sci.* **2007,** *120* (Pt 24), 4243-6.

28.   Bedford, M. T.; Richard, S., Arginine methylation an emerging regulator of protein function. *Mol. Cell* **2005,** *18* (3), 263-72.

29.   Zurita-Lopez, C. I.; Sandberg, T.; Kelly, R.; Clarke, S. G., Human protein arginine methyltransferase 7 (PRMT7) is a type III enzyme forming omega-NG-monomethylated arginine residues. *J. Biol. Chem.* **2012,** *287* (11), 7859-70.

30.   Yang, Y.; Hadjikyriacou, A.; Xia, Z.; Gayatri, S.; Kim, D.; Zurita-Lopez, C.; Kelly, R.; Guo, A.; Li, W.; Clarke, S. G.; Bedford, M. T., PRMT9 is a Type II methyltransferase that methylates the splicing factor SAP145. *Nat Commun* **2015,** *6*, 6428.

31.   Lee, J. H.; Cook, J. R.; Yang, Z. H.; Mirochnitchenko, O.; Gunderson, S. I.; Felix, A. M.; Herth, N.; Hoffmann, R.; Pestka, S., PRMT7, a new protein arginine methyltransferase that synthesizes symmetric dimethylarginine. *J. Biol. Chem.* **2005,** *280* (5), 3656-64.

32.   Cook, J. R.; Lee, J. H.; Yang, Z. H.; Krause, C. D.; Herth, N.; Hoffmann, R.; Pestka, S., FBXO11/PRMT9, a new protein arginine methyltransferase, symmetrically dimethylates arginine residues. *Biochem. Biophys. Res. Commun.* **2006,** *342* (2), 472-81.

33.   Herrmann, F.; Lee, J.; Bedford, M. T.; Fackelmayer, F. O., Dynamics of human protein arginine methyltransferase 1(PRMT1) in vivo. *J. Biol. Chem.* **2005,** *280* (45), 38005-10.

34.   Dhar, S.; Vemulapalli, V.; Patananan, A. N.; Huang, G. L.; Di Lorenzo, A.; Richard, S.; Comb, M. J.; Guo, A.; Clarke, S. G.; Bedford, M. T., Loss of the major Type I arginine methyltransferase PRMT1 causes substrate scavenging by other PRMTs. *Sci. Rep.* **2013,** *3*, 1311.

35.   Zhang X, Z. L., Cheng XD, Crystal structure of the conserved core of protein arginine methyltransferase PRMT3. *Embo. J.* **2000,** *19* (14), 3509.

36.   Zhang, X.; Cheng, X., Structure of the Predominant Protein Arginine Methyltransferase PRMT1 and Analysis of Its Binding to Substrate Peptides. *Structure* **2003,** *11* (5), 509-520.

37.   Zhang, R.; Li, X.; Liang, Z.; Zhu, K.; Lu, J.; Kong, X.; Ouyang, S.; Li, L.; Zheng, Y. G.; Luo, C., Theoretical insights into catalytic mechanism of protein arginine methyltransferase 1. *PLoS One* **2013,** *8* (8), e72424.

38.   Antonysamy, S.; Bonday, Z.; Campbell, R. M.; Doyle, B.; Druzina, Z.; Gheyi, T.; Han, B.; Jungheim, L. N.; Qian, Y.; Rauch, C.; Russell, M.; Sauder, J. M.; Wasserman, S. R.; Weichert, K.; Willard, F. S.; Zhang, A.; Emtage, S., Crystal structure of the human PRMT5:MEP50 complex. *Proc. Natl. Acad. Sci. U. S. A.* **2012,** *109* (44), 17960-5.

39.   Gui, S.; Wooderchak-Donahue, W. L.; Zang, T.; Chen, D.; Daly, M. P.; Zhou, Z. S.; Hevel, J. M., Substrate-induced control of product formation by protein arginine methyltransferase 1. *Biochemistry* **2013,** *52* (1), 199-209.

40.   Gui, S.; Gathiaka, S.; Li, J.; Qu, J.; Acevedo, O.; Hevel, J. M., A remodeled protein arginine methyltransferase 1 (PRMT1) generates symmetric dimethylarginine. *J. Biol. Chem.* **2014,** *289* (13), 9320-7.

41.   Bedford, M. T.; Clarke, S. G., Protein arginine methylation in mammals: who, what, and why. *Mol. Cell* **2009,** *33* (1), 1-13.

42.   Tripsianes, K.; Madl, T.; Machyna, M.; Fessas, D.; Englbrecht, C.; Fischer, U.; Neugebauer, K. M.; Sattler, M., Structural basis for dimethylarginine recognition by the Tudor domains of human SMN and SPF30 proteins. *Nat. Struct. Mol. Biol.* **2011,** *18* (12), 1414-20.

43.   Cheung, N.; Chan, L. C.; Thompson, A.; Cleary, M. L.; So, C. W., Protein arginine-methyltransferase-dependent oncogenesis. *Nat. Cell. Biol.* **2007,** *9* (10), 1208-15.

44.   Scorilas, A.; Black, M. H.; Talieri, M.; Diamandis, E. P., Genomic organization, physical mapping, and expression analysis of the human protein arginine methyltransferase 1 gene. *Biochem. Biophys. Res. Commun.* **2000,** *278* (2), 349-59.

45.   Frietze, S.; Lupien, M.; Silver, P. A.; Brown, M., CARM1 regulates estrogen-stimulated breast cancer growth through up-regulation of E2F1. *Cancer Res.* **2008,** *68* (1), 301-6.

46.   Wang, L.; Pal, S.; Sif, S., Protein arginine methyltransferase 5 suppresses the transcription of the RB family of tumor suppressors in leukemia and lymphoma cells. *Mol. Cell. Biol.* **2008,** *28* (20), 6262-77.

47.   Pal. S, S. S., Interplay Between Chromatin Remodelers and Protein Arginine Methyltransferases. *J. Cell. Physiol.* **2007,** *213*, 306-315.

48.   Kim, J. M. S., H. Y.; Yoon, S. Y.; Oh, J. H.; Yang, J. O.; Kim, J. H.; Song, K. S.; Rho, S. M.; Yoo, H.S.; Kim, Y.S.; Kim, J. G.; Kim, N. S., Identification of Gastric Cancer-Related Genes Using a cDNA Microarray Containing Novel Expressed Sequence Tags Expressed in Gastric Cancer Cells. *Clin. Cancer. Res.* **2005,** *11*, 473-482.

49.   Julianne M. Yost, I. K., Feng Liu, Cen Gao and Jian Jin, Targets in Epigenetics: Inhibiting the Methyl Writers of the Histone Code. *Current Chemical Genomics* **2011,** *5*, 72-84.

50.   Hu, H.; Qian, K.; Ho, M.-C.; Zheng, Y. G., Small Molecule Inhibitors of Protein Arginine Methyltransferases. *Expert Opinion on Investigational Drugs* **2016,** *25* (3), 335-358.

51.   Strahl, B. D.; Briggs, S. D.; Brame, C. J.; Caldwell, J. A.; Koh, S. S.; Ma, H.; Cook, R. G.; Shabanowitz, J.; Hunt, D. F.; Stallcup, M. R., Methylation of histone H4 at arginine 3 occurs in vivo and is mediated by the nuclear receptor coactivator PRMT1. *Curr. Biol.* **2001,** *11* (12), 996-1000.

52.   Rajpurohit, R.; Lee, S. O.; Park, J. O.; Paik, W. K.; Kim, S., Enzymatic methylation of recombinant heterogeneous nuclear RNP protein A1. Dual substrate specificity for S-adenosylmethionine: histone-arginine N-methyltransferase. *J. Biol. Chem.* **1994,** *269* (2), 1075-1082.

53.   Lin, W.-J.; Gary, J. D.; Yang, M. C.; Clarke, S.; Herschman, H. R., The mammalian immediate-early TIS21 protein and the leukemia-associated BTG1 protein interact with a protein-arginine N-methyltransferase. *Journal of Biological Chemistry* **1996,** *271* (25), 15034-15044.

54.   Abramovich, C.; Yakobson, B.; Chebath, J.; Revel, M., A protein‐arginine methyltransferase binds to the intracytoplasmic domain of the IFNAR1 chain in the type I interferon receptor. *The EMBO journal* **1997,** *16* (2), 260-266.

55.   Tang, J.; Kao, P. N.; Herschman, H. R., Protein-arginine methyltransferase I, the predominant protein-arginine methyltransferase in cells, interacts with and is regulated by interleukin enhancer-binding factor 3. *J. Biol. Chem.* **2000,** *275* (26), 19866-19876.

56.   Kwak, Y. T.; Guo, J.; Prajapati, S.; Park, K.-J.; Surabhi, R. M.; Miller, B.; Gehrig, P.; Gaynor, R. B., Methylation of SPT5 regulates its interaction with RNA polymerase II and transcriptional elongation properties. *Mol. Cell* **2003,** *11* (4), 1055-1066.

57.	Herrmann, F.; Bossert, M.; Schwander, A.; Akgün, E.; Fackelmayer, F. O., Arginine methylation of scaffold attachment factor A by heterogeneous nuclear ribonucleoprotein particle-associated PRMT1. *J. Biol. Chem.* **2004,** *279* (47), 48774-48779.

58.	Boisvert, F.-M.; Rhie, A.; Richard, S.; Doherty, A. J., The GAR motif of 53BP1 is arginine methylated by PRMT1 and is necessary for 53BP1 DNA binding activity. *Cell Cycle* **2005,** *4* (12), 1834-1841.

59.	Boisvert, F.-M.; Déry, U.; Masson, J.-Y.; Richard, S., Arginine methylation of MRE11 by PRMT1 is required for DNA damage checkpoint control. *Genes Dev.* **2005,** *19* (6), 671-676.

60.	Dolzhanskaya, N.; Merz, G.; Denman, R. B., Alternative splicing modulates protein arginine methyltransferase-dependent methylation of fragile X syndrome mental retardation protein. *Biochemistry* **2006,** *45* (34), 10385-10393.

61.	Rho, J.; Choi, S.; Jung, C.-R.; Im, D.-S., Arginine methylation of Sam68 and SLM proteins negatively regulates their poly (U) RNA binding activity. *Arch. Biochem. Biophys.* **2007,** *466* (1), 49-57.

62.	Le Romancer, M.; Treilleux, I.; Leconte, N.; Robin-Lespinasse, Y.; Sentis, S.; Bouchekioua-Bouzaghou, K.; Goddard, S.; Gobert-Gosse, S.; Corbo, L., Regulation of estrogen rapid signaling through arginine methylation by PRMT1. *Molecular cell* **2008,** *31* (2), 212-221.

63.	Zhao, X.; Jankovic, V.; Gural, A.; Huang, G.; Pardanani, A.; Menendez, S.; Zhang, J.; Dunne, R.; Xiao, A.; Erdjument-Bromage, H., Methylation of RUNX1 by PRMT1 abrogates SIN3A binding and potentiates its transcriptional activity. *Genes Dev.* **2008,** *22* (5), 640-653.

64.	Jobert, L.; Argentini, M.; Tora, L., PRMT1 mediated methylation of TAF15 is required for its positive gene regulatory function. *Exp. Cell Res.* **2009,** *315* (7), 1273-1286.

65.   Jansson, M.; Durant, S. T.; Cho, E. C.; Sheahan, S.; Edelmann, M.; Kessler, B.; La Thangue, N. B., Arginine methylation regulates the p53 response. *Nat. Cell Biol.* **2008,** *10* (12), 1431-9.

66.   Martin, G.; Ostareck-Lederer, A.; Chari, A.; Neuenkirchen, N.; Dettwiler, S.; Blank, D.; Rüegsegger, U.; Fischer, U.; Keller, W., Arginine methylation in subunits of mammalian pre-mRNA cleavage factor I. *RNA* **2010,** *16* (8), 1646-1659.

67.   Butler, J. S.; Zurita-Lopez, C. I.; Clarke, S. G.; Bedford, M. T.; Dent, S. Y., Protein-arginine methyltransferase 1 (PRMT1) methylates Ash2L, a shared component of mammalian histone H3K4 methyltransferase complexes. *J. Biol. Chem.* **2011,** *286* (14), 12234-12244.

68.   Perreault, A.; Lemieux, C.; Bachand, F., Regulation of the nuclear poly (A)-binding protein by arginine methylation in fission yeast. *J. Biol. Chem.* **2007,** *282* (10), 7552-7562.

69.   An, W.; Kim, J.; Roeder, R. G., Ordered Cooperative Functions of PRMT1, p300, and CARM1 in Transcriptional Activation by p53. *Cell* **2004,** *117* (6), 735-748.

70.   Aletta, J. M.; Cimato, T. R.; Ettinger, M. J., Protein methylation: a signal event in post-translational modification. *Trends Biochem. Sci.* **1998,** *23* (3), 89-91.

71.   Zhang, L.; Wang, R.; Su, H.; Abdel-Wahab, O.; Hrick, T.; Levine, R. L.; Deng, H.; Liu, Y.; Zheng, Y.; Luo, M., Arginine Methylation Of RBM15 By PRMT1 Controls Alternative Splicing Of Genes Involved In Megakaryocyte Differentiation. *Blood* **2013,** *122* (21), 2443-2443.

72.   Zakrzewicz, D.; Zakrzewicz, A.; Preissner, K. T.; Markart, P.; Wygrecka, M., Protein arginine methyltransferases (PRMTs): promising targets for the treatment of pulmonary disorders. *International journal of molecular sciences* **2012,** *13* (10), 12383-12400.

73.   Sun, Q.; Yang, X.; Zhong, B.; Jiao, F.; Li, C.; Li, D.; Lan, X.; Sun, J.; Lu, S., Upregulated protein arginine methyltransferase 1 by IL-4 increases eotaxin-1 expression in airway epithelial cells and participates in antigen-induced pulmonary inflammation in rats. *The Journal of Immunology* **2012,** *188* (7), 3506-3512.

74.   Sun, Q.; Liu, L.; Roth, M.; Tian, J.; He, Q.; Zhong, B.; Bao, R.; Lan, X.; Jiang, C.; Sun, J.; Yang, X.; Lu, S., PRMT1 Upregulated by Epithelial Proinflammatory Cytokines Participates in COX2 Expression in Fibroblasts and Chronic Antigen-Induced Pulmonary Inflammation. *The Journal of Immunology* **2015,** *195* (1), 298-306.

75.   Vallance, P.; Leiper, J., Cardiovascular biology of the asymmetric dimethylarginine: dimethylarginine dimethylaminohydrolase pathway. *Atertio. Thromb. Vasc. Biol.* **2004,** *24* (6), 1023-1030.

76.   Bouras, G.; Deftereos, S.; Tousoulis, D.; Giannopoulos, G.; Chatzis, G.; Tsounis, D.; W Cleman, M.; Stefanadis, C., Asymmetric dimethylarginine (ADMA): a promising biomarker for cardiovascular disease? *Curr. Top. Med. Chem.* **2013,** *13* (2), 180-200.

77.   Lajer, M.; Tarnow, L.; Jorsal, A.; Teerlink, T.; Parving, H.-H.; Rossing, P., Plasma concentration of asymmetric dimethylarginine (ADMA) predicts cardiovascular morbidity and mortality in type 1 diabetic patients with diabetic nephropathy. *Diabetes Care* **2008,** *31* (4), 747-752.

78.   Iwasaki, H., Impaired PRMT1 activity in the liver and pancreas of type 2 diabetic Goto–Kakizaki rats. *Life Sci.* **2009,** *85* (3), 161-166.

79.   Baylis, C., Arginine, arginine analogs and nitric oxide production in chronic kidney disease. *Nature Clinical Practice Nephrology* **2006,** *2* (4), 209-220.

80.   Schwedhelm, E.; Böger, R. H., The role of asymmetric and symmetric dimethylarginines in renal disease. *Nature Reviews Nephrology* **2011,** *7* (5), 275-285.

81.   Cvetković, T.; Pavlović, R.; Đorđević, V.; Stojanović, I.; Veličković-Radovanović, R.; Ignjatović, A.; Stefanović, N.; Živanović, S.; Đorđević, V., Dimethylarginine – biomarkers in progression of kidney disease *Journal of Medical Biochemistry* **2012,** *31* (4), 301-308.

82.   Raptis, V.; Kapoulas, S.; Grekas, D., Role of asymmetrical dimethylarginine in the progression of renal disease. *Nephrology* **2013,** *18* (1), 11-21.

83.   Lakowski, T.; Frankel, A., Kinetic analysis of human protein arginine N-methyltransferase 2: formation of monomethyl-and asymmetric dimethyl-arginine residues on histone H4. *Biochem. J* **2009,** *421*, 253-261.

84.   Qi, C.; Chang, J.; Zhu, Y.; Yeldandi, A. V.; Rao, S. M.; Zhu, Y.-J., Identification of protein arginine methyltransferase 2 as a coactivator for estrogen receptor α. *J. Biol. Chem.* **2002,** *277* (32), 28624-28630.

85.   Buss, H.; Dörrie, A.; Schmitz, M. L.; Frank, R.; Livingstone, M.; Resch, K.; Kracht, M., Phosphorylation of serine 468 by GSK-3β negatively regulates basal p65 NF-κB activity. *J. Biol. Chem.* **2004,** *279* (48), 49571-49574.

86.   Meyer, R.; Wolf, S. S.; Obendorf, M., PRMT2, a member of the protein arginine methyltransferase family, is a coactivator of the androgen receptor. *The Journal of steroid biochemistry and molecular biology* **2007,** *107* (1), 1-14.

87.   Zhong, J.; Cao, R.-X.; Hong, T.; Yang, J.; Zu, X.-Y.; Xiao, X.-H.; Liu, J.-H.; Wen, G.-B., Identification and expression analysis of a novel transcript of the human PRMT2 gene resulted from alternative polyadenylation in breast cancer. *Gene* **2011,** *487* (1), 1-9.

88.	Zhong, J.; Cao, R. X.; Zu, X. Y.; Hong, T.; Yang, J.; Liu, L.; Xiao, X. H.; Ding, W. J.; Zhao, Q.; Liu, J. H., Identification and characterization of novel spliced variants of PRMT2 in breast carcinoma. *FEBS J.* **2012,** *279* (2), 316-335.

89.	Yildirim, A. O.; Bulau, P.; Zakrzewicz, D.; Kitowska, K. E.; Weissmann, N.; Grimminger, F.; Morty, R. E.; Eickelberg, O., Increased protein arginine methylation in chronic hypoxia: role of protein arginine methyltransferases. *Am. J. Respir. Cell Mol. Biol.* **2006,** *35* (4), 436-443.

90.	Swiercz, R.; Cheng, D.; Kim, D.; Bedford, M. T., Ribosomal protein rpS2 is hypomethylated in PRMT3-deficient mice. *J. Biol. Chem.* **2007,** *282* (23), 16917-16923.

91.	Bachand, F.; Silver, P. A., PRMT3 is a ribosomal protein methyltransferase that affects the cellular levels of ribosomal subunits. *The EMBO journal* **2004,** *23* (13), 2641-2650.

92.	Chen, X.; Niroomand, F.; Liu, Z.; Zankl, A.; Katus, H.; Jahn, L.; Tiefenbacher, C., Expression of nitric oxide related enzymes in coronary heart disease. *Basic Res. Cardiol.* **2006,** *101* (4), 346-353.

93.	Matsuguma, K.; Ueda, S.; Yamagishi, S.-i.; Matsumoto, Y.; Kaneyuki, U.; Shibata, R.; Fujimura, T.; Matsuoka, H.; Kimoto, M.; Kato, S.; Imaizumi, T.; Okuda, S., Molecular Mechanism for Elevation of Asymmetric Dimethylarginine and Its Role for Hypertension in Chronic Kidney Disease. *J. Am. Soc. Nephrol.* **2006,** *17* (8), 2176-2183.

94.	Schurter, B. T.; Koh, S. S.; Chen, D.; Bunick, G. J.; Harp, J. M.; Hanson, B. L.; Henschen-Edman, A.; Mackay, D. R.; Stallcup, M. R.; Aswad, D. W., Methylation of histone H3 by coactivator-associated arginine methyltransferase 1. *Biochemistry* **2001,** *40* (19), 5747-5756.

95.	Lee, J.; Bedford, M. T., PABP1 identified as an arginine methyltransferase substrate using high‐density protein arrays. *EMBO reports* **2002,** *3* (3), 268-273.

96.	Lee, Y.-H.; Coonrod, S. A.; Kraus, W. L.; Jelinek, M. A.; Stallcup, M. R., Regulation of coactivator complex assembly and function by protein arginine methylation and demethylimination. *Proc. Natl. Acad. Sci. U. S. A.* **2005,** *102* (10), 3611-3616.

97.	Ito, T.; Yadav, N.; Lee, J.; Furumatsu, T.; Yamashita, S.; Yoshida, K.; Taniguchi, N.; Hashimoto, M.; Tsuchiya, M.; Ozaki, T., Arginine methyltransferase CARM1/PRMT4 regulates endochondral ossification. *BMC Dev. Biol.* **2009,** *9* (1), 47.

98.	Fujiwara, T.; Mori, Y.; Chu, D. L.; Koyama, Y.; Miyata, S.; Tanaka, H.; Yachi, K.; Kubo, T.; Yoshikawa, H.; Tohyama, M., CARM1 regulates proliferation of PC12 cells by methylating HuD. *Mol. Cell. Biol.* **2006,** *26* (6), 2273-2285.

99.	Chen, S. L.; Loffler, K. A.; Chen, D.; Stallcup, M. R.; Muscat, G. E., The Coactivator-associated Arginine Methyltransferase Is Necessary for Muscle Differentiation CARM1 COACTIVATES MYOCYTE ENHANCER FACTOR-2. *J. Biol. Chem.* **2002,** *277* (6), 4324-4333.

100.	Jeong, S.-J.; Lu, H.; Cho, W.-K.; Park, H. U.; Pise-Masison, C.; Brady, J. N., Coactivator-Associated Arginine Methyltransferase 1 Enhances Transcriptional Activity of the Human T-Cell Lymphotropic Virus Type 1 Long Terminal Repeat through Direct Interaction with Tax. *J. Virol.* **2006,** *80* (20), 10036-10044.

101.	Pal, S.; Vishwanath, S. N.; Erdjument-Bromage, H.; Tempst, P.; Sif, S., Human SWI/SNF-associated PRMT5 methylates histone H3 arginine 8 and negatively regulates expression of ST7 and NM23 tumor suppressor genes. *Molecular and cellular biology* **2004,** *24* (21), 9630-9645.

102.	Migliori, V.; Müller, J.; Phalke, S.; Low, D.; Bezzi, M.; Mok, W. C.; Sahu, S. K.; Gunaratne, J.; Capasso, P.; Bassi, C., Symmetric dimethylation of H3R2 is a newly identified

histone mark that supports euchromatin maintenance. *Nat. Struct. Mol. Biol.* **2012,** *19* (2), 136-144.

103. Baldwin, G.; Carnegie, P., Specific enzymic methylation of an arginine in the experimental allergic encephalomyelitis protein from human myelin. *Science* **1971,** *171* (3971), 579-581.

104. Brahms, H.; Raymackers, J.; Union, A.; De Keyser, F.; Meheus, L.; Lührmann, R., The C-terminal RG dipeptide repeats of the spliceosomal Sm proteins D1 and D3 contain symmetrical dimethylarginines, which form a major B-cell epitope for anti-Sm autoantibodies. *J. Biol. Chem.* **2000,** *275* (22), 17122-17129.

105. Barth, S.; Liss, M.; Voss, M. D.; Dobner, T.; Fischer, U.; Meister, G.; Grässer, F. A., Epstein-Barr virus nuclear antigen 2 binds via its methylated arginine-glycine repeat to the survival motor neuron protein. *J. Virol.* **2003,** *77* (8), 5008-5013.

106. Shire, K.; Kapoor, P.; Jiang, K.; Hing, M. N. T.; Sivachandran, N.; Nguyen, T.; Frappier, L., Regulation of the EBNA1 Epstein-Barr virus protein by serine phosphorylation and arginine methylation. *J. Virol.* **2006,** *80* (11), 5261-5272.

107. Yang, M.; Sun, J.; Sun, X.; Shen, Q.; Gao, Z.; Yang, C., Caenorhabditis elegans protein arginine methyltransferase PRMT-5 negatively regulates DNA damage-induced apoptosis. **2009**.

108. Powers, M. A.; Fay, M. M.; Factor, R. E.; Welm, A. L.; Ullman, K. S., Protein arginine methyltransferase 5 accelerates tumor growth by arginine methylation of the tumor suppressor programmed cell death 4. *Cancer Res.* **2011,** *71* (16), 5579-5587.

109. Bandyopadhyay, S.; Harris, D. P.; Adams, G. N.; Lause, G. E.; McHugh, A.; Tillmaand, E. G.; Money, A.; Willard, B.; Fox, P. L.; DiCorleto, P. E., HOXA9 Methylation by PRMT5 Is

Essential for Endothelial Cell Expression of Leukocyte Adhesion Molecules. *Mol. Cell. Biol.* **2012,** *32* (7), 1202-1213.

110.   Wei, H.; Wang, B.; Miyagi, M.; She, Y.; Gopalan, B.; Huang, D.-B.; Ghosh, G.; Stark, G. R.; Lu, T., PRMT5 dimethylates R30 of the p65 subunit to activate NF-κB. *Proceedings of the National Academy of Sciences* **2013,** *110* (33), 13516-13521.

111.   Deng, X.; Gu, L.; Liu, C.; Lu, T.; Lu, F.; Lu, Z.; Cui, P.; Pei, Y.; Wang, B.; Hu, S., Arginine methylation mediated by the Arabidopsis homolog of PRMT5 is essential for proper pre-mRNA splicing. *Proceedings of the National Academy of Sciences* **2010,** *107* (44), 19114-19119.

112.   Andreu-Perez, P.; Esteve-Puig, R.; de Torre-Minguela, C.; Lopez-Fauqued, M.; Bech-Serra, J. J.; Tenbaum, S.; Garcia-Trevijano, E. R.; Canals, F.; Merlino, G.; Avila, M. A., Protein arginine methyltransferase 5 regulates ERK1/2 signal transduction amplitude and cell fate through CRAF. *Science signaling* **2011,** *4* (190), ra58-ra58.

113.   Nishida, K. M.; Okada, T. N.; Kawamura, T.; Mituyama, T.; Kawamura, Y.; Inagaki, S.; Huang, H.; Chen, D.; Kodama, T.; Siomi, H., Functional involvement of Tudor and dPRMT5 in the piRNA processing pathway in Drosophila germlines. *The EMBO journal* **2009,** *28* (24), 3820-3831.

114.   Gu, Z.; Li, Y.; Lee, P.; Liu, T.; Wan, C.; Wang, Z., Protein arginine methyltransferase 5 functions in opposite ways in the cytoplasm and nucleus of prostate cancer cells. *PLoS One* **2012,** *7* (8), e44033.

115.   Bode-Böger, S. M.; Scalera, F.; Kielstein, J. T.; Martens-Lobenhoffer, J.; Breithardt, G.; Fobker, M.; Reinecke, H., Symmetrical dimethylarginine: a new combined parameter for renal function and extent of coronary artery disease. *J. Am. Soc. Nephrol.* **2006,** *17* (4), 1128-1134.

116.   Ratovitski, T.; Arbez, N.; Stewart, J. C.; Chighladze, E.; Ross, C. A., PRMT5-mediated symmetric arginine dimethylation is attenuated by mutant huntingtin and is impaired in Huntington's Disease (HD). *Cell Cycle* **2015,** (just-accepted), 00-00.

117.   Quan, X.; Yue, W.; Luo, Y.; Cao, J.; Wang, H.; Wang, Y.; Lu, Z., The protein arginine methyltransferase PRMT5 regulates Aβ‐induced toxicity in human cells and Caenorhabditis elegans models of Alzheimer's disease. *J. Neurochem.* **2015,** *134* (5), 969-977.

118.   Waldmann, T.; Izzo, A.; Kamieniarz, K.; Richter, F.; Vogler, C.; Sarg, B.; Lindner, H.; Young, N. L.; Mittler, G. M. J.; Garcia, B. A., *Methylation of H2AR29 is a novel repressive PRMT6 target*. Bibliothek der Universität Konstanz: 2011.

119.   Guccione, E.; Bassi, C.; Casadio, F.; Martinato, F.; Cesaroni, M.; Schuchlautz, H.; Lüscher, B.; Amati, B., Methylation of histone H3R2 by PRMT6 and H3K4 by an MLL complex are mutually exclusive. *Nature* **2007,** *449* (7164), 933-937.

120.   Frankel, A.; Yadav, N.; Lee, J.; Branscombe, T. L.; Clarke, S.; Bedford, M. T., The novel human protein arginine N-methyltransferase PRMT6 is a nuclear enzyme displaying unique substrate specificity. *J. Biol. Chem.* **2002,** *277* (5), 3537-3543.

121.   Singhroy, D. N.; Mesplède, T.; Sabbah, A.; Quashie, P. K.; Falgueyret, J.-P.; Wainberg, M. A., Automethylation of protein arginine methyltransferase 6 (PRMT6) regulates its stability and its anti-HIV-1 activity. *Retrovirology* **2013,** *10* (1), 73.

122.   Boulanger, M.-C.; Liang, C.; Russell, R. S.; Lin, R.; Bedford, M. T.; Wainberg, M. A.; Richard, S., Methylation of Tat by PRMT6 regulates human immunodeficiency virus type 1 gene expression. *J. Virol.* **2005,** *79* (1), 124-131.

123.   Sgarra, R.; Lee, J.; Tessari, M. A.; Altamura, S.; Spolaore, B.; Giancotti, V.; Bedford, M. T.; Manfioletti, G., The AT-hook of the chromatin architectural transcription factor high mobility

group A1a is arginine-methylated by protein arginine methyltransferase 6. *J. Biol. Chem.* **2006,** *281* (7), 3764-3772.

124.   El-Andaloussi, N.; Valovka, T.; Toueille, M.; Steinacher, R.; Focke, F.; Gehrig, P.; Covic, M.; Hassa, P. O.; Schär, P.; Hübscher, U., Arginine methylation regulates DNA polymerase β. *Mol. Cell* **2006,** *22* (1), 51-62.

125.   Neault, M.; Mallette, F. A.; Vogel, G.; Michaud-Levesque, J.; Richard, S., Ablation of PRMT6 reveals a role as a negative transcriptional regulator of the p53 tumor suppressor. *Nucleic Acids Res.* **2012,** *40* (19), 9513-9521.

126.   Stein, C.; Riedl, S.; Rüthnick, D.; Nötzold, R. R.; Bauer, U.-M., The arginine methyltransferase PRMT6 regulates cell proliferation and senescence through transcriptional repression of tumor suppressor genes. *Nucleic Acids Res.* **2012,** *40* (19), 9522-9533.

127.   Di Lorenzo, A.; Yang, Y.; Macaluso, M.; Bedford, M. T., A gain-of-function mouse model identifies PRMT6 as a NF-κB coactivator. *Nucleic Acids Res.* **2014**, gku530.

128.   Xie, B.; Invernizzi, C. F.; Richard, S.; Wainberg, M. A., Arginine Methylation of the Human Immunodeficiency Virus Type 1 Tat Protein by PRMT6 Negatively Affects Tat Interactions with both Cyclin T1 and the Tat Transactivation Region. *J. Virol.* **2007,** *81* (8), 4226-4234.

129.   Karkhanis, V.; Wang, L.; Tae, S.; Hu, Y.-J.; Imbalzano, A. N.; Sif, S., Protein arginine methyltransferase 7 regulates cellular response to DNA damage by methylating promoter histones H2A and H4 of the polymerase δ catalytic subunit gene, POLD1. *Journal of Biological Chemistry* **2012,** *287* (35), 29801-29814.

130.   Wang, Y.-C.; Peterson, S. E.; Loring, J. F., Protein post-translational modifications and regulation of pluripotency in human stem cells. *Cell Res.* **2014,** *24* (2), 143-160.

131.   Biermann, K.; Steger, K., Epigenetics in male germ cells. *J. Androl.* **2007,** *28* (4), 466-480.

132.   Jelinic, P.; Stehle, J.-C.; Shaw, P., The testis-specific factor CTCFL cooperates with the protein methyltransferase PRMT7 in H19 imprinting control region methylation. *PLoS Biol.* **2006,** *4* (11), e355.

133.   Yao, R.; Jiang, H.; Ma, Y.; Wang, L.; Wang, L.; Du, J.; Hou, P.; Gao, Y.; Zhao, L.; Wang, G., PRMT7 induces epithelial-to-mesenchymal transition and promotes metastasis in breast cancer. *Cancer Res.* **2014,** *74* (19), 5656-5667.

134.   Sayegh, J.; Webb, K.; Cheng, D.; Bedford, M. T.; Clarke, S. G., Regulation of protein arginine methyltransferase 8 (PRMT8) activity by its N-terminal domain. *J. Biol. Chem.* **2007,** *282* (50), 36444-36453.

135.   Kim, J.-D.; Kako, K.; Kakiuchi, M.; Park, G. G.; Fukamizu, A., EWS is a substrate of type I protein arginine methyltransferase, PRMT8. *Int. J. Mol. Med.* **2008,** *22* (3), 309-315.

136.   Lee, J.; Sayegh, J.; Daniel, J.; Clarke, S.; Bedford, M. T., PRMT8, a new membrane-bound tissue-specific member of the protein arginine methyltransferase family. *J. Biol. Chem.* **2005,** *280* (38), 32890-32896.

137.   Hadjikyriacou, A.; Yang, Y.; Espejo, A.; Bedford, M. T.; Clarke, S. G., Unique Features of Human Protein Arginine Methyltransferase 9 (PRMT9) and Its Substrate RNA Splicing Factor SF3B2. *J. Biol. Chem.* **2015,** *290* (27), 16723-16743.

138.   Uhlén, M.; Fagerberg, L.; Hallström, B. M.; Lindskog, C.; Oksvold, P.; Mardinoglu, A.; Sivertsson, Å.; Kampf, C.; Sjöstedt, E.; Asplund, A., Tissue-based map of the human proteome. *Science* **2015,** *347* (6220), 1260419.

139. Li, K. K.; Luo, C.; Wang, D.; Jiang, H.; Zheng, Y. G., Chemical and biochemical approaches in the study of histone methylation and demethylation. *Med. Res. Rev.* **2012,** *32* (4), 815-67.

140. Spannhoff, A.; Machmur, R.; Heinke, R.; Trojer, P.; Bauer, I.; Brosch, G.; Schule, R.; Hanefeld, W.; Sippl, W.; Jung, M., A novel arginine methyltransferase inhibitor with cellular activity. *Bioorg. Med. Chem. Lett.* **2007,** *17* (15), 4150-3.

141. Wooderchak, W. L.; Zhou, Z. S.; Hevel, J., Assays for S-adenosylmethionine (AdoMet/SAM)-dependent methyltransferases. *Curr. Protoc. Toxicol.* **2008,** *Chapter 4*, Unit4 26.

142. Zeng, H., Xu, W., Enzymatic Assays of Histone Methyltransferase Enzymes. In *Epigenetic Technological Applications*, Zheng, Y. G., Ed. Academic Press: San Diego, 2015; pp 333-361.

143. Luo, M., Current Chemical Biology Approaches to Interrogate Protein Methyltransferases. *ACS Chemical Biology* **2012,** *7* (3), 443-463.

144. Castellano, S.; Milite, C.; Ragno, R.; Simeoni, S.; Mai, A.; Limongelli, V.; Novellino, E.; Bauer, I.; Brosch, G.; Spannhoff, A.; Cheng, D.; Bedford, M. T.; Sbardella, G., Design, synthesis and biological evaluation of carboxy analogues of arginine methyltransferase inhibitor 1 (AMI-1). *ChemMedChem* **2010,** *5* (3), 398-414.

145. Spannhoff, A.; Heinke, R.; Bauer, I.; Trojer, P.; Metzger, E.; Gust, R.; Schüle, R.; Brosch, G.; Sippl, W.; Jung, M., Target-based approach to inhibitors of histone arginine methyltransferases. *J. Med. Chem.* **2007,** *50* (10), 2319-2325.

146.   Dowden, J.; Hong, W.; Parry, R. V.; Pike, R. A.; Ward, S. G., Toward the development of potent and selective bisubstrate inhibitors of protein arginine methyltransferases. *Bioorg. Med. Chem. Lett.* **2010,** *20* (7), 2103-5.

147.   Dowden, J.; Pike, R. A.; Parry, R. V.; Hong, W.; Muhsen, U. A.; Ward, S. G., Small molecule inhibitors that discriminate between protein arginine N-methyltransferases PRMT1 and CARM1. *Org Biomol Chem* **2011,** *9* (22), 7814-21.

148.   Bonham, K.; Hemmers, S.; Lim, Y. H.; Hill, D. M.; Finn, M. G.; Mowen, K. A., Effects of a novel arginine methyltransferase inhibitor on T-helper cell cytokine production. *FEBS J.* **2010,** *277* (9), 2096-108.

149.   Sinha, S. H.; Owens, E. A.; Feng, Y.; Yang, Y.; Xie, Y.; Tu, Y.; Henary, M.; Zheng, Y. G., Synthesis and evaluation of carbocyanine dyes as PRMT inhibitors and imaging agents. *Eur. J. Med. Chem.* **2012,** *54*, 647-59.

150.   Yan, L.; Yan, C.; Qian, K.; Su, H.; Kofsky-Wofford, S. A.; Lee, W. C.; Zhao, X.; Ho, M. C.; Ivanov, I.; Zheng, Y. G., Diamidine compounds for selective inhibition of protein arginine methyltransferase 1. *J. Med. Chem.* **2014,** *57* (6), 2611-22.

151.   Purandare, A. V.; Chen, Z.; Huynh, T.; Pang, S.; Geng, J.; Vaccaro, W.; Poss, M. A.; Oconnell, J.; Nowak, K.; Jayaraman, L., Pyrazole inhibitors of coactivator associated arginine methyltransferase 1 (CARM1). *Bioorg. Med. Chem. Lett.* **2008,** *18* (15), 4438-4441.

152.   Liu, F.; Li, F.; Ma, A.; Dobrovetsky, E.; Dong, A.; Gao, C.; Korboukh, I.; Liu, J.; Smil, D.; Brown, P. J.; Frye, S. V.; Arrowsmith, C. H.; Schapira, M.; Vedadi, M.; Jin, J., Exploiting an allosteric binding site of PRMT3 yields potent and selective inhibitors. *J. Med. Chem.* **2013,** *56* (5), 2110-24.

153.   Huynh, T.; Chen, Z.; Pang, S.; Geng, J.; Bandiera, T.; Bindi, S.; Vianello, P.; Roletto, F.; Thieffine, S.; Galvani, A., Optimization of pyrazole inhibitors of coactivator associated arginine methyltransferase 1 (CARM1). *Bioorg. Med. Chem. Lett.* **2009,** *19* (11), 2924-2927.

154.   Therrien, E.; Larouche, G.; Manku, S.; Allan, M.; Nguyen, N.; Styhler, S.; Robert, M.-F.; Goulet, A.-C.; Besterman, J. M.; Nguyen, H., 1, 2-Diamines as inhibitors of co-activator associated arginine methyltransferase 1 (CARM1). *Bioorg. Med. Chem. Lett.* **2009,** *19* (23), 6725-6732.

155.   Sack, J. S.; Thieffine, S.; Bandiera, T.; Fasolini, M.; Duke, G. J.; Jayaraman, L.; Kish, K. F.; Klei, H. E.; Purandare, A. V.; Rosettani, P.; Troiani, S.; Xie, D.; Bertrand, J. A., Structural basis for CARM1 inhibition by indole and pyrazole inhibitors. *Biochem. J.* **2011,** *436* (2), 331-9.

156.   Wan, H.; Huynh, T.; Pang, S.; Geng, J.; Vaccaro, W.; Poss, M. A.; Trainor, G. L.; Lorenzi, M. V.; Gottardis, M.; Jayaraman, L., Benzo[d]imidazole inhibitors of Coactivator Associated Arginine Methyltransferase 1 (CARM1)—Hit to Lead studies. *Bioorg. Med. Chem. Lett.* **2009,** *19* (17), 5063-5066.

157.   Baiocchi, R. A.; Li, C.; LAI, H.; SIF, S. Inhibitors of prmt5 and methods of their use. WO2014145214 A2, 2014.

158.   Selvi, B. R.; Batta, K.; Kishore, A. H.; Mantelingu, K.; Varier, R. A.; Balasubramanyam, K.; Pradhan, S. K.; Dasgupta, D.; Sriram, S.; Agrawal, S.; Kundu, T. K., Identification of a novel inhibitor of coactivator-associated arginine methyltransferase 1 (CARM1)-mediated methylation of histone H3 Arg-17. *J. Biol. Chem.* **2010,** *285* (10), 7143-52.

159.   Wang, J.; Chen, L.; Sinha, S. H.; Liang, Z.; Chai, H.; Muniyan, S.; Chou, Y. W.; Yang, C.; Yan, L.; Feng, Y.; Li, K. K.; Lin, M. F.; Jiang, H.; Zheng, Y. G.; Luo, C., Pharmacophore-

based virtual screening and biological evaluation of small molecule inhibitors for protein arginine methylation. *J. Med. Chem.* **2012,** *55* (18), 7978-87.

160.   Feng, Y.; Li, M.; Wang, B.; Zheng, Y. G., Discovery and mechanistic study of a class of protein arginine methylation inhibitors. *J. Med. Chem.* **2010,** *53* (16), 6028-39.

161.   Rathert, P.; Cheng, X.; Jeltsch, A., Continuous enzymatic assay for histone lysine methyltransferases. *BioTechniques* **2007,** *43* (5), 602, 604, 606 passim.

162.   Dhayalan, A.; Dimitrova, E.; Rathert, P.; Jeltsch, A., A continuous protein methyltransferase (G9a) assay for enzyme activity measurement and inhibitor screening. *J. Biomol. Screen.* **2009,** *14* (9), 1129-33.

163.   Ibanez, G.; Shum, D.; Blum, G.; Bhinder, B.; Radu, C.; Antczak, C.; Luo, M.; Djaballah, H., A high throughput scintillation proximity imaging assay for protein methyltransferases. *Comb Chem High Throughput Screen* **2012,** *15* (5), 359-71.

164.   Hu, H.; Owens, E. A.; Su, H.; Yan, L.; Levitz, A.; Zhao, X.; Henary, M.; Zheng, Y. G., Exploration of Cyanine Compounds as Selective Inhibitors of Protein Arginine Methyltransferases: Synthesis and Biological Evaluation. *J. Med. Chem.* **2015**.

165.   Siarheyeva, A.; Senisterra, G.; Allali-Hassani, A.; Dong, A.; Dobrovetsky, E.; Wasney, G. A.; Chau, I.; Marcellus, R.; Hajian, T.; Liu, F.; Korboukh, I.; Smil, D.; Bolshan, Y.; Min, J.; Wu, H.; Zeng, H.; Loppnau, P.; Poda, G.; Griffin, C.; Aman, A.; Brown, P. J.; Jin, J.; Al-Awar, R.; Arrowsmith, C. H.; Schapira, M.; Vedadi, M., An allosteric inhibitor of protein arginine methyltransferase 3. *Structure* **2012,** *20* (8), 1425-35.

166.   Kaniskan, H. Ü.; Szewczyk, M. M.; Yu, Z.; Eram, M. S.; Yang, X.; Schmidt, K.; Luo, X.; Dai, M.; He, F.; Zang, I.; Lin, Y.; Kennedy, S.; Li, F.; Dobrovetsky, E.; Dong, A.; Smil, D.; Min, S.-J.; Landon, M.; Lin-Jones, J.; Huang, X.-P.; Roth, B. L.; Schapira, M.; Atadja, P.; Barsyte-

Lovejoy, D.; Arrowsmith, C. H.; Brown, P. J.; Zhao, K.; Jin, J.; Vedadi, M., A Potent, Selective and Cell-Active Allosteric Inhibitor of Protein Arginine Methyltransferase 3 (PRMT3). *Angew. Chem. Int. Ed.* **2015,** *54* (17), 5166-5170.

167.   Zheng, W.; Ibáñez, G.; Wu, H.; Blum, G.; Zeng, H.; Dong, A.; Li, F.; Hajian, T.; Allali-Hassani, A.; Amaya, M. F.; Siarheyeva, A.; Yu, W.; Brown, P. J.; Schapira, M.; Vedadi, M.; Min, J.; Luo, M., Sinefungin Derivatives as Inhibitors and Structure Probes of Protein Lysine Methyltransferase SETD2. *J. Am. Chem. Soc.* **2012,** *134* (43), 18004-18014.

168.   Mitchell, L. H.; Drew, A. E.; Ribich, S. A.; Rioux, N.; Swinger, K. K.; Jacques, S. L.; Lingaraj, T.; Boriack-Sjodin, P. A.; Waters, N. J.; Wigle, T. J.; Moradei, O.; Jin, L.; Riera, T.; Porter-Scott, M.; Moyer, M. P.; Smith, J. J.; Chesworth, R.; Copeland, R. A., Aryl Pyrazoles as Potent Inhibitors of Arginine Methyltransferases: Identification of the First PRMT6 Tool Compound. *ACS Med. Chem. Lett.* **2015,** *6* (6), 655-659.

169.   Eram, M. S.; Shen, Y.; Szewczyk, M. M.; Wu, H.; Senisterra, G.; Li, F.; Butler, K. V.; Kaniskan, H. Ü.; Speed, B. A.; dela Seña, C.; Dong, A.; Zeng, H.; Schapira, M.; Brown, P. J.; Arrowsmith, C. H.; Barsyte-Lovejoy, D.; Liu, J.; Vedadi, M.; Jin, J., A Potent, Selective, and Cell-Active Inhibitor of Human Type I Protein Arginine Methyltransferases. *ACS Chem. Biol.* **2015**.

170.   Smil, D.; Eram, M. S.; Li, F.; Kennedy, S.; Szewczyk, M. M.; Brown, P. J.; Barsyte-Lovejoy, D.; Arrowsmith, C. H.; Vedadi, M.; Schapira, M., Discovery of a Dual PRMT5–PRMT7 Inhibitor. *ACS Med. Chem. Lett.* **2015,** *6* (4), 408-412.

171.   Wu, J.; Xie, N.; Feng, Y.; Zheng, Y. G., Scintillation Proximity Assay of Arginine Methylation. *J. Biomol. Screen.* **2012,** *17* (2), 237-244.

172.   Cook, N. D., Scintillation proximity assay: a versatile high-throughput screening technology. *Drug Discov. Today* **1996,** *1* (7), 287-294.

173.   Glickman, J. F.; Schmid, A.; Ferrand, S., Scintillation proximity assays in high-throughput screening. *Assay Drug Dev. Technol.* **2008,** *6* (3), 433-55.

174.   Fontán, N.; García-Domínguez, P.; Álvarez, R.; de Lera, Á. R., Novel symmetrical ureas as modulators of protein arginine methyl transferases. *Biorg. Med. Chem.* **2013,** *21* (7), 2056-2067.

175.   Cheng, D.; Yadav, N.; King, R. W.; Swanson, M. S.; Weinstein, E. J.; Bedford, M. T., Small molecule regulators of protein arginine methyltransferases. *J. Biol. Chem.* **2004,** *279* (23), 23892-23899.

176.   van Haren, M.; van Ufford, L. Q.; Moret, E. E.; Martin, N. I., Synthesis and evaluation of protein arginine N-methyltransferase inhibitors designed to simultaneously occupy both substrate binding sites. *Org Biomol Chem* **2015,** *13* (2), 549-60.

177.   Heinke, R.; Spannhoff, A.; Meier, R.; Trojer, P.; Bauer, I.; Jung, M.; Sippl, W., Virtual screening and biological characterization of novel histone arginine methyltransferase PRMT1 inhibitors. *ChemMedChem* **2009,** *4* (1), 69-77.

178.   Bissinger, E. M.; Heinke, R.; Spannhoff, A.; Eberlin, A.; Metzger, E.; Cura, V.; Hassenboehler, P.; Cavarelli, J.; Schule, R.; Bedford, M. T.; Sippl, W.; Jung, M., Acyl derivatives of p-aminosulfonamides and dapsone as new inhibitors of the arginine methyltransferase hPRMT1. *Bioorg. Med. Chem.* **2011,** *19* (12), 3717-31.

179.   Rioux, N.; Duncan, K. W.; Lantz, R. J.; Miao, X.; Chan-Penebre, E.; Moyer, M. P.; Munchhof, M. J.; Copeland, R. A.; Chesworth, R.; Waters, N. J., Species differences in

metabolism of EPZ015666, an oxetane-containing protein arginine methyltransferase-5 (PRMT5) inhibitor. *Xenobiotica* **2015**, 1-10.

180.   Xie, Y.; Zhou, R.; Lian, F.; Liu, Y.; Chen, L.; Shi, Z.; Zhang, N.; Zheng, M.; Shen, B.; Jiang, H.; Liang, Z.; Luo, C., Virtual screening and biological evaluation of novel small molecular inhibitors against protein arginine methyltransferase 1 (PRMT1). *Org Biomol Chem* **2014,** *12* (47), 9665-73.

181.   Duncan, K. W.; Rioux, N.; Boriack-Sjodin, P. A.; Munchhof, M. J.; Reiter, L. A.; Majer, C. R.; Jin, L.; Johnston, L. D.; Chan-Penebre, E.; Kuplast, K. G.; Porter Scott, M.; Pollock, R. M.; Waters, N. J.; Smith, J. J.; Moyer, M. P.; Copeland, R. A.; Chesworth, R., Structure and Property Guided Design in the Identification of PRMT5 Tool Compound EPZ015666. *ACS Med. Chem. Lett.* **2016,** *7* (2), 162-166.

182.   Yu, X.-R.; Tang, Y.; Wang, W.-J.; Ji, S.; Ma, S.; Zhong, L.; Zhang, C.-H.; Yang, J.; Wu, X.-A.; Fu, Z.-Y.; Li, L.-L.; Yang, S.-Y., Discovery and structure–activity analysis of 4-((5-nitropyrimidin-4-yl)amino)benzimidamide derivatives as novel protein arginine methyltransferase 1 (PRMT1) inhibitors. *Bioorg. Med. Chem. Lett.* **2015**.

183.   Collazo, E.; Couture, J. F.; Bulfer, S.; Trievel, R. C., A coupled fluorescent assay for histone methyltransferases. *Anal. Biochem.* **2005,** *342* (1), 86-92.

184.   Wang, R.; Ibanez, G.; Islam, K.; Zheng, W.; Blum, G.; Sengelaub, C.; Luo, M., Formulating a fluorogenic assay to evaluate S-adenosyl-L-methionine analogues as protein methyltransferase cofactors. *Mol Biosyst* **2011,** *7* (11), 2970-81.

185.   Copeland, R. A.; Solomon, M. E.; Richon, V. M., Protein methyltransferases as a target class for drug discovery. *Nat. Rev. Drug Discov.* **2009,** *8* (9), 724-32.

186.   Pugh, C. S. G.; Borchardt, R. T.; Stone, H., Inhibition of Newcastle Disease Virion Messenger RNA (guanine-7-)-Methyltransferase by Analogues of S-Adenosylhomocysteine. *Biochemistry* **1977,** *16*.

187.   Pugh, C. S. G.; Borchardt, R. T.; Stone, H., Sinefungin, a Potent Inhibitor of Virion mRNA(guanine-7-)-methyltransferase, mRNA(nucleoside-2'-)-methyltransferase, and Viral Multiplication. *J. Biol. Chem.* **1978,** *263*.

188.   Daigle, S. R.; Olhava, E. J.; Therkelsen, C. A.; Majer, C. R.; Sneeringer, C. J.; Song, J.; Johnston, L. D.; Scott, M. P.; Smith, J. J.; Xiao, Y.; Jin, L.; Kuntz, K. W.; Chesworth, R.; Moyer, M. P.; Bernt, K. M.; Tseng, J. C.; Kung, A. L.; Armstrong, S. A.; Copeland, R. A.; Richon, V. M.; Pollock, R. M., Selective killing of mixed lineage leukemia cells by a potent small-molecule DOT1L inhibitor. *Cancer Cell* **2011,** *20* (1), 53-65.

189.   Yu, W.; Chory, E. J.; Wernimont, A. K.; Tempel, W.; Scopton, A.; Federation, A.; Marineau, J. J.; Qi, J.; Barsyte-Lovejoy, D.; Yi, J.; Marcellus, R.; Iacob, R. E.; Engen, J. R.; Griffin, C.; Aman, A.; Wienholds, E.; Li, F.; Pineda, J.; Estiu, G.; Shatseva, T.; Hajian, T.; Al-Awar, R.; Dick, J. E.; Vedadi, M.; Brown, P. J.; Arrowsmith, C. H.; Bradner, J. E.; Schapira, M., Catalytic site remodelling of the DOT1L methyltransferase by selective inhibitors. *Nat Commun* **2012,** *3*, 1288.

190.   Trapp, J.; Meier, R.; Hongwiset, D.; Kassack, M. U.; Sippl, W.; Jung, M., Structure-activity studies on suramin analogues as inhibitors of NAD+-dependent histone deacetylases (sirtuins). *ChemMedChem* **2007,** *2* (10), 1419-31.

191.   Ragno, R.; Simeoni, S.; Castellano, S.; Vicidomini, C.; Mai, A.; Caroli, A.; Tramontano, A.; Bonaccini, C.; Trojer, P.; Bauer, I., Small molecule inhibitors of histone arginine

methyltransferases: homology modeling, molecular docking, binding mode analysis, and biological evaluations. *J. Med. Chem.* **2007,** *50* (6), 1241-1253.

192.   Mai, A.; Cheng, D.; Bedford, M. T.; Valente, S.; Nebbioso, A.; Perrone, A.; Brosch, G.; Sbardella, G.; De Bellis, F.; Miceli, M., Epigenetic multiple ligands: mixed histone/protein methyltransferase, acetyltransferase, and class III deacetylase (sirtuin) inhibitors. *J. Med. Chem.* **2008,** *51* (7), 2279-2290.

193.   Dillon, M. B.; Bachovchin, D. A.; Brown, S. J.; Finn, M.; Rosen, H.; Cravatt, B. F.; Mowen, K. A., Novel inhibitors for PRMT1 discovered by high-throughput screening using activity-based fluorescence polarization. *ACS Chem. Bio.* **2012,** *7* (7), 1198-1204.

194.   Morales, Y.; Cáceres, T.; May, K.; Hevel, J. M., Biochemistry and regulation of the protein arginine methyltransferases (PRMTs). *Arch. Biochem. Biophys.* **2016,** *590*, 138-152.

195.   Bocobo, F. C.; Curtis, A. C.; Harrell, E. R.; Conner, V., In Vitro Fungistatic Activity of Stilbamidine, Propamidine, Pentamidine and Diethylstilbestrol1. *J. Invest. Dermatol.* **1953,** *21* (3), 149-156.

196.   Purfield, A. E.; Tidwell, R. R.; Meshnick, S. R., Interactions of DB75, a novel antimalarial agent, with other antimalarial drugs in vitro. *Antimicrob. Agents Chemother.* **2008,** *52* (6), 2253-5.

197.   Allan, M.; Manku, S.; Therrien, E.; Nguyen, N.; Styhler, S.; Robert, M. F.; Goulet, A. C.; Petschner, A. J.; Rahil, G.; Robert Macleod, A.; Deziel, R.; Besterman, J. M.; Nguyen, H.; Wahhab, A., N-Benzyl-1-heteroaryl-3-(trifluoromethyl)-1H-pyrazole-5-carboxamides as inhibitors of co-activator associated arginine methyltransferase 1 (CARM1). *Bioorg. Med. Chem. Lett.* **2009,** *19* (4), 1218-23.

198.   Cheng, D.; Valente, S.; Castellano, S.; Sbardella, G.; Di Santo, R.; Costi, R.; Bedford, M. T.; Mai, A., Novel 3,5-bis(bromohydroxybenzylidene)piperidin-4-ones as coactivator-associated arginine methyltransferase 1 inhibitors: enzyme selectivity and cellular activity. *J. Med. Chem.* **2011,** *54* (13), 4928-32.

199.   Alinari, L.; Mahasenan, K. V.; Yan, F.; Karkhanis, V.; Chung, J. H.; Smith, E. M.; Quinion, C.; Smith, P. L.; Kim, L.; Patton, J. T.; Lapalombella, R.; Yu, B.; Wu, Y.; Roy, S.; De Leo, A.; Pileri, S.; Agostinelli, C.; Ayers, L.; Bradner, J. E.; Chen-Kiang, S.; Elemento, O.; Motiwala, T.; Majumder, S.; Byrd, J. C.; Jacob, S.; Sif, S.; Li, C.; Baiocchi, R. A., Selective inhibition of protein arginine methyltransferase 5 blocks initiation and maintenance of B-cell transformation. *Blood* **2015**.

200.   Hamzeh-Mivehroud, M.; Alizadeh, A. A.; Morris, M. B.; Church, W. B.; Dastmalchi, S., Phage display as a technology delivering on the promise of peptide drug discovery. *Drug Discov. Today* **2013,** *18* (23-24), 1144-57.

201.   Osborne, T.; Weller Roska, R. L.; Rajski, S. R.; Thompson, P. R., In situ generation of a bisubstrate analogue for protein arginine methyltransferase 1. *J. Am. Chem. Soc.* **2008,** *130* (14), 4574-4575.

202.   Obianyo, O.; Causey, C. P.; Osborne, T. C.; Jones, J. E.; Lee, Y. H.; Stallcup, M. R.; Thompson, P. R., A chloroacetamidine-based inactivator of protein arginine methyltransferase 1: design, synthesis, and in vitro and in vivo evaluation. *ChemBioChem* **2010,** *11* (9), 1219-23.

203.   Lakowski T M, t. H. P., Ahern C A, et al., N-etha-Substituted Arginyl Peptide Inhibitors of Protein Arginine N-Methyltransferases. *ACS chembio* **2010,** (11), 1053-1063.

204.   Thomas, D.; Koopmans, T.; Lakowski, T. M.; Kreinin, H.; Vhuiyan, M. I.; Sedlock, S. A.; Bui, J. M.; Martin, N. I.; Frankel, A., Protein arginine N-methyltransferase substrate

preferences for different neta-substituted arginyl peptides. *ChemBioChem* **2014,** *15* (11), 1607-13.

205.   t Hart, P.; Lakowski, T. M.; Thomas, D.; Frankel, A.; Martin, N. I., Peptidic partial bisubstrates as inhibitors of the protein arginine N-methyltransferases. *ChemBioChem* **2011,** *12* (9), 1427-32.

206.   t Hart, P.; Thomas, D.; van Ommeren, R.; Lakowski, T. M.; Frankel, A.; Martin, N. I., Analogues of the HIV-Tat peptide containing Nη-modified arginines as potent inhibitors of protein arginine N-methyltransferases. *MedChemComm* **2012,** *3* (10), 1235.

207.   Chesworth, R.; Mitchell, L. H.; Shapiro, G.; Kuntz, K. W., Arginine methyltransferase inhibitors and uses thereof. Google Patents: 2014.

208.   Chesworth, R.; Moradei, O. M.; Shapiro, G.; Jin, L.; Babine, R. E., Carm1 inhibitors and uses thereof. Google Patents: 2014.

209.   Mitchell, L. H.; Shapiro, G.; Chesworth, R.; Boriack-Sjodin, P. A.; Moradei, O. M.; Kuntz, K. W., Prmt1 inhibitors and uses thereof. Google Patents: 2014.

210.   Duncan, K. W.; Chesworth, R.; Munchhof, M. J., Prmt5 inhibitors and uses thereof. Google Patents: 2014.

211.   Blanc, R. S.; Richard, S., Arginine Methylation: The Coming of Age. *Mol. Cell* **2017,** *65* (1), 8-24.

212.   Schoenbach, E. B.; Miller, J. M.; Long, P. H., The treatment of systemic blastomycosis with stilbamidine. *Annals of internal medicine* **1952,** *37* (1), 31-47.

213.   Schoenbach, E. B.; Miller, J. M.; Ginsberg, M.; Long, P. H., Systemic blastomycosis treated with stilbamidine: a preliminary report. *Journal of the American Medical Association* **1951,** *146* (14), 1317-1318.

214.   Ecker, H. D.; Lubitz, J. M., Kala-azar In The United States: Review Of The Literature And Report Of Two Cases: Stilbamidine Treatment. *Annals of internal medicine* **1947,** *26* (5), 720-733.

215.   Ansede, J. H.; Anbazhagan, M.; Brun, R.; Easterbrook, J. D.; Hall, J. E.; Boykin, D. W., O-alkoxyamidine prodrugs of furamidine: in vitro transport and microsomal metabolism as indicators of in vivo efficacy in a mouse model of Trypanosoma brucei rhodesiense infection. *J Med Chem* **2004,** *47* (17), 4335-4338.

216.   Ismail, M. A.; Brun, R.; Easterbrook, J. D.; Tanious, F. A.; Wilson, W. D.; Boykin, D. W., Synthesis and antiprotozoal activity of aza-analogues of furamidine. *J Med Chem* **2003,** *46* (22), 4761-4769.

217.   Soeiro, M. N.; De Souza, E.; Stephens, C. E.; Boykin, D., Aromatic diamidines as antiparasitic agents. *Expert opinion on investigational drugs* **2005,** *14* (8), 957-972.

218.   De Souza, E.; Menna-Barreto, R.; Araujo-Jorge, T.; Kumar, A.; Hu, Q.; Boykin, D.; Soeiro, M., Antiparasitic activity of aromatic diamidines is related to apoptosis-like death in Trypanosoma cruzi. *Parasitology* **2006,** *133* (1), 75-79.

219.   Baraldi, P. G.; Bovero, A.; Fruttarolo, F.; Preti, D.; Tabrizi, M. A.; Pavani, M. G.; Romagnoli, R., DNA minor groove binders as potential antitumor and antimicrobial agents. *Medicinal research reviews* **2004,** *24* (4), 475-528.

220.   Boykin, D. W., Antimicrobial activity of the DNA minor groove binders furamidine and analogs. *Journal of the Brazilian Chemical Society* **2002,** *13* (6), 763-771.

221.   Sands, M.; Kron, M. A.; Brown, R. B., Pentamidine: a review. *Reviews of infectious diseases* **1985,** *7* (5), 625-6344.

222.   Bradford, M. M., A rapid and sensitive method for the quantitation of microgram quantities of protein utilizing the principle of protein-dye binding. *Anal. Biochem.* **1976,** *72* (1), 248-254.

223.   Zhang, L.; Tran, N. T.; Su, H.; Wang, R.; Lu, Y.; Tang, H.; Aoyagi, S.; Guo, A.; Khodadadi-Jamayran, A.; Zhou, D.; Qian, K.; Hricik, T.; Cote, J.; Han, X.; Zhou, W.; Laha, S.; Abdel-Wahab, O.; Levine, R. L.; Raffel, G.; Liu, Y.; Chen, D.; Li, H.; Townes, T.; Wang, H.; Deng, H.; Zheng, Y. G.; Leslie, C.; Luo, M.; Zhao, X., Cross-talk between PRMT1-mediated methylation and ubiquitylation on RBM15 controls RNA splicing. *eLife* **2015,** *4*.

224.   Zhang, J.; Qian, K.; Yan, C.; He, M.; Jassim, B. A.; Ivanov, I.; Zheng, Y. G., Discovery of Decamidine as a New and Potent PRMT1 Inhibitor. *Medchemcomm* **2017,** *8* (2), 440-444.

225.   Karkhanis, V.; Hu, Y. J.; Baiocchi, R. A.; Imbalzano, A. N.; Sif, S., Versatility of PRMT5-induced methylation in growth control and development. *Trends Biochem. Sci.* **2011,** *36* (12), 633-41.

226.   Lee, D. Y.; Teyssier, C.; Strahl, B. D.; Stallcup, M. R., Role of protein methylation in regulation of transcription. *Endocr. Rev.* **2005,** *26* (2), 147-70.

227.   Krause CD, Y. Z., Kim YS, Lee JH, Cook JR, Pestka S., Protein arginine methyltransferases: evolution and assessment of their pharmacological and therapeutic potential. *Pharmacol Ther.* **2007,** *113* (1), 50-87.

228.   Gu, Z. P.; Gao, S.; Zhang, F. H.; Wang, Z. Q.; Ma, W. C.; Davis, R. E.; Wang, Z. X., Protein arginine methyltransferase 5 is essential for growth of lung cancer cells. *Biochem. J.* **2012,** *446*, 235-241.

229. Bao, X. X.; Zhao, S.; Liu, T.; Liu, Y.; Liu, Y. Y.; Yang, X. S., Overexpression of PRMT5 Promotes Tumor Cell Growth and Is Associated with Poor Disease Prognosis in Epithelial Ovarian Cancer. *J. Histochem. Cytochem.* **2013,** *61* (3), 206-217.

230. Cho, E. C.; Zheng, S.; Munro, S.; Liu, G.; Carr, S. M.; Moehlenbrink, J.; Lu, Y. C.; Stimson, L.; Khan, O.; Konietzny, R.; McGouran, J.; Coutts, A. S.; Kessler, B.; Kerr, D. J.; Thangue, N. B., Arginine methylation controls growth regulation by E2F-1. *The EMBO journal* **2012,** *31* (7), 1785-97.

231. Pal, S.; Baiocchi, R. A.; Byrd, J. C.; Grever, M. R.; Jacob, S. T.; Sif, S., Low levels of miR-92b/96 induce PRMT5 translation and H3R8/H4R3 methylation in mantle cell lymphoma. *EMBO J.* **2007,** *26* (15), 3558-69.

232. Park, J. H.; Szemes, M.; Vieira, G. C.; Melegh, Z.; Malik, S.; Heesom, K. J.; Von Wallwitz-Freitas, L.; Greenhough, A.; Brown, K. W.; Zheng, Y. G.; Catchpoole, D.; Deery, M. J.; Malik, K., Protein arginine methyltransferase 5 is a key regulator of the MYCN oncoprotein in neuroblastoma cells. *Mol. Oncol.* **2015,** *9* (3), 617-627.

233. Moggs, J. G.; Murphy, T. C.; Lim, F. L.; Moore, D. J.; Stuckey, R.; Antrobus, K.; Kimber, I.; Orphanides, G., Anti-proliferative effect of estrogen in breast cancer cells that re-express ERalpha is mediated by aberrant regulation of cell cycle genes. *J. Mol. Endocrinol.* **2005,** *34* (2), 535-51.

234. Schulz, W. A.; Hoffmann, M. J., Epigenetic mechanisms in the biology of prostate cancer. *Semin. Cancer Biol.* **2009,** *19* (3), 172-80.

235. Chan-Penebre, E.; Kuplast, K. G.; Majer, C. R.; Boriack-Sjodin, P. A.; Wigle, T. J.; Johnston, L. D.; Rioux, N.; Munchhof, M. J.; Jin, L.; Jacques, S. L.; West, K. A.; Lingaraj, T.; Stickland, K.; Ribich, S. A.; Raimondi, A.; Scott, M. P.; Waters, N. J.; Pollock, R. M.; Smith, J.

J.; Barbash, O.; Pappalardi, M.; Ho, T. F.; Nurse, K.; Oza, K. P.; Gallagher, K. T.; Kruger, R.; Moyer, M. P.; Copeland, R. A.; Chesworth, R.; Duncan, K. W., A selective inhibitor of PRMT5 with in vivo and in vitro potency in MCL models. *Nat. Chem. Biol.* **2015,** *11* (6), 432-437.

236.   Wang, M.; Xu, R. M.; Thompson, P. R., Substrate specificity, processivity, and kinetic mechanism of protein arginine methyltransferase 5. *Biochemistry* **2013,** *52* (32), 5430-40.

237.   de Ines, C.; Leynadier, D.; Barasoain, I.; Peyrot, V.; Garcia, P.; Briand, C.; Rener, G. A.; Temple, C., Jr., Inhibition of microtubules and cell cycle arrest by a new 1-deaza-7,8-dihydropteridine antitumor drug, CI 980, and by its chiral isomer, NSC 613863. *Cancer Res.* **1994,** *54* (1), 75-84.

238.   Barbier, P.; Dorleans, A.; Devred, F.; Sanz, L.; Allegro, D.; Alfonso, C.; Knossow, M.; Peyrot, V.; Andreu, J. M., Stathmin and interfacial microtubule inhibitors recognize a naturally curved conformation of tubulin dimers. *The Journal of biological chemistry* **2010,** *285* (41), 31672-81.

239.   Leynadier, D.; Peyrot, V.; Sarrazin, M.; Briand, C.; Andreu, J. M.; Rener, G. A.; Temple, C., Jr., Tubulin binding of two 1-deaza-7,8-dihydropteridines with different biological properties: enantiomers NSC 613862 (S)-(-) and NSC 613863 (R)-(+). *Biochemistry* **1993,** *32* (40), 10675-82.

240.   Dumontet, C.; Jordan, M. A., Microtubule-binding agents: a dynamic field of cancer therapeutics. *Nat. Rev. Drug Discov.* **2010,** *9* (10), 790-803.

241.   Lu, Y.; Chen, J.; Xiao, M.; Li, W.; Miller, D. D., An overview of tubulin inhibitors that interact with the colchicine binding site. *Pharmaceutical research* **2012,** *29* (11), 2943-71.

242.   Hurwitz, A. A.; Foster, B. A.; Allison, J. P.; Greenberg, N. M.; Kwon, E. D., *The TRAMP mouse as a model for prostate cancer*. 2001; Vol. Chapter 20, p Unit 20.5.

243. Waud, W. R.; Leopold, W. R.; Elliott, W. L.; Dykes, D. J.; Laster, W. R.; Temple, C. G.; Harrison, S. D.; Griswold, D. P., Antitumor Activity of Ethyl 5-Amino-1,2-dihydro-2-methyl-3-phenylpyrido[3,4-b]pyrazin-7-ylcarbamate 2-Hydroxyethanesulfonate, Hydrate (NSC 370147) against Selected Tumor Systems in Culture and in Mice. *Cancer Res.* **1990,** *50* (11), 3239-3244.

244. Kunschner, L. J.; Fine, H.; Hess, K.; Jaeckle, K.; Kyritsis, A. P.; Yung, W. K., CI-980 for the treatment of recurrent or progressive malignant gliomas: national central nervous system consortium phase I-II evaluation of CI-980. *Cancer Invest.* **2002,** *20* (7-8), 948-54.

245. Werbovetz, K., Diamidines as antitrypanosomal, antileishmanial and antimalarial agents. *Current opinion in investigational drugs (London, England: 2000)* **2006,** *7* (2), 147-157.

246. Christison, I. B.; Conant, N. F., Antifungal activity of some aromatic diamidines. *Translational Research* **1953,** *42* (4), 638-640.

247. Ming, X.; Ju, W.; Wu, H.; Tidwell, R. R.; Hall, J. E.; Thakker, D. R., Transport of Dicationic Drugs Pentamidine and Furamidine by Human Organic Cation Transporters. *Drug Metabolism and Disposition* **2009,** *37* (2), 424-430.

248. Lansiaux, A.; Dassonneville, L.; Facompré, M.; Kumar, A.; Stephens, C. E.; Bajic, M.; Tanious, F.; Wilson, W. D.; Boykin, D. W.; Bailly, C., Distribution of furamidine analogues in tumor cells: influence of the number of positive charges. *J Med Chem* **2002,** *45* (10), 1994-2002.

249. Lansiaux, A.; Tanious, F.; Mishal, Z.; Dassonneville, L.; Kumar, A.; Stephens, C. E.; Hu, Q.; Wilson, W. D.; Boykin, D. W.; Bailly, C., Distribution of furamidine analogues in tumor cells: targeting of the nucleus or mitochondria depending on the amidine substitution. *Cancer research* **2002,** *62* (24), 7219-7229.

250.   Sklarin, N. T.; Lathia, C. D.; Benson, L.; Grove, W. R.; Thomas, S.; Roca, J.; Einzig, A. I.; Wiernik, P. H., A phase I trial and pharmacokinetic evaluation of CI-980 in patients with advanced solid tumors. *Invest. New Drugs* **1997,** *15* (3), 235-246.

251.   Rowinsky, E. K.; Long, G. S.; Noe, D. A.; Grochow, L. B.; Bowling, M.; Sartorius, S. E.; Donehower, R. C., Phase I and pharmacological study of CI-980, a novel synthetic antimicrotubule agent. *Clin. Cancer. Res.* **1997,** *3* (3), 401-407.

252.   Thomas, J. P.; Moore, T.; Kraut, E. H.; Balcerzak, S. P.; Galloway, S.; Vandre, D. D., A phase II study of CI-980 in previously untreated extensive small cell lung cancer: an Ohio State University phase II research consortium study. *Cancer Invest.* **2002,** *20* (2), 192-198.

253.   Whitehead, R. P.; Unger, J. M.; Flaherty, L. E.; Eckardt, J. R.; Taylor, S. A.; Didolkar, M. S.; Samlowski, W.; Sondak, V. K., Phase II Trial of CI-980 in Patients with Disseminated Malignant Melanoma and no Prior Chemotherapy–A Southwest Oncology Group Study. *Invest. New Drugs* **2001,** *19* (3), 239-243.

254.   Patel, S. R.; Burgess, M. A.; Papadopolous, N. E.; Sidhu, G.; Gray, R.; Plager, C.; Jenkins, J.; Benjamin, R. S., Phase II study of CI-980 (NSC 635370) in patients with previously treated advanced soft-tissue sarcomas. *Invest. New Drugs* **1998,** *16* (1), 87-92.

255.   Pazdur, R.; Meyers, C.; Diaz-Canton, E.; Abbruzzese, J.; Patt, Y.; Grove, W.; Ajani, J., Phase II trial of intravenous CI-980 (NSC 370147) in patients with metastatic colorectal carcinoma. *Am. J. Clin. Oncol.* **1997,** *20* (6), 573-576.

256.   Kudelka, A. P.; Hasenburg, A.; Verschraegen, C. F.; Edwards, C. L.; Meyers, C. A.; Varma, D.; Freedman, R. S.; Forman, A.; Conrad, C. A.; Grove, W., Phase II study of iv CI-980 in patients with advanced platinum refractory epithelial ovarian carcinoma. *Anti-Cancer Drugs* **1998,** *9* (5), 405-409.

257.   Zhu, T.; Cao, S.; Su, P.-C.; Patel, R.; Shah, D.; Chokshi, H. B.; Szukala, R.; Johnson, M. E.; Hevener, K. E., Hit Identification and Optimization in Virtual Screening: Practical Recommendations Based Upon a Critical Literature Analysis. *J. Med. Chem.* **2013,** *56* (17), 6560-6572.

258.   Shoichet, B. K., Virtual screening of chemical libraries. *Nature* **2004,** *432* (7019), 862-865.

259.   McInnes, C., Virtual screening strategies in drug discovery. *Curr. Opin. Chem. Biol.* **2007,** *11* (5), 494-502.

260.   Hu, H.; Luo, C.; Zheng, Y. G., Transient Kinetics Define a Complete Kinetic Model for Protein Arginine Methyltransferase 1. *J. Biol. Chem.* **2016,** *291* (52), 26722-26738.

261.   Lakowski, T. M.; Frankel, A., A kinetic study of human protein arginine N-methyltransferase 6 reveals a distributive mechanism. *Journal of Biological Chemistry* **2008,** *283* (15), 10015-10025.

262.   Kölbel, K.; Ihling, C.; Bellmann-Sickert, K.; Neundorf, I.; Beck-Sickinger, A. G.; Sinz, A.; Kühn, U.; Wahle, E., Type I arginine methyltransferases PRMT1 and PRMT-3 act distributively. *Journal of Biological Chemistry* **2009,** *284* (13), 8274-8282.

263.   Obianyo, O.; Thompson, P. R., Kinetic mechanism of protein arginine methyltransferase 6 (PRMT6). *Journal of Biological Chemistry* **2012,** *287* (8), 6062-6071.